Instituto Tecnológico y de Estudios Superiores de Monterrey

Campus Monterrey

School of Engineering and Sciences

Real-Time Simulation of Mechanical Properties on Virtual Reality: A Methodology to Improve Geometric Segmentation, Mathematical Modeling and Characterization of Soft Tissues

A dissertation presented by

Mario Regino Moreno Guerra

Submitted to the
School of Engineering and Sciences
in partial fulfillment of the requirements for the degree of

Doctor of Philosophy

In

Engineering Sciences

Major in Mechatronics and Advanced Manufacturing

Monterrey Nuevo León, June 14th, 2022

Dedication

I would like to dedicate this work and achievement to those who have always supported me across my professional and personal life, no matter what.

First of all, to GOD because it was His will to put me through this process of the never-ending pursuit of growth and learning. He allowed me to achieve what sometimes seemed an impossible goal.

To my family that was always with me, even being apart. My parents, who sacrificed everything of themselves to be able to see me fulfilled, planted in me a tireless spirit of dedication and hard work. My sister, who was always able to listen and comfort me when I needed it the most.

To my friends, who always helped me see things from a different perspective. And to my professors, who advised me wisely during these years and who I admire professionally and personally.

Additionally, thank you to whoever is getting to read this work. This is the product of years of my life, I appreciate the fact that you are taking the time to review it.

These last years have been really complex for everyone and if someone have told me what this path was going to be, I would probably have not believed it. But it is in challenging times that most of the opportunities arise. This is not the end of a phase, but the start of a new one.

Acknowledgments

I would like to express my deepest gratitude to all those who have supported my long journey to get to this point. Particularly, for all that I have learned, all the advice, guidance, and trust provided by Dr. Alex Elías Zúñiga, Dr. Ciro A. Rodríguez, Dr. José Antonio Díaz Elizondo, Dr. Oscar Martínez Romero, Dr. Luis Manuel Palacios Pineda and Dr. Daniel Olvera Trejo. I will be eternally grateful to all of you for being so supportive, tolerant, and understanding with me.

This project would not be possible without the scholarship support from the Instituto Tecnológico y de Estudios Superiores de Monterrey (ITESM), Campus Monterrey, as well as the financial support of the Consejo Nacional de Ciencia y Tecnología (CONACyT). I owe them everything I have done professionally, for both my Master's and PhD. I, like many other students with limited resources, would never be able to access this level of academic education without their support. Thank you for providing opportunities for everyone willing to work for a better future.

In addition, I am thankful for the collaboration with my friends, colleagues, and institutions from Brazil, like the support provided by Dr. Jorge V. Lopes da Silva, Thiago Franco de Moraes and Paulo Henrique Junqueira Amorim from the Centro de Tecnologia da Informação Renato Archer (CTI), the classes and teaching from Dra. Wu Shin-Ting at the Universidade Estadual de Campinas (UNICAMP) and the support from the Conselho Nacional de Desenvolvimento Científico e Tecnológico (CNPq).

Also, I would like to give special thanks to the School of Medicine and Health Sciences of the Tecnológico de Monterrey for the collaboration with Dr. José Antonio Díaz Elizondo and Dr. Eduardo Flores Villalba, who provided medical knowledge that was fundamental for the development of this research project.

Additionally, I am grateful for the support from special teachers and colleagues at the Tecnológico de Monterrey, like Dra. Karen Lorena Baylon Quiñones, Dra. Erika García Lopez, Dra. Raquel Tejeda Alejandre. All of them provided me with help and advice, motivating me to keep going even when I was in my darkest times. I will always cherish and remember with great appreciation those moments.

And last, but not least I would like to thank Navistar International Corporation, a TRATON Group company. I appreciate the flexibility that allowed me to finish this degree while I was also performing my duties as Chassis Engineering Manager of Steering and Suspension Product Development teams in NMxTC. Particularly to Enrique A. Garza, Marco Anaya and Marco Zapiain.

I would like to add that this dissertation, a journal article, and the final steps of the PhD were performed following Scrum principles, which is an agile methodology for project management. I am deeply grateful that got this framework into my life. I think it has a lot of opportunities and applications for R&D projects.

Real-Time Simulation of Mechanical Properties on Virtual Reality: A Methodology to Improve Geometric Segmentation, Mathematical Modeling and Characterization of Soft Tissues

By

Mario Regino Moreno Guerra

Abstract

In this research project, it is presented a methodology to achieve the development of technological tools and material knowledge that support the real-time simulation of soft tissues for virtual reality. Particularly, this work is focused on two main areas that were identified in previous work as opportunities for improvement: Geometrical and Material Modeling. These areas are key to develop not only medical training processes, but also other research projects that involve soft tissue and composite materials characterization, design and development of biomedical devices, and augmented reality tools, among others.

As one of the goals, it is proposed to create virtual tools that allow the interaction, processing, and segmentation of medical images in a semi-automatic way. This was detected by questioning how to increase the applicability of the simulation framework to other anatomical geometries and simplify the creation of new and customized medical cases based on their own set of images.

The solution proposed is to provide the user with access to an interactive learning experience based on 3D rendering of medical images. This will not only allow visualization of medical cases but also have a relatively quick and simple process to get anatomically realistic 3D geometries for simulation, design of new products or 3D printing of models. In this path, it was developed the module *VISUALIX*, which is able to provide said interaction, and the results are presented in chapter 4. Also, a proposal for fractal structure analysis was done using microtomography images, creating *FractalCells* module with the implemented tools.

For material modeling and characterization of soft tissue, a new hybrid formulation is proposed by questioning how a simple technique like Spring-Mass Model (SMM) can describe the soft tissue mechanical properties, if it is based on linear elasticity theory and therefore it can only be used to predict small deformations (<10%).

The solution proposed is based on the application of a constitutive model able to describe the mechanical behavior of soft tissue, as well as other composite materials. For this purpose, it is created a hybrid construction of a Strain Energy Density Function (SEDF) used to find an energy equivalence with a variable stiffness SMM. This formulation was named Equivalent Energy Spring Model (EESM) and is

presented in chapter 5. It is able to characterize soft tissue properties of non-linearity, anisotropy, and Mullin's effect, to predict its response at large deformation (>10%).

Finally, and in order to validate the proposed model, an experimental phase was defined to perform uniaxial and biaxial cyclical tensile tests with porcine tissue samples in order to have experimental data for material characterization using EESM. This experimental phase is described in chapter 6. The results for the characterization of porcine liver and abdominal wall tissues, as well as the predictions of the EESM formulation are presented in chapter 7, including an evaluation of its accuracy and its capacity to perform in real-time.

List of Figures

List of Tables

Contents

Chapter 1

Introduction

During the past years, the world has been made aware of the high necessity of efficient and well-trained health care systems. Challenges that can be presented unexpectedly by many different reasons are able to disturb and shake our current way of living in our day-to-day basis, and to be properly prepared for a quick response and with a high quality and efficient healthcare systems has never been a huge necessity as today.

With that in mind, the fusion of medical knowledge, science, and technology has a great opportunity today to find novelty solutions that allow healthcare professionals to be as well prepared as possible. Therefore, research and development focused on the creation of methodologies and tools that improve current academic procedures for training physicians could represent a great contribution to our society.

In this particular project, it has been proposed to create virtual reality tools that allow healthcare staff to visualize and represent accurate mechanical behavior of soft tissues. This is in order to have an additional training tool that allow direct interaction in the performance of surgical procedures, inside a safe environment. It is believed that this will improve the training process, reduce the infrastructure requirements and ethical implications, and increase the accuracy of the training method.

1.1 Motivation

Within the different branches of medical specialties, the surgical ones present a high degree of difficulty related to the learning of procedures and the development of skills that involve capacities, knowledge, and manual skills. In general, these skills are acquired through practice and experience, resulting in an initial dilemma: You cannot develop these skills without practicing, but you cannot practice directly on the patient without mastering

these skills. Based on the above need, multiple alternative methods have been developed for the training of students and residents of specialties in medical areas.

In medical schools, clinics, and hospitals of the healthcare system it is required efficient ways for learning and skill development. In the case of surgical training, it is important to consider methods without involving any risk to patients.

There are diverse alternative methods that are used by medical institutions for the development of surgical skills and training of surgical procedures. Some of these are animal models, cadavers, box simulators, and virtual simulators, among others.

Each of these methods has different advantages and opportunity areas but in general, these are aimed to represent the hand movement, environment, conditions, and situations present in surgical procedures, seeking to adhere as closely as possible to reality.

However, the development of new medical techniques and technologies, a high number of students and a lack of resources for training affect the quality of medical education and the acquisition of surgical skills. In some cases, the students have to learn skills just by watching others perform these activities, as shown in Fig. 1.

Fig. 1 Surgical training on cadaver at Escuela de Medicina y Ciencias de la Salud, Tecnológico de Monterrey

This represents an opportunity area for the development of technological tools that improve current learning and training methods, in particular for those considering virtual reality and computational simulations.

In order to develop this work, it was required to get in close contact with the surgical and medical environment to learn and understand the requirements of the area and the users. To get this knowledge, the author of this dissertation participated in multiple interactions with the training center at the Escuela de Medicina y Ciencias de la Salud, Tecnológico de Monterrey, the Centro de Tecnologia da Informação Renato Archer (CTI) and the Facultade de Ciências Médicas, UNICAMP.

Months of interactions with surgeons, medical students, hospitals, training centers, radiologist, medical image experts and developers, and centers for medical image acquisition were required to understand their language, how the healthcare system works and how can this project contribute to the development of knowledge, tools and skills.

It is highly recommended to keep the interaction between engineering professionals and medical area experts since the key to develop new technology and tools for this area relies in understanding their day-to-day issues and necessities.

1.1.1 Training Methods for Laparoscopic Surgery

The first laparoscopic cholecystectomy was performed in 1990 in the United States by McKernan and Saye. Since then, laparoscopic surgery has become one the most popular kinds of minimally invasive techniques used in surgery today.

Laparoscopic surgery requires insufflating the abdominal cavity with CO_2 to create an open workspace inside the patient. Then, a video camera, lighting, and specialized instruments are inserted through small incisions on the abdominal wall. The surgeon is only guided by video images provided by the inserted camera.

The main challenges of the laparoscopic surgery are the following (Kremer et al. 2001, Soper et al. 2009):

(1) Visualization:
The surgeon cannot directly see the operating site and must rely on a 2D video image in a monitor. This causes problems of spatial orientation due to the lack of depth perception.

(2) Motion Range:
Since the instruments and the camera are introduced through small holes into a narrow space, their movements are restricted.

(3) Limited Feedback:
Surgeons have reduced visual and haptic feedback during these interventions and cannot rely on traditional hand-eye coordination.

(4) Learning Curve:
Skills development in laparoscopy procedures takes more practice compared to traditional surgical procedures.

Given the proven benefits of this minimally invasive technique, the use of laparoscopic surgery has rapidly increased around the world, bringing an associated need to train an increasing number of surgeons with a set of demanding skills. The training methods for laparoscopic surgery include the following:

- Training on patients
- Training on cadavers
- Training on animals
- Box trainer
- Virtual reality simulator

The first three methods are considerably limited. Training on patients, it is required to have strong skills and knowledge, and it is only allowed for experienced surgeons due to inherent risk.

Training on cadavers has a lot of legal and ethical implications, and not all medical schools have access to this method, requiring special infrastructure to be able to maintain this service (Vázquez, 2013, Secretaría de Salud, 2014, Secretaría de Salud (B), 2014).

Training on animals is also controversial, this method involves several ethical and legal implications as well, and with limited access to anatomical properties of real human surgery. (Dirección General de Normas, 2001, SENASICA, 2012, SENASICA (B), 2012).

Fig. 2 Surgical training methods at Escuela de Medicina y Ciencias de la Salud, Tecnológico de Monterrey

It is important to consider that despite representing the human body anatomically, they do not fully reproduce the conditions present in the operating room, compared with the implications they present. Based on this, Box trainers and Virtual reality simulators are both great options to allow the development of skills and training in a low-risk and academic environment, as shown in Fig. 2. In the next points, these two methods are going to be described better.

1.1.2 Box trainer

This method is basic and accessible, but it does not intend to reproduce the real surgery. The abdominal cavity is represented by a box. Manipulation of real instruments to practice with several objects is monitored through an internal video camera, as shown in Fig. 3.

Fig. 3 Use of a Box trainer in the Escuela de Medicina y Ciencias de la Salud, Tecnológico de Monterrey

In order to develop skills, the trainee has to perform certain activities inside the box using real-life instruments, being inserted into similar ports than would be in surgery.

They have a couple of additaments that ask for them to perform certain tasks that are designed to represent movements that would be required during surgery, like grabbing objects, pulling an elastic band (representing a tissue) or even to peel off a grape.

These tasks are only for academic purposes, and the idea is to develop hand skills without any risk. It is relatively easy to assemble and inexpensive, as shown in Fig. 4 (even some provided as a free offer from corporates that develop surgical devices).

Fig. 4 Surgical training methods at Escuela de Medicina y Ciencias de la Salud

1.1.3 Virtual reality for training

This method can reproduce surgery-like scenarios with a considerable level of fidelity and allows the user for repetitive practice in an environment free of risk and implications, by using technological tools and virtual reality.

Likewise, this method allows for establishing performance feedback tools and helps to measure progress in learning and the development of skills and abilities (Shetty et al., 2014, Smutny et al, 2019, Palter et al., 2010).

Virtual Reality (VR) is a key technology for planning and training complex activities in a fully controllable, practical, and out-of-danger environment (Smutny et al., 2019).

Additionally, it can help in a wide set of skills ranging from surgical procedures to factory operations (Radhakrishnan et al., 2021).

Lately, VR has been applied to multiple areas in order to improve the way users interact with software. In the industry, VR systems provide support in a wide range of operations such as manufacturing process training. Some examples of the activities that take advantage of the VR in the manufacturing industry are teaching how to work with industrial robots, remote training for assembly steps and maintenance processes to new staff, among others (Radhakrishnan et al., 2021).

In medicine, VR systems find use in surgery planning and training, rehabilitation, and design of medical devices, among many other applications. It can help to acquire skills that require a set of steps or sequences, a high level of hand-eye coordination and have a better spatial perception between objects (Goldenberg et al., 2017, Smutny et al., 2019, Shetty et al., 2014, Radhakrishnan et al., 2021).

The effectiveness of commercial VR simulators as a teaching tool for laparoscopic surgery training (shown in Fig. 5) has been previously validated by several studies. It has been conclusive that high-fidelity simulators facilitate learning among trainees when used under the right conditions (Flores-Villalba et al. 2012, Goldenberg et al., 2017, Hernández-Irizarry et al., 2016, Shetty et al., 2014).

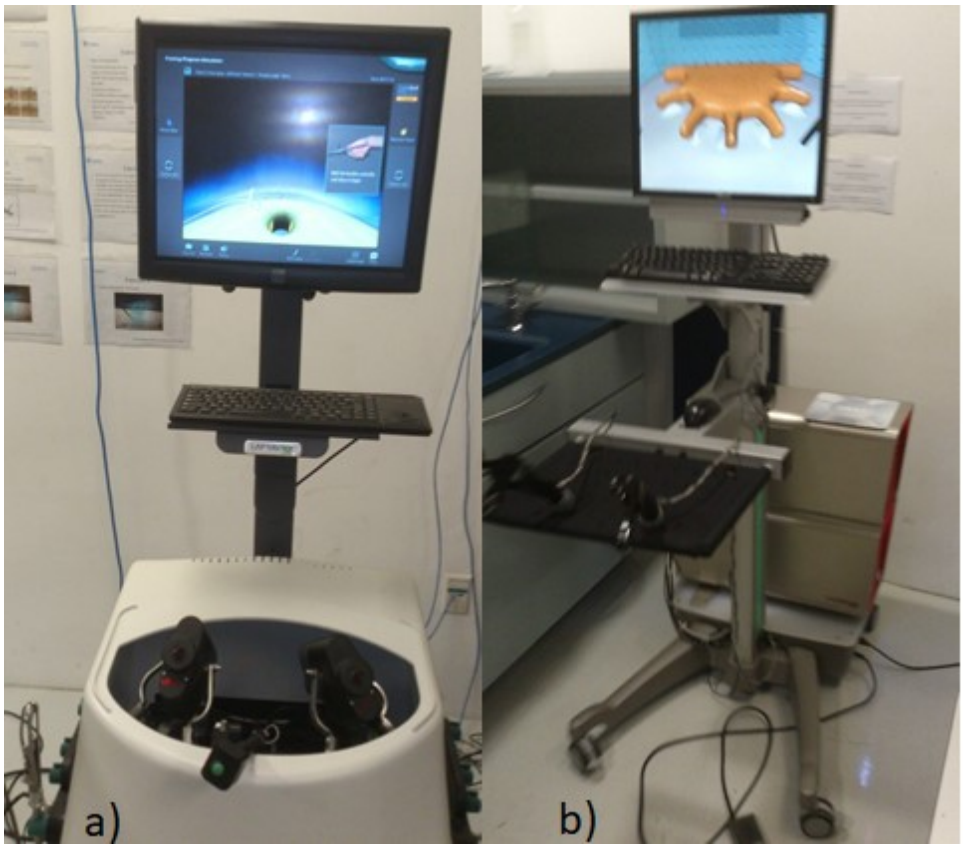

Fig. 5 a) Virtual Simulator Simbionix from J&J, b) Virtual Simulator SymSurgery

However, the cost associated with the establishment and operation of laparoscopic skills laboratories with VR systems can be significant. The work presented here shows an open-source low-cost development of laparoscopic surgery virtual simulator. This approach provides a reduction in cost for this kind of virtual simulator and wider access to this technology.

It has been evaluated and proven that the surgical virtual simulation is a source of cost-effective training by the reduction of the time and materials used for laparoscopic inguinal repairs (Hernández-Irizarry et al., 2016).

As a learning tool, one of the most important contributions of virtual surgical simulators is the representation of a real-life surgery with a high degree of fidelity in a controlled environment. These types of experiences support the development of basic skills such as hand-eye coordination, depth perception, complete procedures, and even crisis management (Goldenberg et al., 2017, Nguyen et al., 2020, Serna-Ojeda et al., 2012, Shetty et al., 2014).

It has been proven that the use of laparoscopic surgical simulators improves the training of the surgeons in the early stages of their development and learning (Goldenberg et al., 2017, Hernández-Irizarry et al. 2016, Shetty et al., 2014). Also, the skills learned in the simulation environment are transferred into the operating room performance (Shetty et al., 2014).

From a technological point of view, it is in virtual simulators that an opportunity opens up for the application of knowledge in multiple branches of science and engineering. IT is required the use of mechatronic devices with virtual tools, as well as the computational implementation of methods with strong theoretical bases in mathematical models for characterizing the behavior of materials. This has been widely studied in order to propose solutions to realistically simulate the scenario present in surgical procedures (Mhod et al., 2021, Nguyen et al., 2020, Zhang et al., 2017).

A virtual simulator is made up of three main areas: an input device for instrument emulation, the virtual reality system that performs computational processes, and an output device for graphic feedback.

In this case, the user interaction tool that emulates the instruments is the input device, the virtual reality system is represented by the graphic environment that performs the necessary computational processes and calculations, and the output device is a monitor that provides the user with graphic feedback on the interaction with the system. This architecture is schematically represented in the diagram shown in Fig. 6.

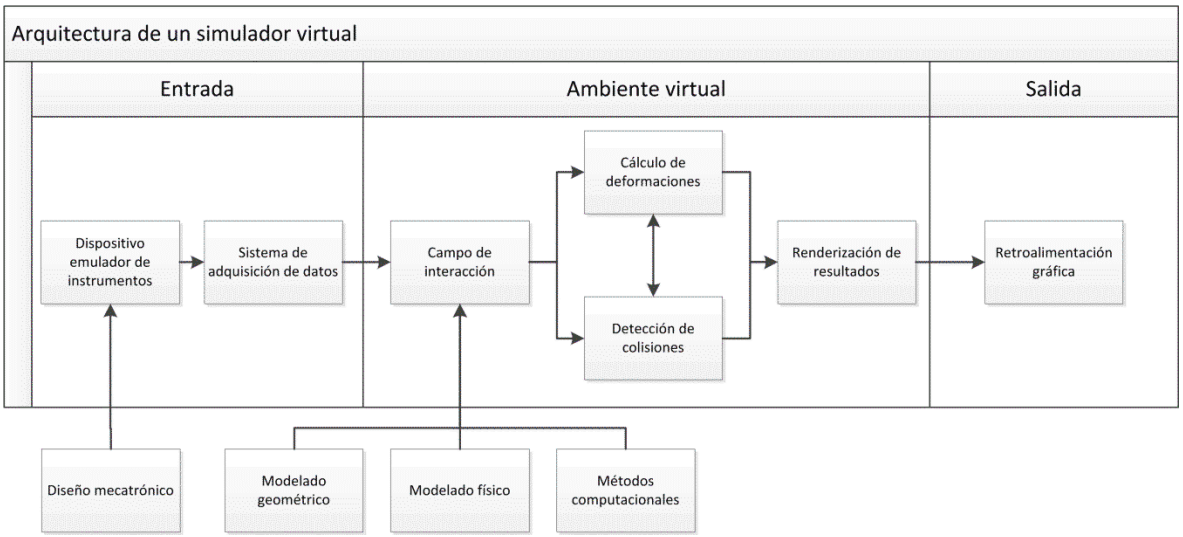

Fig. 6 Product architecture of a Virtual Reality Simulator

The operation of virtual simulators is based on the interaction with the virtual environment through the use of the input device, which generates signals that when acquired by the system can be transformed into the control angles of the virtual instrument (Coles et al., 2011, Guiatni et al., 2013, Herman et al., 2011, Zhang et al., 2018).

Based on this interaction, the virtual environment generates rendered visualizations of objects and anatomical structures and represents the response of the system to the actions that the user performs. This system must be able to show this feedback graphically in real time in the output device and sometimes provide force feedback through the same input device (Guiatni et al., 2013, Nguyen et al., 2020, Zhang et al., 2017, Zhang et al., 2018).

The development of applications for virtual simulators implies the creation of an anatomical graphic environment to represent the interior of the abdominal cavity and the contained organs. The creation of such an environment requires anatomically realistic geometric models, computational methods that perform calculations in real time and mathematical models that characterize the behavior and properties of tissues deformation (Nguyen et al., 2020, Omar et al., 2022, Zhang et al., 2017, Zhang et al. 2018).

1.2 Problem Statement and Context

There have been multiple approaches for development of technological tools that improve the way surgical training is performed by virtual reality and simulations. Some are focused on the computational improvement, others on the interaction's devices as well as the system architecture or clinical applicability (Nguyen, et. al., 2020). Even so, each one of these works is based on different considerations and assumptions, making them really specific for the application they are focusing.

In a first approach carried out as research by the author of this proposal to obtain the degree of Master of Science in Manufacturing Systems with a Major in Design and Innovation of Products, it was possible to develop a framework that allows applications to perform real-time simulations in virtual reality with a focus on laparoscopic surgery procedures.

This development was achieved by integrating computational methods in real time with a simplified model that represents the behavior of the material in a linear way, setting an initial framework to develop applications for surgical simulation but leaving opportunity areas identified during this process for future works.

At the end of the development of this first approach, there were identified two main improvement paths remaining.

(1) Geometrical modeling:

The procedure to obtain anatomically realistic 3D models was done using InVesalius, an Open-Source software that allows the processing of medical images. In this initial approach, anatomical geometries of the liver and gallbladder were manually segmented from a particular case using medical images.

These geometries were used to create the simulation, but it was limited to reproduce only these geometries. If a different case was required to be simulated, the methodology proposed to get the 3D model had to be performed again and again, limiting the applicability of this first approach.

(2) Material modeling:

The material model applied in the original approach, was based on a simplified model that represented the behavior of the tissue as linear. It allowed the calibration of the constants and control parameters in order to do a “tunning” of the simulation to represent how it would look like in real life, but without any basis on the physical and mechanical properties of the tissue that was wanted to be simulated.

This calibration process was performed manually and if the geometry used to simulate changed, this process must be run again, relying on the subjective perception of the running the calibration process to define if the simulation resembles the reality.

In this doctoral research and dissertation, solutions to these problems are being explored in order to improve previous works. It is expected to contribute to different knowledge areas by the creation of a methodology and tools that:

Allows the creation of any anatomically realistic 3D model using medical images, without performing a manual process. This is in order to increase the applicability of the developed framework.

A material model that considers the mechanical properties of soft tissues and therefore it could be calibrated using experimental data of physical tests. By doing this, it will improve the accuracy of the simulation and correlate to the real behavior of the material, increasing its applicability.

1.3 Research Questions

Considering the identified problems, several questions were raised that are within the goals of this research:

(1) How can SMM be used to predict the mechanical behavior of soft tissues, if it is based on the linear elasticity theory?

(2) How can We create a mathematical model that represents material properties like non-linearity, hyperelasticity, anisotropy and softening with a real-time response?

(3) How could this model be applied to any anatomical geometry for simulation of their mechanical properties?

(4) Is it possible to define a process to create a 3D mesh from 2D images by just selecting it?

1.4 Solution Overview

For this project, the solution is going to be based on a holistic approach. Two main areas are going to be explored in order to solve the problem statements and answer the research questions described before.

The solution proposals in order to improve the real-time simulation of mechanical properties in virtual reality are explained below.

(1) Geometrical modeling:

The current VR engine could be enhanced by considering a module for visualization, interaction, and segmentation of medical images to create 3D models, that can be used for simulation purposes.

This is based on the idea that there could be created an interactive segmentation method for medical images. This tool should allow the user to create geometrical meshes compatible with the simulation framework to apply a mathematical model for deformation.

In order to achieve the desired solution, it is expected to develop and implement semi-automatic algorithms for interactive image processing to create 3D models. This will allow to import new cases for interactive visualization and segmentation

of anatomical structure from medical images that any student or researcher is working with

(2) Material modeling:

To develop a material model that can be used to characterize the physical properties of soft tissues and allows real-time simulation.

This is based on the idea that it is possible to find a methodology to enhance the SMM in order to predict the mechanical behavior of abdominal organs. It is believed that by using a constitutive model that characterizes the mechanical behavior of soft tissue, could be possible to create a hybrid formulation with the SMM and keep the time response required for real-time simulation.

In order to achieve this proposed solution, the hybrid model should consider two phases, a precomputed mathematical model that consider the mechanical properties of soft tissue based on experimental data to find an equivalent stiffness parameter that takes the SMM to the same behavior for each deformation level.

That describes the creation of a formulation that allows calculations to be used by the virtual reality simulation. An experimental phase for mechanical characterization will be required in order to get data from soft tissue behavior that represent accurately the physical properties of the material.

1.5 Expected contributions

This research aims to define a modeling methodology capable of characterizing the mechanical behavior of soft tissue in real-time simulations, applied to virtual reality training of laparoscopic surgery.

The general objective is to define a methodology and tools for real-time simulation that represent the anatomical geometry and mechanical properties of soft tissue using an accurate material model.

In order to achieve this research project goal, a set of specific objectives were established:

(1) Define tools to interact and create anatomically realistic geometrical models of the internal organs based on medical images.

(2) Allow the creation of customized meshes that can be used in the implementation of a material model to be applied for simulation.

(3) Define a hybrid mathematical model that can be implemented for real-time simulation.

(4) Perform experimental tests for characterization of mechanical properties of soft tissue.

(5) Calibrate the hybrid mathematical model proposed to predict soft tissue behavior using experimental data.

(6) Apply the proposed hybrid mathematical model that predicts the mechanical properties of soft tissue on anatomically realistic geometrical models to perform simulations.

1.6 Dissertation Organization

This dissertation is distributed in 8 chapters, including this introduction. During the next chapters, the process in which the proposed solution and contributions were conceived, developed, and implemented is going to be explained in detail, as well as their results and conclusions will be presented.

- Chapter 2 Background: In this chapter, previous development on this area is presented in order to explain the context and starting point of this research project. It includes the discussion of opportunity areas identified in previous works that are proposed to be addressed in this project. State-of-the-art of material modeling is presented, as well as mechanical characterization and experimental procedure.

- Chapter 3 Methodology: The process followed for Geometrical and Material modeling is exposed in this section. It contains a brief description of the activities that were proposed, the scope, materials and resources required to develop this work as well as the expected results of this project.

- Chapter 4 Interactive Segmentation for Geometrical Modeling: In this chapter, all the development and results achieved for the improvement of the geometrical modeling process are exposed. It is presented the *VISUALIX* module, developed in this research project for interactive processing of medical images. A proposal for fractal structure analysis using microtomography images is done, presenting *FractalCells* module.

- Chapter 5 Material Modeling of Mechanical Properties: The core of the research project is described in this section. The main issue of modeling and characterization of soft tissues in real-time is aborded in detail, resulting in the proposal of a new hybrid model that considers the non-linear, anisotropic behavior at large deformation for extension and softening by including Mullin's effect.

- Chapter 6 Experimental Testing for Mechanical Characterization: Detailed description of the experimental phase of the research project, performing uniaxial and biaxial cyclical tensile tests in porcine tissue samples of liver and abdominal

wall. Results are exposed in this chapter and are used for characterization and modeling with the proposed EESM formulation.

- Chapter 7 Material Modeling Final Results: This chapter presents an analysis of the characterization and predictions obtained with the EESM formulation. It also includes a comparison with a simple SMM prediction and experimental data to validate this model. Results show a smaller error range than using SMM for extension and without comparison for softening properties, since no work in the literature was found to represent the Mullin's effect with a formulation of the SMM.

- Chapter 8 Conclusions & Future Works: A brief summary of the main contributions to the geometrical and material modeling areas is presented. In this section, it is included the general conclusions about the results of this research project as well as opportunities for future work in different branches.

- Appendix A Acronyms & Repositories: The list of acronyms used in this work is included, as well as the list of online repositories where the script and codes developed in this project can be downloaded.

- Appendix B Volumetric formulation using Finite Element Method (FEM): Description of the preliminary work performed on the volumetric formulation of the EESM.

- Appendix C Flow diagrams for simulation framework: In this appendix are contained flow diagrams that explain the simulation framework. This was used as a reference for the development of the proposals included in this dissertation.

Chapter 2

Background

In order to achieve the proposed goals by this project, it is required to have a proper background on several topics, since this involves not only the development of a virtual reality tool and the creation of a hybrid mathematical model but also the experimental mechanical characterization of soft tissues.

In this chapter, background information will be presented in order to explain how this project was developed in the different main areas. All these areas were explored during this research in order to achieve desired results and each one is a massive and exciting field that could be explored independently in future works and articles, but now it will be limited only to the scope for development of this project.

2.1 Related Work

One of the key elements in real-time surgery simulation is the soft tissue mathematical model used to predict material behavior. This model is used to calculate the response of the simulation mesh used to graphically represent the interaction between surgical instruments and the abdominal organs.

The literature shows a wide range of models for tissue deformation, such as the Spring-Mass Model (SMM) or tensor-mass model (TMM), solved through Finite Differences Method (FDM), Finite Element Method (FEM), Boundary Element Method (BEM) among others (Duan et al. 2014, Kot et al. 2015, Nguyen et al. 2020, Omar et al., 2022, Zhang et al. 2017, Zhang et al. 2018).

Most of the works departs from the geometric characteristics that are going to be used in order to calculate the deformation of the simulation mesh. Two main approaches have been found, based on one-dimensional elements and volumetric elements.

Some of the related works in the literature proposed with one-dimensional elements, are based on hybrid variations of SMM with different approaches (Nguyen et al. 2020, Omar et al., 2022, Zhang et al., 2017), on force distribution in a loop (Waters et al. 2018), considering volume preservation (Duan et al., 2014), multi-constant with a complex mesh (Patete et al., 2013), among others.

For volumetric elements, there can be found other works based on tissue interactions with FEM (Freutel et al., 2014), on reaction-diffusion mechanics (Zhang et al., 2018), using a BEM and FEM (Kim et al., 2013).

In section 2.5 for Material modeling, it is performed a more detailed analysis of what has been proposed in the literature for this application. However, it is important to give a detailed summary of what was done previously on this topic by the author of this dissertation. The next section was included in order to provide a general background of the departure point of this research work.

2.2 Previous works

During the Master's degree of the author of this dissertation, an initial approach was proposed for training using real-time simulation of soft tissue in virtual reality (Moreno-Guerra, 2012). This previous work proposed the creation of an open-source real-time simulation system for laparoscopic surgery training.

The elements required to perform a laparoscopic surgery simulation system included: a) medical knowledge, b) surgical instrument emulation, c) VR environment engine, d) tissue deformation models, and d) simulation display and feedback.

All elements of this open-source simulation system were done in parallel developments by multiple works. This effort resulted in the creation of a prototype for a low-cost VR laparoscopic surgery simulator, shown in Fig. 7 (Moreno-Guerra et al., 2012).

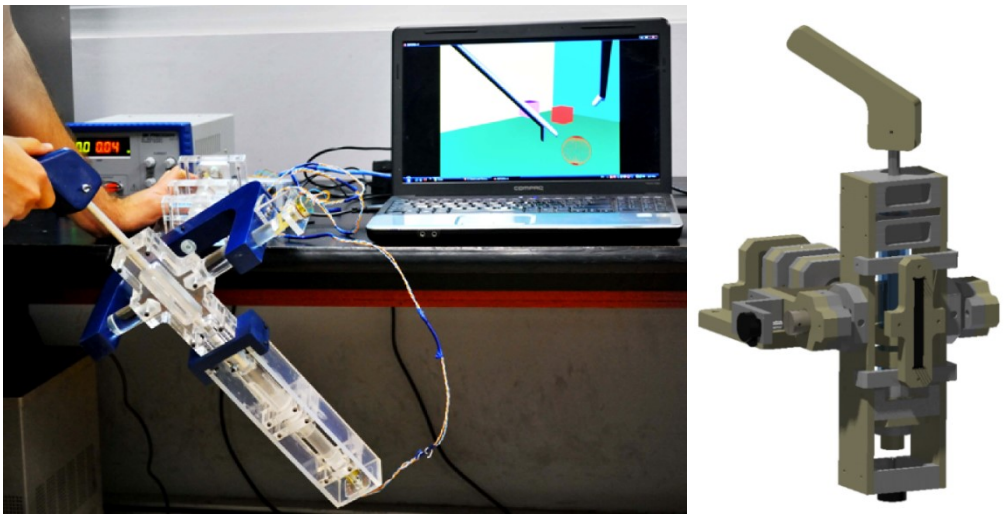

Fig. 7 Laparoscopic surgery instrument emulator interacting with the VR environment.

Fig. 8 shows the architecture of the proposed system. The contribution of the author of this dissertation was mainly focused on the VR environment engine and was presented as a partial requirement to get the Master's degree at Tecnológico de Monterrey (Moreno-Guerra, 2012).

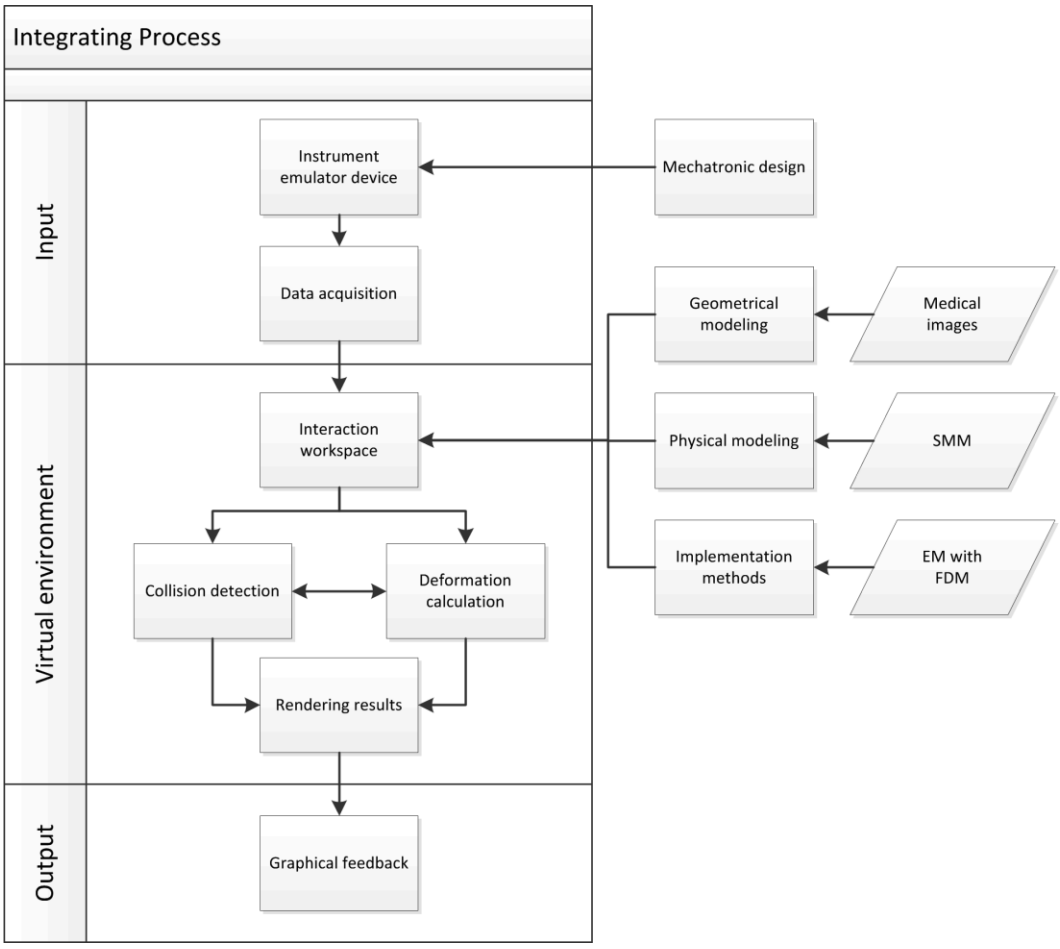

Fig. 8 VR system architecture.

A detailed description of the VR environment engine is presented in this section (2.2 Previous Works) as the background of this research project. Also, a compendium of details and information about the application developed can be found in Appendix C.

These are included since are considered to be relevant for awareness of the foundations for the methodology and developments presented in this dissertation. Everything outside section 2.2 and Appendix C are the results of the research project performed by the author during PhD program at Tecnológico de Monterrey.

The main focus of the previous work was to develop a VR framework for the simulation of laparoscopic surgical training. This system was created with an open-source approach in order to facilitate access to this training technology and to create a community of open-source developments that further enrich the initial system.

The open-source tools used in this research include *Python* programming language, *Visualization Toolkit* (VTK) library, *InVesalius* software for medical image processing, and *MeshLab* for organ model processing.

Master's degree contribution was the first approach that allowed basic interactions based on a simple material model that will be described in the next pages. The use of a simplified material model was identified as the main opportunity for future works, and this is the main objective of the research project performed for this Doctoral dissertation.

2.2.1 3D model and mesh creation

The anatomically realistic organs are based on complex surfaces, whose acquisition and processing are important issues in the surgery simulation. In order to represent the real anatomy of the human body and organs, the geometrical models were acquired through InVesalius, a free access software developed by the Centro de Tecnologia da Informação Renato Archer (CTI) in Brazil.

The InVesalius software (Martins et al. 2008) includes several tools for visualization, segmentation and processing of medical images. Some of the medical imaging techniques that can be processed with this software are Magnetic Resonance Imaging (MRI) and Computerized Tomography (CT), stored through Digital Imaging and Communication in Medicine (DICOM) standard file format.

These image techniques are considered as the main source of volumetric data on human anatomy and multiples approaches can be found in the literature to process this information (Abdallah et al., 2015, Bennai et al., 2020, Fajar et al., 2020, Tan et al., 2019, Wen et al., 2021).

These DICOM files are processed with InVesalius for segmentation, 3D reconstruction, and mesh generation (in STL format) of the desired geometry by using the marching cubes algorithm to generate triangular polygonal meshes (Moraes et al. 2011). Then, additional graphics tools can be used to process these models.

As an illustration, an example from CTI's database is processed. A CT file composed by 242 slices with a 0.7099 mm x 0.7099 mm x 2 mm spacing was selected for this application, from which the liver and gallbladder geometry were segmented and exported in STL format, providing an anatomically realistic geometric model, as shown in Fig. 9.

Using this process, the liver and gallbladder geometry were acquired. The STL triangular mesh obtained directly from InVesalius has several irregularities caused by the segmentation process and the image resolution.

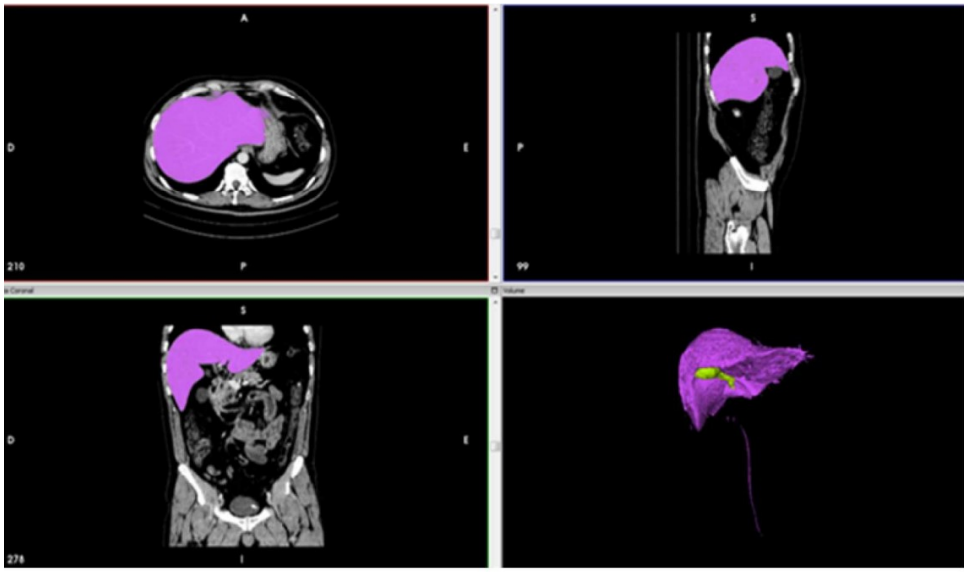

Fig. 9 Liver and gallbladder segmentation process from medical images through InVesalius software 370x217mm (96 x 96 DPI)

From InVesalius, the surface when exported had a rough finish with a large number of faces as shown in Fig. 10a (liver: 156788 vertex / 315213 faces, gallbladder: 8235 vertex / 16493 faces), meaning a high computational cost for a real-time interactive simulation.

A simplified mesh is required in order to achieve a better interactive response by lowering the amount of data calculated by the simulation model (Nguyen et al. 2020, Omar et al., 2022, Zhang et al. 2008). The open-source software *MeshLab* (Cignoni et al. 2008) can be useful in order to improve mesh quality or any other topological issue found.

Different procedures were applied in order to improve the mesh quality. Table *1* shows the recommended methods and parameters in order to process segmented 3D models. The aim is to have a realistic model with a small number of vertexes and faces in order to facilitate real-time processing (Moreno-Guerra, 2012).

The degree of distortion generated by the model processing was monitored with the Hausdorff distance method (Aspert et al. 2002). The original mesh surface was reconstructed for noise reduction without rearranging the vertexes as shown in Fig. 10b and then softened to achieve an improved mesh as shown in Fig. 10c. However, at this point the models have an excessive number of vertexes.

A simplification method was applied in order to lower the number of vertexes. However, the appearance was too rough as shown in Fig. 10d. Then visual filters for softening were applied directly in VTK (such as iterative softening and Gouraud shading). After this process, a mask shaded and rendered based on the rough mesh was used for interaction, as shown in Fig. 10e. Visualization and interaction with the user are based on the model in Fig. 10e. However, the deformation calculations are based on the model in Fig. 10d.

The parameters and results from this process are shown in Table *1*, in this case the Hausdorff Distance was used to validate that the higher geometrical change on the messes by applying this process is less than 1 mm.

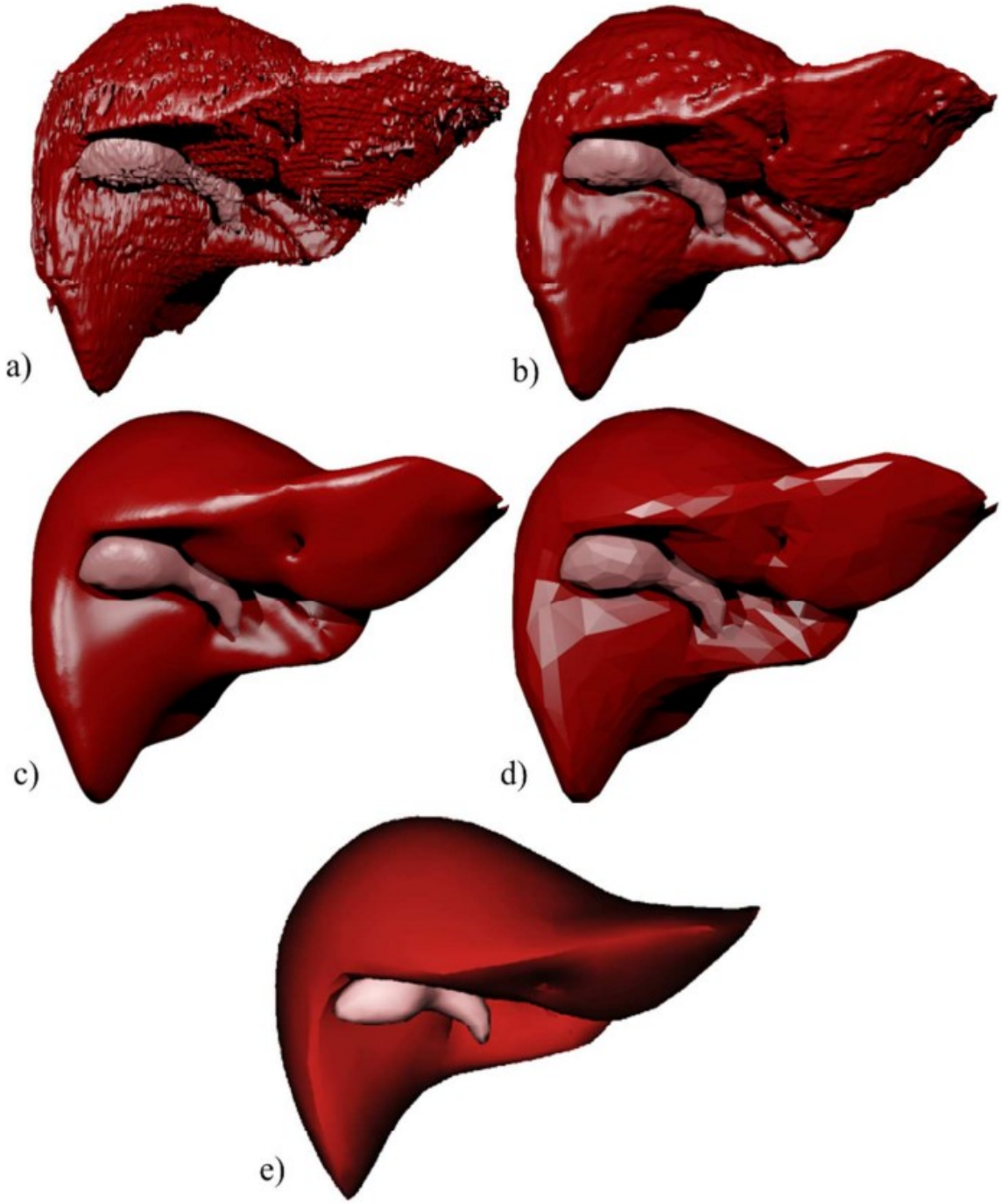

Fig. 10 Stages of geometric model processing: a) Original mesh; b) Reconstructed surface; c) Smooth and regular surface; d) Simplified mesh; e) Final shaded mesh for visualization (Moreno-Guerra, 2012).

Table 1 Mesh processing parameters

Procedure	Method		Mesh Features after Processing		Mean Node Displacement (Hausdorff Distance)
	Type	Parameters	Vertexes	Faces	
Surface Reconstruction (Fig. 10b)	Poisson surface reconstruction	Octree depth: 8 Solver divide: 8 Samples per node: 3	Liver: 122,230 Gallbladder: 7,921	Liver: 244,456 Gallbladder: 15,830	0.207 mm 0.202 mm
Surface Softening (Fig. 10c)	Taubin smoothing algorithm	Lambda: 1 Mu: 2 Smoothing steps: 20 iterations for liver & 1 iterations for gallbladder	Liver: 122,223 Gallbladder: 7,921	Liver: 244,460 Gallbladder: 15,830	0.599 mm 0.399 mm
Surface Simplification (Fig. 10d)	Quadric edge collapse decimation algorithm	Preserve topology, Quality threshold: 0.3	Liver: 626 Gallbladder: 154	Liver: 1,254 Gallbladder: 296	0.681 mm 0.435 mm

As discussed before, this process allows to create a mesh for simulation and interaction, but is a limited approach, since the user will only have access to this segmented mesh. In order to create new content or simulate other patients or geometries, new research will have to be performed to manually create the mesh that the user is going to simulate.

2.2.2 Tissue Deformation Model

One of the challenges in the surgery simulation is the balance between surgery's reality and the visual interaction feedback. With a significant time, the delay between the user actions and the graphical response, the whole VR system loses the reality experience.

Therefore, the selection of the proper real-time algorithm for tissue deformation is a critical issue for creating an effective VR environment in laparoscopic surgery simulation. This was true during the development of the previous work, and it is still valid currently according to the literature (Nguyen, 2020, Omar et al., 2022, Zhang et al., 2017).

With this in mind, a hybrid method based on the SMM with a skeleton structure was proposed and implemented to represent the deformation and material behavior of the organ tissue (Moreno-Guerra, 2012). This was performed for the specific case of a mesh from a liver and a gallbladder obtained as described before.

In the SMM an object is modeled as a set of mass points interconnected by springs with known elastic properties. With this discretization concept, an object can be represented by a mesh where the vertexes are the localized masses and the edges of the faces are the springs that allow and limit their displacement, as shown in Fig. 11.

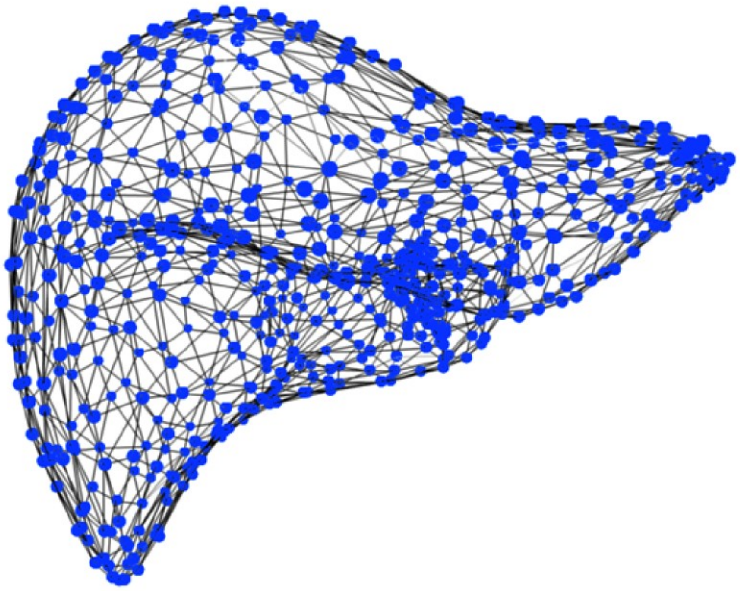

Fig. 11 Liver surface mesh

The triangular mesh resulting from the preprocessing only represents the surface of an anatomically realistic organ. In order to include the internal behavior of the organ in the model calculation, an internal organ skeleton structure has to be defined. This structure is formed by an offset mesh of control points created from the simplification of the organ surface.

The offset proportion is calculated using the quadric edge collapse decimation and the Poisson Surface Reconstruction (with 2:1 offset) and correlated to the center of the geometry, as shown in Fig. 12. This internal organ skeleton is used to calculate the internal propagation of forces and deformation.

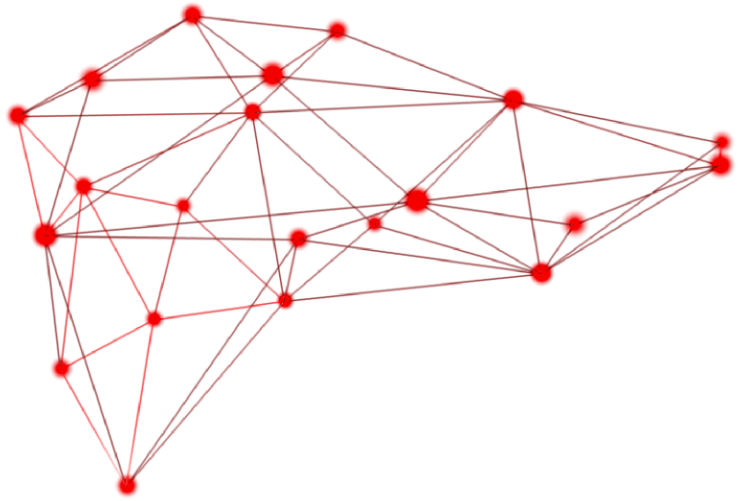

Fig. 12 Internal skeleton for liver model based on offset mesh of control points

Each triangular face of the surface geometry is linked with the nearest vertexes of the offset mesh of control points (internal skeleton) as shown in Fig. 13a, and each triangular face of the mesh of control points is linked with the center of the geometry (Moreno-Guerra, 2012).

The union of the surface mesh and the internal skeleton structure creates a new geometric representation of the organ as shown in Fig. 13b and will be used to apply the deformation model. Each level of this modified organ model has different elastic coefficients in order to obtain a realistic mechanical behavior.

a) 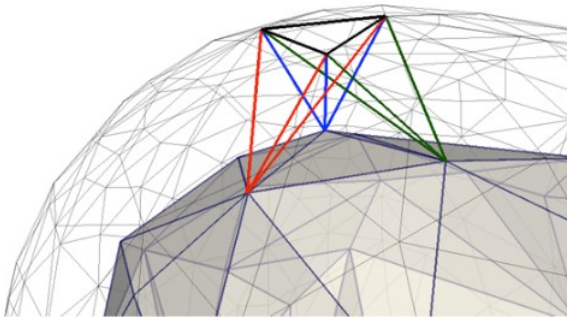 b) 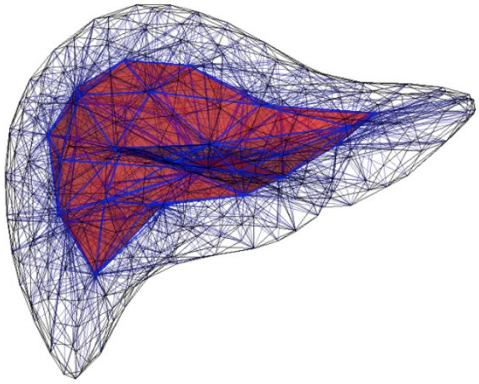

Fig. 13 Modified organ geometric model: a) internal skeleton structure and b) integration of the surface mesh and the skeleton structure.

Now, with the combination of the SMM and the new organ model (consider surface and the internal skeleton structure), it is possible to calculate the elastic restoring force F_i that the displacement of a point P_i applies on a point P_j, considering its connected neighboring points $N(P_i)$ and using the Hooke's law (Moreno-Guerra, 2012, Duan et al. 2014, Kot et al. 2015). Equation (1) summarizes the necessary calculations.

Eq. 1
$$\boldsymbol{F_i} = \sum_{\boldsymbol{j \in N(P_i)}} \boldsymbol{k_{ij}} \left(\left\| \boldsymbol{P_i P_j} \right\| - \boldsymbol{l_{ij}^0} \right) \frac{\boldsymbol{P_i P_j}}{\left\| \boldsymbol{P_i P_j} \right\|}$$

Where k_{ij} is the stiffness coefficient of the spring that connects the point P_i and P_j , and l_{ij}^0 is the original length of the spring in its rest position. By knowing the force applied to the point P_j caused by the displacement of the point P_i, it is possible to calculate the displacement of the point P_j using a second-order differential equation based on Newton's motion law, as indicated in Equation (2).

Eq. 2
$$\boldsymbol{m_j} \frac{\boldsymbol{d^2 u}}{\boldsymbol{dt^2}} + \boldsymbol{d_j} \frac{\boldsymbol{du}}{\boldsymbol{dt}} + \boldsymbol{k_{ij} u} = \boldsymbol{Fi}$$

where m_j is the mass of the point P_j, d_j is a damping coefficient and k_{ij} is the stiffness coefficient of the spring.

The numerical method implemented to solve the system's equation was Euler's method (EM) with a central finite difference (CFD). The calibration parameters were defined based on the following testing.

The model was tested for deformation defining a set of fixed vertexes as constraints, applying gravity force and user interaction as shown in Fig. 14a and Fig. 14b. Also, a color level visualization was defined for deformation illustration, based on the distance of each vertex to the center of the mesh at its actual position compared with the distance to the center at the reference (rest) position.

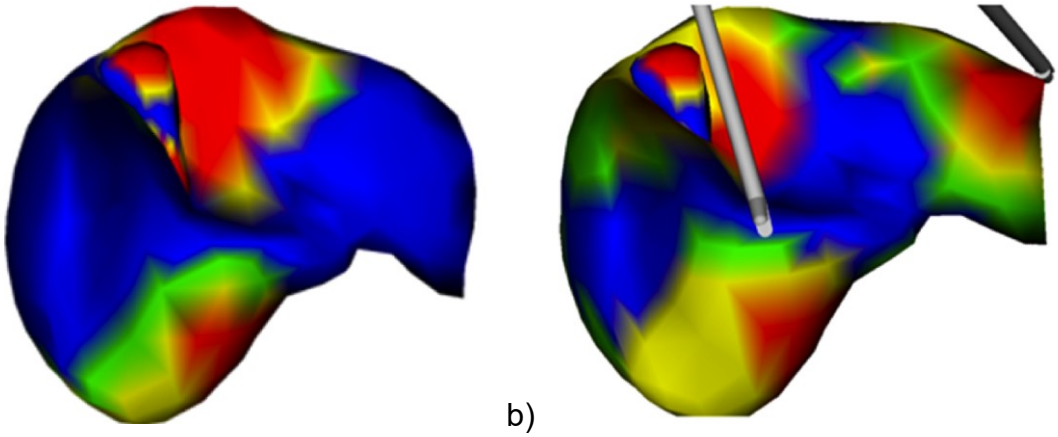

a) b)

Fig. 14 Tissue deformation: a) liver and gallbladder mesh under deformation by gravity force and b) liver and gallbladder mesh under deformation by the user's interaction

2.2.3 Collision Detection

A collision detection method was implemented in order to represent the deformation caused by the collision of the simulated surgical instruments with the simulated organ. The implemented method is based on the collision sphere tree approach. In this case, the mesh space is partitioned in segments.

Then a k-dimensional tree (KD-Tree) data structure is used to make proximity queries. The nearest vertex to the center of each segment is stored as a collision control point and used as the center of a collision sphere. Then, all the vertexes inside the sphere's diameter are considered as its collision subdomain (Banihani, 2009, Moreno-Guerra, 2012, Banihani et al., 2013). Fig. 15 shows a representation of this method applied to the liver (a) and surgical instrument (b) models.

This hierarchical method improves the collision detection speed by limiting the collision search only to the collision spheres. Once an object of interest is inside a particular collision sphere, the search is focused only on the vertexes in the subdomain of that collision sphere.

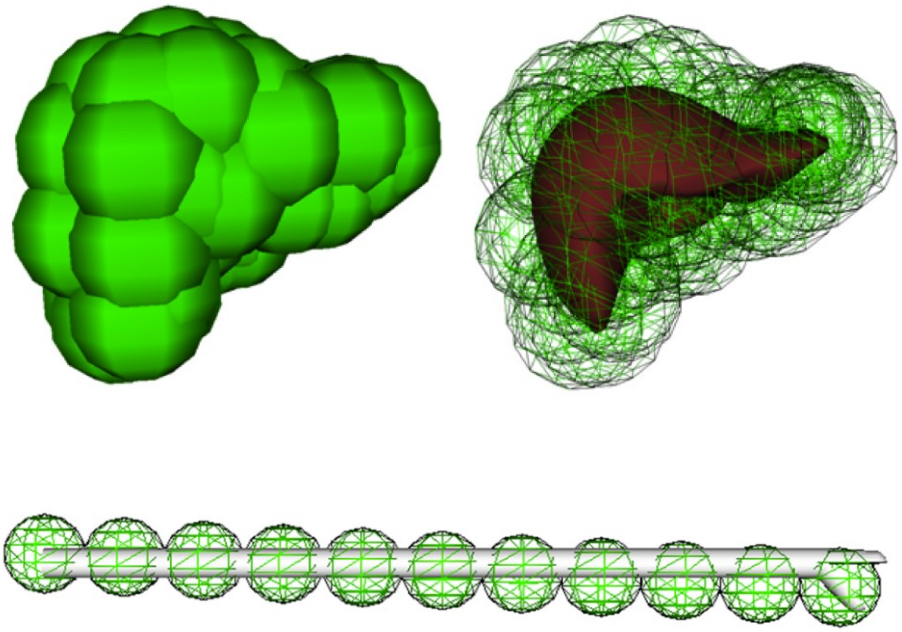

a)

b)

Fig. 15 a) The collision sphere's tree of the liver model, b) The instrument with the collision sphere's tree method applied.

When a collision control point of the surgical instrument of interest is inside a collision sphere, a set of preventive collision points is defined around it as shown in Fig. 16. Then a query starts to find the vertexes inside that subdomain that could be involved in a face collision.

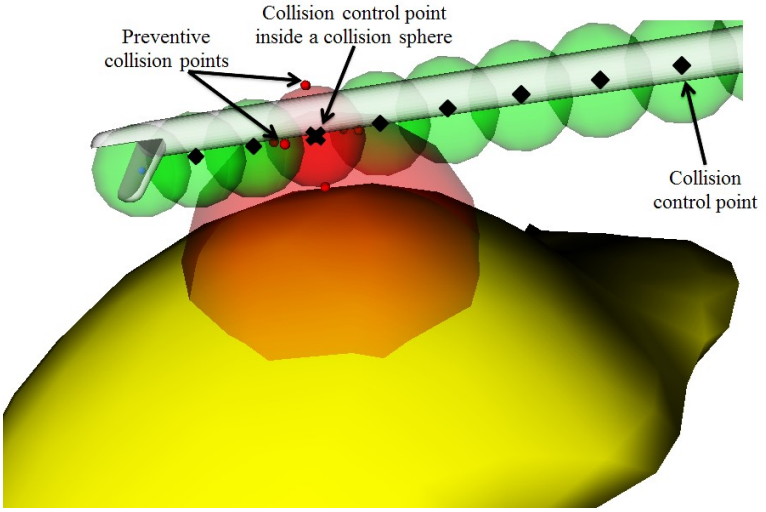

Fig. 16 Illustration of the collision detection process.

The faces that include those vertexes are used for a simple volumetric measurement with each of the preventive collision points, in order to know if a preventive collision point already has passed through its surface. This method is better illustrated in Fig. 17.

This volumetric measurement determines if a preventive collision point is at the same side (negative volume) or at the opposite side (positive volume) regarding the direction of the face normal vector. If a preventive collision point is at the opposite side of a face normal vector, it means that this point has passed through this face and is inside of the organ's mesh.

Therefore the collision control point is nearly intersecting that face, detecting a collision and showing a deformation when this happens. This method was implemented and tested with the liver and gallbladder models.

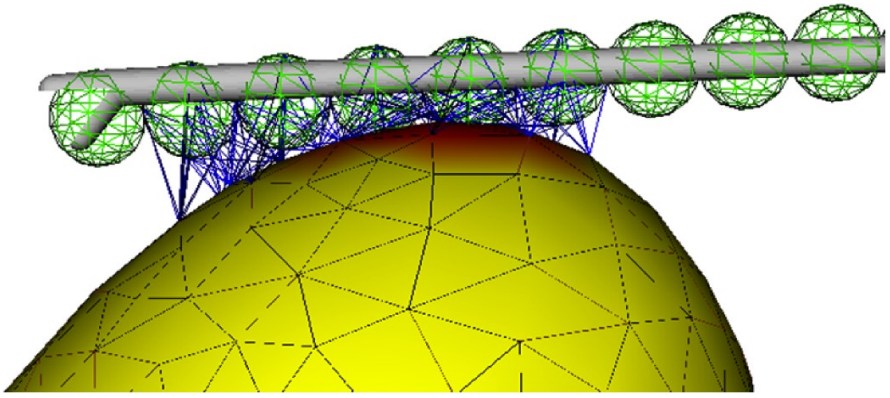

Fig. 17 Graphical description of the collision detection method for the liver and the instrument (the colliding faces are shown in red).

2.2.4 VR Environment Engine

The VR environment in the laparoscopic surgery simulator is a component specifically dedicated to creating the interaction between the user and the simulated patient. This environment has the function to simulate the real surgery conditions and lets the user interact with simulated human organs in order to improve skills and acquire specific knowledge.

First, the training methods and real surgical procedures were reviewed in order to specify the simulator's functional requirements, defining the following kinds of applications:

Basic laparoscopy skills. In this kind of application, the task objectives are limited to improving basic hand-eye coordination skills, such as camera navigation and object manipulation applications. Basic skills are developed in a non-anatomical environment, as shown in Fig. 18.

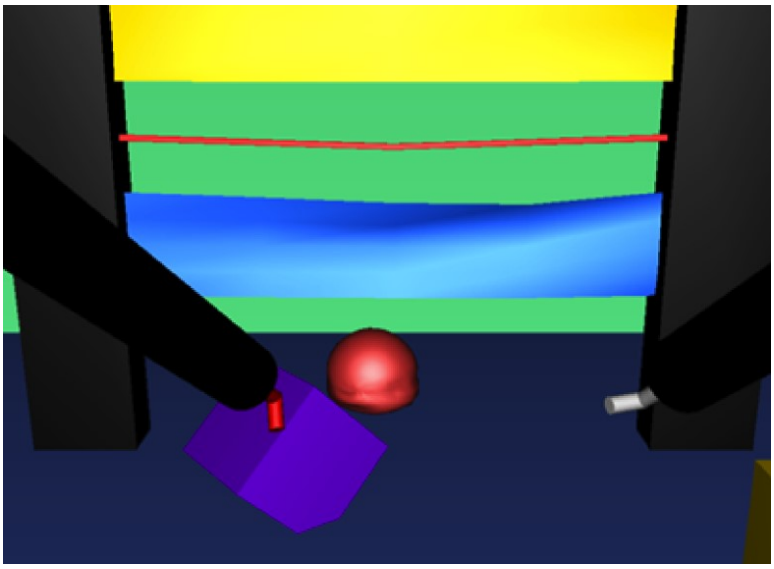

Fig. 18 Application for basic skills with a simple environment in VR system.

Specific laparoscopy procedure skills: In this kind of application, simulation tasks are associated with selected surgical procedures, such as clipping and cutting the cystic duct and artery of the gallbladder in a cholecystectomy (gallbladder removal). Specific procedure skills are developed in an anatomical environment, as shown in Fig. 19.

The development of applications for specific procedure skills implies the creation of an anatomically realistic environment, requiring realistic human organs and models for interaction. The process to represent tissue properties and organs in the anatomically realistic environment are presented next, including the geometric modeling and the deformation model.

As previously mentioned, one of the most challenging issues for the development of VR interactive applications is the graphical feedback required. For this type of surgery simulator, an update rate of 15-20 Hz provides an acceptable perception of an object moving in a scene.

The methods exposed in this work were implemented in *Python* programming language, and different tests were done for the parameters calibration and the validation of the system performance in computational time (on a PC Intel® Core™ i7 2.2 GHz CPU). In the pre-processing phase of the VR environment, the creation of the model with skeleton structure (for liver and gallbladder meshes) was achieved in 445.09 ms and the collision spheres tree was achieved in 228.15 ms.

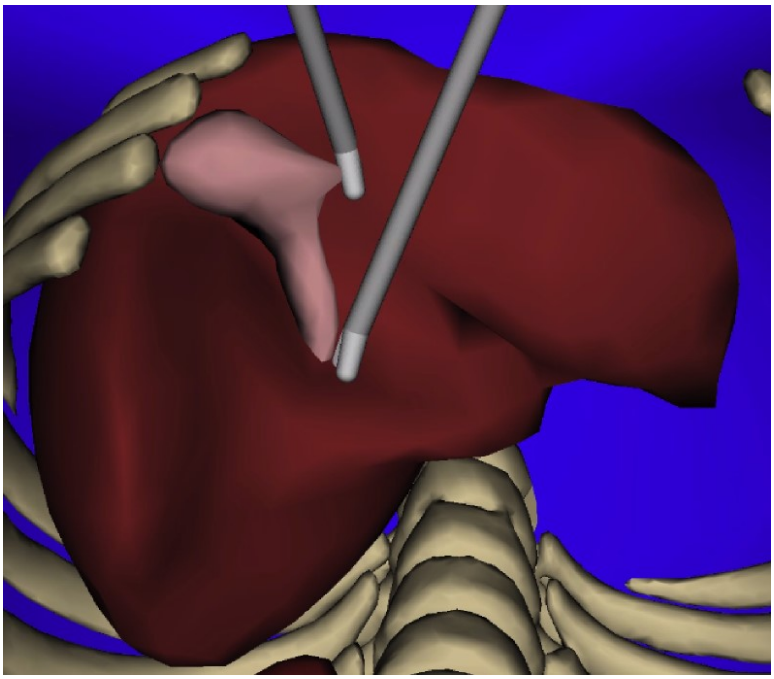

Fig. 19 Application for specific skills with anatomically realistic geometric models.

For the case of the liver and gallbladder simulation shown in Fig. 19, organ deformation was computed in 32.29 ms, and the collision detection was computed in 11.54 ms. The complete cycle time (including the rendering time) was 43.83 - 50.73 ms, achieving an update rate of 19-23 Hz with collision detection and 27-30 Hz for graphical feedback only.

At the current stage of development, the VR simulator shows an adequate level of performance, allowing 25-30 frames per second (FPS) on graphic feedback is acceptable for this kind of application (Goldenberg et al., 2017, Goulette & Chen, 2015, Nguyen et al., 2020). This means that in order to achieve this performance, the computational time should be lower than 40 ms.

It should be considered that for this application, the geometrical and mechanical modeling of the anatomical structures represent a huge challenge and therefore have a high impact on the computational time required to perform this simulation. If a different application was intended, other methods more accurate but with a non-real-time response could be applied.

2.3 Discussion and opportunity areas

During the evaluation of previous works performed during the Master's degree, there were several important opportunity areas that were identified. These were considered to be developed in future works and were part of the proposal for investigation during the Doctoral studies that this dissertation is prepared for.

We can classify the opportunity areas into two main topics.

(1) Geometrical modeling:

As previously mentioned, in the previous approach a methodology was proposed to create 3D models that represent the anatomical structures using open-source software for medical image processing, called *InVesalius*. On an initial approach, geometries were manually segmented from a set of medical images provided by one of the study cases of CTI Renato Archer.

Even when these models were enough for the initial approach to create a simulation framework, it put a constrain on the applicability of the proposed model. In order to change or perform a different simulation, the whole methodology for acquisition and processing of a new anatomical model would have to be performed, including the manual segmentation of medical images. This would require not only time but also experience and skills to perform this procedure.

(2) Material modeling:

The material model applied in the original approach, was based on a simplified model that represented the behavior of the tissue as linear. It allowed the calibration of the constants and control parameters in order to do a “tunning” of the simulation to represent how it would look like in real life, but without any basis on the physical and mechanical properties of the tissue wanted to be simulated.

This calibration process was performed manually and if the geometry used to simulate changed, this process must be run again, relying on the subjective perception of the running the calibration process to define if the simulation resembles the reality.

In the next points, both topics will be described in more detail.

2.4 Geometrical modeling

The initial approach proposed during the Master’s degree only allowed the interaction with a particular geometry that was obtained during the research process. But… What would happen if another geometry would like to be used? The system would have to be manually modified and another research process runs in order to segment manually the geometry of a different organ or subject.

So, it was identified this is a limitation for use in multiple scenarios. Other geometries and particular cases for the study of medical trainees, researchers, and surgeons would not be possible to be simulated.

The proposal in this Doctoral dissertation is to create a module that allows interaction with any medical image in order to allow visualization, interaction and segmentation tools (Fan, & Lee, 2015, Shrivastava et al., 2020). This idea is in order to obtain meshes that could be used not only for simulation, but also for other applications, like 3D printing, Surgical

Planning among other visualization uses (Abdallah et al., 2015, Fajar et al., 2020, Williams et al., 2019).

This would represent a great contribution in order to interact with both systems and allow wider opportunities to apply the material model.

2.5 Material modeling

The efficacy of simulators as training tools is directly related to the development of the virtual environment. In this case, the high-precision computational methods used for the prediction of deformations, and the characterization models of the behavior of the materials used to represent the properties of the tissues, allow the generation of reliable simulations with a high degree of adherence to reality.

That is why within the specific objectives of this research proposal is the search for mathematical models that accurately and computationally represent the behavior of soft tissues. This objective is based on the difficulty of simulating the non-linear mechanical characteristics of soft tissues subjected to large deformations present in surgical procedures, as well as calculating the reaction forces for tactile feedback.

Likewise, it is intended to develop algorithms that allow the implementation of said mathematical models for real-time simulation in virtual reality systems, using computational processes.

As stated before, for the development of the initial approach during the Master's degree, a simplified Spring-Mass Model (SMM) was used to represent the mechanical properties of the organ that was simulated.

This model allowed the calibration of its variables in order to get the desired response based only on subjective evaluation of how it responds versus how it should respond. Also, since it is based on the linear elastic theory it can only represent the behavior of soft tissue at small deformations (<10%) where it behaves linear (Zhang et al., 2017, Zhang et al., 2018), as shown in Fig. 20.

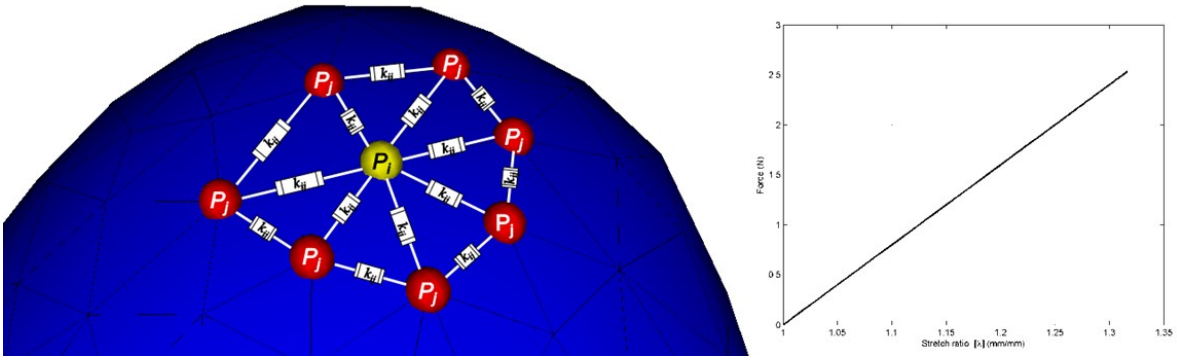

Fig. 20 Behavior of the SMM element implemented for deformation of a mesh

For large deformations (>10%), it is expected that the soft tissue presents a non-linear behavior, and therefore it can not be predicted by a constant of stiffness (Duan et al., 2014, Nguyen et al., 2021, Omar et al., 2022, Zhang et al., 2017, Zhang et al., 2018). It was strongly questioned about how it was possible to bring real material behaviors to these simulations in order to validate their reality.

If the material model used was only a simplified equation with a linear behavior. How could be used to characterize real mechanical properties in order to predict soft tissue behavior?

This matter is considered of high complexity, not only because it involved knowledge in materials mechanics and mathematical modeling for the development of a new model. Also, this new formulation should be able to predict the non-linear anisotropic behavior of soft tissues but be able to run on real-time computing.

The main roadblock for this opportunity area in the research was that in order to implement such a material model, it will imply getting experimental data to validate the model and with this, the proper ethical protocol to collect, prepare and perform mechanical tests on physical tissue samples.

With this in mind, a review of current mathematical models applied to soft tissue simulation is done in the next points, based on one-dimensional and volumetric elements.

2.5.1 Models based on one-dimensional elements

It considers the object as a set of punctual masses, united by means (one-dimensional elastic elements) and dampeners with different constants of elasticity, as conceptualized in Fig. 21. It is generally based on the laws of Hooke and Newton. Different hybrid models have been developed to try to simulate the behavior of soft tissue.

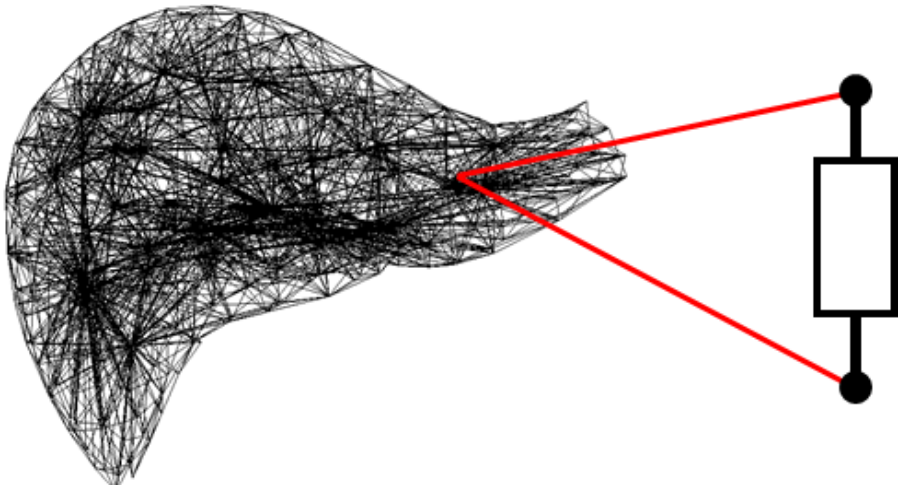

Fig. 21 Concept of material modeling using one-dimensional elements

- Advantages

(1) It constitutes a discrete representation of the object
(2) Easy to implement
(3) Use of a low amount of parameters
(4) Low computational cost

- Disadvantages

(1) They represent, in a limited way, small deformations by means of one-dimensional elastic elements.
(2) It has difficulties validating itself in the three dimensions.
(3) Its constants are difficult to calibrate y in relation to the physical parameters of the material.
(4) Does not consider the volume of the object

- Models using one-dimensional elements:

(1) Multi-constant with complex mesh (Patete et al., 2013).
(2) With force distribution in a loop (Waters et al. 2018).
(3) Coupled with BEM functions (Zhu et al. 2012).
(4) Volume preservation (Duan et al., 2014).
(5) Spring-mass model using Young's modulus and Poisson's ratio (Natsupakpong et al., 2010, Lloyd et al., 2012, Kot et al., 2015, Nikolaev et al., 2013).
(6) Using Guccione and Mooney Rivlin models to calibrate the spring parameters (Mohr et al., 2003) and nonlinear coefficient (Chen et al., 2007).
(7) Using Ogden model to calibrate parameters for a spring cube (San-Vicente et al., 2012).

2.5.2 Models based on volumetric elements

Volumetric elements allow representing the behavior of the soft tissues considering the elasticity by measuring the Lamé-Hooke equations and the Newtonian dynamics, using tensor calculations (tensor-mass model). Models such as St. Venant-Kirchhoff, Fung, Veronda-Westmann, Mooney-Rivlin and Kelvin-Voigt have been used within this classification to generate hybridizations with hyperelastic characteristics. A conceptual representation is shown in Fig. 22.

- Advantages

(1) Allows continuous representation of the object
(2) Do not depend on the geometry of the mesh.
(3) Parameters have physical relation.
(4) It is valid for large deformations.

- Disadvantages

(1) High computational cost (time for processing and calculation)
(2) Requires a high number of parameters
(3) Difficult to implement

- Models using volumetric elements:

(1) Using BEM and FEM (Kim et al., 2013).
(2) Using tissue interactions with FEM (Freutel et al., 2014).
(3) Using reaction-diffusion mechanics (Zhang et al., 2018).
(4) Using a meshfree method with Galerkin (Abdi et al., 2012).
(5) Using point collocation method of finite spheres (Banihani et al., 2013).
(6) Using St Venant-Kirchhoff model for hyperelasticity (Delingette et al., 2008).
(8) Using Spencer and Fung models static (Picinbono et al., 2001) & quasi-static (Delingette et al., 2004), and Viscoelastic (Liu et al., 2011).

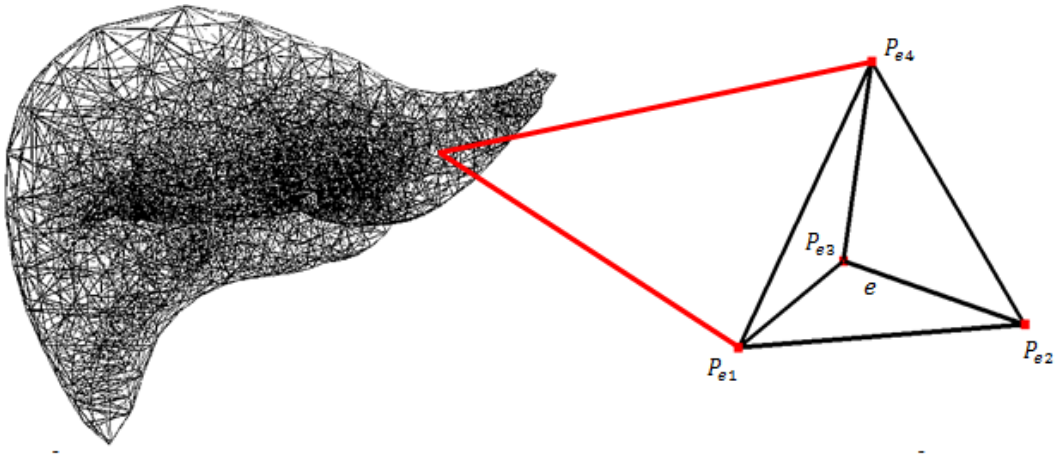

Fig. 22 Concept of material modeling using volumetric elements

2.5.3 Mechanical characterization

One of the biggest challenges in the biological tissue research field is the development of the experimental phase over human patients due to the ethical implications involved in it. This problem is not exempt in the performance of mechanical tests where large tissue samples are required to properly execute the experimentation.

The difficulties that arose in the validation of biomedical research are leading to the necessity of alternatives to test hypotheses and obtain real data to verify the functionality of applications. Among the alternatives, the use of animal models is frequently, given the advantage to recreate the human properties for experimentation in controlled environments.

When working with animal models multiple questions arise, which need to be defined to provide support to the research and justify the experimental phase. It is for this, that is necessary to establish and meet an overview of the experimental process to validate the investigations related to the medical field, particularly those involving the real behavior of tissues.

Some of the investigations contemplated within this approach have among their implementation objectives: a) the study of tissue damage suffered due to car accident injuries, b) understanding and characterization of tissue for behavioral prediction, c) development and validation of medical devices (i.e. prosthesis, aortic valves, stents, virtual reality simulators for medical training, etc.).

The aim of this background is to expose the current scenario in the experimentation process over biological tissue, starting from the selection of the appropriate animal model for the research to the types of tissue most widely used and their applications.

When performing animal experimentation protocols, the selection of the appropriate model for each case of study is a major decision. This is why many factors must be considered at the moment of selecting the animal species, since not only anatomical similarities should be taken into account, but also not all species are suitable for biomedical research.

In general, a suitable animal model for the development of a research must meet certain conditions (Isselhard & Kushe, 1986):

(1) Represent the characteristic that is intended to be measured
(2) To be accessible and common for another research
(3) To have available enough material for getting several samples with the same specimen
(4) To consider the size of the model and infrastructure requirements
(5) To be able to work with and manipulate for the sampling process
(6) To be conserved in proper conditions to warranty the results are not affected
(7) To meet the criteria of the study in which their data is going to be used
(8) To consider the legal and ethical implications of working with such model

The investigator should consider using previous models when feasible, justifying the relevance of them for research purposes.

- Liver

The liver is the largest internal organ and gland in the human body, weighing around 1500 g. The diaphragm separates the liver from the pleura, lung, pericardium, and heart. Except for the lipids, any substance absorbed by the alimentary tract is received first by the liver, besides developing metabolic functions, the liver stores glycogen and secretes bile (Moore et al., 2010).

Depending on the purpose of the research, it is possible to analyze from different perspectives the liver properties through mechanical tests. One arises from its composition, considering that this organ is formed by a capsular tissue overlying the parenchyma and vascular tissue. Hence, in the literature can be found many studies dedicated to experimentation in liver specimens, composite samples either exclusively parenchyma or including the capsular tissue membrane.

Some investigations have opted for developing tests with full organ, in order to consider the combined composition (Ahn & Jung, 2010, Carter et al., 2001, Stingl et al., 2002). These differ from other studies in which sectional samples are taken with cutting and stamping tools from parenchyma and capsule (Brunon et al., 2010, Gao et al., 2010; Kemper et al., 2010, Umale et al., 2013).

Considering the purpose and application of these researches protrude those related with material understanding and characterization for the behavioral prediction (Ahn & Jung, 2010, Carter et al., 2001, Gao et al., 2010, Stingl et al., 2002). These studies are based on the description of the mechanical properties of the tissue by mathematical models, which can be validated with computational simulations such as FEM.

Also, another branch widely investigated for this organ, is related to the study of the damage suffered by car accident injuries (Brunon et al., 2010, Kemper et al., 2010, Umale et al., 2013). This kind of research seeks to establish tolerance parameters related to tissue, which support the development of systems to reduce injuries and traumas in such mishaps.

- Spleen

The spleen is a mobile ovoid lymphoid organ of size, shape, and weight variable. Usually is approximately 12 centimeters long and 7 centimeters in width, which corresponds in proportion to the size and shape of a clenched fist (Moore et al., 2010). It is located in the left upper quadrant, in the region between the stomach and diaphragm. Across the spleen pass the splenic artery, splenic vein, and efferent lymphatic.

The spleen plays important role in regard to red blood cells and the immune system. It removes old red blood cells, holds a reserve of red blood cells (more than a third of the supply of the body) and produces red blood cells during the fetal stage (Tortora & Derrickson, 2009).

Similar to the liver, various contributions have been made to the literature regarding the evaluation of the spleen damage suffered in car accident injuries (Kemper et al., 2012, Stingl et al., 2002, Umale et al., 2013).

In this case, the main objective of this research is to analyze the mechanical properties to establish the critical acceleration with which the spleen can be injured during the accidents, as well as the use of FEM simulations to validate results.

The mathematical characterization of the spleen has been found in the literature less than the liver´s one, but it has been proposed to apply models of 5 viscoelastic elements to describe the tissue (Wang et al., 2013).

As mentioned previously, the principal function of the spleen is related to the lymphatic and circulatory systems, therefore its structural composition is formed largely by vascular

tissue. It is for this that different research chose the development of tests with full organ, since their volume and structure are affected by the loss of blood in the vascular tissue (Umale et al., 2013). Furthermore, it is possible to find studies where mechanical tests are performed on sectioned samples of the organ, regardless of the blood loss (Wang et al., 2013, Kemper et al., 2012, Stingl et al., 2002).

- Kidney

The kidneys are paired, reddish organs located just above the waist, between the peritoneum and the posterior abdominal wall. Usually, an adult kidney is approximately 10-12 centimeters in length, 5-7 centimeters wide, and 4 centimeters thick, weighting from 135 to 150 g. (Tortora & Derrickson, 2009). The main function of the kidneys is to filter blood and remove waste products through urine, which drains through the ureters into the bladder (Moore et al., 2010).

The kidney is composed of a capsule that covers completely the renal cortex, renal medulla, and vascular tissue. Within the literature, the properties of the renal cortex have been analyzed to characterize the behavior of this kind of tissue, performing mechanical tests over renal cortex samples, obtained by removing the renal capsule (Umale et al., 2013, Farshad et al., 1999).

Considering kidneys as one of the organs most affected when a car accident occurs, the renal cortex has been studied in order to understand its mechanical properties and characteristics to trauma, with the purpose of predicting its behavior and resistance through FEM simulations (Umale et al., 2013).

Also, has been seeking to get information about the mechanical response of this material under critical loading conditions using FEM simulations, in order to analyze the mechanisms of traumatic injuries of this organ (Farshad et al., 1999).

2.5.4 Experimental procedure

Since there are multiple approaches about how can be performed mechanical testing and characterization of biological tissue, it is important to analyze and consider the appropriate method to ensure the validity of results.

In the literature, there were found three methods mainly used in research for developing mechanical tests to characterize the behavior of biological tissues. These methods are based on uniaxial testing under stress in tension, compression, or indentation.

The main features of these methods are:

- Tissue sampling process
- Dimensions and geometry of the used samples
- Parameters in the experimental process
- Instrumentation

For this project, the testing method selected was tension testing. This was due to the specifications of testing equipment available and characteristics of the tissues that were relevant to this research.

Normally, samples of biological tissue used in mechanical testing are obtained from animal models postmortem (Brunon et al., 2010, Jones et al, 1995, Kemper et al, 2010, Lally et al., 2004, Rodriguez et al., 2011, Stingl et al., 2002, Umale et al, 2013). The geometry of specimens used for tensile tests is dog bone shaped (Brunon et al., 2010, Kemper et al., 2010, Kemper et al., 2012) or rectangular (Farshad et al., 1999, Ferraresi et al., 1999 , Lally et al., 2004, Umale et al, 2013), both on a wide range of dimensions.

Preservation of the tissue samples is performed by immersion in solutions such as Dlbecco's Modified Eagle Medium (DMEM), antibiotic or saline solutions. The storage temperature varies depending on the purpose of the author's study, which can be between 4 and 6 ° C (Kemper et al, 2010, Kemper et al., 2012, Lally et al., 2004, Umale et al., 2013) or freezing temperatures below -18 ° C (Brunon et al., 2010, Ehrensberger et al., 2013, Jones et al., 1995, Rodriguez et al., 2011).

The mechanical testing parameters are defined considering the objective of the research study. If the experimental target is to determine the tissue's stiffness should be established a uniaxial tension test, but if the objective is to know the material’s response to repetitive movements and study their properties, behavior and wear caused by fatigue, a cyclic test (Ehresberger et al., 2013) should be performed.

Given the tissue nature in some cases, sandpaper or plastic is used on clamp faces to avoid slipping, dislocation or releasing of the sample when the test is performed. Also, studies in the literature consider values in strain rates between 0.01 and 10 1 / s, which will be further analyzed during the discussion section.

The instrumentation used is generally based on a Universal Testing Machine (UTM), adding optical equipment for measuring the cross-sectional area of the tissue sample, high-speed cameras to record the deformation of the material, and in some cases special equipment for temperature control while the experiment is performed.

On the Centro de Innovación y Diseño Estratégico de Productos (CIDEP) of the Tecnológico de Monterrey, an experimental area for mechanical testing of materials is available. For this research, uniaxial and biaxial tensile mechanical tests were performed.

Chapter 3

Methodology

The development of skills and learning about surgical procedures is a very important objective within medical training in different branches of the health area. Currently, several technologies have been applied to facilitate and improve the method by which physicians acquire experience and practical knowledge, in order to avoid risking patients' lives in this process.

Simulation and virtual reality are computational tools that allow the generation of controlled scenarios, free of risk and with high fidelity in relation to the real world, so it is possible to create virtual simulators for surgical training. In this type of device, the user (the physician) can interact with the system to complete specific tasks repetitively, allowing for the detection of errors and measurement of improvement, until reaching the level of quality necessary to perform the actual procedure (Goldenberg et al., 2017, Hernández-Irizarry et al., 2016, Schijven, 2013, Serna-Ojeda et al., 2012, Shetty et al., 2014, Palter et al., 2010).

The effectiveness of virtual simulators as learning tools has been previously validated in several studies, concluding that highly attached simulations actually facilitate the training of surgeons when used under appropriate conditions (Flores-Villalba et al., 2012, Palter et al., 2010, Nguyen et al., 2020).

The development of simulation tools with greater fidelity in the real world depends on great computational performance, whether through efficient algorithms or specific hardware, this is a research area with high potential for generating applications, solving problems, and meeting needs in the Health area. In this project, research is proposed in

virtual reality software and interactive simulation for the development of surgical training tools with a free and public approach.

Key areas include: 1) anatomically realistic geometries using medical imaging software 2) mathematical models for the characterization of human tissues; 3) new computational methods with great precision and good performance.

3.1 Geometrical modeling

As previously mentioned, in the previous approach a methodology was proposed to create 3D models that represent the anatomical structures using open-source software for medical image processing, called *InVesalius*. On an initial approach, geometries were manually segmented from a set of medical images provided by one of the study cases of CTI Renato Archer.

Even when these models were enough for the initial approach to create a simulation framework, it put a constrain in the applicability of the proposed model. In order to change or perform a different simulation, the whole methodology for acquisition and processing of a new anatomical model would have to be performed, including the manual segmentation of medical images. This would require not only time but also experience and skills to perform this procedure.

In order to improve this condition, the next steps are proposed:

(1) Create a module for reading and processing medical images using Phyton, in order to define a platform for the implementation of interactive tools (Abdallah et al., 2015, Fajar et al., 2020, Williams & Drew, 2019).

(2) Review state-of-the-art visualization algorithms, and implement interactive tools to use them for image processing and segmentation purposes, like the Volume Direct Rendering (VDR) and Intensity Projection (MIP).

(3) Define filtering and processing tools for medical images based on threshold and histogram analysis using the intensity.

(4) Define an algorithm for automatic segmentation of medical images using the created platform, based on 2D image object selection (Saeed & Saleh, 2020, Wen et al., 2021).

(5) Create 3D models and export STL meshes using this module in order to allow simulation and other applications (Fajar et al., 2020).

3.2 Material modeling and simulation

(1) Define an energy equivalence between two mathematical models: based on experimental parameters and considering nonlinearity and anisotropy of soft tissues and a simplified mechanical system able to solve in real-time (Brunon et al., 2010, Elías-Zúñiga et al., 2014, Elías-Zúñiga et al., 2020, Zhang et al., 2017, Zhang et al., 2018).

(2) Establish an algorithm for precomputing the non-real-time part of the model and a computational method to combine with the real-time part.

(3) Create a computational platform for simulation based on the hybrid model defined in this research, focused on increasing accuracy, and predicting behavior at softening. There was not found any work in the literature that uses a variant of the SMM with Mullin's effect (Nguyen et al., 2020, Omar et al., 2022, Zhang et al., 2017).

(4) Perform characterization of soft tissue and biological materials, running mechanical tests with porcine tissue samples (Brunon et al., 2010, Fu et al., 2013, Umale et al., 2013).

(5) Validate the simulations obtained through the proposed model with experimental data.

3.3 Scope and process

The proposal for this Doctoral dissertation was to work on the implementation of medical image processing tools that solve geometrical model opportunity areas and also develop a hybrid model that can represent the mechanical properties of soft tissue.

Part of these goals were performed during a research internship in Campinas, Sao Paulo, Brazil as a part of the Doctoral program on Tecnológico de Monterrey. This was planned since it provided the possibility to interact and learn from specialist in software development from the Centro de Tecnologia da Informacion (CTI) Renato Archer and with the Universidade Estadual de Campinas (UNICAMP).

After getting an improvement on the virtual part, the medical protocol for collecting the samples, processing and physical testing was performed in Tecnológico de Monterrey, with support from the Escuela de Medicina y Ciencias de la Salud and the Centro de Innovación y Diseño Estratégico de Productos.

In the next chapters, there is a detailed description of the process performed for the development of this research project.

- Creation of tools for geometric modeling

  (1) Implementation of algorithms for the visualization of medical images.
  (2) Define interaction strategy with the visualization module.
  (3) Interaction with images to create interactive selection tools.
  (4) Algorithms for semi-automated segmentation of anatomical structures based on medical images.
  (5) Creation of 3D mallets of anatomical structures in STL format to allow simulation and/or interaction with the deformation model.

- Modeling of the behavior of soft tissues

  (1) Literature review on constitutive, discretized, and hybrid models.
  (2) Constitutive model selection and analysis of its equations.
  (3) Mathematical formulation of a hybrid model with one-dimensional elements.
  (4) Review the use of the proposed formulation with volumetric elements.
  (5) Characterization of soft tissue behavior using a hybrid model.
  (6) Validation of the hybrid model with experimental data.

- Experimentation with animal tissue

  (1) Literature review on mechanical testing for characterization of soft tissue, sample preparation, and procedures.
  (2) Medical protocol for the extraction of tissue samples.
  (3) Tension tests and obtaining experimental data for mechanical properties of soft tissue.
  (4) Data analysis and characterization with constitutive models.

3.4 Materials and Resources

In order to perform this research, it was required the support of multiple organizations, laboratories, special equipment, and materials.

- Escuela de Medicina y Ciencias de la Salud of the Tecnológico de Monterrey
  (1) Bioterio
  (2) Amphitheater/Morgue
  (3) Surgical Simulation Laboratory
  (4) Tissue simples

- Centro de Innovación y Diseño Estratégico de Productos (CIDEP) of the Tecnológico de Monterrey

  (1) Instron™ 6635 electromechanical universal testing system
  (2) Electroforce™ Biaxial TestBench

- Centro de Tecnologia da Informação (CTI) Renato Archer, where the author of this dissertation did a research internship for collaboration with the DT3D - Divisão de Tecnologias Tridimensionais.
  (1) InVesalius
  (2) Medical Images
  (3) Microtomographys
  (4) OsiriX

- Universidade Estadual de Campinas (UNICAMP), where the author of this dissertation studied a year of classes in computational graphics at the Facultade de Engheneria Electrica e de Computação.

3.5 Expected results

The main outcome that is expected from this research is to generate a new hybrid model, based on an energy equivalence between an SEDF and the SMM.

The hypothesis is that using this hybrid construction it can be possible to simulate one-dimensional elements with the accuracy of the proposed SEDF to describe hyperelastic, anisotropic, non-linear, and softening behaviors (in function of their orientation), keeping the real-time response of the SMM.

In addition, it is expected to create a set of tools that allow the visualization and segmentation of medical images, facilitate the generation of anatomically realistic geometric models, and can be used for simulations applying the proposed material model (in addition to other uses for investigation and development).

Chapter 4

Interactive Segmentation for Geometrical modeling

In order to perform this research project, getting accurate information about the human body's anatomical structures was one of the biggest objectives. This has been explored in the past, and it has been found that one of the best approaches to get accurate information for geometrical modeling of this kind of complex surface is by using medical imaging current technology.

In this chapter, the process in which medical images were obtained, segmented, and processed in order to create a physically correct anatomical structure will be explained in detail.

During this research and as part of the international exchange and collaboration with the CTI Renato Archer and the UNICAMP, a part of the project was focused on the goal of developing an interactive rendering of medical images.

This goal aimed for interactive visualization and segmentation of medical images. It was developed on Python with OpenGL, NumPy, SciPy, and other libraries (see Download area for more details) and was based on GPU programming for real-time rendering, visualization, and interaction with volumetric data from medical images.

All DICOM images used for the development of this project were obtained from the OsiriX sample datasets available at http://www.osirix-viewer.com/datasets/ for testing and research purposes, no confidential personal information was disclosed.

The main objective was to create an application that provides support for different visualization modes, customized visualizations, histogram information display,

interactions with 3D space and segmentation of medical images, using GPU programming for real time rendering.

On a compendium of multiple techniques available in the literature, this part of the project will be focused on developing a process for renderization of Computed Tomography (CT) and Magnetic Resonance Imaging (MRI) creating volumetric data from medical images, using a specific algorithm called ray-casting.

Direct modes for visualization of volumes and surfaces will be applied (VDR and SDR), as well as Maximum Intensity Projection (MIP) and Maximum Intensity Difference Accumulation (MIDA). Tools for 3D interaction and segmentation will be studied.

In this chapter, the creation of a module for interactive visualization, processing, and segmentation of medical images is presented. This module was called *VISUALIX* by the author of this dissertation and its results are presented at the end of the chapter.

4.1 Medical images

Currently, medical images are used as a part of the diagnosis for diseases in many fields of medicine as well as surgical planning, education, and research proposes.

With technological advances, medical images are more often utilized in the process of identifying medical issues and concerns, diagnosis for diseases, and in many fields of medical research. These tools are also used for surgical planning as well as for training in the medical education system.

The development of tools for improvement of the current visualization process and diagnosis by a specialist in the medical area and radiologist can, by itself, be a great contribution to the science. In order to develop new tools, a solid understanding of the basic concepts of medical imaging, processing, and visualization using programming skills is highly necessary.

Medical images are acquired by exposing the patient body to a signal and measuring its response in order to process, reconstruct and store its anatomy. Currently, the main technologies used for medical imaging are Magnetic Resonance Imaging (MRI) and Computerized Tomography (CT).

These two types of technologies use different kinds of physical principles, one using magnetic fields and the other one x-rays. Even when these processes are different, the results of both are stored through Digital Imaging and Communication in Medicine (DICOM) standard file format.

These DICOM files, represent 2D images of sections of the body that are generated based on the patient's response, and depending on the nature of the signal, each kind of tissue is represented in different ways by intensity levels on each pixel from 0 to 255, as shown on Fig. 23.

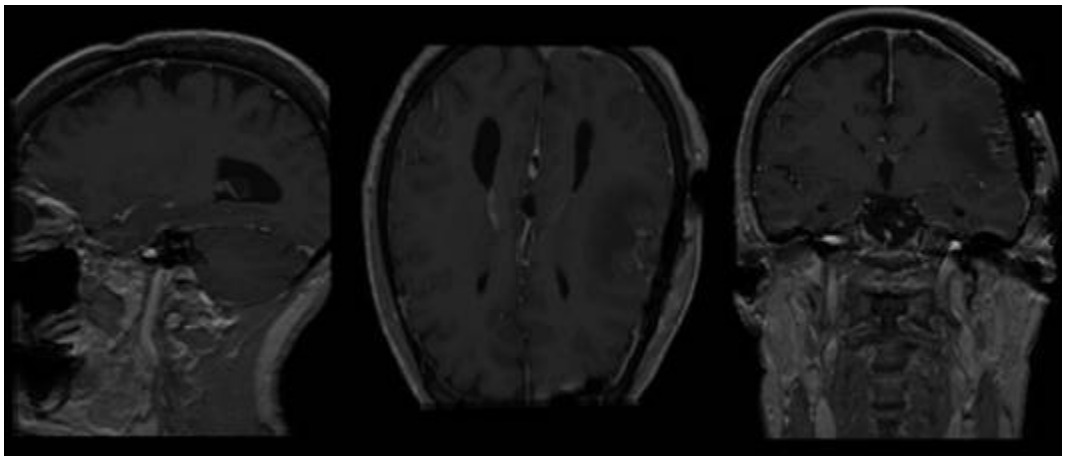

Fig. 23 2D medical images (Sagittal, Axial, and Coronal) of Brainix MRI

With this in mind, a system to read information from DICOM files was developed in order to have access to the intensity value per pixel of all the images to create a tridimensional array that reconstructs the volume of the patient anatomy (as conceptualized in Fig. 24).

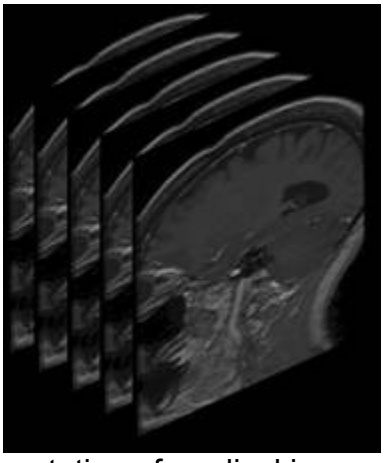

Fig. 24 Conceptual representation of medical images in a tridimensional array

In this research, the approach followed was to create interactive processing tools that allow the user to visualize and process the medical images in order to get the anatomical structure that is required to simulate. This process requires minimal input from the user and allows the creation of an STL mesh that represents a 3D model of the anatomical structure that will be used to apply the material model to simulate mechanical properties.

This chapter describes the process that is followed to interact and process medical images, as well as the tools developed to allow the user to create 3D models to use in the simulation framework.

One of the main goals of this project was the creation of tools that allowed the acquisition of anatomically realistic 3D models from medical images, based on an interactive approach.

This objective was defined in order to allow the user, a medical student, researcher or surgeon, to provide medical images from a particular case that is being worked on and be able to visualize, interact and segmentate a particular anatomical structure of interest in order to apply the material model developed in this research and use it to simulate its behavior.

Just the fact of creating a 3D geometrical model of the anatomical structure in an STL format allows the user to be able to use it for research purposes, 3D printing with additive manufacturing, design of products like prosthetics using such base geometry, surgical planning, etc.

Considering these reasons, the creation of such tools in an open-source approach is a great contribution to the development of new technologies and applications for bioengineering and medical purposes.

In the next points of this chapter, the creation and implementation of a set of tools for interactive visualization, processing, and segmentation of medical images are explained in detail, as well as examples of the results that can be achieved using the developed module, which was named *VISUALIX*.

4.2 *VISUALIX* module for interactive processing of medical images

Using GDCM (gdcmconv --raw) the images were decompressed into raw data. It can be used as a function to convert an entire folder of DICOM images to raw data in another location.

Table 2 Code fragment to convert DICOM images to raw data

```
dcm2raw(){
    for i in $1/*
    do
        fname=$(basename $i)
        oname=${fname%.*}
    gdcmconv -w -i $i -o $2/$oname.raw
    done
}
```

Using Pydicom the raw files were read and stored in a NumPy array on the readicom function.

The pipeline for rendering process defines the steps to create visualizations based on OpenGL:

(1) Vertex Shaders
(2) Tessellation
    a. Tessellation Control shaders
    b. Tessellator
    c. Tessellation Evaluation Shader

(3) Geometry Shader
(4) Clipping
(5) Rasterization
(6) Fragment Shader
(7) Fragment Tests
(8) Framebuffer Blending and Logic
(9) Write Masking
(10) Write to Framebuffer

To initialize it is needed to create the vertex arrays, load vertex and fragment shaders from text files, and create the textures and the framebuffers used in the rendering process.

Table 3 Code fragment to load the pyshaders that will be used

```
def InitGL(self):
   g_texWidth = self.width
   g_texHeight = self.height
   self.initVBO() #Create vertex array
   self.initshader() #Create shaders
   self.set_data_pack() #Define attributes
   size = self.tffsize
   tff = self.tffconfig[self.tffindex]
   data,(w,h,d) = 0,(0,0,0)
   self.g_tffTexObj =
self.transferfunction(np.array(tff,dtype=np.float32)/ float(size),size)
   self.g_bfTexObj = self.facetexture(self.width,self.height)
   self.g_bfTexObjpicking = self.facetexture(self.width,self.height)
   self.g_volTexObj = self.loadvolumedata(data,w,h,d)
   self.g_frameBuffer = self.initFrameBuffer(self.g_bfTexObj, g_texWidth
g_texHeight)
   self.g_frameBufferpicking =
self.initFrameBuffer(self.g_bfTexObjpicking, g_texWidth, g_texHeight)
```

In this process, an OpenGL 3D texture was created with the dataset of all the images, using the loadvolumedata function.

Table 4 Code fragment to load the volumetric data of the medical images

```
def loadvolumedata(self,dataset,w,h,d):
   data = ""
   for ind in range(d):
       data = data + dataset[:,:,ind].tostring()
   g_volTexObj = glGenTextures(1)
   glBindTexture(GL_TEXTURE_3D, g_volTexObj)
   glTexParameteri(GL_TEXTURE_3D, GL_TEXTURE_MAG_FILTER, GL_LINEAR)
   glTexParameteri(GL_TEXTURE_3D, GL_TEXTURE_MIN_FILTER, GL_LINEAR)
   glTexParameteri(GL_TEXTURE_3D, GL_TEXTURE_WRAP_S, GL_CLAMP)
   glTexParameteri(GL_TEXTURE_3D, GL_TEXTURE_WRAP_T, GL_CLAMP)
   glTexParameteri(GL_TEXTURE_3D, GL_TEXTURE_WRAP_R, GL_CLAMP)
   glPixelStorei(GL_UNPACK_ALIGNMENT,1)
   glTexImage3D( GL_TEXTURE_3D, 0, GL_INTENSITY16, w, h, d, 0,
GL_LUMINANCE, GL_UNSIGNED_SHORT, data)
   return g_volTexObj
```

To load the texture 3D on the GPU, it was used the uniform with the location defined by its name on the fragment shader.

Table 5 Code fragment to define volumetric texture used for visualization

```
volumeLoc = glGetUniformLocation(self.g_programHandle, "VolumeTex")
if (volumeLoc >= 0):
    glActiveTexture(GL_TEXTURE2)
    glBindTexture(GL_TEXTURE_3D, self.g_volTexObj)
    glUniform1i(volumeLoc, 2)ef loadvolumedata(self,dataset,w,h,d):
   data = ""
   for ind in range(d):
       data = data + dataset[:,:,ind].tostring()
   g_volTexObj = glGenTextures(1)
   glBindTexture(GL_TEXTURE_3D, g_volTexObj)
   glTexParameteri(GL_TEXTURE_3D, GL_TEXTURE_MAG_FILTER, GL_LINEAR)
   glTexParameteri(GL_TEXTURE_3D, GL_TEXTURE_MIN_FILTER, GL_LINEAR)
   glTexParameteri(GL_TEXTURE_3D, GL_TEXTURE_WRAP_S, GL_CLAMP)
   glTexParameteri(GL_TEXTURE_3D, GL_TEXTURE_WRAP_T, GL_CLAMP)
   glTexParameteri(GL_TEXTURE_3D, GL_TEXTURE_WRAP_R, GL_CLAMP)
   glPixelStorei(GL_UNPACK_ALIGNMENT,1)
   glTexImage3D( GL_TEXTURE_3D, 0, GL_INTENSITY16, w, h, d, 0,
GL_LUMINANCE, GL_UNSIGNED_SHORT, data)
   return g_volTexObj
```

4.3 Ray-casting

Once a 3D texture with the information of all images was generated, it is possible to use a ray-casting algorithm as a rendering method. In this process, a set of rays are created from the observer to the object that wants to be visualized, one for each pixel of the final image (Mensmann et al., 2010, Pietroszek, 2018, Shkarin et al., 2020).

The intersection of these rays with a 3D proxy geometry (a cube) is used to map special coordinates (XYZ) to a voxel position on the 3D texture and then use the information of the image at that point to calculate the color using an illumination model, as conceptualized in Fig. 25.

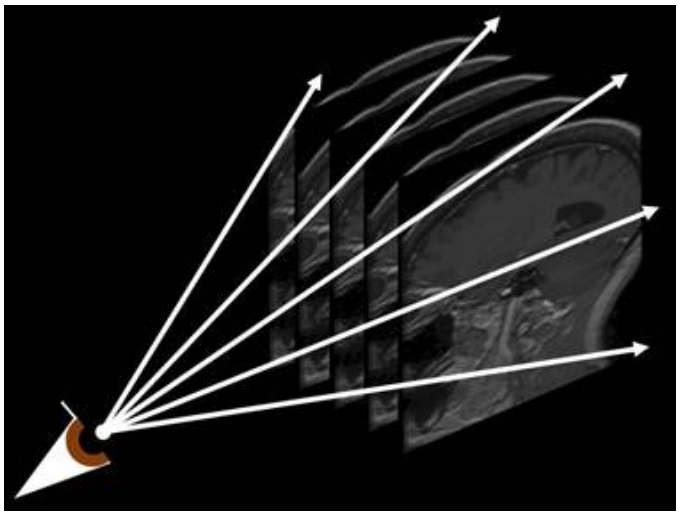

Fig. 25 Conceptual representation of a ray-casting method

This illumination model considered absorption, reflection, and refraction of light by interaction with the voxels. Depending on the visualization mode, it is required information like the position, intensity, accumulation, color, opacity value, and normal vector per voxel.

In this case, two steps rendering method was used for implementing ray-casting. On a first step, the back faces of the proxy geometry are rendered to get the exit point of the rays (by using the XYZ coordinate as RGB color code) and saved in a 2D texture (Mensmann et al., 2010). In a second step, the front faces are rendered to get the entry point, using the exit point for the same pixel calculated in the previous step from the 2D texture saved. Both sets of faces are shown in Fig. 26.

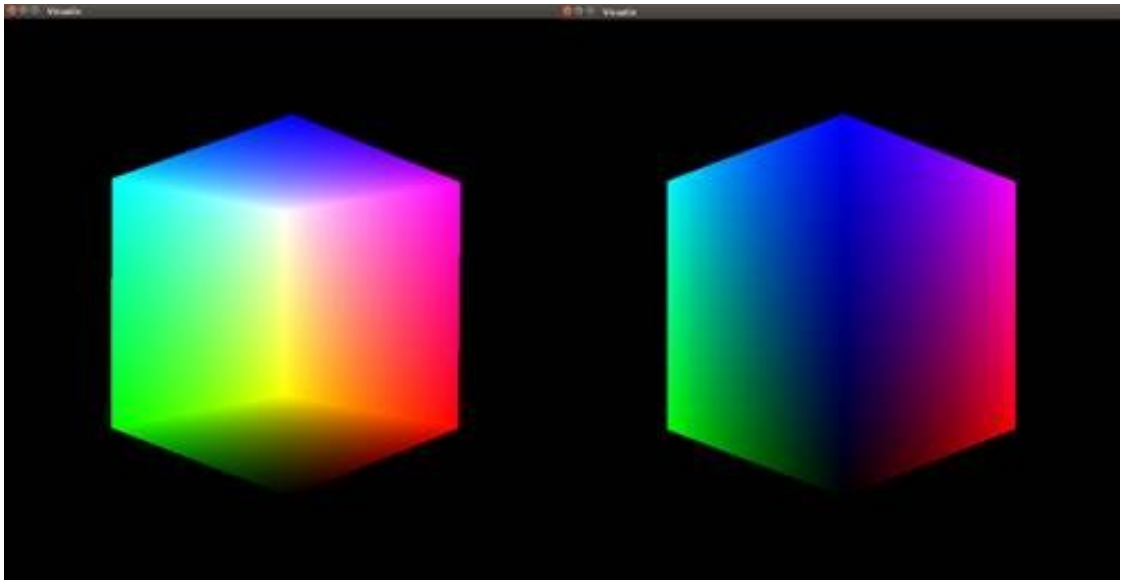

Fig. 26 Back faces and front faces of the proxy geometry

Using the entry and exit points for each pixel, a vector can be calculated. Considering a step size defined by the user, the ray starts to run in the vector direction by increasing for n steps. On each step, the intensity value of that position on space is searched in the 3D texture in order to use it in the visualization mode.

As an advantage of GPU use, it is possible to access to the information of any spatial point inside the 3D texture on the fragment shader, by having an automatic interpolated value of the intensity at that position, as shown in Fig. 27 using Manix data set of medical images from OsiriX library.

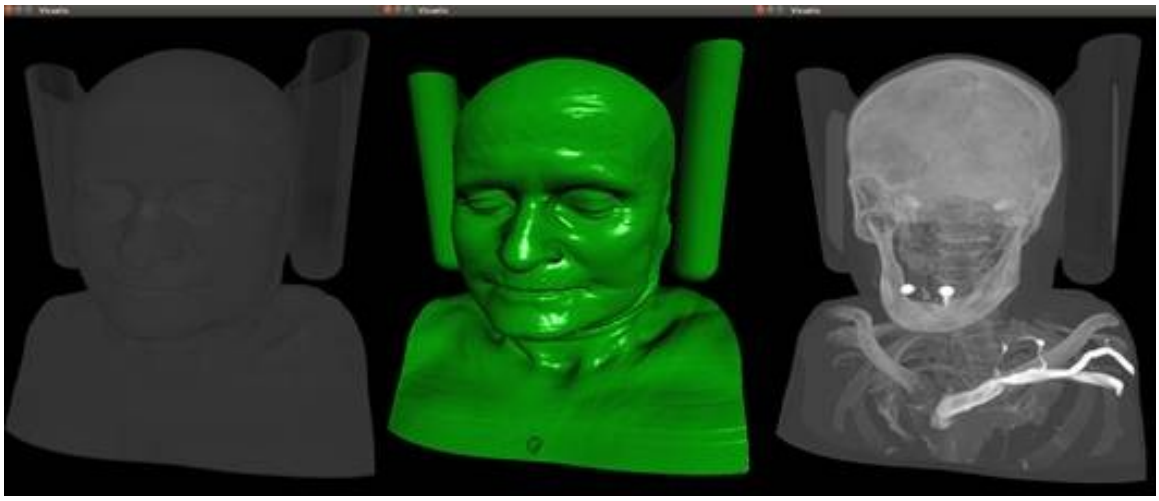

Fig. 27 Different visualization modes achieved with this implementation of ray-casting

4.4 Interactive Visualization

Four principal visualization modes were implemented in the VISUALIX module for interactive processing of medical images based on state-of-the-art techniques, including:

(1) Volume Direct Rendering (VDR)
(2) Surface Direct Rendering (SDR) with the option to show normal vectors
(3) Maximum Intensity Projection (MIP)
(4) Maximum Intensity Difference Accumulation (MIDA)

Each one is based on differences in the ray-casting process on the fragment shader.

4.4.1 Volume Direct Rendering (VDR) implemented in *VISUALIX*

On VDR, each ray used on the fragment shader performs an accumulation of the voxel's color and opacity factor in order to define the final color that will be represented by the pixel (Balsa Rodriguez et al., 2014, Khlebnikov et al., 2014, Weiss et al., 2021). This technique can generate visualization like the one shown in Fig. 28.

Table 6 Code fragment to define the VDR resulting value

```
colorAcum.rgb += (1.0 - colorAcum.a) * colorSample.rgb * colorSample.a;
colorAcum.a += (1.0 - colorAcum.a) * colorSample.a;}
```

Fig. 28 Volume Direct Rendering (VDR) on Panoramix

4.4.2 Surface Direct Rendering (SDR) implemented in *VISUALIX*

On SDR, there is no accumulation process to define each pixel color. For this case, the ray advances on the proxy geometry searching for the first valid voxel to visualize. Once founded, the normal vector on that point of the surface is required to calculate the illumination model based on Phong-Blinn equations (Okuyan et al., 2014).

Since there is no topological information on this surface (considering it is not a mesh, but a 3D texture) is needed a way to estimate the normal vector at each point. In this case, it was used Central Finite Differences (CFD) to calculate the gradient and use it as an estimator of the normal vector, only calculated on the first and last valid voxel (Liu et al., 2015).

It is possible to visualize the normal vectors on the final surface represented as colors (XYZ -> RGB), as shown in Fig. 29.

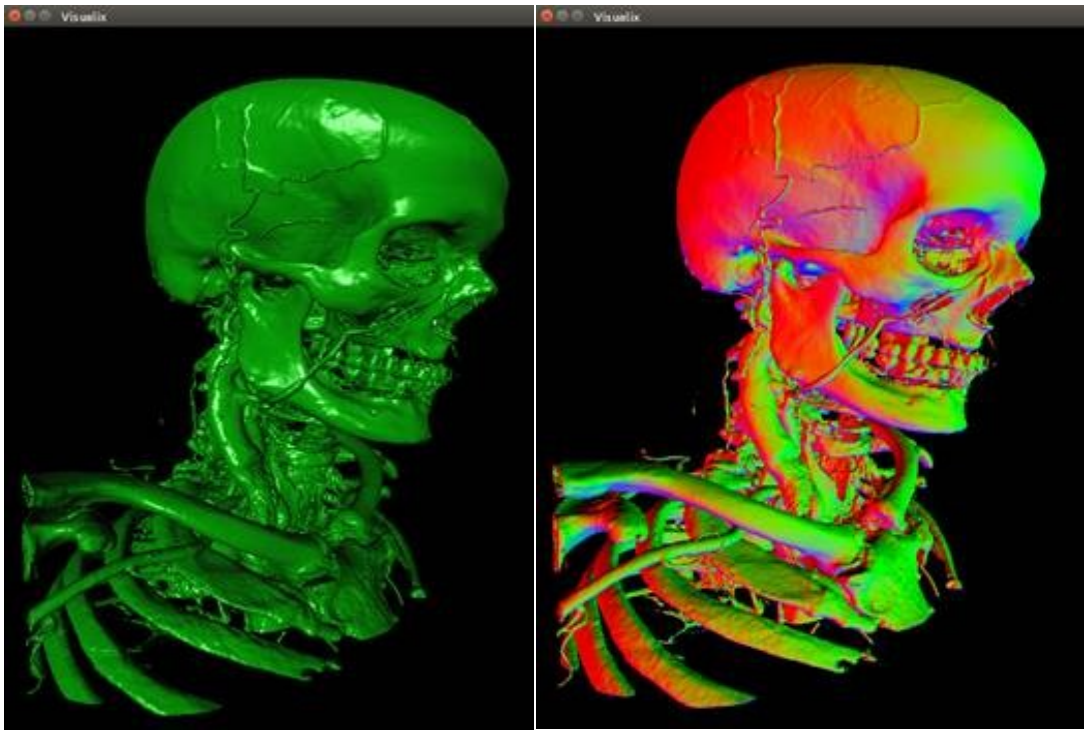

Fig. 29 Surface Direct Rendering (SDR) and normal vector as colors on Manix

4.4.3 Maximum Intensity Projection (MIP) implemented in *VISUALIX*

MIP is a mode commonly used in the medical area to visualize certain kind of tissue or structures, since enhance the visualization of structures of interest (Mroz et al., 2000). In particular, it works well to visualize bone, vascular tissue, and bronchial tubes. Also, it is used to visualize stents, prostheses, and other metal implants (Rosskopf et al., 2020, Zheng et al., 2020), as the cranial implant screws shown in Fig. 30.

Table 7 Code fragment to define the MIP resulting value

```
if (mip < intensity) { colorAcum.rgb = colorSample.rgb; mip = intensity;}
```

Fig. 30 Maximum Intensity Projection (MIP) on Phenix

4.4.4 Maximum Intensity Difference Accumulation (MIDA) implemented in *VISUALIX*

On MIDA, the accumulation of the VDR is calculated by considering not only the maximum intensity, but also the difference between a new maximum intensity and the maximum intensity previously crossed by the same ray (Bruckner & Gröller, 2009). Using this approach, it is possible to enhance structures with maximum intensity on the visualization (like MIP) but without fully excluding other structures, as shown in Fig. 31.

Table 8 Code fragment to define the MIDA resulting value

```
if (mida < intensity) {  dl = intensity - mida; mida = intensity;}
                  else { dl = 0.0;}
float bt = 1.0 - dl*(1+gama);

colorAcum.rgb = (bt*colorAcum.rgb)+(1.0-bt*colorAcum.a)*colorSample.rgb*
colorSample.a;
colorAcum.a = (bt*colorAcum.a)+(1.0-bt*colorAcum.a)*colorSample.a;
```

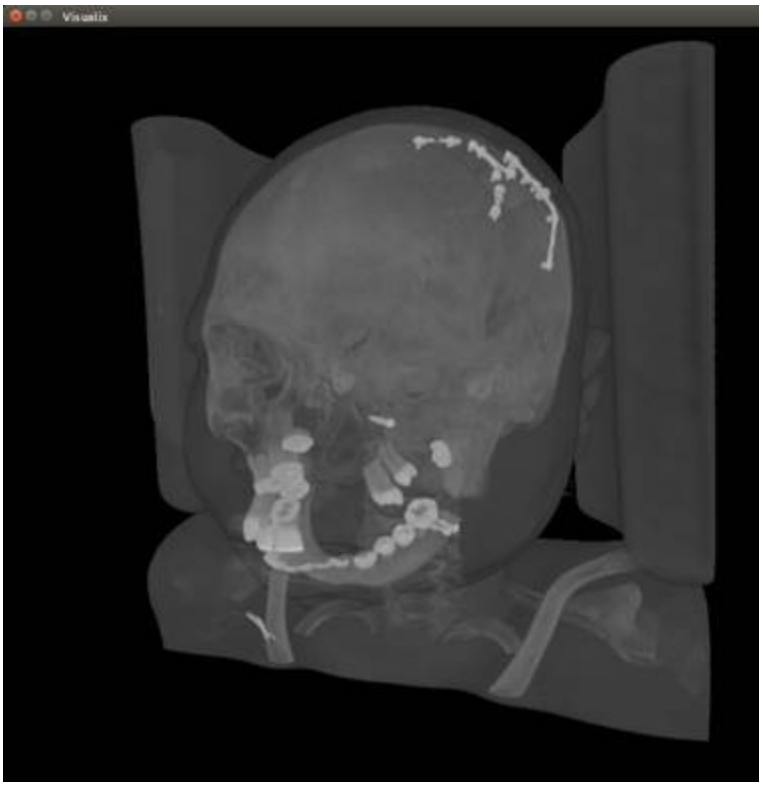

Fig. 31 Maximum Intensity Difference Accumulation (MIDA) on Phenix

All functions are available on four visualization modes.

4.5 Histogram Interaction

A histogram function was added to the project, since this is important information of the images that can be helpful in the visualization and segmentation process. By using the histogram, it is possible to interact with the visualization by creating customized transfer functions and changing the threshold for filter and segmentation of the visualization.

4.5.1 Interactive Transfer Functions (ITF)

As an interaction tool, were included three kinds of shapes for customized transfer functions: 1) Triangular, 2) Ramp and 3) Square functions. Each shape has a particular utility and enables the user to create multiple configurations and combinations of colors by controlling and overlapping each channel (RGB).

A demonstration of the Triangle Transfer Function tool implemented using the histogram for applying the color with VDR using Panoramix data set is shown in Fig. 32, and using MIDA with Manix in Fig. 33. The Ramp Transfer Function tool implemented is shown in Fig. 34 and Fig. 35. Also, the Square Transfer Function tool implemented is shown in Fig. 36, creating a visualization that can help to segmentation of specific regions.

Fig. 32 Histogram with a Triangle Transfer Function on Panoramix (VDR)

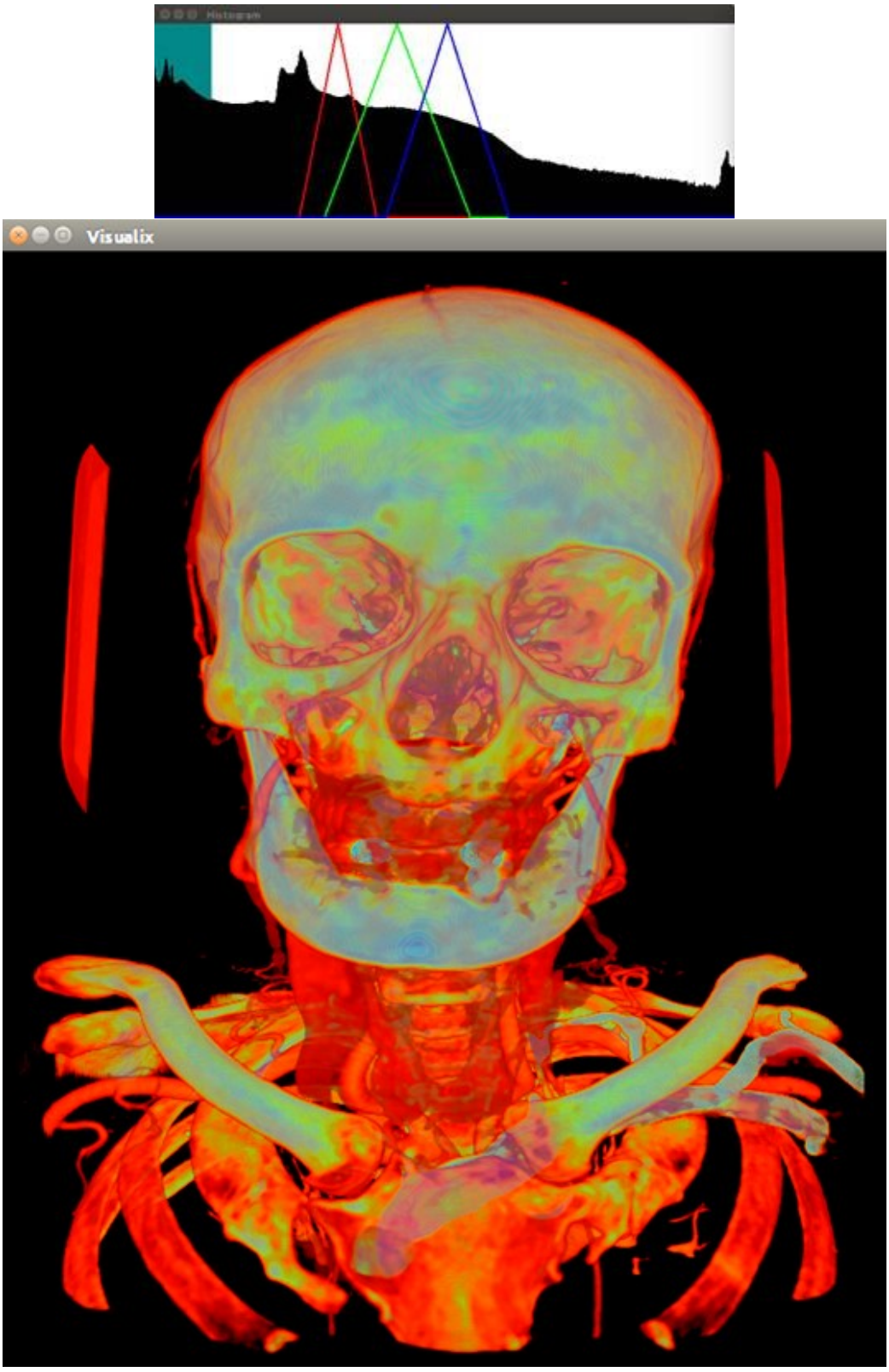

Fig. 33 Histogram with a Triangle Transfer Function and the visualization on Manix (MIDA)

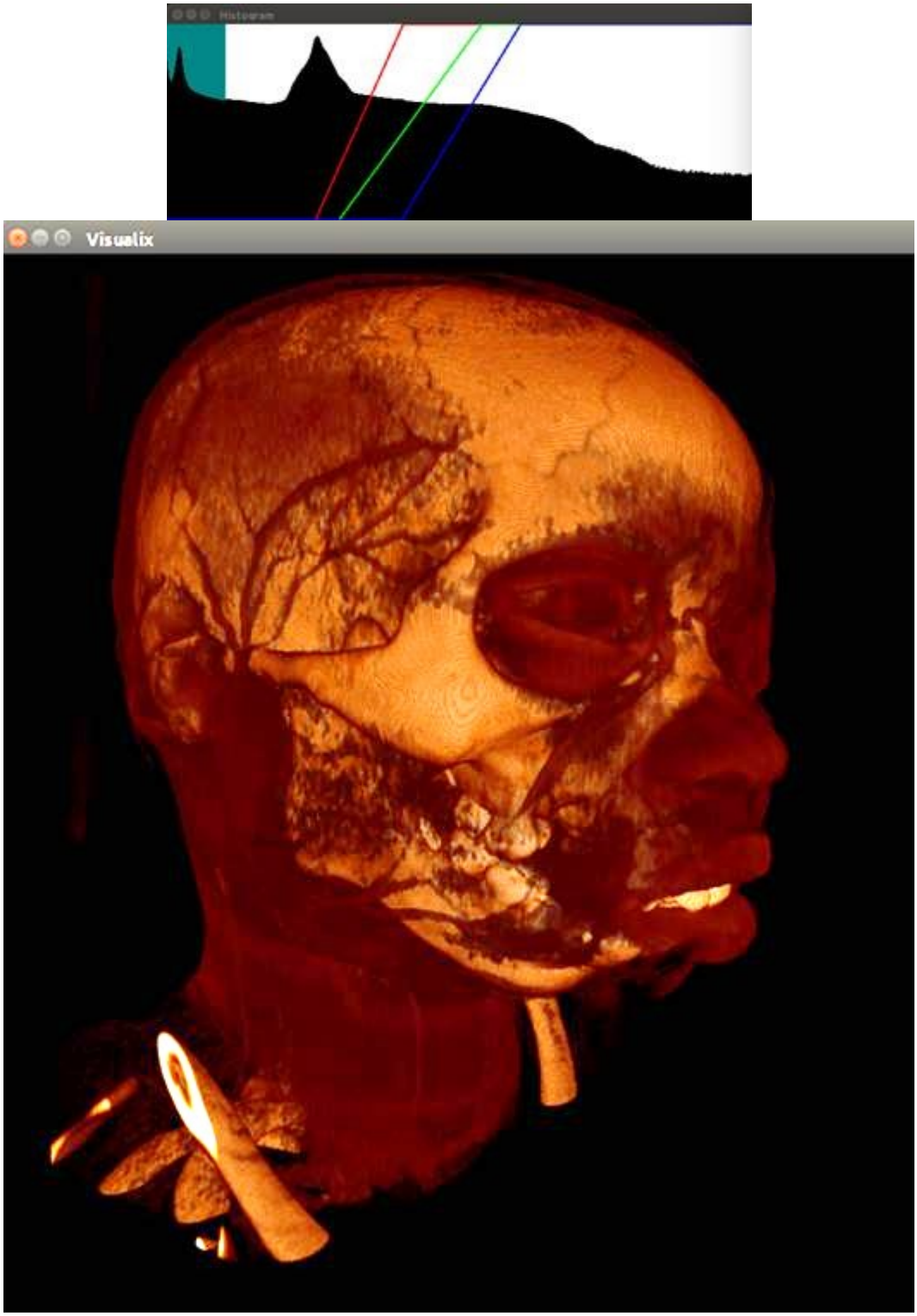

Fig. 34 Histogram with a Ramp Transfer Function and the visualization on Phenix (VDR)

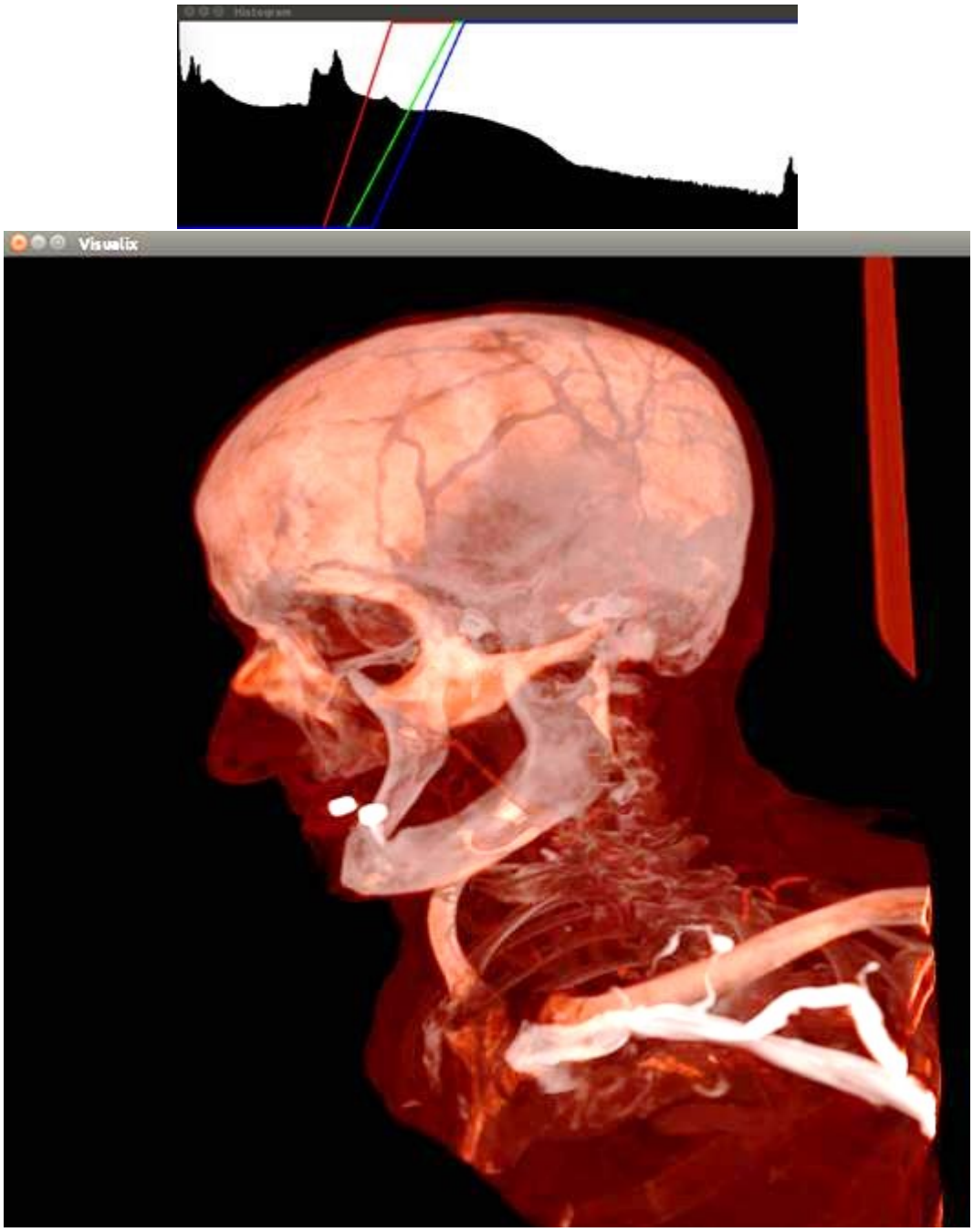

Fig. 35 Histogram with a Ramp Transfer Function and the visualization on Manix (MIP)

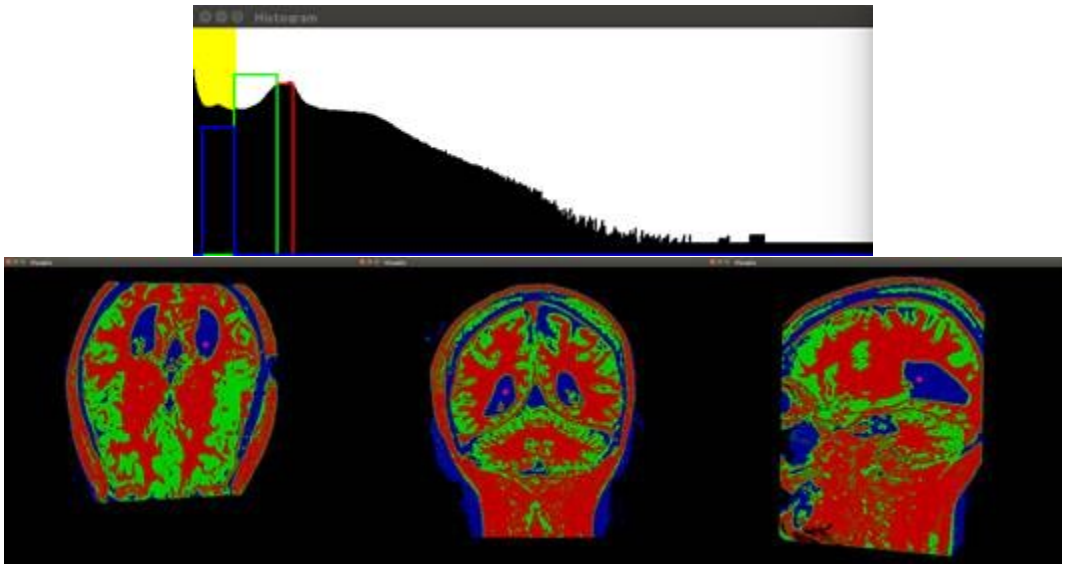

Fig. 36 Histogram with Square Transfer Function visualization on Brainix (VDR)

All three implemented transfer functions shapes tools allow interacting with the histogram to define position and window level for RGB values, and it is possible to save and load configurations previously created.

In this implementation, a protocol for a file format called by the author ****.tff*** (transfer function file) was defined, allowing the users of *VISUALIX* to save their created transfer functions and use them later in multiple images or share them with others to reproduce the same visualization.

A .tff file is a chain of parameters that define the position on the histogram of the RGB transfer function, as well as the window level or intensity.

4.6 Interactive 3D positioning

As one of the main objectives of this project is to generate interactive communication between the user and the visualization. With that purpose in mind, were developed tools to handle users' 2D actions to interact with the 3D visualization space.

A spatial cursor tool was prepared in order to identify the 3D position of the object that the user is trying to select when clicking on the 2D visualization rendered in the window.

4.6.1 Positions map

When the user clicks at a 2D point, a new cycle for refreshing the visualization is started. Before generating and showing the final image on-screen, a position map is created and stored in an offscreen frame buffer.

The position map is a 2D image created in a fragment shader where the pixels represent the 3D coordinates (XYZ) of the first valid voxel crossed by each ray, stored as color codes (RGB) (Batagelo et al., 2005, Andrade et al., 2012).

In this process, the valid voxels are in function of the data that the user is visualizing at that time, considering filters, cuts, and visualization mode as shown in Fig. 37 using VDR/SDR and in Fig. 38 using MIP/MIDA.

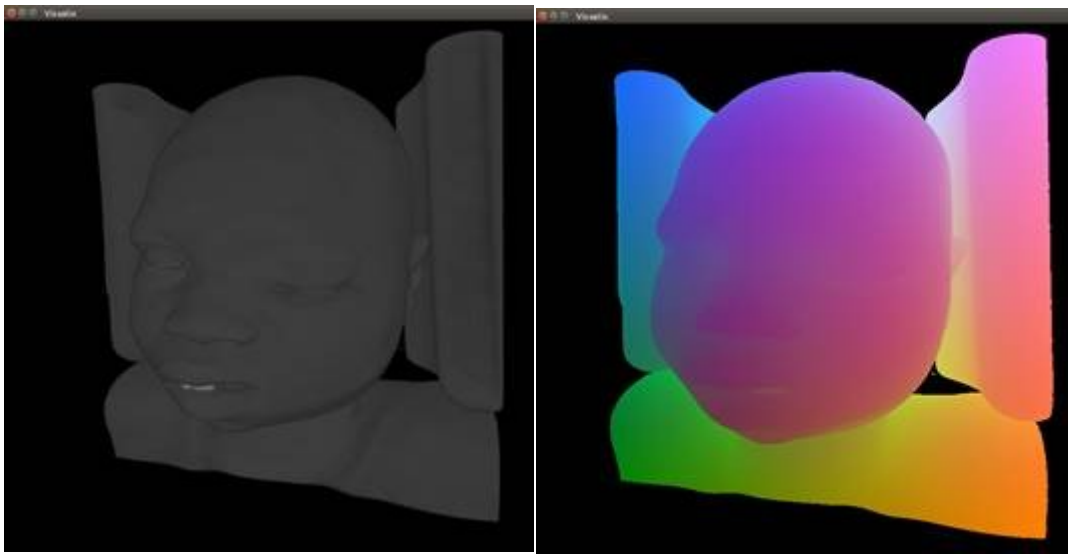

Fig. 37 Positions map of VDR on Phenix (same for SDR)

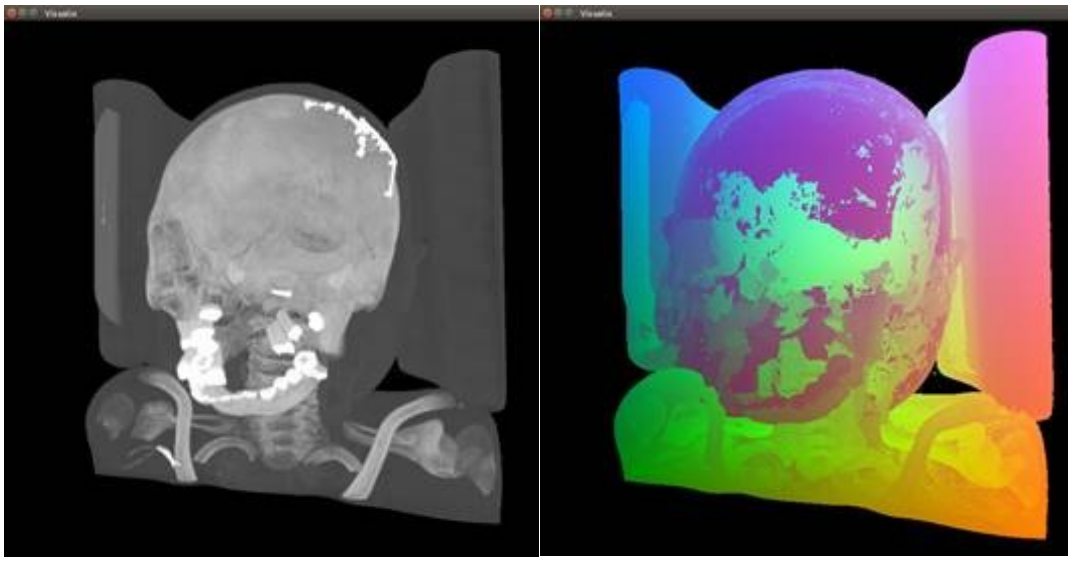

Fig. 38 Positions map of MIP on Phenix (same for MIDA)

When the user picks a point on the visualization, the 2D window coordinates are used to obtain the 3D coordinates of that point on the visualization space, using the color code (RGB) of that pixel on the position map stored. Using this information, the 3D cursor is positioned on that point (shown as a red sphere in Fig. 39).

Fig. 39 Selection of a kidney with the 3D cursor on Panoramix

4.6.2 Cutting Section for Visualization

Using the 3D cursor, it was developed a cutting tool based on the position of the object selected by the user. In this case, each axis coordinate of the cursor is used to define a position for cutting the model at that point, providing better visualization of the object of interest.

It is possible to navigate cutting the model by moving the 3D cursor, as shown in Fig. 40.

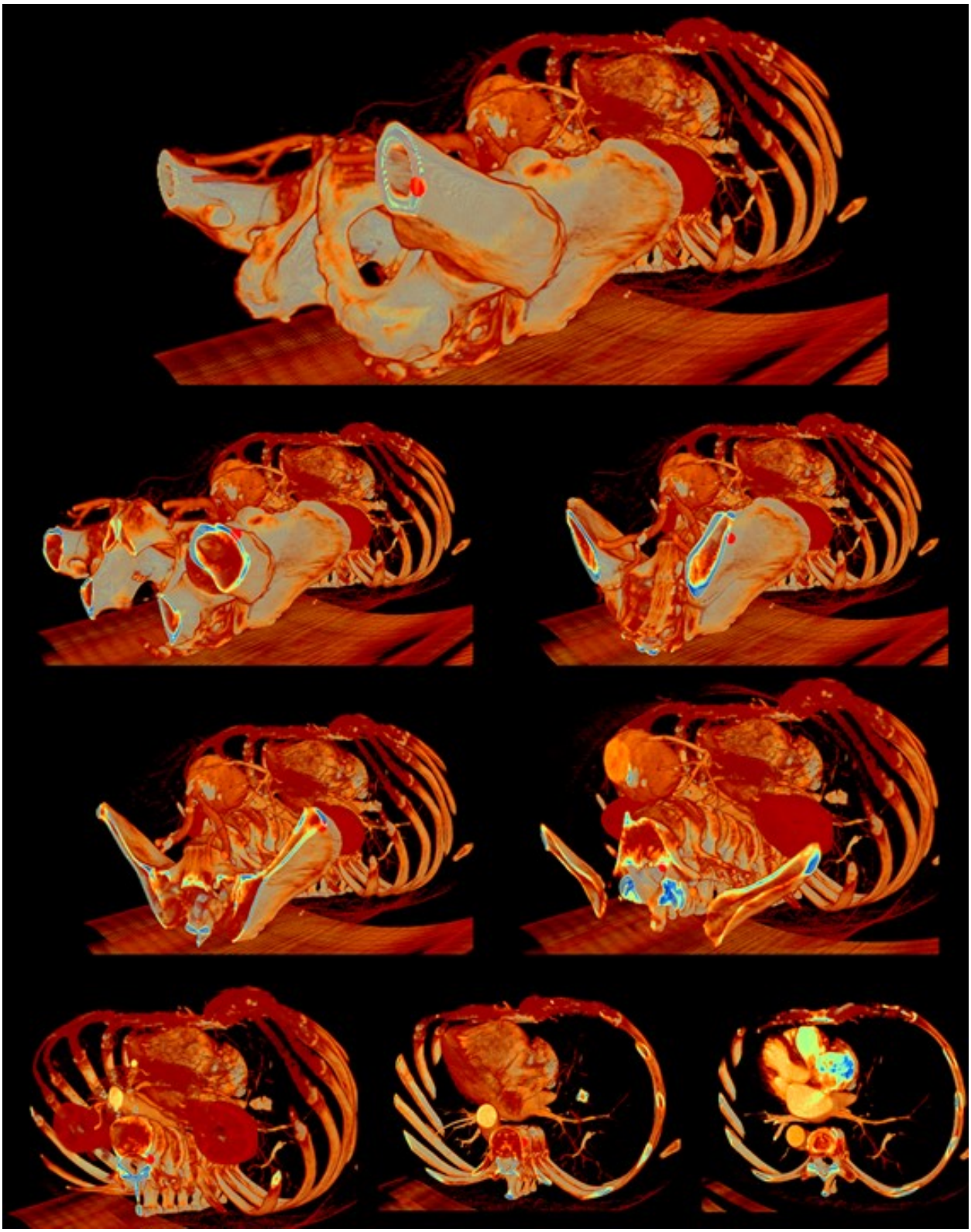

Fig. 40 Using 3D cursor on Panoramix for interacting with the medical images and select where to section the visualization, advancing in the transverse plane.

4.6.3 Selective filtering

As previously explained, it is possible to filter voxels in the visualization through an intensity threshold, but it is not so simple for the user to identify the intensity of any object of interest among the others. With this in mind, selective filtering was developed using the 3D cursor.

When the user selects an object of interest by positioning the 3D cursor, it was implemented a function for selective filtering that will show only the voxels that have an intensity value within a defined threshold, as shown in Fig. 41.

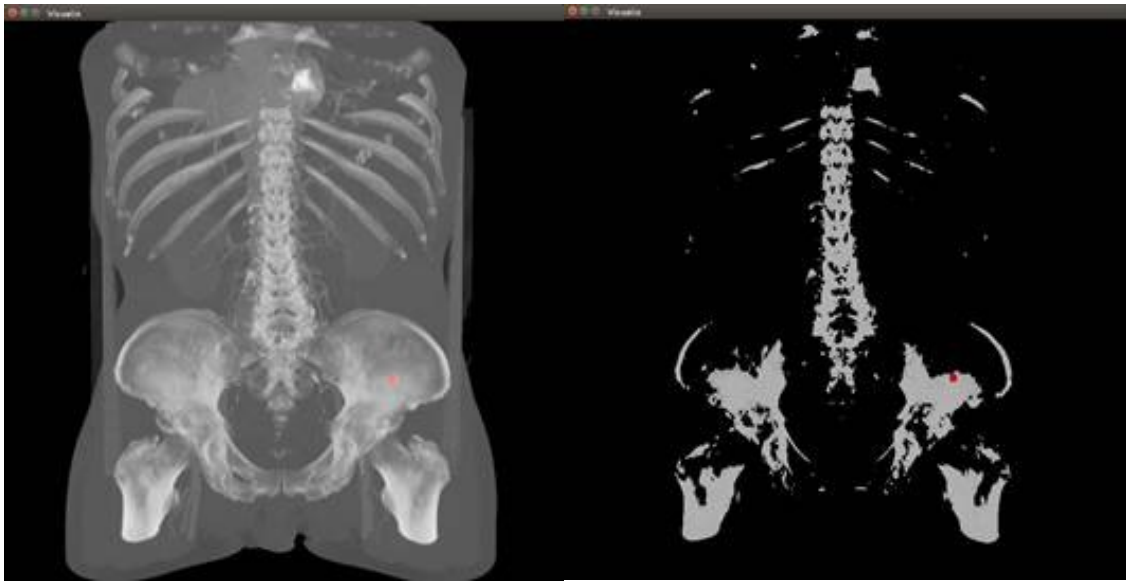

Fig. 41 Selective filtering on Panoramix

The intensity of the selected voxel can be acquired and displayed on the histogram tool with a yellow range, this yellow range represents the values in the histogram that are displayed with the selective filtering tool, as shown in Fig. 42.

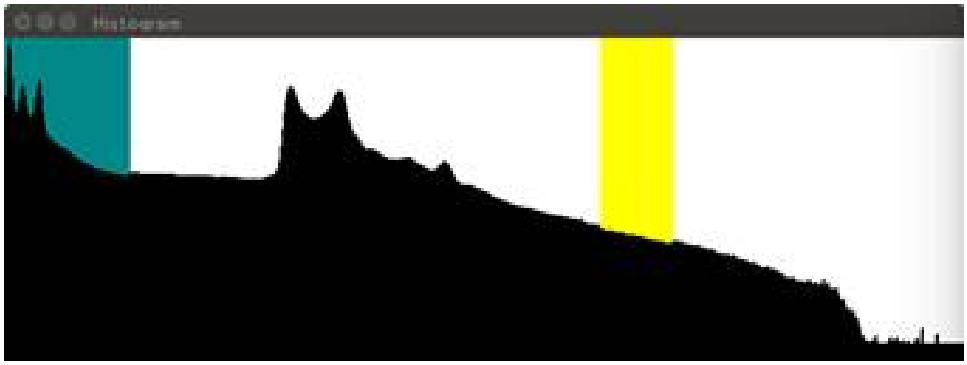

Fig. 42 Histogram before and after increasing threshold

Then, the selected value can be used to define the center of a window range of intensities of valid voxels to visualize, allowing the user to customize this filtering by increasing or reducing the width of this range or by moving the 3D cursor shown in Fig. 43.

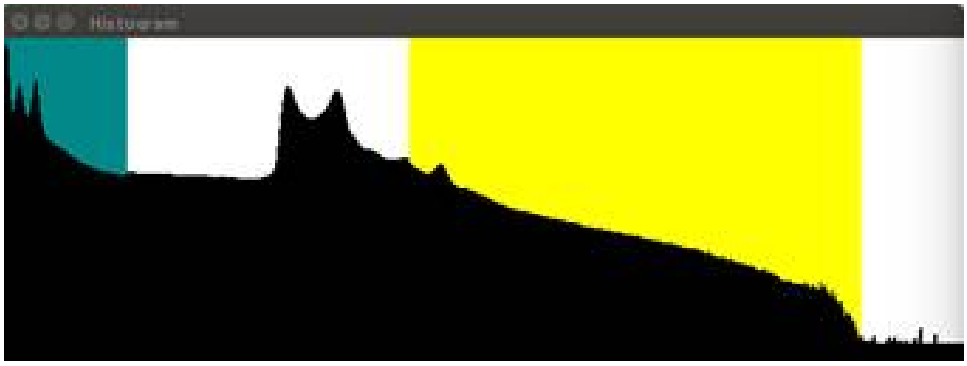

Fig. 43 Histogram before and after increasing threshold

The results from the user increasing the range of values as shown in Fig. 42 and Fig. 43, can be reviewed in Fig. 44. This shows how it is possible to focus the visualization only on a desired and customized set of intensity values by interacting with the 3D cursor and the histogram tools.

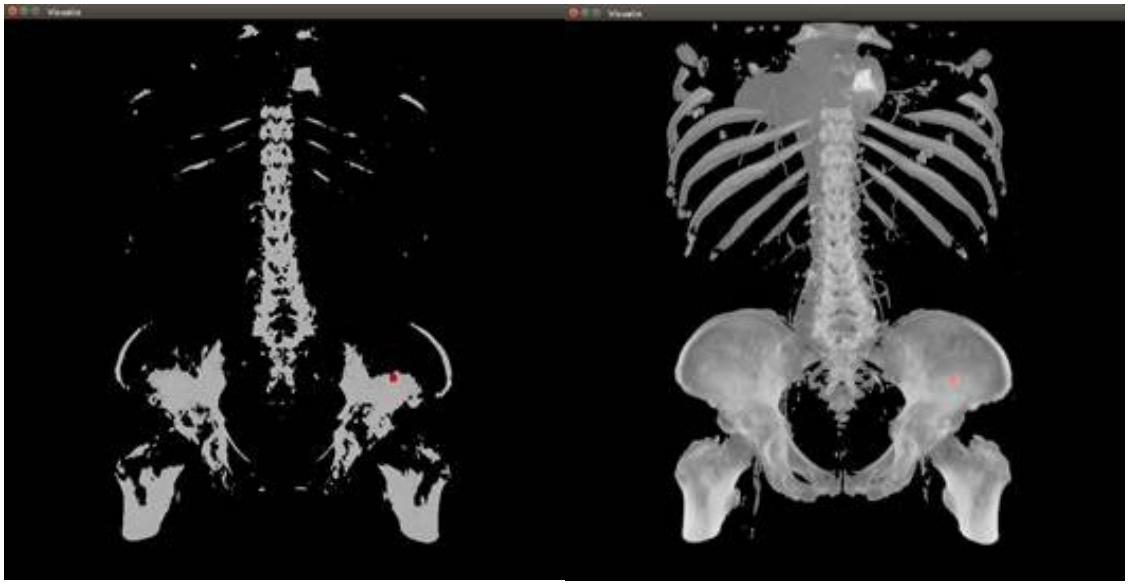

Fig. 44 Selective filtering on Panoramix before and after incresing threshold

4.7 Segmentation process

One of the main objectives of this project was to create tools for segmentation of medical images. The segmentation is a process in which different anatomical structures can be separated or identified with (or without) the interaction of the user. In this case, different tools for segmentation based on the concepts of threshold, seeds for region growing, and boundaries were developed.

4.7.1 Segmentation by threshold filters

When ray-casting is running, it is possible to define an intensity threshold of valid voxels to be considered for visualization as crossed by the rays. Based on that, a simple tool to define the minimum and maximum intensities to be rendered was developed as shown in Fig. 45.

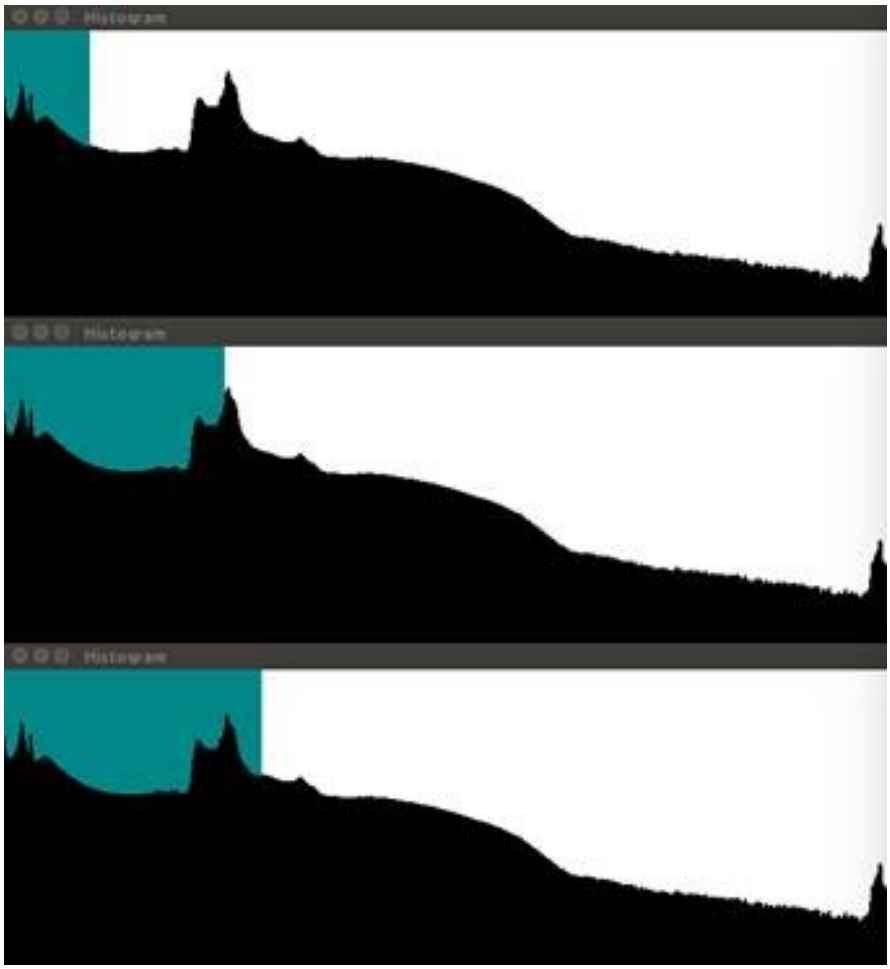

Fig. 45 Histogram with the minimum intensity increasing

Just by changing these parameters, it is possible to see different structures on the images, as skin, muscle, bones and vascular tissue, among others. One example of this tools is selective filtering, and although it can be considered as a segmentation tool, the results of threshold-based segmentations are rarely good or as expected.

It can generate a good visualization of different anatomical structures but can not be used for a specific structure due to lack of control. This is because many structures on the body can have the same intensity values, therefore not all the voxels within the valid range of intensities belong to the structure of interest. Results from the user interacting with this tool in the histogram shown in Fig. 45 can be reviewed in Fig. 46.

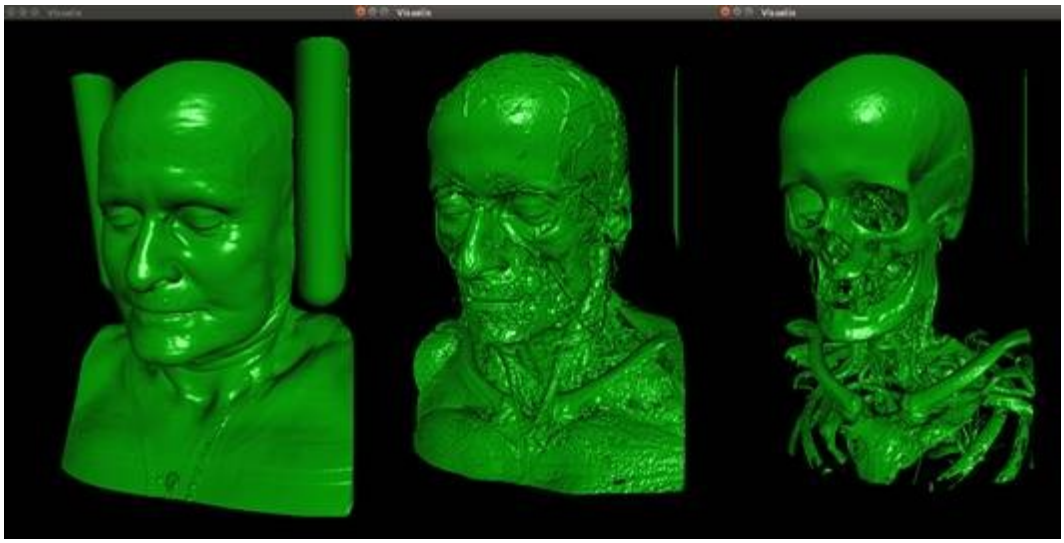

Fig. 46 Changing the minimum intensity valid for Manix

4.7.2 Segmentation by region growing

In order to solve this issue and provide a better segmentation tool, a region-growing algorithm was included on this project.

It has been found in the literature that this algorithm is currently being implemented on specific research cases for medical analysis, like Lung cancer (Alakwaa et al., 2017), Skull and Brain (Tan et al., 2019), Brain tumor (Bennai et al., 2020), among others (Xi et al., 2014, Yuan et al., 2015).

Also, it has been used for segmentation of 2D images of Pectoral Muscle (Saeed, E. & Saleh, H. 2020), Gynecological Malignant Tumor (Wen et al., 2021), Cochlear nerve (Singarayan et al., 2018), Liver (Lu et al., 2014), and even for 2D sandstones (Asmussen et al., 2015).

Based on this, an implementation of region growing for interactive segmentation is proposed, using seeding selection. Using this algorithm, the voxel selected through the 3D cursor position is treated as a seed. In the beginning, this seed searches on his neighbor voxels and if it finds a value on the defined intensity threshold, the seed grows into those voxels and then searches on each new neighborhood (represented in Fig. 47 with an S for selected and N for neighbor).

When the last voxel can not find avalid neighbor to grow, the segmentation process would be finished, and all occupied voxels would be treated as segmented objects. Using this search, it is possible to segmentate medical images by an automated approach, with just a couple of inputs from the user and considering it will be an interactive tool to set up.

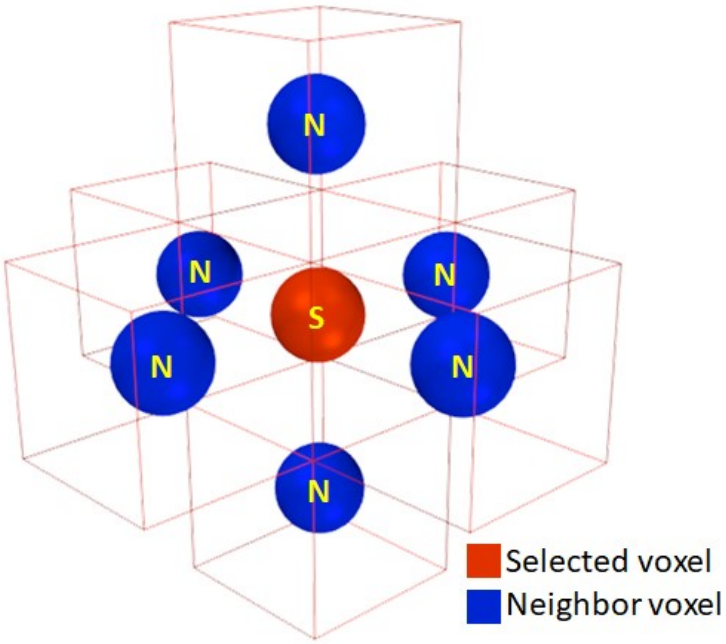

Fig. 47 Concept of the growing segmentation

In this case, it is possible to represent this algorithm in an illustrative way by using a 2D image of how the region growing works, shown step-by-step in Table 9.

Table 9 Step-by-step illustration of the region growing segmentation

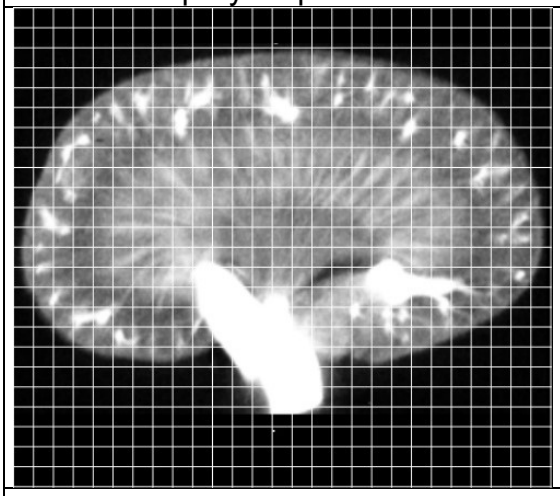	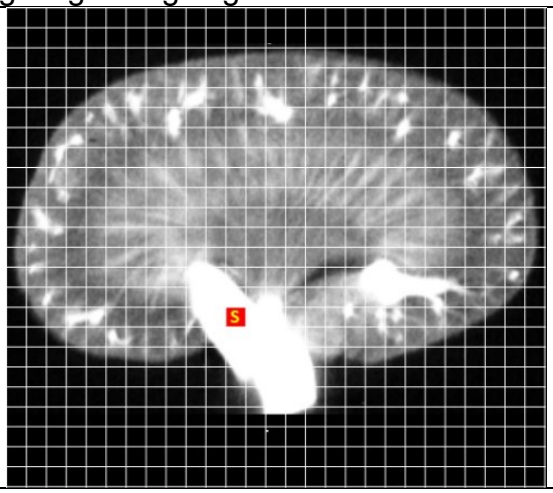
Original 2D image, before being selected an element to segmentate	There was selected a point (shown in 2D) to start a segmentation of a structure of interest (by using the 3D interactive cursor, having xyz cords)

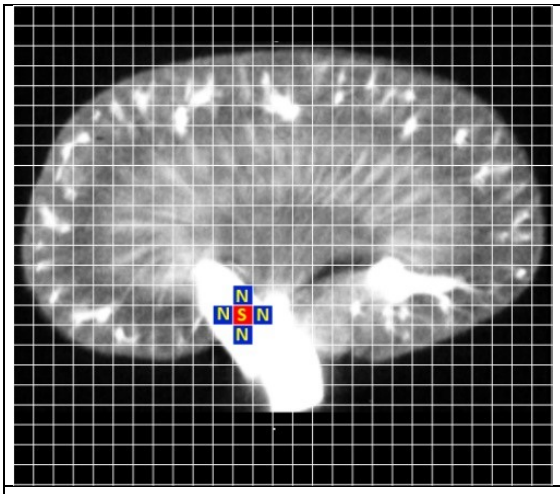	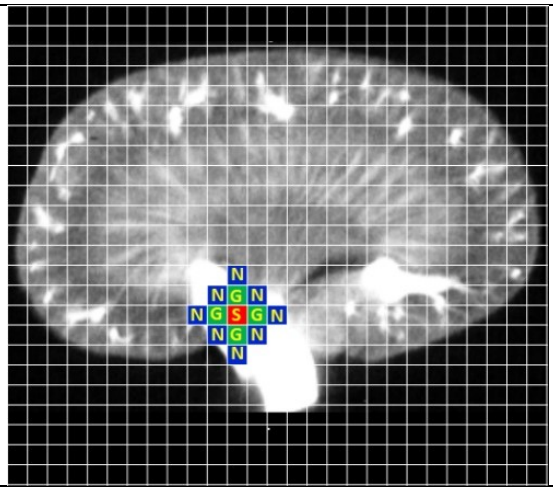
The selected point starts searching in all neighborhood voxels for values of intensity inside the threshold defined.	All neighbors that match the criteria are stored as a part of the geometry intended to be segmented. The search continues in their respective neighborhood of voxels.
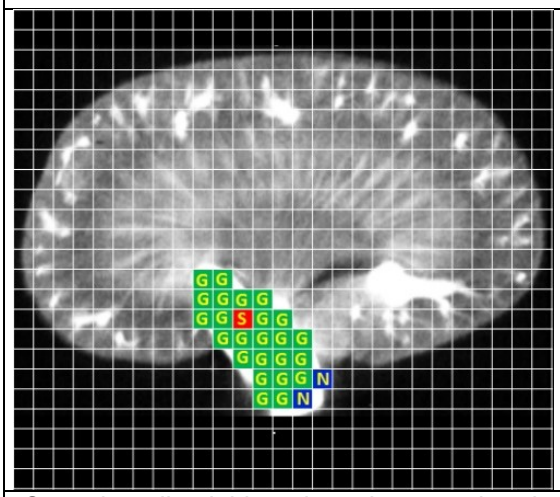	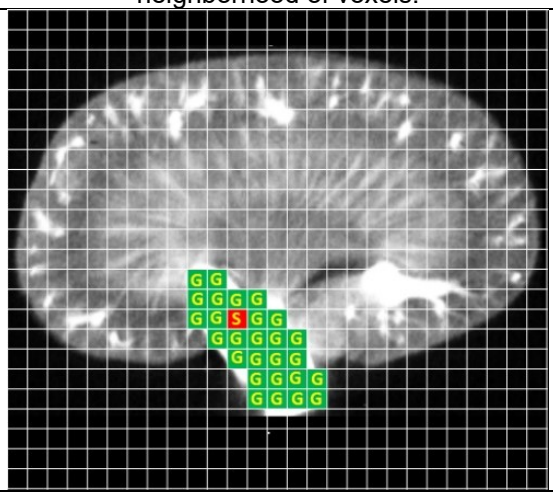
Once that all neighbors have been explored, they keep expanding until only a few neighbors are left to validate in the search. The search is completed once all connected neighbors matching the selection criteria were reviewed and there are no new neighbors to check.	All the voxels that were stored create the volume of the geometry segmented and the contour of this volume is the 3D STL mesh that will be created.

Using this technique, it is possible to create results like the one shown in Fig. 48.

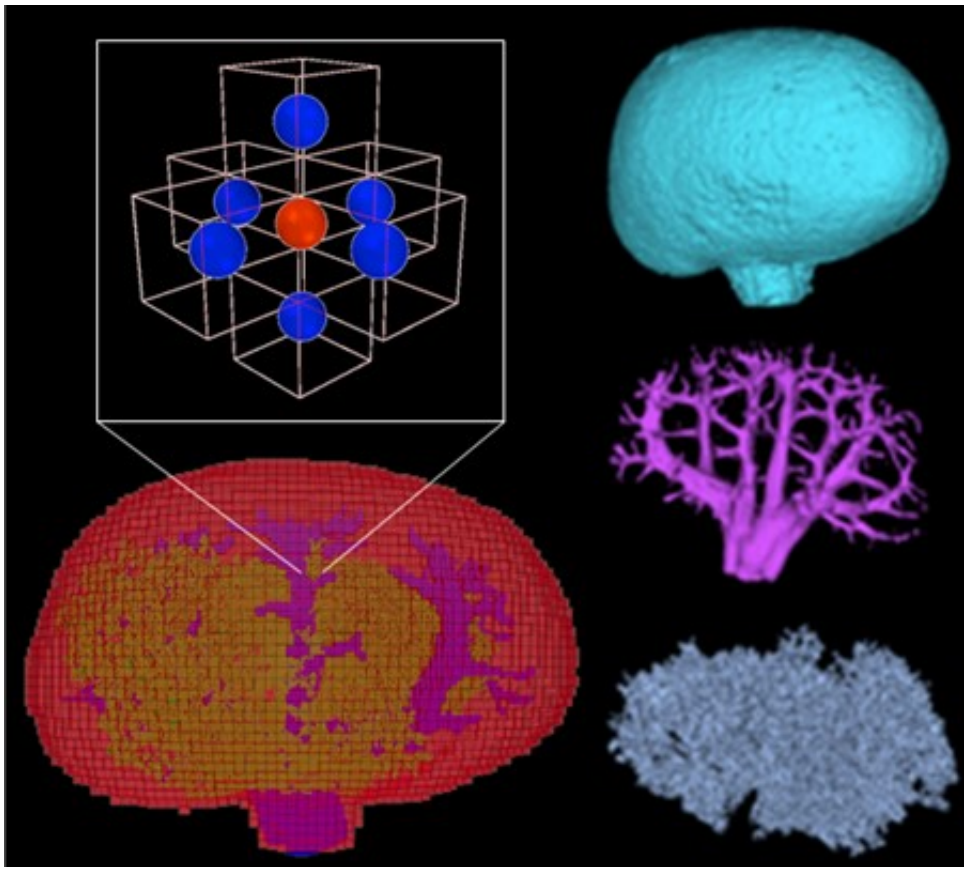

Fig. 48 Segmented parts of a kidney geometry using the proposal approach

Here, the code for the proposed tool for interactive segmentation of medical images based on region growing with a mixture of boundary volumes is presented in Table 10.

Table 10 Code fragment to perform the segmentation by growing region

```
def Segmentation(self,data,point,intensity,tolerance,tmax,tmin,size,
output,xbox,ybox,zbox,rsphere,segmode):
sizex,sizey,sizez = data.shape
ix = int(point[0]*(sizex-1)) #get the index for the point x coordinate
iy = int(point[1]*(sizey-1)) #get the index for the point y coordinate
iz = int(point[2]*(sizez-1)) #get the index for the point z coordinate
valint = intensity*((2**16)-1)
fmin = valint - tolerance*size
fmax = valint + tolerance*size
con1 = data > fmin
con2 = data < fmax
con3 = con1 == con2
mask = np.zeros(data.shape,dtype=np.uint16)
mask[con3] = data[con3] #Add only the data from tolerance of 3D cursor
con1 = data > tmin*((2**16)-1)
con3 = con1
mask[-con3] = 0 #Remain only the data above min threshold
seeds = np.zeros(data.shape,dtype=np.uint16)
seeds[iy,ix,iz] = 1 #define the first seed in iy,ix,iz
grow = 1
indices = np.indices(data.shape)
nextx = indices[0]
```

```
nexty = indices[1]
nextz = indices[2]
count = 0
neig = [-1,0,1]
neigclust = np.zeros((3,27),dtype=np.int16)
for ind1 in range(3):
    sx = neig[ind1]
    for ind2 in range(3):
       sy = neig[ind2]
       for ind3 in range(3):
           sz = neig[ind3]
           neigclust[:,count] = [sx,sy,sz]
           count = count+1
count = 0
while grow == 1: #continue while new seeds remain
    newseeds = seeds==1
    next = [nextx[newseeds],nexty[newseeds],nextz[newseeds]]
    grow = 0
    for seed in range(len(next[0])):
       iy,ix,iz = next[0][seed],next[1][seed],next[2][seed]
       seek = [iy+neigclust[0],ix+neigclust[1],iz+neigclust[2]]
       masksample = mask[seek[0],seek[1],seek[2]]
       seedsample = seeds[seek[0],seek[1],seek[2]]
       a = masksample != 0
       b = seedsample == 0
       c = a*b
       seeds[seek[0][c],seek[1][c],seek[2][c]] = 1 #found new seeds
       if c.any() == True:
           grow = 1
       seeds[iy,ix,iz] = 2 #change current seed into past seeds
    print "Segmentation iteration:", count
    count = count + 1
mask[seeds!=2] = 0
output.put((mask,sizex,sizey,sizez))
return
```

4.7.3 Segmentation boundaries

Even when region growing has good results, it is common to have a leakage problem on this algorithm when having structures near each other and with similar intensities. To solve this problem, a new methodology is proposed in this research work, using interactive segmentation boundaries based on bounding volumes to contain the expansion of the region-growing algorithm.

It was not found in the literature a similar technique for this application, only was found in the segmentation of 2D images for object detection like cars (Mousavian et al., 2017), 2D panoramic pictures (Wu et al., 2017, Yu et al., 2018), and 2D mammographic images (Saeed & Saleh, 2020). In a different approach, it was found totally automated segmentation based on deep learning of neural networks for an area or volume measurements (Alakwaa et al., 2017, Hesamian et al., 2019, Ioffe & Szegedy, 2015, Kawahara et al., 2016, Simonyan et al., 2014).

Therefore, it is considered that this methodology is a novel proposal for interactive semi-automatic segmentation of medical images focused on the creation of quick 3D models.

Based on this idea, it was implemented the semi-automatic segmentation algorithm using region growing with seed selection and bounding volumes, creating a rectangular and spherical shapes. The user is able to change the dimension of the rectangular volume, by controlling length, width and height, and the spherical volume by controlling the sphere radius.

During this search, the algorithm considers that, If the intensity value of the N voxel is inside the threshold set up in the histogram tool and the boundaries selected by the user, it will be appended to a list of voxel's index that will create the volume of the geometry. The process of this proposed methodology for interactive segmentation of medical images performs step-by-step is conceptually illustrated in Table 11.

Table 11 Step-by-step illustration of the segmentation with boundaries

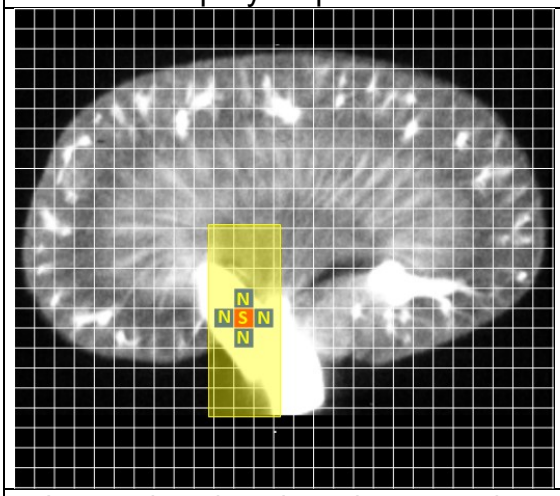	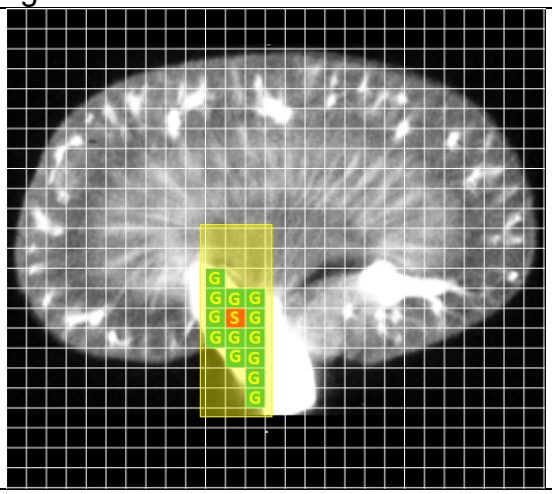
It was selected a point and a rectangular boundary box was defined. As previously implemented, a search in neighborhood starts.	When the search for voxels to be added to the volume of segmentation goes out the boundary box, these voxels are no longer considered.
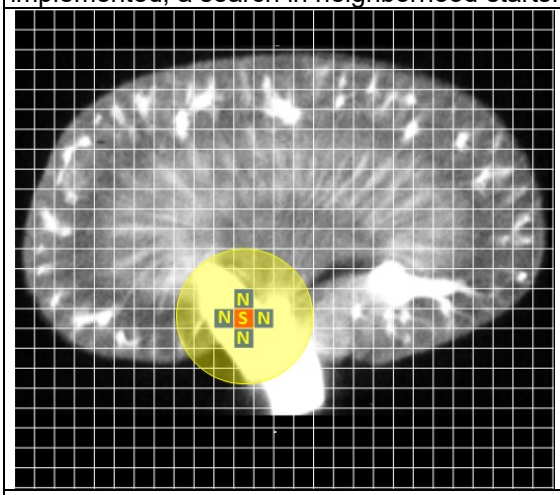	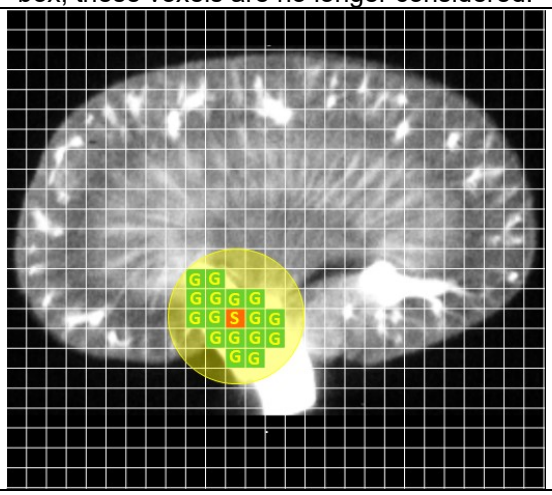
There was selected a point and a boundary sphere was defined. As previously implemented, a search in neighborhood starts	When the search for voxels to be added to the volume of segmentation goes out the boundary box, these voxels are no longer considered.

The dimension of these two volumes can be controlled by the user in order to define what is the specific area of interest to limit its segmentation process. Any voxel outside the boundaries selected by the user will not be considered for the segmentation.

To include this consideration in the segmentation process, the next code was added to the region growing before starting to expand, as shown in Table 12.

Table 12 Code fragment to define segmentation boundaries

```
xbox = xbox*(sizex-1)
ybox = ybox*(sizey-1)
zbox = zbox*(sizez-1)

if segmode == 0:
       segboxx1 = int(ix - xbox/2)
       segboxx2 = int(ix + xbox/2)
       segboxy1 = int(iy - ybox/2)
       segboxy2 = int(iy + ybox/2)
       segboxz1 = int(iz - zbox/2)
       segboxz2 = int(iz + zbox/2)

       if segboxx1 < 1:
            segboxx1 = 1
       if segboxx2 > sizex-1:
            segboxx2 = sizex-1
       if segboxy1 < 1:
            segboxy1 = 1
       if segboxy2 > sizey-1:
            segboxy2 = sizey-1
       if segboxz1 < 1:
            segboxz1 = 1
       if segboxz2 > sizez-1:
            segboxz2 = sizez-1
       mask[0:segboxy1,:,:] = 0
       mask[:,0:segboxx1,:] = 0
       mask[:,:,0:segboxz1] = 0
       mask[segboxy2:sizey-1,:,:] = 0
       mask[:,segboxx2:sizex-1,:] = 0
       mask[:,:,segboxz2:sizez-1] = 0
else:
       xsphere = rsphere*(sizex-1)/2
       ysphere = rsphere*(sizey-1)/2
       zsphere = rsphere*(sizez-1)/2
       xs,ys,zs = np.ogrid[0:sizey,0:sizex,0:sizez]
       xs = xs-iy
       ys = ys-ix
       zs = zs-iz
       mask[(xs**2/xsphere**2 + ys**2/ysphere**2 + zs**2/zsphere**2 > 1)]
= 0
       mask[0,:,:] = 0
       mask[:,0,:] = 0
       mask[:,:,0] = 0
       mask[sizey-1,:,:] = 0
       mask[:,sizex-1,:] = 0
       mask[:,:,sizez-1] = 0
```

4.8 Implementation of *VISUALIX* module

In this chapter, the methodology and development of the tools for visualization, interaction, and segmentation of medical images named by the author of this dissertation "*VISUALIX",* was explained in detail. This module was implemented and tested with an Ubuntu 14.04 computer with Intel Core i7-4510U @ 2.00 GHz x 4, 8 Gb RAM and NVIDIA GeForce 710M.

For the development of *VISUALIX*, the following open-source libraries were used:

- Python 2.7.6
- GDCM 2.2.4
- Pydicom 0.9.9
- wxPython 2.8.12.1
- NumPy 1.8.2
- SciPy 0.13.3
- VTK 5.8.0

The interface to interact with the *VIXUALIX* module was established in a simple way, as shown in Fig. 49. In this way, the objective of this area was achieved, which was to provide the user with a set of interactive and intuitive tools for visualization and segmentation of medical images. This will increase the applicability of the simulation framework and the use of the proposed material model, as well as provide a learning experience.

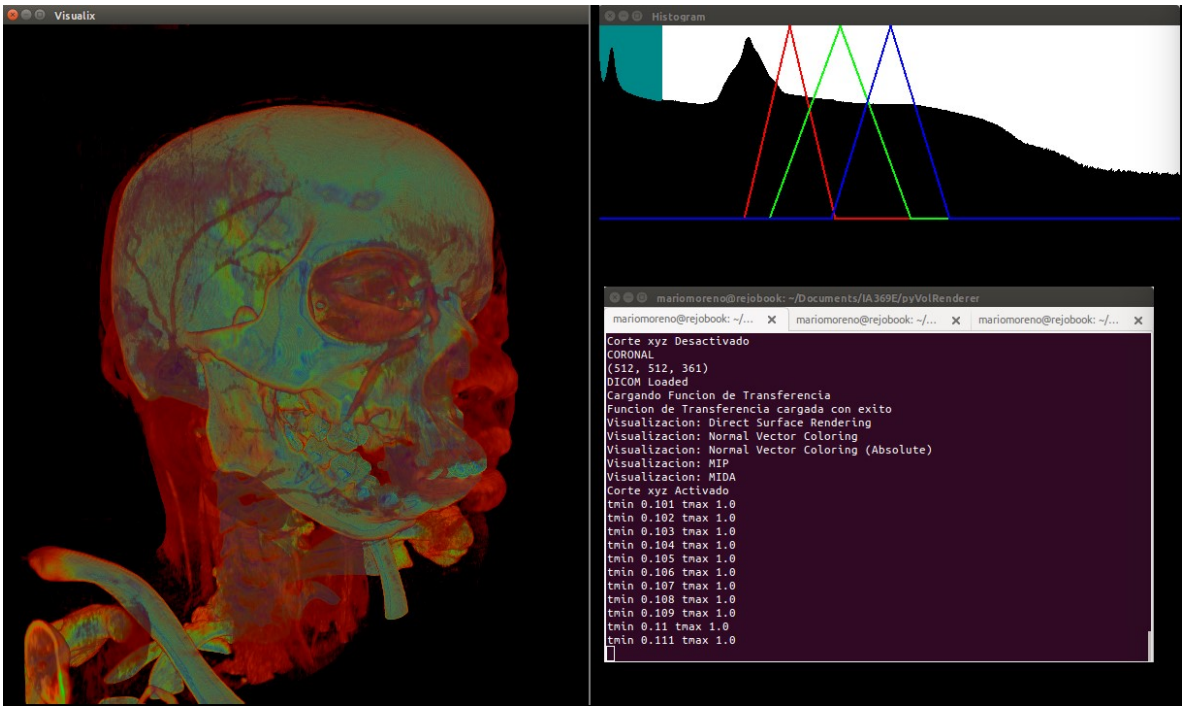

Fig. 49 User interface of the created module *VISUALIX* for interactive visualization and segmentation of medical images showing a Phenix

A set of hotkeys was included in order to provide access to all tools implemented are displayed in Table 13.

Table 13 User interface hotkeys display in the “Help” option

Key	Action or tool activated
-/+	- Zoom Out/In
0	- Activate / Deactivate xyz cutting
1/3	- Increase / Decrease x cut
4/6	- Increase / Decrease y cut
7/9	- Increase / Decrease z cut
5	- Activate / Deactivate multiplanar reconstruction
2/8	- Increase / Decrease position of cutting plane
J/L	- Increase / Decrease azimuth of cutting plane
I/K	- Increase / Decrease elevation of cutting plane
V	- Change of visualization mode
A/S	- Increase / Decrease surface opacity (only in SDR mode)
Z/X	- Increase / Decrease minimum threshold
Q/W	- Increase / Decrease maximum threshold
F	- Change transfer function
R, G, B	- Activate each channel for customized transfer function edition
C	- Deactivate the interaction with any channel for customized transfer function
<->	- Move center on any channel for customized transfer function
^-v	- Open and close the window of any channel for customized transfer function
D	- Save screenshot
E	- 3D cursor cutting
M	- Interactive Segmentation with Bounding Box
N	- Interactive Segmentation with Bounding Sphere
P	- Shows position map
U	- Save last segmented geometry in a stl mesh
Barra	- Selective filtering
T/Y	- Increase/Decrease tolerance for selective filtering & segmentation
Mouse lef button	- Rotation
Mouse right butto	- Define 3d cursor position

The description of features implemented for interaction with the histogram tools can be visualized in Fig. 50. Here, some of the concepts described before are explained in a graphical way for the user.

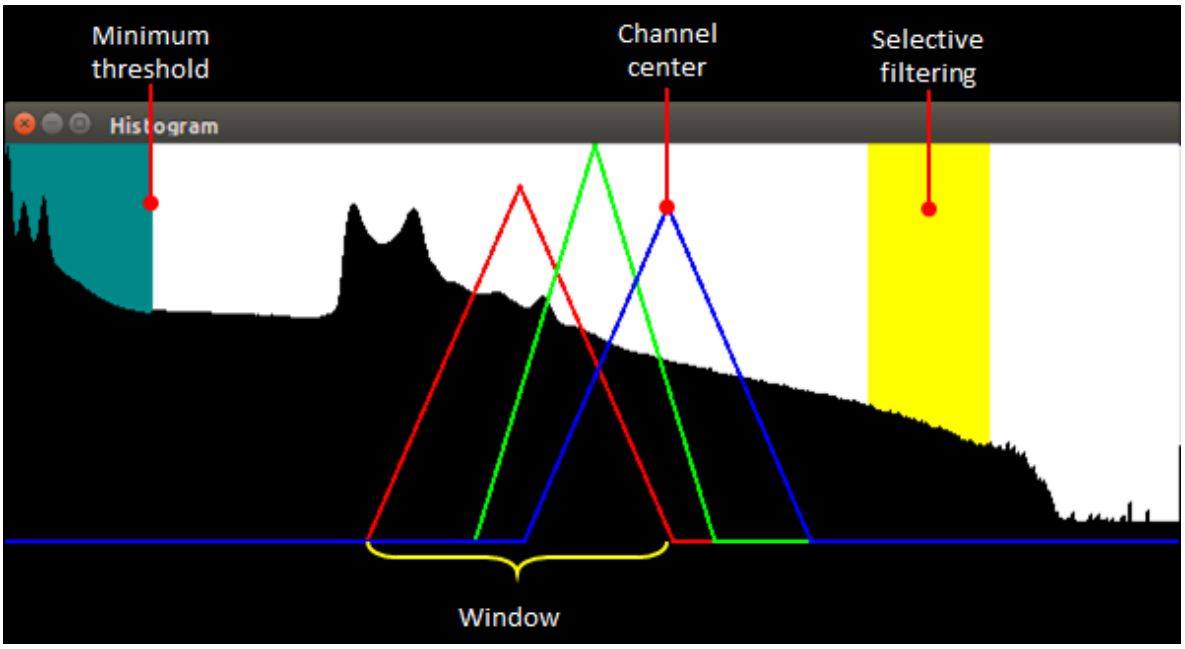

Fig. 50 Description of properties on transfer function channels and threshold

On this module it was possible to define a process for visualization and segmentation of medical images. As an application, it provides the user with tools for visualize in different ways the information obtained from the acquisition of the images.

The implementation for these shaders is included in in the VISUALIX repository (available in Appendix A.2).

4.9 Results of Interactive Segmentation for Geometrical Modeling

In this section, the capacity of *VISUALIX* is presented as one of the results of this research. The main areas included are Visualization, Segmentation, Mesh creation, and Mesh processing.

4.9.1 Visualization results

One of the main functions that provide the module *VISUALIX* is to interact with medical images to create useful visualizations. In the next pages, different examples of how the tools developed can be applied, showing the graphical results, and demonstrating the applicability of this research and implementation process.

For these visualizations, all medical images are cases obtained from the OsiriX sample datasets available at http://www.osirix-viewer.com/datasets/.

A brief description of the visualization intention and tools used to create it is included, providing information on what could be used to apply to that particular set of medical images by a student, a researcher or a surgeon.

Data set: Manix CT DICOM
Source: OsiriX
Visualization with transfer function to allow a detailed focus on bones and vessels

Fig. 51 Visualization of Manix using *VISUALIX* module VDR

Data set: Panoramix CT DICOM
Source: OsiriX
Visualization with transfer function to allow detection of kidneys issues

Fig. 52 Visualization of Panoramix using *VISUALIX* module using MIDA

Data set: Phenix CT DICOM
Source: OsiriX
Sectioned visualization with transfer function to allow review of internal vessels and skull

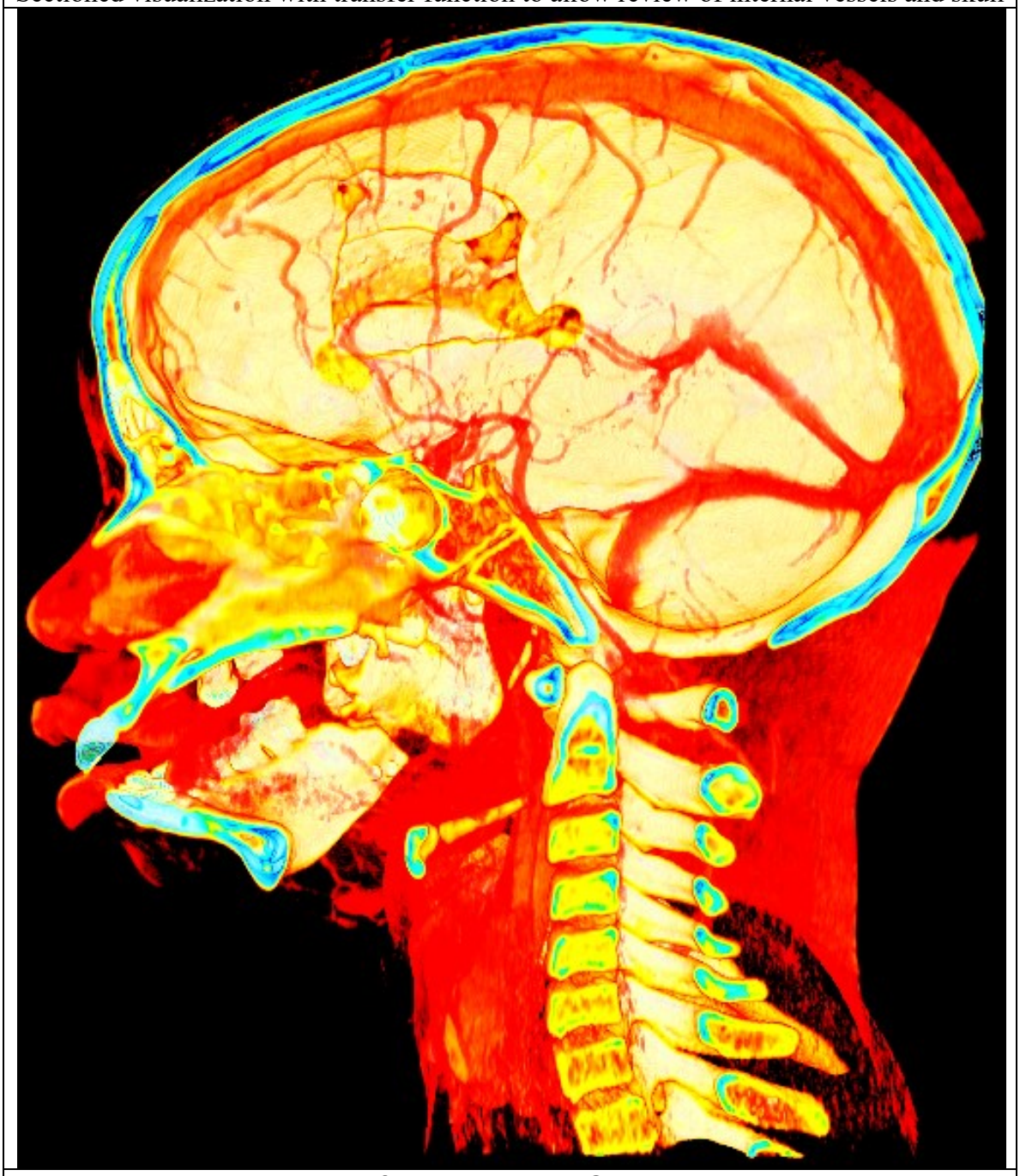

Fig. 53 Visualization of Phenix using *VISUALIX* module with MIDA

Data set: Manix CT DICOM
Source: OsiriX
Sectioned visualization with transfer function to allow review of spine and skull

Fig. 54 Visualization of Manix using *VISUALIX* module with VDR

Data set: Panoramix CT DICOM
Source: OsiriX
Sectioned visualization with transfer function to allow review of spine and Abdomina
Aortic Aneurysm (AAA)

Fig. 55 Visualization of Panoramix using *VISUALIX* module with VDR

Data set: Magix CT DICOM
Source: OsiriX
Visualization with transfer function to allow view of the heart, veins and arteries

Fig. 56 Visualization of Magix using *VISUALIX* module with VDR

4.9.2 Segmentation results

All three ITF allows interaction with the histogram to define position and window level, and it is possible to save and load configurations previously created.

Using the 3D cursor position and before starting the region growing process, was included a step to define a box or spherical boundary with dimensions controlled by the user (Fig. 57 and Fig. 58).

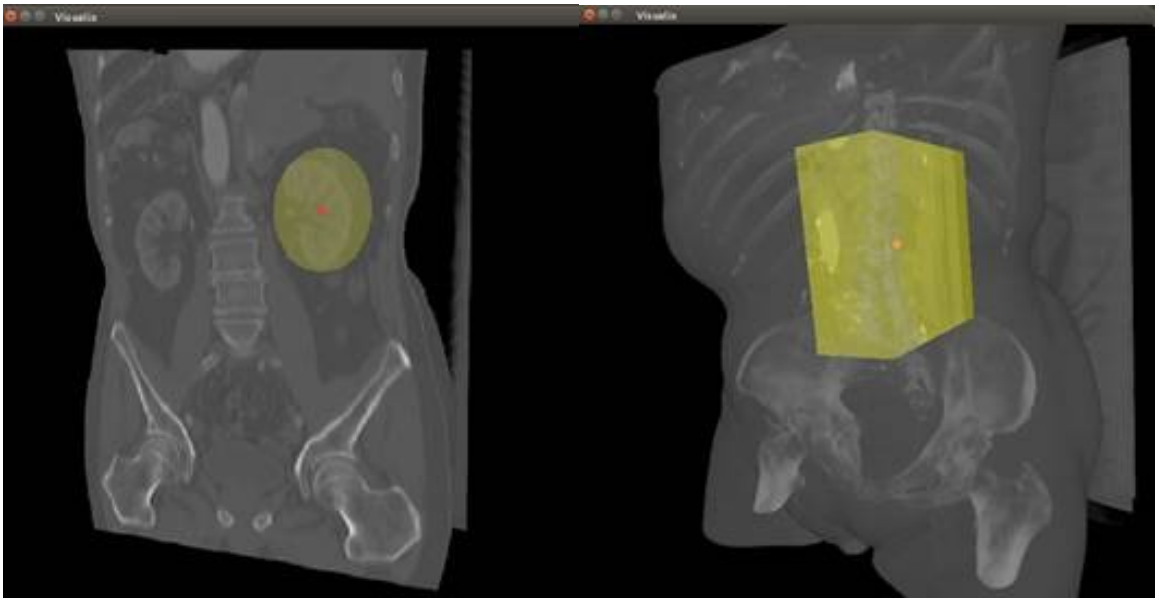

Fig. 57 Interactive segmentation with box and spherical boundary on Panoramix

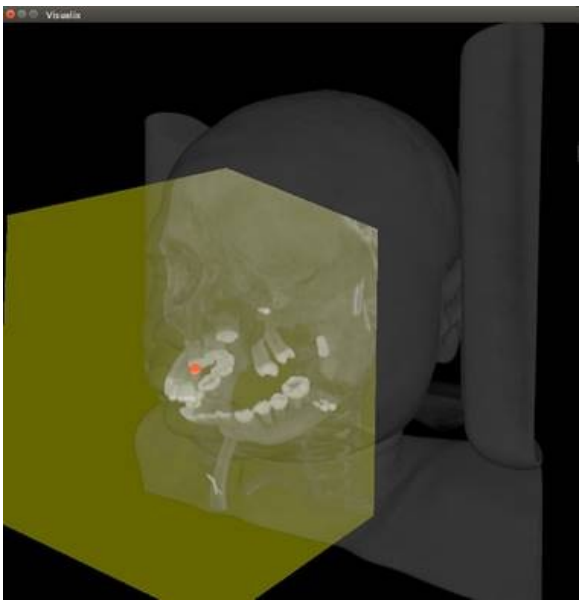

Fig. 58 Interactive segmentation with a rectangular volume as a boundary on Phenix

With this, it is possible to establish or delimit a maximum space that the segmentation can grow and therefore help to avoid the problem of leaking into not desired objects or anatomical structures.

It is possible to get really detailed geometries like the one shown in Fig. 59 or complex geometries like the one shown in Fig. 60.

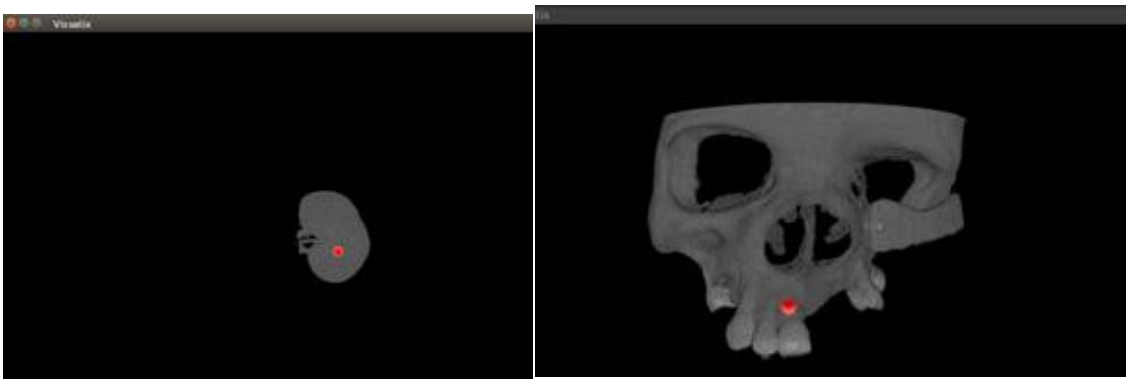

Fig. 59 Visualization of the segmented geometry

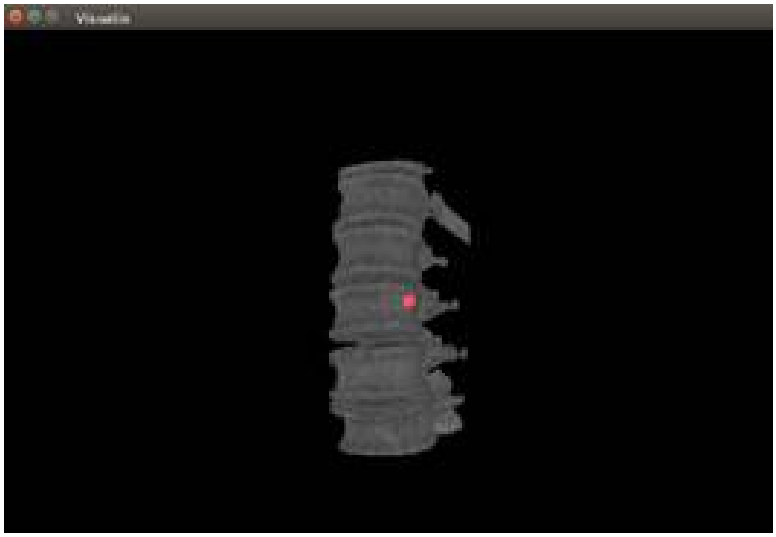

Fig. 60 Visualization of the segmented geometry

4.9.3 Mesh creation for the geometric model

One of the main interests in the segmentation of medical images is the possibility to generate a mesh of a particular structure. This is because even when all previous processes were done only for visualization, they can be used to create geometric models with several applications, such as 3D printing, prosthesis design, simulations, and surgical planning, among others.

With this in mind, it was included a tool to create a 3D mesh of triangles from segmented data by using marching cubes and a smoothing algorithm (on VTK). This mesh is exported in stereolithography (STL) format, which is widely supported by 3D printers and a lot of different software for processing (Fig. 61 and Fig. 62).

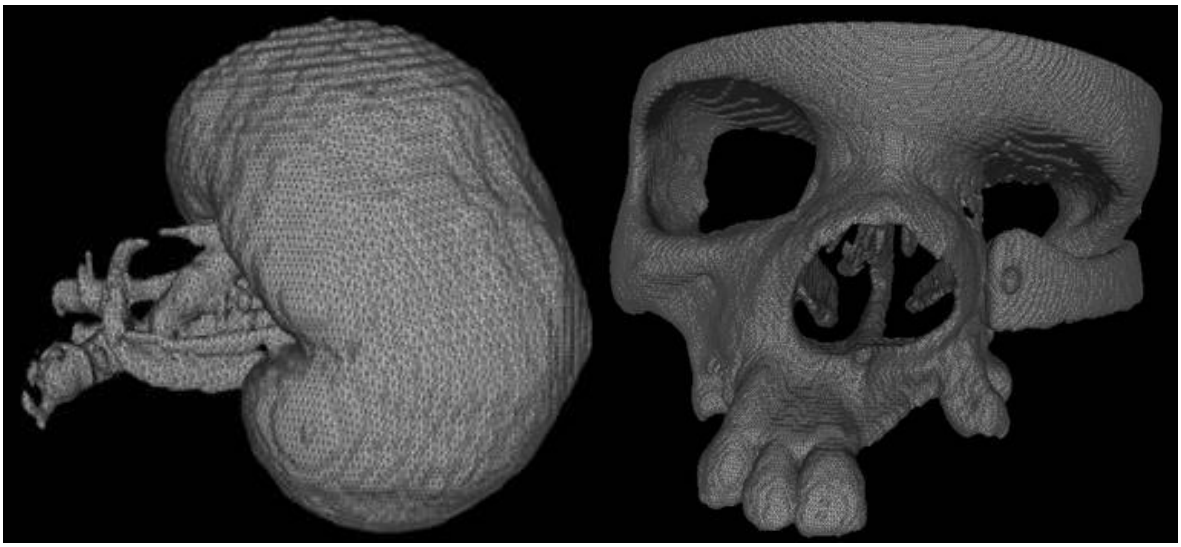

Fig. 61 3D mesh of segmented geometries on STL for a kidney and a skull

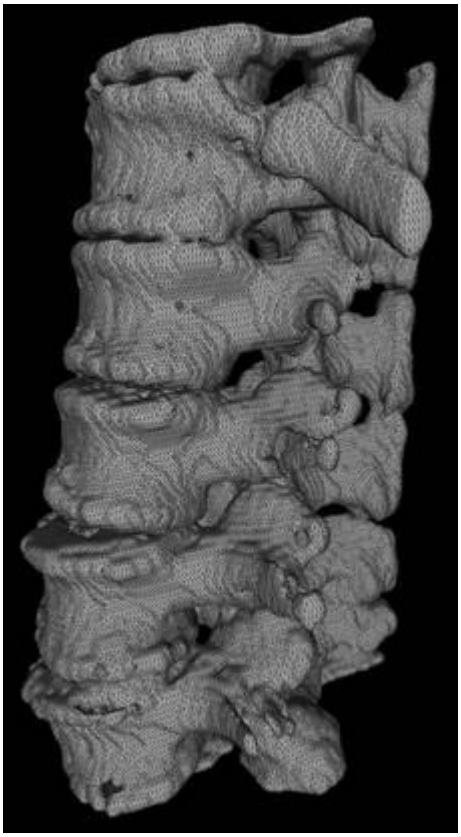

Fig. 62 3D mesh of segmented geometries on STL for a spine

4.10 Contributions of the proposed methodology

The implementation of the VISUALIX module for interactive visualization, processing, and segmentation of medical images not only represents a contribution to the applicability of the simulation framework, but is a development by itself.

VISUALIX can provide open-source support for the visualization of medical images to students, researchers, and surgeons. The user can not only visualize anatomical structures but interact in an easy way with the visualization and create segmented geometries of the desired structure. This segmented geometry can be exported as a 3D mesh in STL file format, using the proposed methodology for quick interactive segmentation.

At this point, *VISUALIX* can be used to create 3D models and geometries that support multiples applications, for example:

- Real-time interactive simulation:

  The proposed method allows the user to create 3D models that can be used with the real-time simulation framework to interact with and apply the proposed material model. This removes the limitation to only one geometry developed in previous works and increases the applicability of this research for any new case that can be provided with medical images.

- Medical training:

  Visualization of medical images and specific study cases in open-source software can allow medical students and staff to train for diagnosis, anatomical knowledge, and understanding of specific patient diseases.

- Virtual surgical planning:

  Provided visualization and interaction tools can be used by a surgeon to study a particular case that will perform surgery in a near future. This can allow the doctor to plan access, technique, assessment of risks, and potential complications. With this tool, the surgeon could decide to segment a geometry and perform a simulation with the proposed framework or print the patient geometry for its physical manipulation and practice.

- Design of biomedical devices based on anatomical geometry:

  To create new devices in the biomedical field, it is usually required to have a base geometry to use as a representation of the human anatomy. These are usually obtained by the collaboration of experts in medical imaging, but now it could be possible to use *VISUALIX* by non-medical trained professionals.

This module creates computational tools that can be used by engineers, designers, product owners, and researchers, among others, in an open-source approach.

This allows acquiring anatomically realistic geometry to base their design or to perform its validation in an easy and inexpensive way.

- CAE simulation for validation of products and testing:

3D models created from medical images using *VISUALIX* can be used for studies and research for the validation of biomedical products, testing, and analysis of the impact of certain conditions. These can be simulated using CAE commercial software for FEA.

Usually, the process to get an anatomical model requires interaction with an expert in medicine, scanning a physical sample or using a representative design modeled based on sculpturing. This can be avoided by the usage of medical images and segmentation tools like *VISUALIX*.

- 3D printing of anatomical geometries:

STL files can be used to create rapid prototypes of the anatomical geometries and structures of interest with additive manufacturing. This could be done for academic, research or surgical planning purposes.

4.11 Scientific relevance of this work

In order to define the scientific relevance of the proposed methodology for interactive segmentation, it was performed a review of recent works found in the literature. A detailed comparison with the state-of-the-art is presented below.

The methodologies found in recent works have a focus on deep learning techniques based on neural networks, stating that it is of great relevance and the future for segmentation of images (Alakwaa et al., 2017, Hesamian et al., 2019, Kawahara et al., 2016, Shrivastava et al., 2020). With this approach, the objective is to create a fully automated trained system that does not require user interaction to perform the segmentation of medical images.

The results presented by these works are highly relevant for the generation of artificial intelligence tools, machine learning, neural networks, and deep learning techniques. These results could be compared with the one presented in this dissertation by two main points: 1) user interaction and 2) data needed for development.

4.11.1 User interaction

The application of neural network methods is linked to the diagnosis of conditions through volumetric measurements of anatomical structures and the detection of anomalies (Alakwaa et al., 2017, Kawahara et al., 2016). Also, it includes research to correlate geometric dimensions of structures with specific diseases, monitoring of the evolution of detected cases, and effectivity of treatment to reduce the volume of anomalies, among others (Hesamian et al., 2019, Ioffe & Szegedy, 2015, Simonyan et al., 2014).

The methodology proposed in this dissertation is based on semi-automated algorithms, which focus on interaction with the user to give a set of inputs. Then using those specific inputs, it performs the process for which the algorithm was implemented, that is to segment the anatomical structures intended by the user.

The main objective of this implementation is to give the user tools to process, select, constrain, and segment medical images. This methodology used concepts such as thresholding filtering, 2D-3D selection using raycasting position map, and region growing, similar to those applied by other works (Bayazit 2019, Bennai et al., 2020, Lu et al., 2014, Singarayan et al., 2018, Xi et al., 2014, Yuan et al., 2015). Therefore, there have been recently relevant developments using region growing as an alternative of deep learning techniques.

The methodology for semi-automatic segmentation proposed in this dissertation was based on a region-growing algorithm with seed selection, applying bounding volumes to constrain the expansion. This methodology has not been found in the literature.

Recently has been published works with a similar approach using bounding boxes for segmentation of 2D images to detect objects like cars in movement (Mousavian et al., 2017), 2D panoramic pictures (Singarayan et al., 2018, Wu et al., 2017, Yu et al., 2018) and 2D mammographic images (Saeed & Saleh, 2020). However, it has not been applied for semi-automatic segmentation of medical images to create 3D models.

It is important to remind that the application of the proposed methodology in this dissertation is not the total automation of the segmentation process. Also, it is not the detection of anomalies in patients. Particularly, it is not to perform volumetric measurements that can support the diagnosis of diseases, raising the concern towards human error reduction to avoid false negatives/positives, and searching to improve the accuracy and standardize the process. Especially, it is not to generate a system that does not require interaction with the user, but quite the opposite.

The proposed methodology is intended for the creation of 3D models that represents an anatomical structure that is geometrically realistic, in a short time and with relatively little effort for the user. The visualization and interaction with the user are fundamental since this application has training, academic, and knowledge development purposes. This goal would be lost by having a fully automated system that does not allow or require interaction with the user.

4.11.2 Data needed for development

For the development of deep learning techniques, it is required a large amount of data previously labeled manually for “training” of the system. Later, it must be validated with experiments using another set of data. This data set must be different from those used for system training in order to be able to detect how accurate the system performs with new data.

Among recent developments of deep learning techniques for fully automated segmentation, it was required:

- 1,300 sample images for training (Kawahara et al., 2016).
- 248,580 sample images for training (Alakwaa et al., 2017).
- 1.3 million images for training, additionally 50,000 images for validation, and 100,000 images for testing (Simonyan et al., 2014).
- Up to 10,000,000 previously tagged images for neural network training using another 150,000 for validation and testing (Ioffe & Szegedy, 2015).

The training time is variable. In a particular case, it required from 12 - 18 weeks (for 6 neural networks) using equipment with 4 NVIDIA Titan Black GPUs (Simonyan et al., 2014). Another case required up to 30,000,000 training steps (Ioffe & Szegedy, 2015).

The algorithm proposed and implemented in this dissertation does not require a training process, as it is a semi-automated algorithm that allows interaction with the user. In fact, the interaction is a fundamental part of the objective of the creation of these tools. Therefore, the methodology and techniques proposed and implemented in this dissertation simplify the development process, fulfilling the objective of creating segmentation tools for the application that is intended.

With these points, it can be determined that the methodology proposed in this dissertation is focused in a different direction than others found in the literature (Abdallah et al., 2015, Alakwaa et al., 2017, Fajar et al., 2020, Hesamian et al., 2019, Kawahara et al., 2016, Shrivastava et al., 2020, Williams & Drew, 2019). All with their respective relevance, applicability, and scientific contributions.

4.12 Microtomography images for material characterization

During this research, it was identified an opportunity to apply microtomography images for modeling and characterization of composite materials. Initial developments and preliminary results are presented in this dissertation, but it is left for future works to fully apply this concept with the tools that were created in this research.

As it will be explained in more detail in chapter 5, to model the behavior of tissues it can be considered as a composite material. This considering that the mechanical properties of soft tissues are related to their cell composition, which gives these materials non-uniform properties.

In this work, tissues were considered as a material composed by a filling matrix with an isotropic behavior mixed with a volumetric fraction of reticular fibers that provides a resulting non-linear anisotropic behavior. This composite construction of the soft tissue can be compared with the fractal structure found in other biological materials, like the trabecular bone structure that can be segmented from microtomography images, shown in Fig. 63.

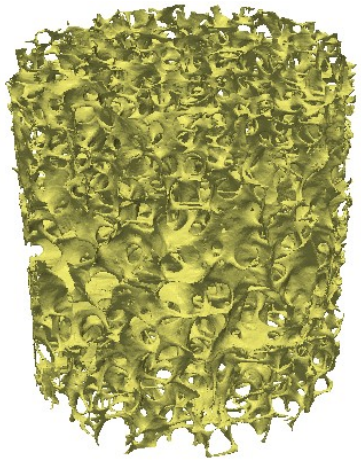

Fig. 63 Fractal structure of trabecular bone sample obtained by segmentation of microtomography images.

If the fractal structure can be segmented from the microtomography images, therefore its main characteristics and principal directions can be analyzed to define its influence on the mechanical behavior. Also, it could be applied for soft tissue characterization, considering it is relevant to know the fiber volumetric fractions and orientations, as well as the contribution of these fibers to the general behavior of the material.

It was reviewed in the literature for current state-of-the-art techniques used for the fractal analysis (Alomari et al., 2017, Chappard et al., 2015, He & Ain, 2020, Korolj et al., 2019, Gómez-García et al., 2020). It was found that these techniques are applied to specific cases, and do not correlate the geometrical structure for distribution of the mechanical properties in a simulation mesh nor evaluate its contribution to the anisotropic behavior.

In this case, microtomography images of a rat kidney processed are used as a reference case to illustrate the concept (see Fig. 64). Other materials and organs could be used to study their geometrical composition and structure.

It is important to mention that these images are from a rat kidney, to understand the level of microscopic detail that can be achieved by microtomography and its superiority to other imagining techniques. Also, this procedure can be used not only for biological material but also could be used to scan the internal structure of a composite material with nanoparticles, ceramics, and geological materials, among others.

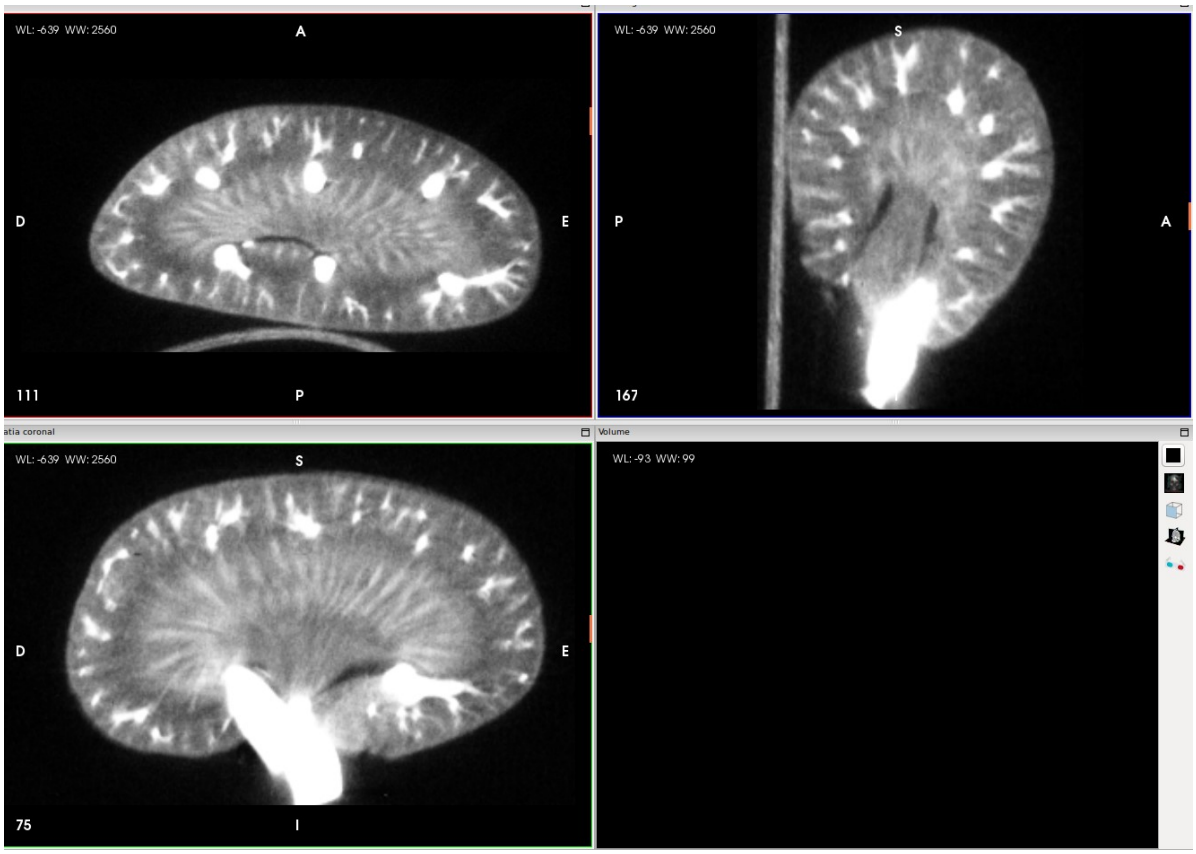

Fig. 64 Rat kidney Microtomography

It is possible to generate illustrative geometries of the generalized kidney composition into three main groups (as shown in Fig. 65) of phases with different materials/cells/components and consequently represent direct contributions to the anisotropic behavior of the whole body and material. For this case, these were classified as capillaries, parenchyma, and fibers.

Fig. 65 Virtual segmentation of a composite material based on Microtomography

Each of these phases has a volumetric fraction in the composition of the organ or sample to be simulated and, therefore, they have to be calculated and studied as a function of the percentage of the total volume of the segmented images. Doing

segmentation of each phase is something that can be achieved using the *VISUALIX* module developed in this research project.

The model of the organ or a sectioned sample of kidney tissue (see Fig. 66) should be studied considering it to be composed of:

- Volumetric fraction f_1 of capillaries
- f_2 volumetric fraction of fibers
- Volumetric fraction 1 - f_1 - f_2 of parenchyma

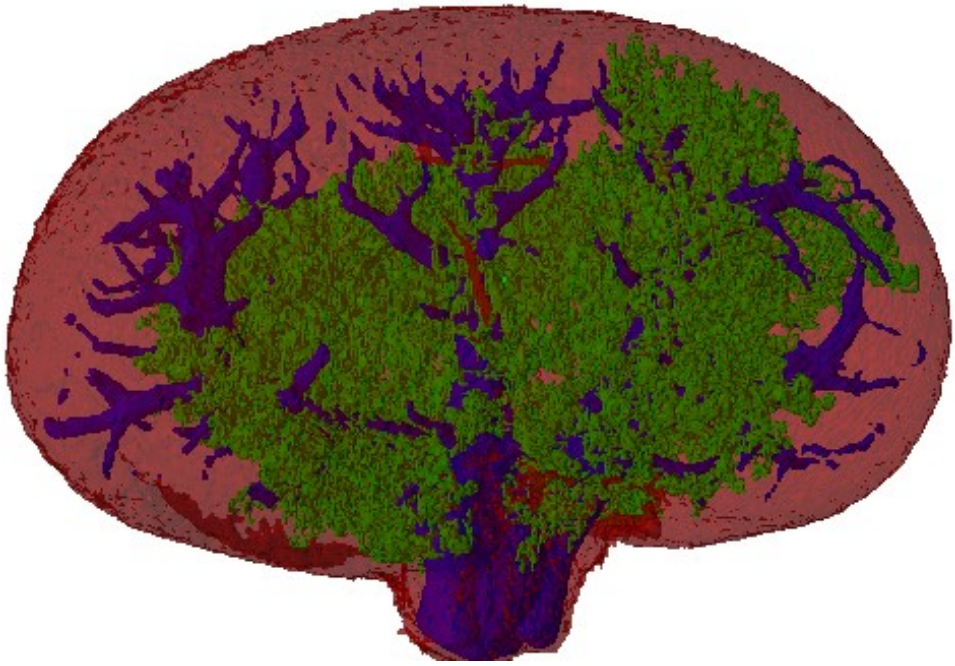

Fig. 66 Virtual internal structure of a composite material based on Microtomography image processing

If the segmentation of these volumetric fractions can be done, why not can be determined the main direction and orientation that these structures have and how they contribute to the mechanical properties?

This was the question that started a review of the fractal analysis and how can be used to characterize the mechanical behavior of the materials. Being able to determine the main directions $\boldsymbol{ai}$ for each volumetric fraction $\boldsymbol{f_i}$ found in a particular material in function of its fractal structure, allows to represent the sample composition and the material in general. This information is normally lost when simplifying the modeling, characterization, and simulation process of composite materials with internal structure.

Using this concept, it is possible to create tools to determine the composition and orientation of any section that can be taken from this non-homogeneous material.

Therefore, it could be possible to represent how these different phases/fractions interact and how are distributed in the sample that wants to be characterized.

By analyzing this fractal composition, it is possible to have a map of the particular distribution and orientation of certain composite materials, as conceptually presented in Fig. 67.

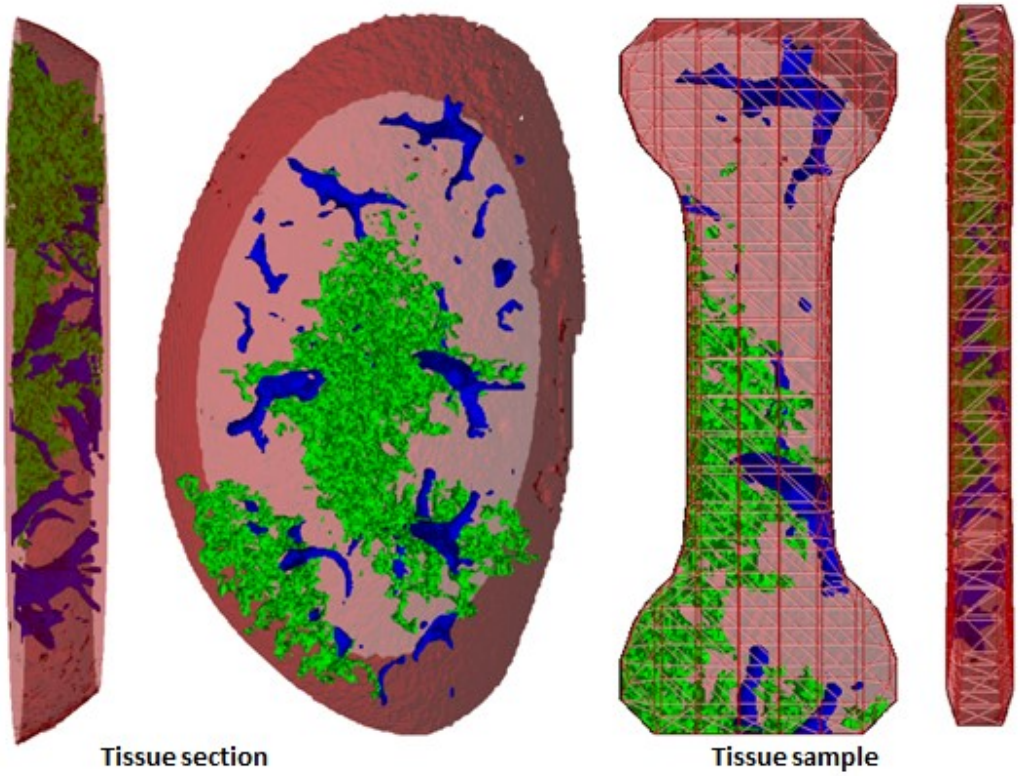

Fig. 67 Virtual internal structure of a tissue section and tissue sample from a kidney created by segmentation of Microtomography images

Using a virtual sample composition, a volumetric mesh formed by uniform tetrahedral elements can be generated, which will be used for real-time simulation of the behavior of the soft tissue with the fractal structure data extracted from the images.

Now, in current simulation processes, when performing the discretization and using a surface mesh to represent the geometry, the structural composition of the simulated object would be considered homogeneous, and the material properties would be applied in the same way to all elements, regardless of the material composition, the internal fractal structure and main direction of its fractions (particularly in biological materials, like organs and bones).

In this project, the hybrid EESM model was developed for one-dimensional elements. In the case of volumetric elements, a similar formulation was generated starting from the construction of stiffness matrices of the tetrahedral elements generated from the

original geometry, calculating the parameters that lead the model to an energy equivalence.

With this proposal, the energy equivalence would be using information from the structural composition of the material to consider the distribution of the stiffness and mechanical properties in the simulation mesh, as shown conceptually in Fig. 68.

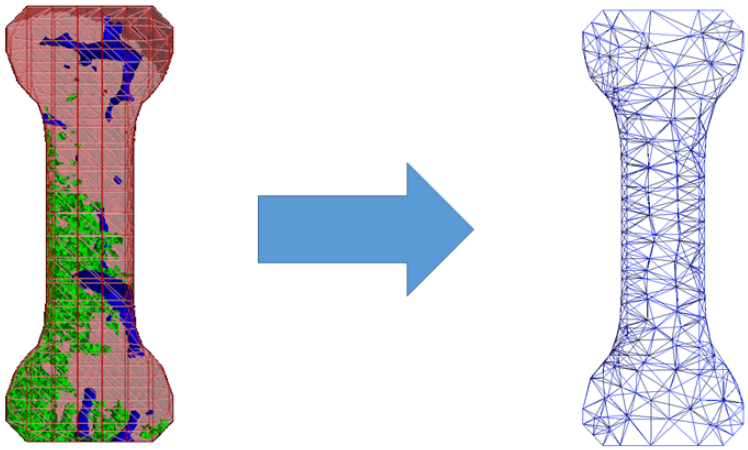

Fig. 68 Mesh considers homogenous material based on the experimental data

Using the volumetric formulation, it is possible to assemble the global matrices from the ones of each element and the relationship between the degrees of freedom in the tetrahedron mesh. Based on Hooke's law and using said global matrices, the effort for each element can be calculated and subsequently the deformation using the stiffness matrix.

Using this formulation and the appropriate parameters in the main directions, different behaviors can be obtained that can represent the anisotropic characteristics of tissues in an organ (as shown in Fig. 69).

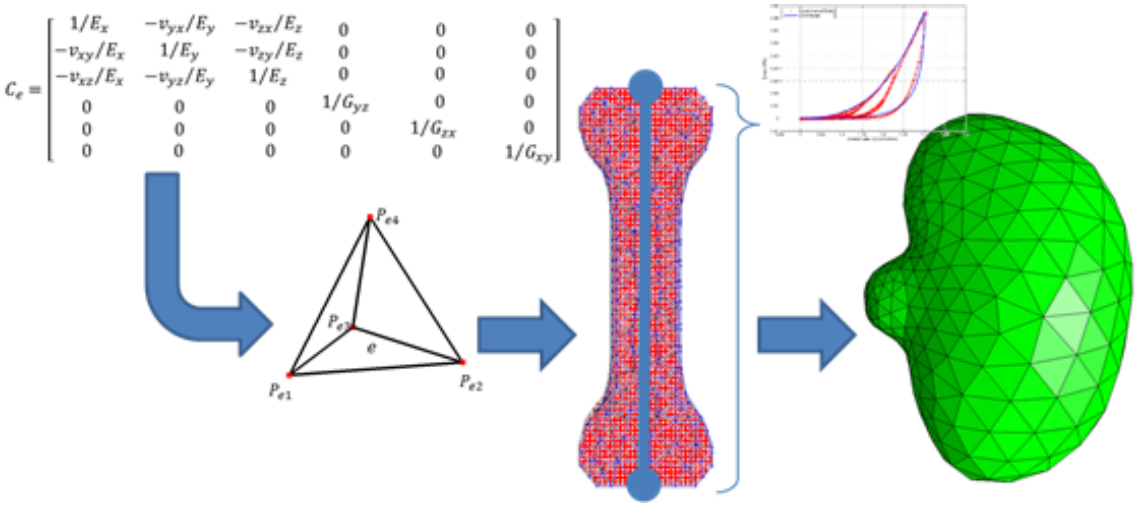

Fig. 69 Current process to simulate mechanical properties on volumetric elements

By using the proposed method, which is called by the author of this dissertation as a fractal map, it is believed that is possible to use this information as parameters to determine the distribution of the stiffness and its contribution to the anisotropic behavior of the material. The idea is to use the variations in the intensity of microtomography images to analyze and measure the curvature and direction of the fractal structure in the organ, tissue, or material sample.

With this in mind, it is possible to make a comparison of the intensity for each voxel and its vicinity in the reconstruction of the fractal structure with the images (as shown in Fig. 70), in order to weight the main direction where the intensity is increased and thus represent the orientation angle of the structure.

Using the information on the proportion of the main directions, the Young E modulus can be weighted for each of the directions $\{\boldsymbol{E_x}, \boldsymbol{E_y}, \boldsymbol{E_z}\}$ to define its contribution to the global matrixes. This would be called the Equivalent Stiffness Matrix and it could define the behavior for a particular voxel and allow to calculate the average of the voxels that conforms an element, being included in its local array.

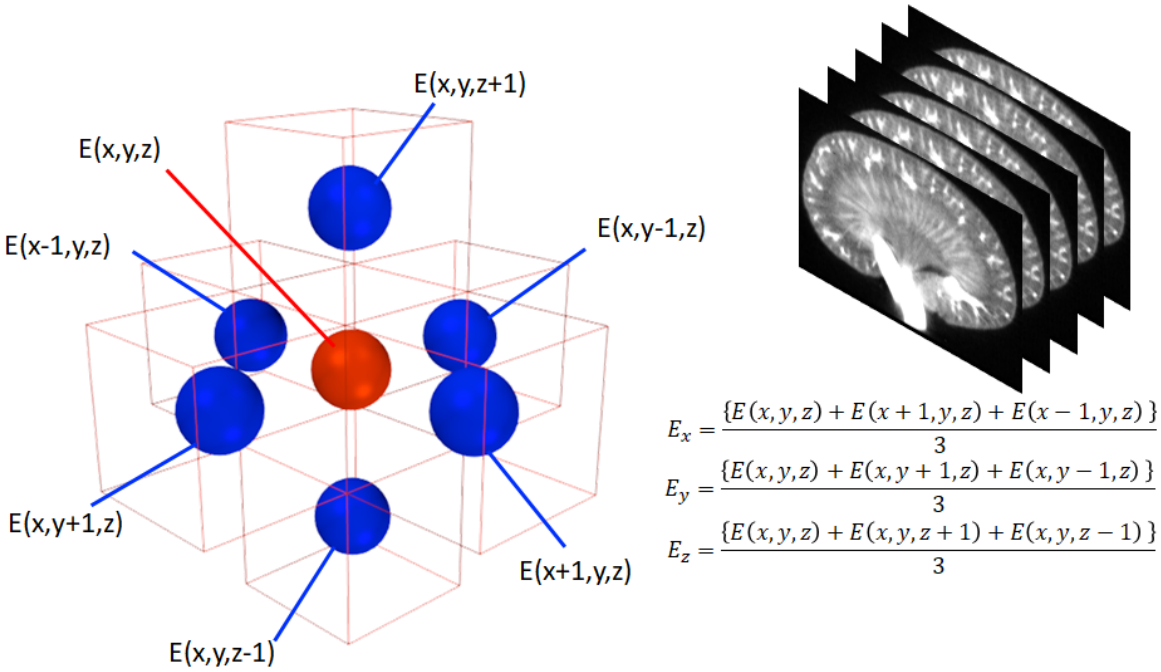

Fig. 70 Ponderation method for the principal direction of each voxel using the neighborhood

The proposed method was implemented in an algorithm developed using Python, NumPy, and OpenGL, in order to generate the main direction data that will be stored in matrices for each voxel to be loaded in the simulation in real-time by weighting Young's modulus (*E*) to define the Equivalent Stiffness Matrix in a volumetric mesh, as conceptually described in Fig. 71.

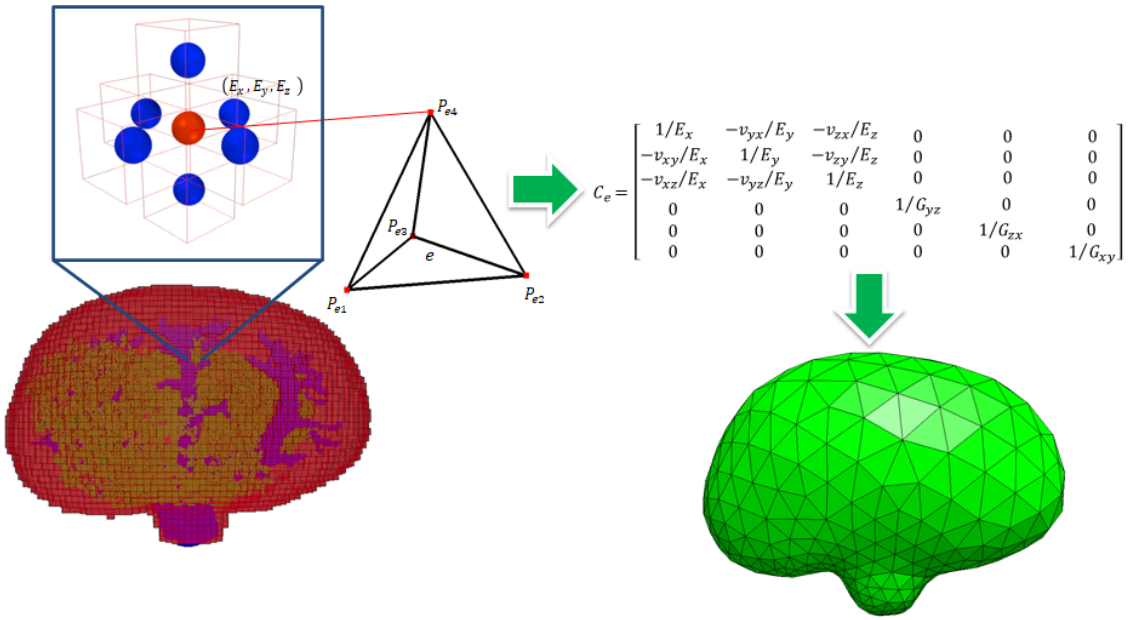

Fig. 71 Process to define Equivalent Stiffness Parameters for each node in the volumetric element formulation

4.12.1 *FractalCells* module for Interactive Fractal Analysis

Using the *VISUALIX* module, anatomically realistic geometrical models were created, using the interactive semi-automatic segmentation algorithm proposed and implemented. These models are intended to create a simulation mesh to calculate its deformation, and it is possible to process the geometry to create one-directional or volumetric elements.

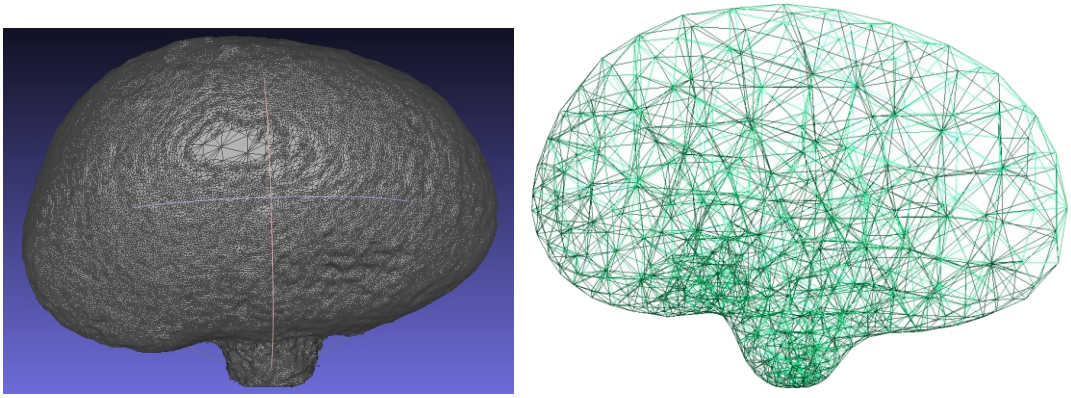

Fig. 72 Simulation mesh created from the segmented model (volumetric elements)

The proposed method for ponderation of mechanical parameters using microtomography images for the volumetric formulation was initially implemented using the *VISUALIX* module. This idea was used to develop a new module called *FractalCells (name proposed by Dr. Alex Elías-Zúñiga)*. This module is intended to provide interactive tools for analysis of the fractal structure on biological and composite

materials based on microtomography images (scripts available online in the *FractalCells* repository included in Appendix A.2).

The process for calculating and visualizing the main directions of the fractal structure was implemented using OpenGL Shading Language. The first and second derivatives in the microtomography images were calculated, generating the normal vector and direction vector of the material structures. These are calculated at each voxel as a function of the intensity of the neighborhood, similar to the way it was calculated to visualize the SDR in 4.4.2.

In Fig. 73 it is included the first and second partial derivatives, using the {x,y,z} values of the vectors displayed in RGB, representing the gradient and curvature of the fractal structure. The result of this process is the calculation of unitary direction vectors at each voxel that represent the direction cosines of the fractal structure.

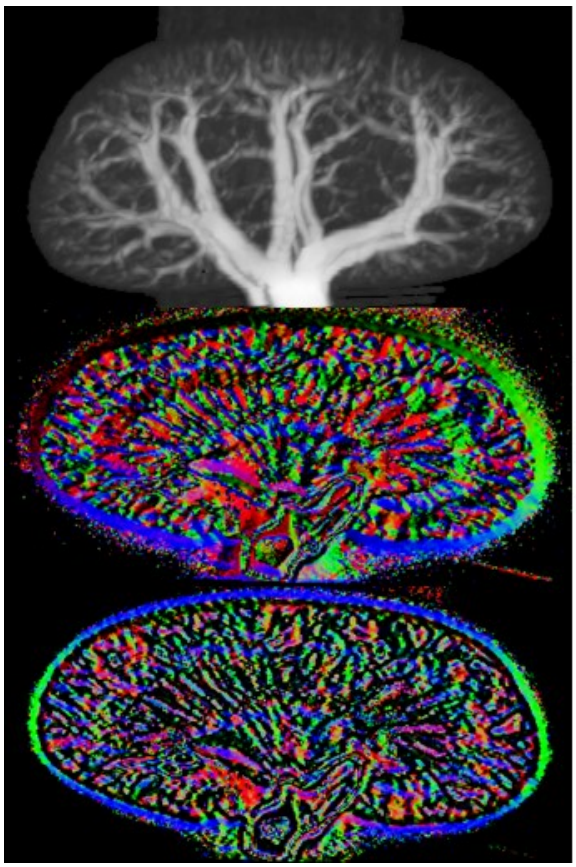

MicroTomography image

First partial derivative (gradient)
To obtain the normal vector of each voxel

$$f' = \left[\frac{\partial f}{\partial x}, \frac{\partial f}{\partial y}, \frac{\partial f}{\partial z}\right] = N$$

Second partial derivative (curvature)
To obtain the main directions per point

$$f'' = \left[\frac{\partial f'}{\partial x}, \frac{\partial f'}{\partial y}, \frac{\partial f'}{\partial z}\right] = C$$

Fig. 73 Microtomography image used to calculate the first and second derivative of the rat kidney structure

This proposed technique is used to generate a 3D texture with the direction vectors coordinates {x,y,z} used as an RGB color at each voxel (as shown in Fig. 74). This 3D texture was called a fractal map, and it represents the direction of the fractal structure per voxel, which has a direct impact on the material properties.

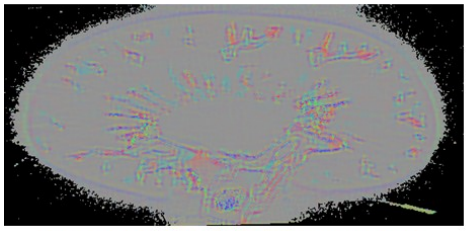

Anisotropy map based in the internal structure

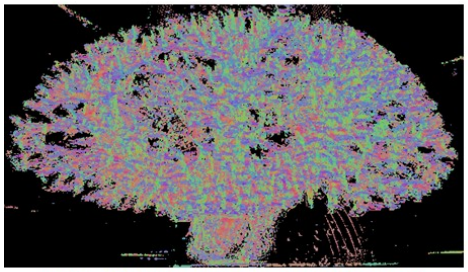

Principal directions vector used as RGB per Voxel

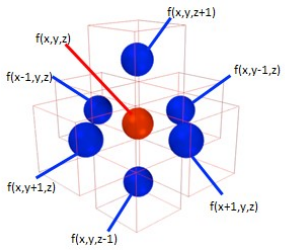

Process to calculate the unit vector for ponderation

$$a_x = \{f(x,y,z) + f(x+1,y,z) + f(x-1,y,z)\}$$

$$a_y = \{f(x,y,z) + f(x,y+1,z) + f(x,y-1,z)\}$$

$$a_z = \{f(x,y,z) + f(x,y,z+1) + f(x,y,z-1)\}$$

$$a = \frac{[a_x, a_y, a_z]}{\|a_x, a_y, a_z\|}$$

The unit vector ***a*** that weights the proportion of the principal directions of the intensity of the Voxel

Fig. 74 Map of the rat kidney fractal structure based on principal directions (vectors values for {x,y,z} are represented as a color combination of RGB)

The results of the principal directions of the fractal structure are calculated for each voxel using the images and can be viewed in any section of the organ (see Fig. 75).

Then, all red spots in Fig. 75 can be considered voxels where the fractal structure has a direction vector mainly oriented on X-axis, green voxels would represent an orientation on Y-axis and blue spots on Z-axis. All intermediate colors were removed since represent that there is no principal direction on the X, Y, and Z-axis.

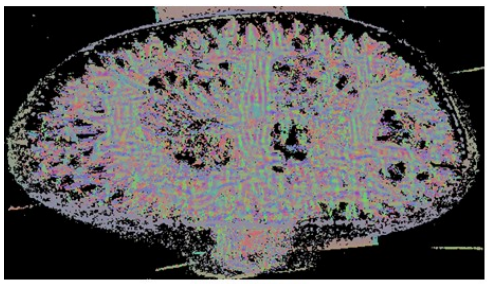

FRONT VIEW

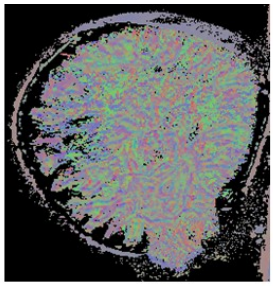

SIDE VIEW

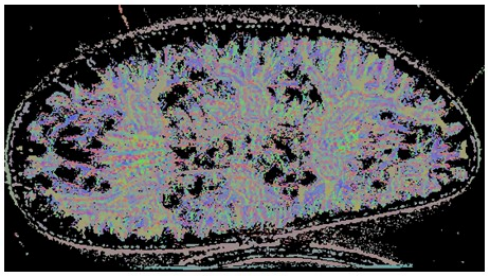

TOP VIEW

The information calculated is stored in a matrix for each voxel and it can be used to weight the elasticity module and calculate the volumetric fraction.

Fig. 75 Sections views of the rat kidney fractal structure, showing the vector for the principal directions {x,y,z} as RGB per voxel

This proposed method can be used to calculate the main directions of material samples, such as in the case of trabecular bone (shown in Fig. 63).

The microtomography images were processed and the fractal structure was analyzed by the proposed methodology using the implemented algorithm on *FractalCells* module (developed in this research project). It was possible to calculate the main directions of the fractal structure in the sample based on its composition and it was called a fractal map.

This map was applied in texture coordinates calculated and rendered with GPU using (shown in Fig. 76). The proposal is to use this information to correlate and understand the distribution of the properties found in mechanical tests after the microtomography images.

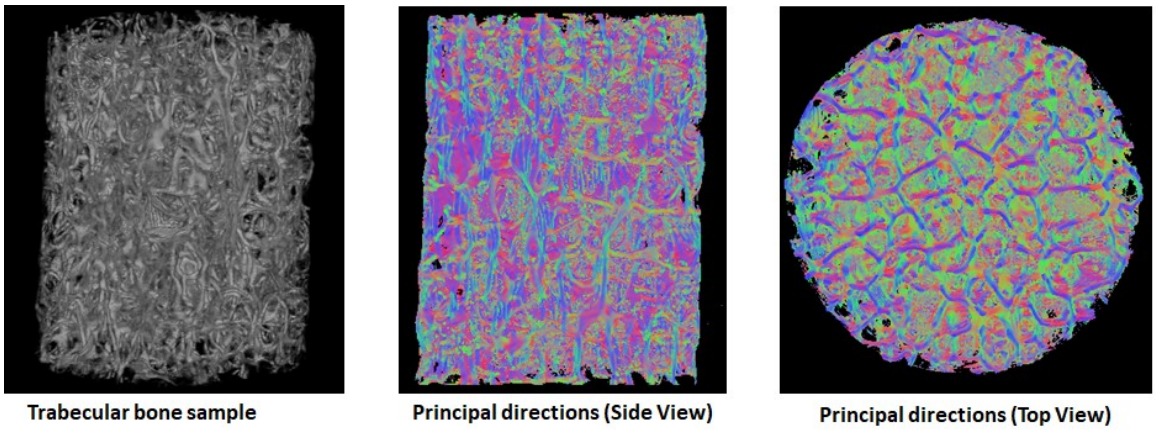

Fig. 76 Trabecular bone sample analyzed using the proposed method for characterization of anisotropy and mechanical properties based on the fractal structure

The fractal map can be stored in a NumPy matrix, and it can be used to weight the mechanical characteristics of the material in each direction. This could be applied during the calculation of the global matrixes of the volumetric formulation for the simulation of the material model.

More important, *FractalCells* module provides the same tools for interaction that were developed on *VISUALIX*, plus the main direction analysis. This creates an open-source framework for the development of new tools based on the fractal analysis for microtomography images and the proposed methodology using GPU volumetric rendering and ray-casting.

As described before, the fractal map was calculated by processing the microtomography image of tissue samples of a rat kidney (Fig. 75) and trabecular bone (Fig. 76). The model parameters could be calibrated using this method to consider the physical characteristics of the sample such as porosity, volume fraction, and direction or curvature of internal structures of different materials.

It is believed that this will allows to consider the fractal structure concept in a simulation with a solid simplified mesh as shown in Fig. 77. This proposal is better described and presented in section 8.2.2 for future works.

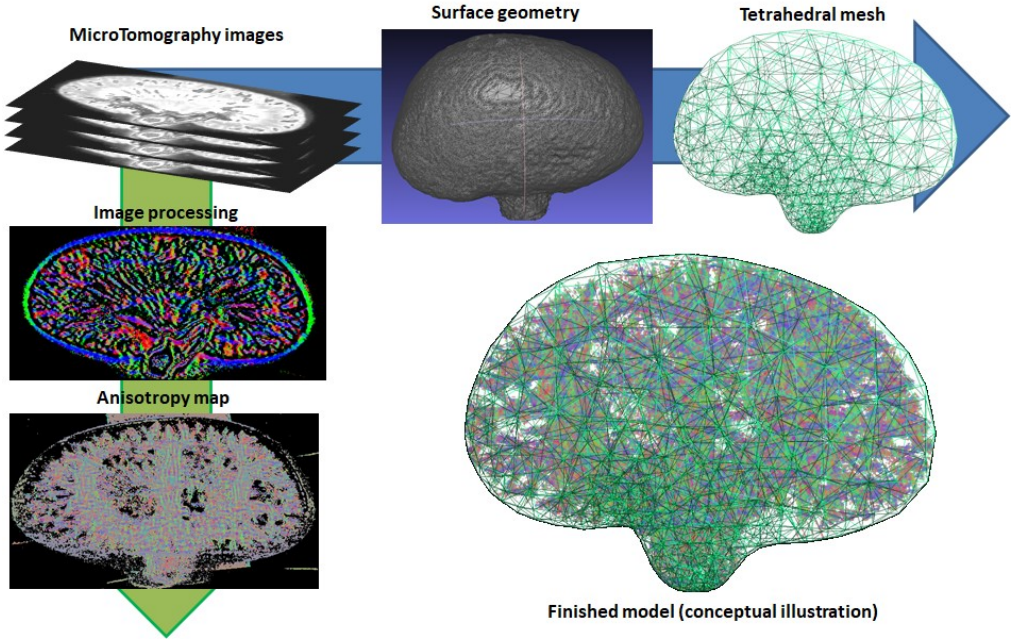

Fig. 77 Process for the usage of the proposed method of anisotropy maps for mesh parameters ponderation

This proposal is considered a new methodology to what has been found in the literature for fractal analysis (Alomari et al., 2017, Chappard et al., 2015, He & Ain, 2020, Korolj et al., 2019, Gómez-García et al., 2020). It will allow to perform a partial calculation of segment of the fractal structure and be able to use this information to perform simulations in the whole structure, using less computational time than currently is taking.

A similar approach was found on soil structure (Tseng et al., 2018), sand compression (Zhao et al., 2019), porosity in foam elements (Borovinsek et al., 2021), and the first one related to fibers was just published last year (Shkarin et al., 2020). An even in these developments, the techniques do not correlate the geometrical structure for distribution of the mechanical properties in a simulation mesh. These also do not evaluate its contribution to the anisotropic behavior. Research on both features is included as a proposal for future works (described in section 8.2.2) by applying the methodology implemented in this dissertation with *FractalCells* module.

Chapter 5

Material Modeling of Mechanical Properties

In this chapter, the proposal of a new hybrid model for real-time simulation of soft tissue mechanical properties is proposed. First, a review of the constitutive models found in the literature that are proposed for soft tissue is done in order to show state-of-the-art.

5.1 Soft Tissue Modeling

Multiple works can be found in the literature that is proposed to mathematically describe the mechanical behavior of materials. Particularly, it is possible to find constitutive models that describe the hyperelastic behavior of the soft tissues.

One of the most used models is the one defined by Mooney-Rivlin (Mooney, 1940). As shown in Eq. 3, this model uses two parameters to characterize the behavior of materials.

Eq. 3 $$\Psi(I_1, I_2) = C_{10}(I_1 - 3) + C_{01}(I_2 - 3)$$

Also, it can be found Fung model (Fung, 1967) shown in Eq. 4. This model proposes a different two parameters formulation that aims to describe the hyperelastic behavior of soft tissues.

Eq. 4 $$\Psi = \frac{k_1}{k_2}\{\exp[k_2(\lambda - 1) - 1]\}$$

Then, the Arruda-Boyce model was proposed initially for rubber materials (Arruda & Boyce, 1993) using a four parameters formulation shown in Eq. 5. Later, this model was proposed for the characterization of soft tissues by relating its nature to a composite material.

Eq. 5 $$T = \frac{\mu\beta}{3\lambda_r}\left(\lambda^2 - \frac{1}{\lambda}\right) \text{ with } \lambda_r = \sqrt{\frac{I_1}{3N}},\ \beta = L^{-1}(\lambda_r) = \coth\beta - \frac{1}{\beta}$$

Another highly used model in the literature is the one proposed by Holzapfel in his multiple works (Holzapfel, 2001, Holzapfel et al., 2005, Holzapfel & Ogden, 2008). This formulation of three parameters was proposed as a constitutive model for arteries in (Holzapfel & Ogden, 2008), as shown in Eq. 6.

Eq. 6 $$\Psi(I_1, I_4) = \frac{k_1}{k_2}\{\exp\{\, k_2[(1-\rho)(I_1-3)^2 + \rho(I_4 - I_4^0)^2]\} - 1\}$$

In this work, a new algorithm for real-time simulation is proposed based on a hybrid construction of the SMM and an energetic equivalence with a Strain Energy Density Function (SEDF) defined by the rule of mixtures, solved in a pre-computation stage.

For this formulation, soft tissues were considered as a composite material, formed by an isotropic matrix and an anisotropic fraction of collagen fibers, which provides anisotropy and non-linear deformation properties to be represented in the time simulation real.

5.2 Computational method and simulation of soft biological tissue

To apply the constitutive models previously exposed for validation of medical devices, strain-energy density functions which define soft biological tissue behavior must be implemented on algorithms based on computational methods in order to be solved in a specific geometric space. These methods can be classified by how continuous domain is considered for the volumetric model, having methods that use a mesh discretization and others meshfree.

Among the most used computational methods for this kind of application are:

(1) Finite Element Method (FEM)
(2) Boundary Elements Method (BEM)
(3) Finite Differences Method (FDM).

For this case, FEM is one of the most important methods due to its accurate calculations, usually based on Lagrangian or Hermitian interpolations and implemented with Euler, Gauss, Adams-bashforth or Runge-Kutta numerical integration methods (Roy et al., 2012, Freutel et al., 2014, Kim et al., 2013, Zhang et al., 2018).

Computational modeling of soft biological tissue using FEM has been applied as a validation tool of medical research in many fields, like endovascular stents for abdominal aortic aneurysms (Roy et al., 2012), failure mechanisms of articular cartilage (Wilson et al., 2005), and for virtual surgery simulation (Delingette et al., 2008, Freutel et al., 2014, Kim et al., 2013, Zhang et al., 2018).

As discussed in Chapter 2 Background, in previous works it was proposed a surgery simulator, based on the Spring Mass Model (SMM) represents the mechanical behavior of soft tissue in a simplified way. It was applied to one-dimensional elements implemented with the Finite Difference Method (FDM)

Based in the concept of the SMM model applied to this framework, it could consider that a body can be represented by a combination of mass points linked by springs with certain elasticity properties, as shown in Fig. 78. Since it is based on Hooke's law, the elasticity properties are characterized by a constant of stiffness (*k*).

(1) They represent, in a limited way, small deformations by means of one-dimensional elastic elements.
(2) It has difficulties validating itself in the three dimensions.
(3) Its constants are difficult to calibrate y in relation to the physical parameters of the material.
(4) Does not consider the volume of the object

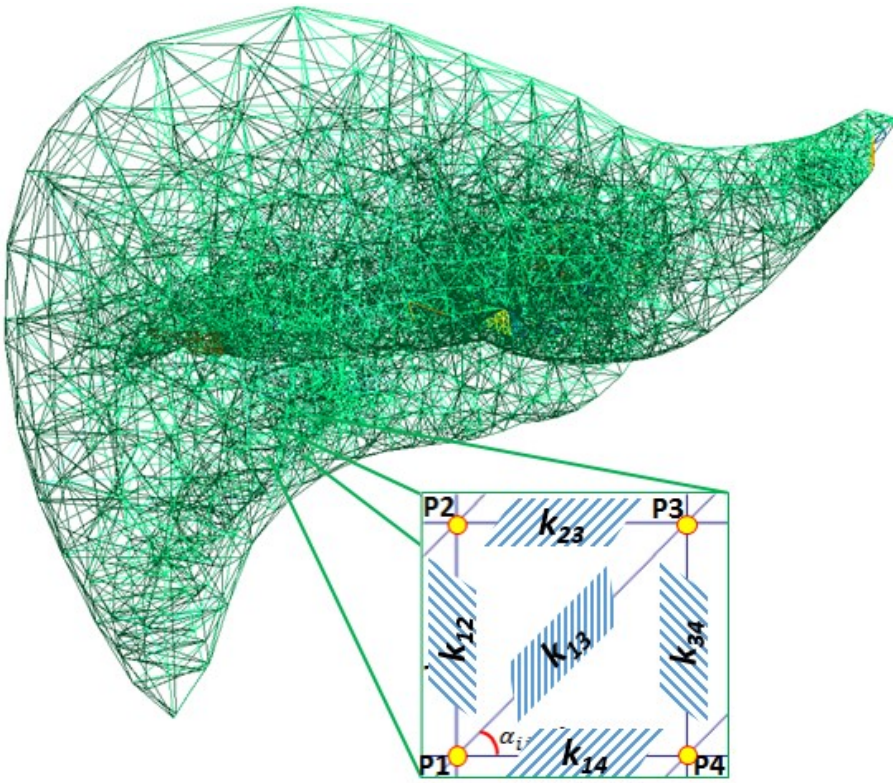

Fig. 78 A mesh of springs represented with one-dimensional elements using the SMM

During the main refresh cycle on the real-time simulation, it is possible to calculate the force Fi at a point Pi in a mesh by using the Hooke's Law as (Duan et al., 2014) and others (Omar et al., 2022, Zhang et al., 2017) have done. This is defined as the force of a spring with linear elasticity that connects Pi with Pj, calculated by using a stiffness

constant (kij), the initial length of the spring (Lij), and the length of the spring at the time of the calculation:

Eq. 7 $$\mathrm{F_i} = k_{ij}\left(\left|P_j - P_i\right| - L_{ij}\right)\frac{P_j - P_i}{\left|P_j - P_i\right|}$$

Good results were found in previous works (Moreno-Guerra, 2012), but there was one main issue: there was no physical relationship between the mechanical properties of the soft tissues and the parameters used to model and predict the behavior of the soft tissues/organs (in this case, the stiffness constants used on the SMM for each element). In this case, each spring represents direct stiffness in the model and are not limited to a maximum deformation.

In order to find the elasticity parameters to be applied, a trial-error calibration process had to be run manually to define how should look like the deformation for each mesh, based on the subjective perspective of the one performing said process.

Also, considering it uses a stiffness constant, this model represents the mechanical behavior of the soft tissue as linear. This is a major simplification since based on its non-homogeneous composition, it is known that the mechanical behavior of the soft tissues is non-linear. Models like SMM and others based on the linear elasticity theory are only valid on small deformations (<10%), it cannot be applied to large deformations since the mechanical behavior of the soft tissues is no longer linear.

5.3 Equivalent Energy Spring Model (EESM)

For this research, it was developed a new approach which proposes a mathematical model that allows the characterization of mechanical properties of soft tissue using experimental data, but keeping the efficiency of the SMM to perform in a real-time simulation.

In this chapter, it will be presented a new hybrid formulation proposed by this research project, based on an energy equivalence of the SMM and a constitutive model for a Strain Energy Density Function (SEDF) in order to have a spring element with variable stiffness parameter depending on its deformation stage.

This will be called the stiffness function and it is part of the formulation proposed in this work. It represents the value that matches the strain energy of a one-dimensional spring with the one calculated using the constitutive model based on the rule of mixtures of energies.

This model considers the soft tissues as a composite material of an isotropic matrix with a volumetric fraction of fibers that provide properties of anisotropy, nonlinearity, and hyperelasticity. It calculates the total strain energy as the contributions from the isotropic and anisotropic volumetric fractions of the material (Elías-Zúñiga et al., 2014), (Cantournet et al., 2007).

This proposed hybrid construction is called by the author of this dissertation as Equivalent Energy Spring Model (EESM) and its formulation will be described in detail below. It is intended to address one of the main concerns of real-time simulation of soft tissue behavior, which is to provide an accurate prediction based on material mechanical properties but within the time response required.

In the EESM model, the composition of the object continues to be considered as a mix of springs and masses but in this case, the stiffness is precalculated to have a different value based on the deformation at which the spring is at that time.

The SEDF based on the rule of mixture defines the total strain energy of a material as follows:

Eq. 8 $$\boldsymbol{W_1 = (1 - f)W_{iso} + fW_{aniso}}$$

Where W_{iso} represents the strain energy of the isotropic part, and W_{aniso} represents the contribution of the strain energy of the anisotropic part *f*, which is the anisotropic volumetric fraction. The two energies are calculated based on constitutive models applicable to each case, as defined in (Elías-Zúñiga et al., 2014).

In this case, the isotropic volumetric fraction was modeled using the Arruda-Boyce model (Arruda & Boyce, 1993), which considers the strain energy as a function of the draw ratio $\boldsymbol{\lambda_i}$ in the main directions:

Eq. 9 $$\boldsymbol{W_{iso}(\lambda_1, \lambda_2, \lambda_3) = \mu\left[N\left(\beta\lambda_r + ln\left(\frac{\beta}{sinh\ \beta}\right)\right) - ln\left(\frac{\beta}{\lambda_r}\right)\right] + c}$$

Where *N* is the number of the chair, μ is the shear module of the material, c is an energy constant, λ_r is the relative chain stretch presented in Eq. 10 and is presented in Eq. 11:

Eq. 10 $$\boldsymbol{\lambda_r = \frac{\sqrt{I_1/3}}{\sqrt{N}} = \frac{\sqrt{(\lambda_1^2+\lambda_2^2+\lambda_3^2)/3}}{\sqrt{N}}}$$

Eq. 11 $$\beta = \frac{3\lambda_r}{1-\lambda_r^3}$$

For the anisotropic part, (Elías-Zúñiga et al., 2014) presented an isotropized formulation to calculate the strain energy based on (Spencer, 1984) model:

Eq. 12 $$\boldsymbol{W_{aniso}(\lambda_1, \lambda_2, \lambda_3) = A_1\left(\lambda_{fibrai}^2 - 1\right) + A_2\left(\lambda_{fibrai}^2 - 1\right)^2 - 2A_1 ln\sqrt{J_i}}$$

Considering $\boldsymbol{\lambda_{fibrai}^2 = I_{4i} = a_i C a_i}$,, and where $\boldsymbol{a_i}$ represents the direction angle of the fibers family *i*. In this particular case, it was considered families associated with the 55 °

angle described by $\boldsymbol{a_i} = [\mathbf{1}, \mathbf{1}, \mathbf{1}]$ (and all variations $[-\mathbf{1}, \mathbf{1}, \mathbf{1}], [\mathbf{1}, -\mathbf{1}, \mathbf{1}]$, $[\mathbf{1}, \mathbf{1}, -\mathbf{1}]$, etc.). This is in order to perform an isotropization of $\boldsymbol{\lambda_{fibrai}^2} = \boldsymbol{\lambda_1^2 \alpha_1^2} + \boldsymbol{\lambda_2^2 \alpha_2^2} + \boldsymbol{\lambda_3^2 \alpha_3^2} = \boldsymbol{I_{1i}/3}$, in the same way as the formulations of (Cantournet et al., 2007) and (Elías-Zúñiga et al., 2014) used, but considering that other direction angles can be studied. In this way, it is possible to represent:

Eq. 13 $$\boldsymbol{W_{aniso}(\lambda_1, \lambda_2, \lambda_3)} = \frac{\boldsymbol{A_1}}{\mathbf{3}}(\boldsymbol{I_{1i}} - \mathbf{3}) + \frac{\boldsymbol{A_2}}{\mathbf{9}}(\boldsymbol{I_{1i}} - \mathbf{3})^{\mathbf{2}} - \frac{\mathbf{2}\boldsymbol{A_1}}{\mathbf{3}}\boldsymbol{ln}\sqrt{\boldsymbol{I_{2i}}}$$

Eq. 14 $$W_T = \left[(1-f)\left(\mu\left[N\left(\beta\lambda_r + ln\left(\frac{\beta}{sinh\ \beta}\right)\right) - ln\left(\frac{\beta}{\lambda_r}\right)\right] + c\right) + (f)\left(\frac{A_1}{3}(I_{1i} - 3) + \frac{A_2}{9}(I_{1i} - 3)^2 - \frac{2A_1}{3}ln\sqrt{I_{3i}}\right)\right]$$

Using Eq. 14, it is possible to calculate and characterize the mechanical behavior of soft tissues and composite materials, but its application for real-time simulation would be limited by the computational time required to solve this model at each frame and achieve a proper time response.

For this purpose, the hybrid formulation is proposed in order to get the accuracy of the SEDF proposed by (Elías-Zúñiga et al., 2014) with the computational cost of a simpler model like SMM (Moreno-Guerra et al., 2015). This construction was done based on an energy equivalence and isotropizing the behavior of the soft tissue, which is introduced as the Equivalent Energy Spring Model (EESM).

In this case, the equivalence is done with a Neo-Hookean model for a one-dimensional spring with variable stiffness, where the total strain energy at a certain deformation λ_S is considered to be equivalent to the one proposed by the SEDF at the same λ.

Eq. 15 $$W_S(\lambda_S) = \frac{\sigma\epsilon}{2} = \frac{F(\lambda_S - 1)}{2v_{ij}} = \frac{\kappa_S \lambda_S}{2v_{ij}}(\lambda_S - 1) = W_T(\lambda_1, \lambda_2, \lambda_3)$$

Where W_S is the total strain energy of the EESM element, v_{ij} is a geometrical parameter that represents the transversal area of the tissue sample that was used to find the characterization parameters of the material model, λ_S is the strain in the spring element and κ_S is the stiffness function of an EESM element. WT is considered the total strain energy from the SEDF, where it will be formulated using the assumption of uniaxial tension of an incompressible material, having $\boldsymbol{\lambda_1} = \boldsymbol{\lambda}$ and that $\boldsymbol{\lambda_2} = \boldsymbol{\lambda_3} = \mathbf{1}/\sqrt{\boldsymbol{\lambda}}$.

Therefore, it is possible to define the parameters of each spring to individually represent the non-linear behavior of the soft tissue in order to improve the prediction of the deformation.

The stiffness function is an energy equivalence pre-calculated as a parameter in function of the SEDF of the isotropic and anisotropic volumetric fractions contributions, using Arruda-Boyce and Spencer model with the Rule of Mixtures as (Elías-Zúñiga et al., 2014). This function uses the parameters that characterize the behavior of the material obtained using data from mechanical testing of porcine tissue samples.

Eq. 16 $$\kappa_S(\lambda) = \frac{2v_{ij}[(1-f)W_{iso}+fW_{aniso}]}{(\lambda_S^2-\lambda_S)}$$

This hybrid model allows calculating a stiffness parameter that causes a stretched spring to reach the same strain energy as the soft tissue described by the constitutive model at the same deformation ratio.

In this case, κ_S is calculated for a specific configuration of the EESM element, using the parameters that characterize the mechanical behavior of the material from tensile test data. Each EESM element represents a spring with variable *k*, representing direct stiffness and providing a behavior response following experimental data until reaching the maximum deformation achieved in the mechanical test before material failure.

Now the construction with the SMM is performed by considering the creation of EESM elements in a simulation mesh. Each EESM element is a one-dimensional spring that has as its initial length the distance between two points connected (Pi and Pj), as shown in Fig. 79.

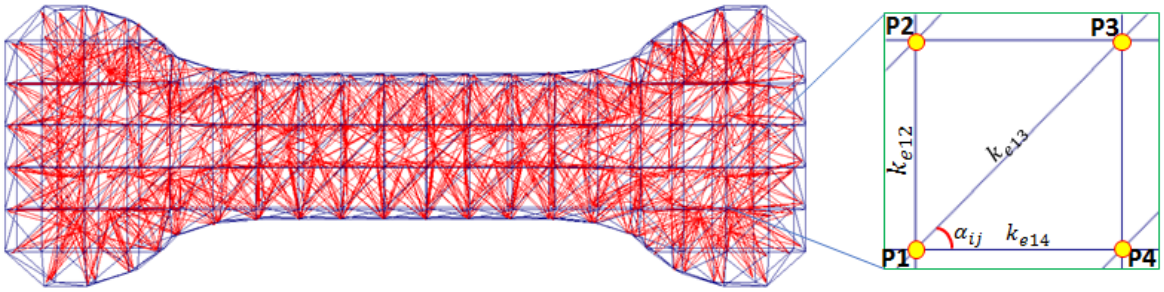

Fig. 79 Conceptual graphic representation of the creation of mesh of EESM elements that are used for real-time simulation.

In the implementation, the EESM stiffness function is used for each strain value to define a 3D array k_{ij} created in the initialization stage. This array is pre-calculated based on the parameters that characterize the mechanical behavior of the material, defining a variable stiffness parameter for each deformation λ_S.

Eq. 17 $$k_{ij}(\lambda_S) = [\boldsymbol{\kappa_S}(\lambda_S),\ \boldsymbol{\kappa_S}(\lambda_S),\ \boldsymbol{\kappa_S}(\lambda_S)]$$

By using this method, it is possible to define parameters on a simplified model that allow real-time simulation using mechanical properties of soft tissues by tension experimental results, as shown in Fig. 80.

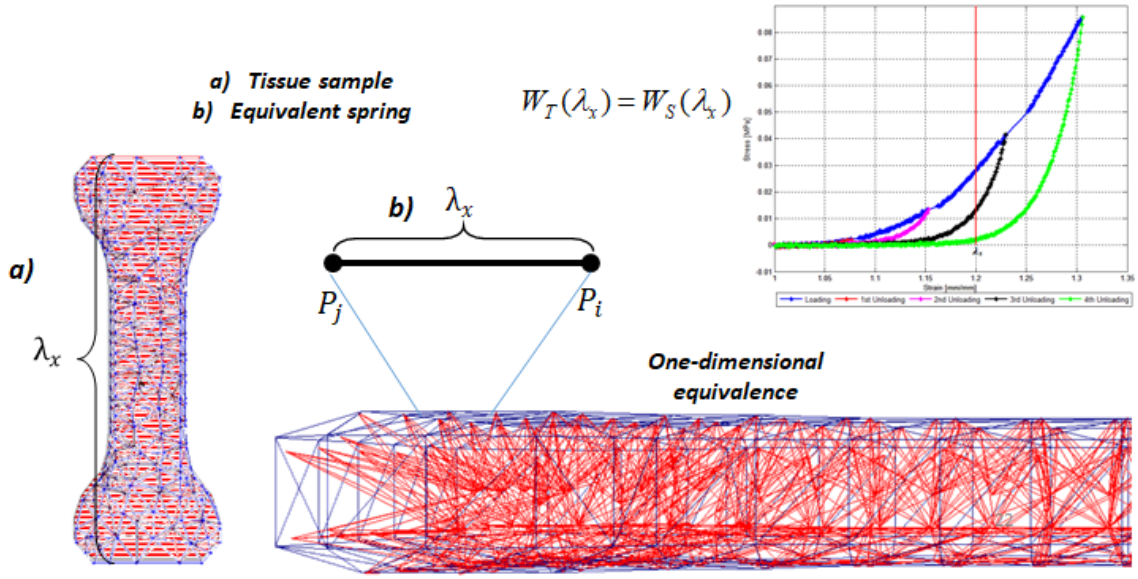

Fig. 80 Concept of the EESM to use the strain energy to calculate the stiffness value that makes the deformed spring have equivalent energy

As mentioned before when reviewing the proposed SEDF, an isotropization of the material was performed as (Cantournet et al., 2007) and (Elías-Zúñiga et al., 2014). This was done by considering the main direction of the fibers to be 55°.

Based on this, it was possible to consider the material as a random distribution of the contribution of the fibers in the three main axes, and that the properties obtained are distributed based on the main orientation, so it is also considered on the κS stiffness function.

The EESM formulation for uniaxial tension considers that the contribution of the stiffness in the three main directions is the one that is described in the model and used to predict its mechanical behavior as shown in Fig. 81.

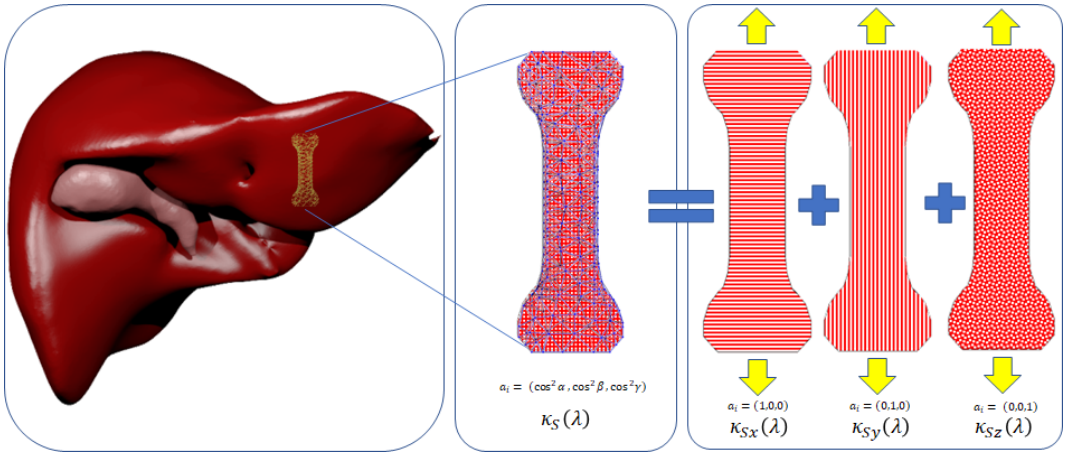

Fig. 81 Graphic representation of uniaxial mechanical test for characterization of anisotropic mechanical properties of soft tissue.

Considering that soft tissue presents anisotropic behavior, the biaxial tension test was evaluated in order to define the applicability of the proposed model for this case and review the impact of the assumption of the main orientation of the fibers.

In a material with a volumetric fraction of fibers randomly and homogeneously distributed, this assumption will be true. Now it could be reviewed if this would be the case for a material with the volumetric fraction of fibers oriented in a dominant direction.

Following the previous idea, cyclical biaxial tensile tests were performed to analyze and characterize the mechanical behavior of soft tissue. Using the proposed model, an adequation to the stiffness function should be done to consider the contribution of each axle on a virtual mesh, as shown in Fig. 82.

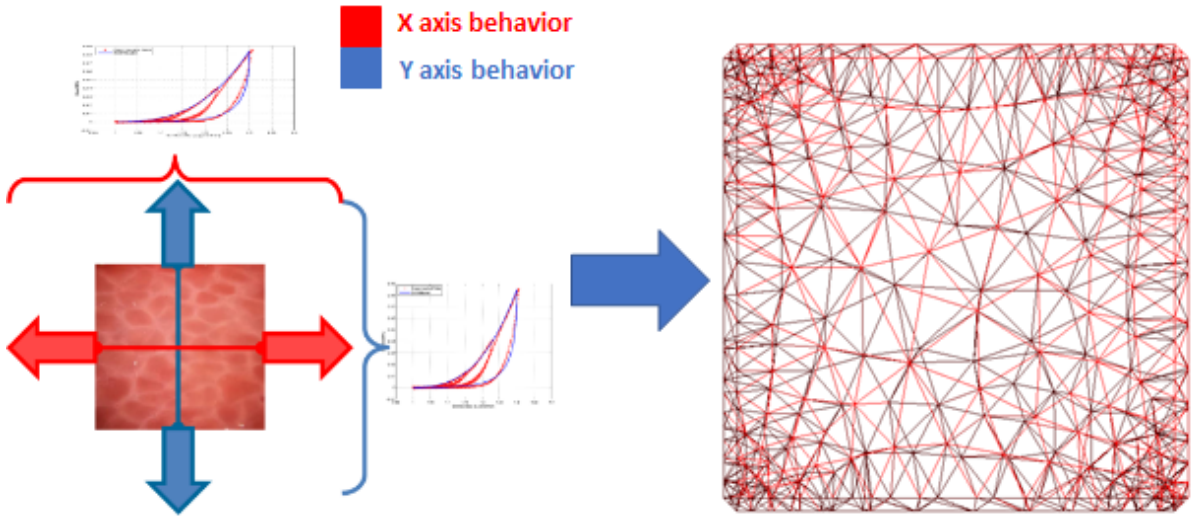

Fig. 82 Graphic representation of biaxial mechanical test for characterization of anisotropic mechanical properties of soft tissue

As it was defined in Eq. 15, W_S is the total strain energy of the EESM element, but now it will consider that the element is equivalent to W_T of a case of biaxial extension on an incompressible material, so $\boldsymbol{\lambda_1 = \lambda_2 = \lambda}$ and that $\boldsymbol{\lambda_3 = 1/\lambda^2}$.

Eq. 18 $$W_S(\lambda_S) = \frac{\sigma\epsilon}{2} = \frac{F(\lambda_S - 1)}{2v_{ij}} = \frac{\kappa_S \lambda_S}{2v_{ij}}(\lambda_S - 1) = W_T(\lambda_1, \lambda_2, \lambda_3);\ \boldsymbol{\lambda_1 = \lambda_2 = \lambda, \lambda_3 = 1/\lambda^2}$$

Then, the stiffness function for an EESM element considering biaxial tension would be represented by:

Eq. 19 $$k_{ij}(\lambda_S) = \left[cos^2\,\alpha\,\boldsymbol{\kappa_{Sx}}(\lambda_1),\ cos^2\,\beta\,\boldsymbol{\kappa_{Sy}}(\lambda_2),\ cos^2\,\gamma\,\boldsymbol{\kappa_{Sz}}(\lambda_3)\right]$$

Using this proposal it is possible to define a κ_S for each axis and use the directional cosines of the EESM element orientation (α,β,γ) to weight the contribution of the stiffness function on each axis.

In this case, $\kappa_{Sx}(\lambda_1)$ represents the stiffness function for an EESM element in direction of the X-axis at a specific λ deformation, using the experimental data in this axis obtained from biaxial testing. Same for $\kappa_{Sy}(\lambda_2)$ based on Y-axis experimental data. For Z-axis, $\kappa_{Sz}(\lambda_3)$ is calculated based on the other two axes. This concept is represented in Fig. 83.

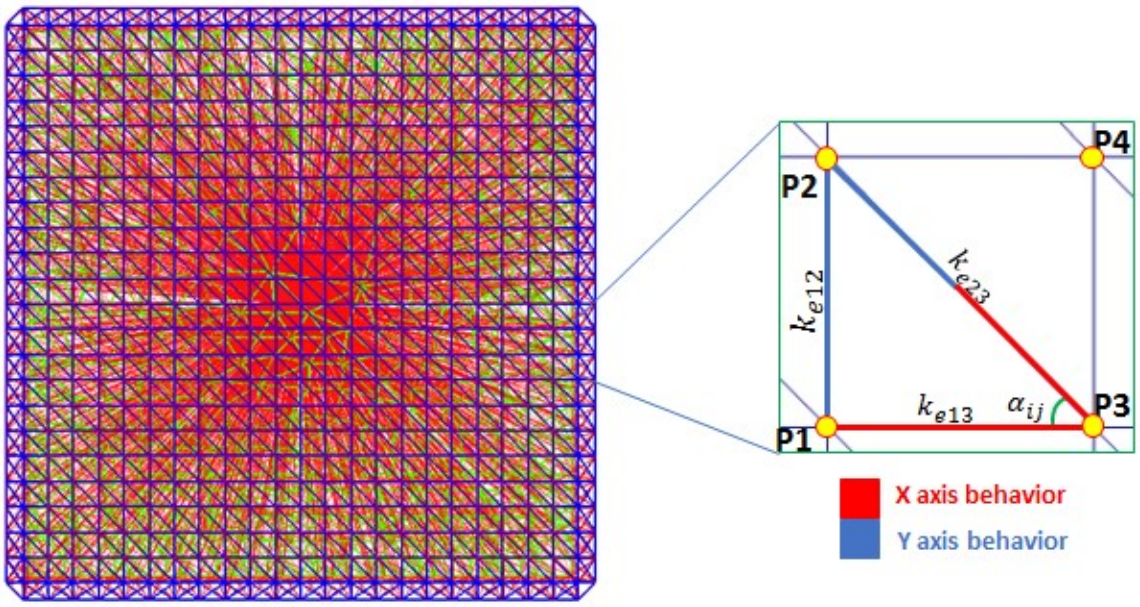

Fig. 83 Virtual mesh used for testing of biaxial application of the proposed model on real-time simulation

Following this idea, the stiffness parameters k_{ij} of a particular EESM element will be in function of two things: 1) The characterization of the material mechanical behavior at biaxial tension with the SEDF and; 2) The EESM element's initial orientation in X,Y, and Z-axis based on the directional cosines.

For the implementation, this parameter is calculated and stored in the initialization phase for each EESM at all values of λ_S. During the main refresh cycle of the real-time simulation, the method uses this value as the stiffness parameter of the EESM element for the particular deformation level λ_S at that time.

5.4 Implementation of EESM formulation in real-time simulation

EESM was implemented as a material model for a real-time simulation of soft tissue behavior using Python, Visualization Toolkit (VTK), NumPy, SciPy and Wx, replacing the previous material model used in the original framework, but keeping all the tools that were

implemented like Collision Detection and main interaction cycle for the virtual environment, as shown in Fig. 84.

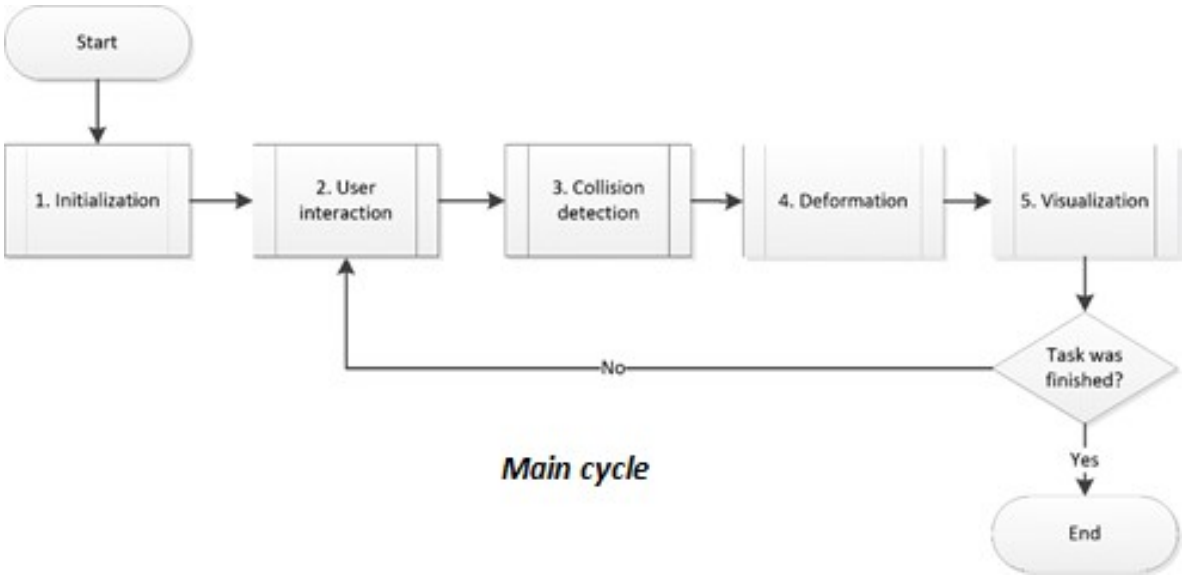

Fig. 84 Flow diagram for implementation of the proposed model for pre-calculation of mechanical behavior in a virtual environment

As shown in Fig. 85, it is in step 1 (Initialization) where the model calculates the constants for the EESM springs formed with the organ geometry, using the parameters that calibrate the model to represent the tissue to be simulated (it is considered that these parameters were previously found using experimental data).

For the EESM, the strain energy of a linear spring was based on a case of the Neo-Hookean model for one-dimensional elements Eq. 16 and will be found an energetic equivalence to the SEDF using Eq. 14 from $\lambda = 1$ to λmax with step $d\lambda$ and stored in the stiffness array k_{ij} as Eq. 17 describes on the initialization phase.

For a spring at λ, using $\kappa(\lambda_S)$ make it achieve the same deformation energy that the soft tissue sample at the same λ. The same case for the biaxial formulation, only using Eq. 18 consideration for the biaxial case and Eq. 19 for the stiffness array k_{ij}.

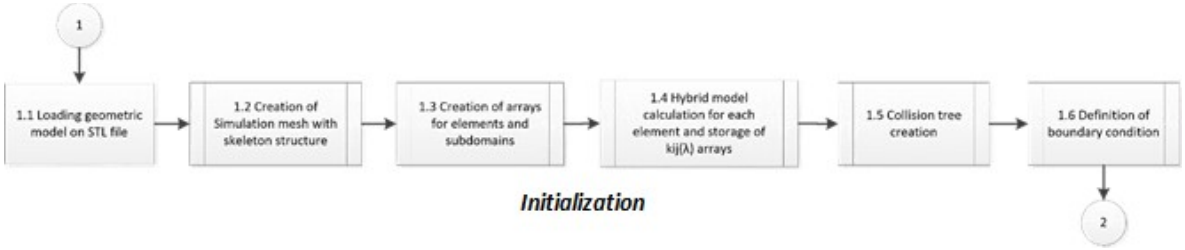

Fig. 85 Flow diagram for implementation of proposed model for pre-calculation of mechanical behavior in a virtual environment

Also, in Fig. 85 it is possible to find step 1.6, where the boundary conditions are set for each mesh and organ. This step was carried over from the previous implementation of the simulation virtual environment developed in previous works (Moreno-Guerra et al., 2012). In this case, boundary conditions are defined for each organ to fix themselves into what would be the abdominal wall and are used to calculate initial deformations and loads during simulation steps.

Defining boundary conditions are important and should be done at the start of each new application module that is developed. For future virtual environments or tests, defining these are required based on each mesh geometry and topology. In order to represent cutting procedures, it is recommended to use the boundary conditions as part of the section that is planned to be performed between two independent meshes.

In Fig. 86, the EESM calculation for each element is detailed, considering the tissue characterization parameters, and calculating and storing k_{ij} for each value of λ in each element.

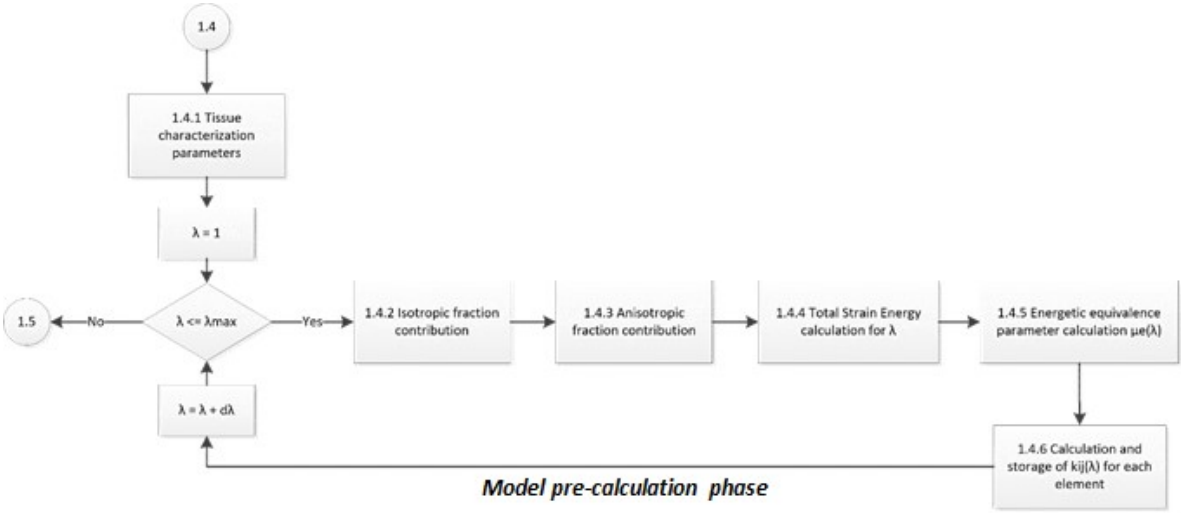

Fig. 86 Flow diagram for implementation of proposed model for pre-calculation of mechanical behavior in a virtual environment

The testing phase was defined to collect experimental data from porcine liver tissue samples at uniaxial and biaxial tensile tests, and from porcine abdominal wall tissue samples at biaxial tensile tests. These processes are presented in Chapter 6.

Using the experimental data collected, the parameters to characterize the mechanical behavior of soft tissue with the EESM formulation were calculated and presented in Chapter 7. Predictions were performed and compared with experimental data and a simple SMM, evaluating results to measure the performance on accuracy and time response.

Chapter 6

Experimental Testing for Mechanical Characterization

Once the material model was implemented, experimental validation was required to obtain data to prove and improve the proposed model and scheme. In order to acquire data on the mechanical properties of the materials, uniaxial and biaxial tensile tests were performed.

Different materials were tested in order to obtain experimental information to retrofit the material model implemented. The selection of these materials was based on the best interest of this project, in order to create a database of materials based on their mechanical properties that could be used on a simulation engine for tissues and composites, such as liver, heart, kidney, nanofibers, surgical mesh, and polymers.

On this chapter, the experimental setup to acquire mechanical properties data, sample preparation, data processing, and results are exposed. For this dissertation, only will be considered experimental tests with tissue samples of liver and abdominal wall.

The experimental step was considered crucial for this research and the results obtained in this stage itself are a valuable contribution to material characterization, providing a methodology for testing and a better understanding of the mechanical behavior of tissue and composites materials for multiple applications.

6.1 Tissue sample collection

For this research project, it was considered to use porcine tissue, since in addition to primates, pigs are the laboratory animal species closest to humans in terms of anatomy and physiology. The procedure to collect and manipulate the tissue samples was

performed in collaboration with the Escuela de Medicina y Ciencias de la Salud from Tecnológico de Monterrey.

A protocol was established for multiple research purposes, among those to collect the tissue samples used for this investigation. An ethical committee (Comité Institucional para el Cuidado y Uso de Animales de Laboratiorio, CICUAL), medical and veterinarian specialists were in charge that the specimen was treated humanely and cared properly, as shown in Fig. 87.

Also, this procedure was performed as specified in the protocol to consider the ethical and legal implications of performing and collecting these samples. The protocol followed the current laws and standards for animal trials, as specified by Mexican authorities (Dirección General de Normas, 2011, Secretaría de Salud (B), 2014, SENASICA, 2012, SENASICA (B), 2012).

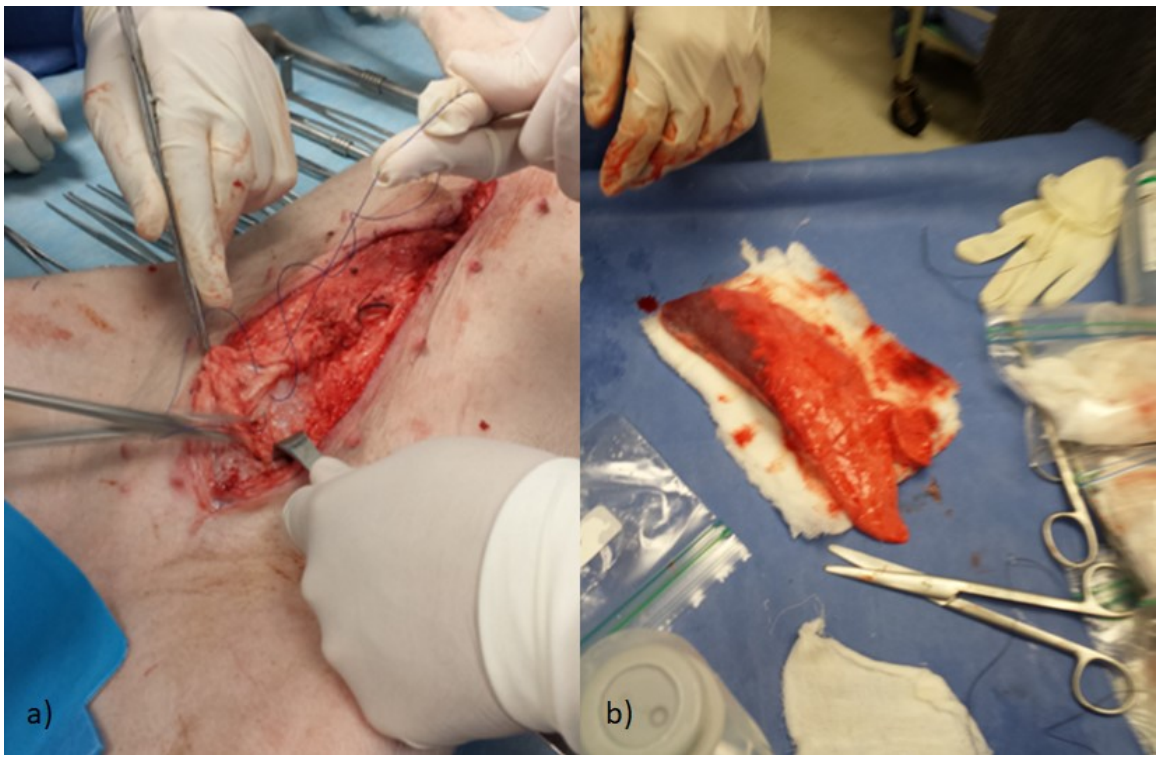

Fig. 87 Procedure to collect tissue samples based on a research medical protocol. Liver and abdominal wall tissues were evaluated for mechanical characterization.

From this medical protocol, porcine tissue samples were obtained for many different research works, among the tissues that were collected and stored were: liver, kidney, skin, trachea, spleen, stomach, esophagus, facia, lung, veins, and heart.

Multiple research projects have been done thanks to this medical protocol. In this dissertation, porcine tissue samples were used to perform experimental testing to characterize the mechanical properties of the tissue.

The results of this research work can help to understand better the behavior of this organ and can be used to improve the training of medical students and surgeons. Eventually, it is expected that this research will provide benefits by having higher quality healthcare systems and saving more lives in surgeries.

In addition, other applications can use this material model to develop new biomedical devices, impacts test for safety and crashes, and for other research purposes related to the mechanical properties of soft tissues (shown in Fig. 88). Just developing a model that characterizes the mechanical behavior of this kind of tissue is a great contribution to bioengineering, materials, and natural sciences.

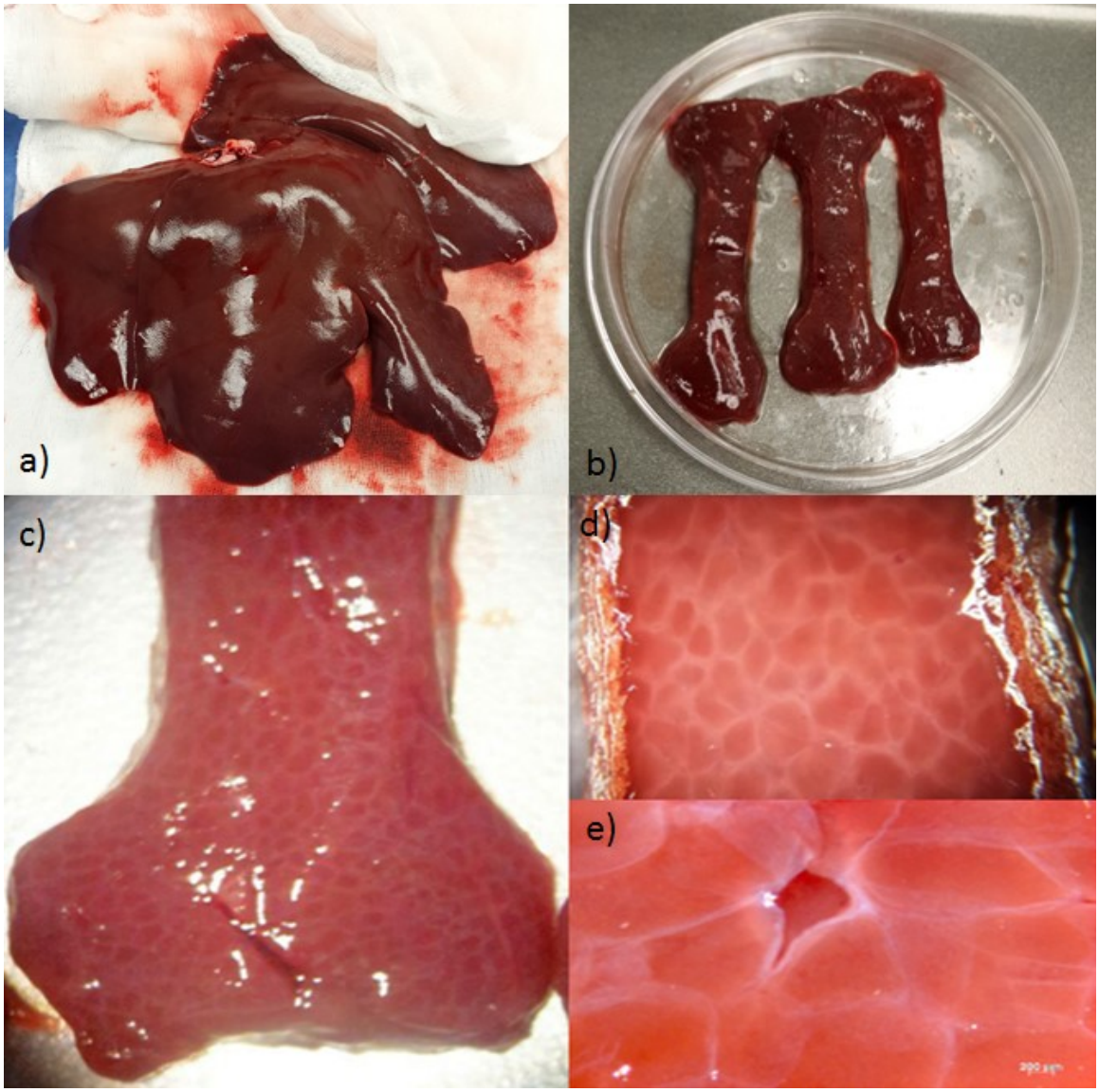

Fig. 88 Thanks to this medical protocol it was possible to get a) Porcine Liver used to take b) Tissue samples with specific geometry c) Close-up section of tissue sample d) Microscopy view of tissue sample e) Histological composition of tissue

6.2 Uniaxial mechanical tests

Uniaxial tensile tests were performed using and Instron™ electromechanical universal testing system with ±1kN Pneumatic Wedge Grips, as shown in Fig. 89. Cyclical tensile tests were performed to obtain experimental data for porcine liver tissue.

Fig. 89 Setup for Instron™ electromechanical universal testing system

The specs of this equipment are as follow:

- Capacity: 1kN Pneumatic Grips (up to 5kN capacity)
- Minimum speed: 0.005 mm/min
- Maximum speed: 500 mm/min
- Crosshead travel: 1122 mm
- Vertical test space: 1193 mm
- Colum spacing: 420 mm
- Footprint dimensions: 158 x 76 x 71 cm

6.2.1 Samples preparation

In order to prepare the samples, first a standard geometry had to be defined to use for the characterization of the tissue. The standard geometry was based on an analysis of the literature, where it was found that a *dog bone* shape is used and accepted for tensile tests (Brunon et al., 2010, Fu et al., 2013, Kemper et al., 2010, Kemper et al., 2012, Umale et al., 2013).

In this case, the *dog bone* shape was defined, and the dimensions were determined in accordance with the availability of the material. Even having a specific shape, the next concern was to make sure that all samples had the same geometry. Considering the complexity of a *dog bone* cut, it was a challenge to reproduce 20 samples manually.

For this purpose, it was designed a tooling used to get standardized samples as shown in Fig. 90. This tooling design was done specifically for the characterization of tissue and to define a standard geometry for the preparation of tissue samples by our research group to analyze the mechanical properties at uniaxial tensile tests. The general dimension of the samples used in this research was 55 x 20 x 5 mm.

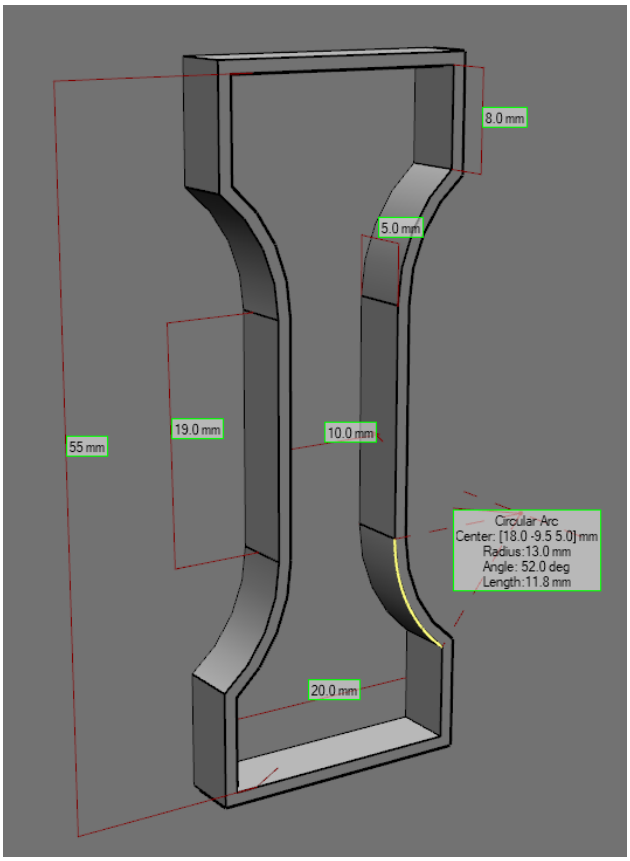

Fig. 90 *Dog bone* tooling design that defines the standard geometry and dimensions for the tissue sample

It important to mention that the composition of the sample is not homogeneous, and therefore the results obtained in this test are considered the contribution of the different volumetric fractions of fibers and tissue with multiple orientations. All samples were taken considering that the general orientation of the sample was the same, using the designed tooling as shown in Fig. 91.

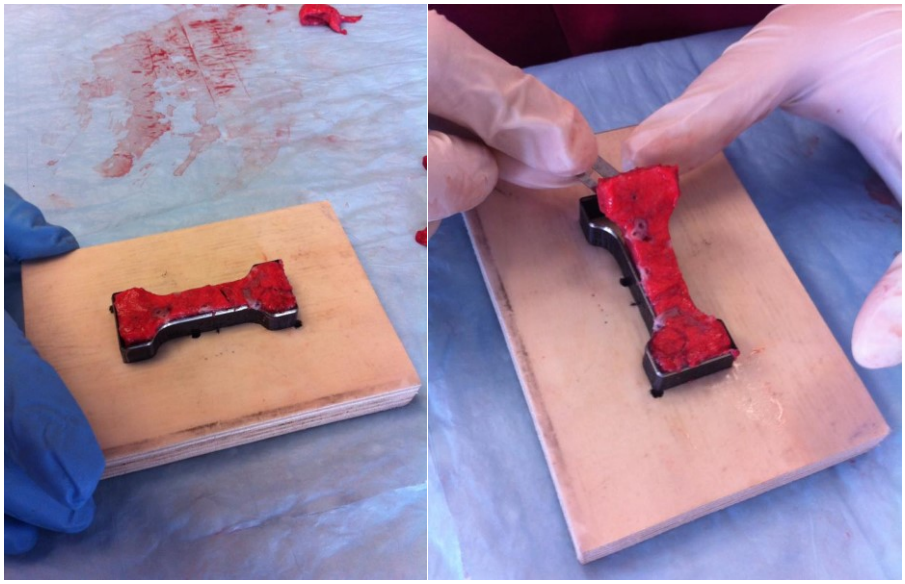

Fig. 91 *Dog bone* tooling used to cut the samples with a standard shape

Also, these samples were frozen in order to keep them from losing properties. They were rehydrated with saline solution and left at room temperature while the setup of the testing equipment was being done, as shown in Fig. 92.

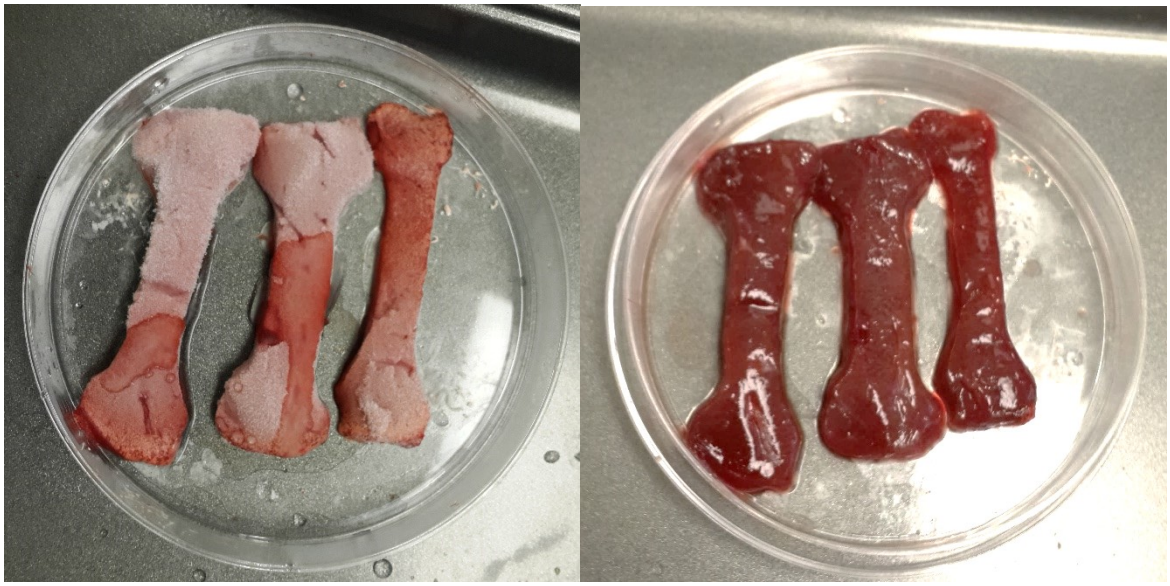

Fig. 92 Tissue samples of liver tissue for uniaxial testing

6.2.2 Experimental phase

Destructive tests were performed on 5 samples of porcine liver tissue, as shown in Fig. 93. These were done using uniaxial tensile tests, and the experimental data was used to define the cyclical test parameters that were going to be performed, as shown in Fig. 94.

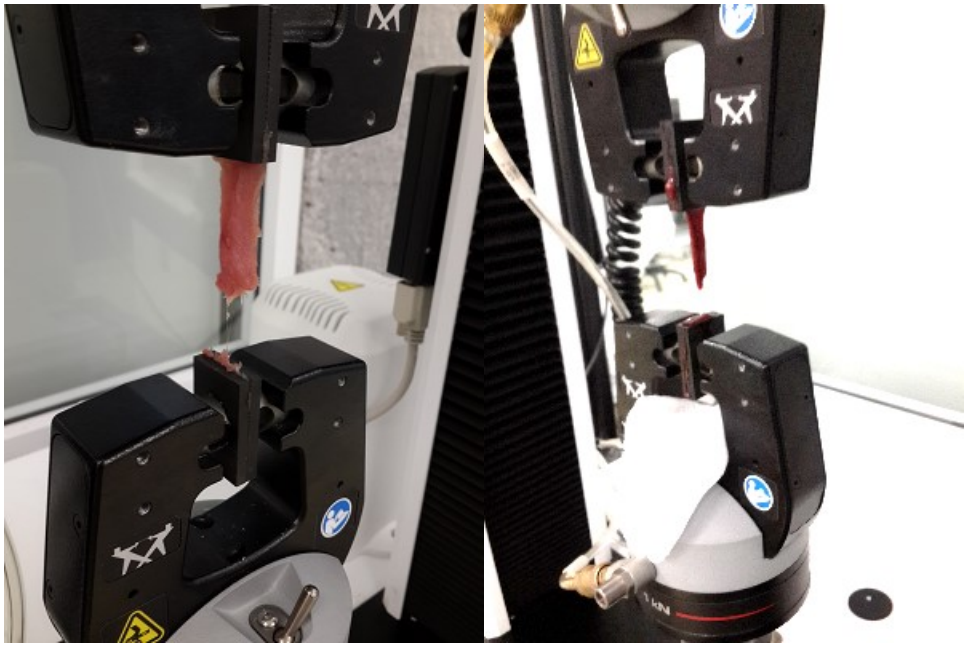

Fig. 93 Experimental tension test to failure to define parameters for cyclical test

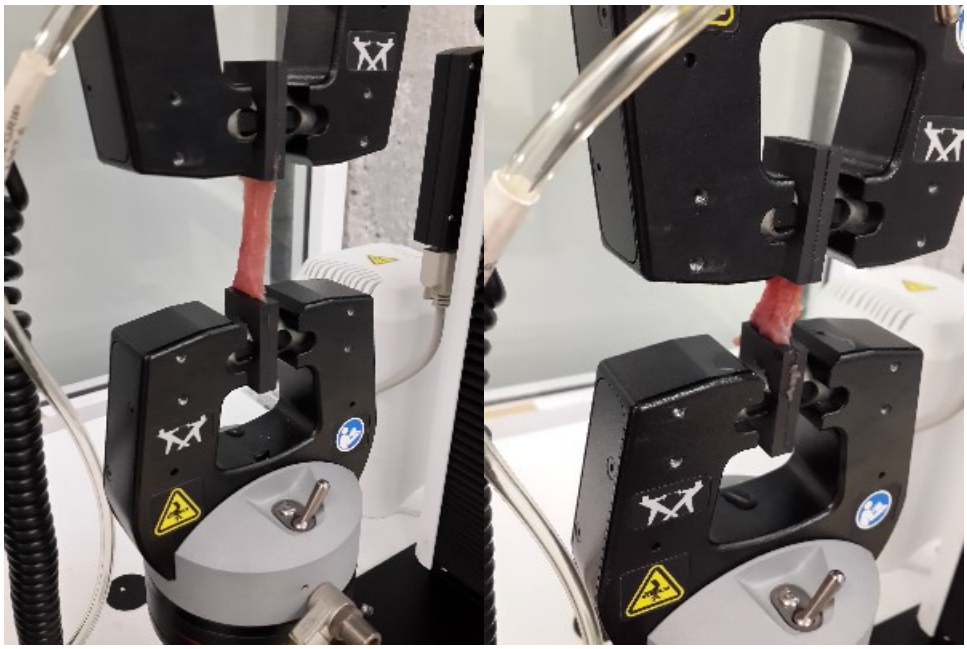

Fig. 94 Experimental tension cyclical test, left picture show maximum tension and right picture shows the permanent deformation after the unload curve

Uniaxial tensile tests were cyclically performed on 15 samples of porcine liver tissue. The experimental results were processed and used to characterize the mechanical behavior of porcine liver tissue (Baylon et al., 2015, Moreno-Guerra et al. 2015).

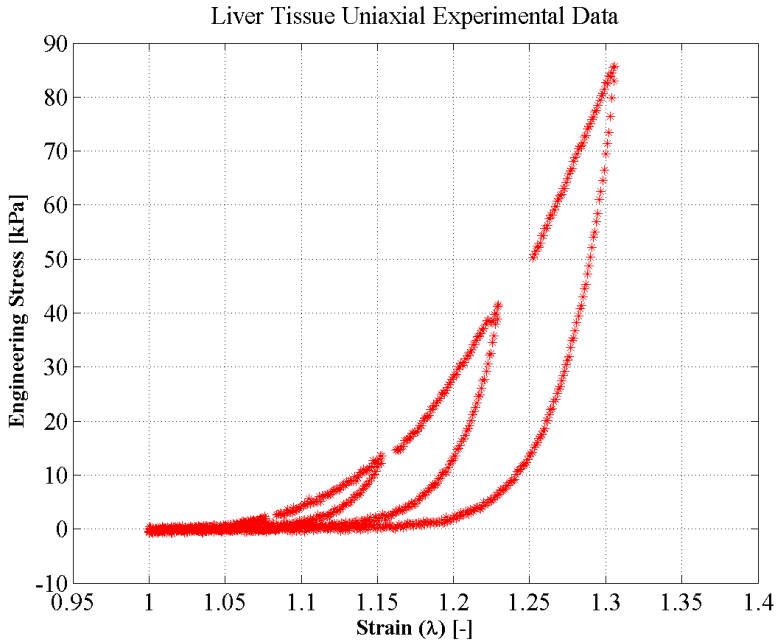

Fig. 95 Experimental data for uniaxial tensile test on porcine liver tissue samples.

6.3 Biaxial mechanical tests

For the experimental setup, it was used an Electroforce™ Biaxial TestBench with 4 independent linear actuators of 200N with 20N loadcells on each axis, as shown in Fig. 96. In addition to a GOM Aramis™ system of stereoscopic cameras in order to record the experimental test and analyses for imaging correlation to obtain accurate 3D deformation/displacement (average frequency of 20 Hz).

The specs of this equipment are as follows:

- Peak force capacity: ± 200 N
- Static force capacity: ± 140 N
- Range of displacement: 12.5 mm
- Maximum frequency: 100 Hz
- Reaction base dimension: 609 x 609 x 51 mm (width x depth x thickness)
- Available test space: 0 – 267 mm (with load cell)
- Reaction base weight: 36 kg
- LM1 motor weight: 4.5 kg
- Saline bath chamber with temperature control
- Resistance Temperature Detector (RTD)
- 2D Digital Video Extensometer (DVE)

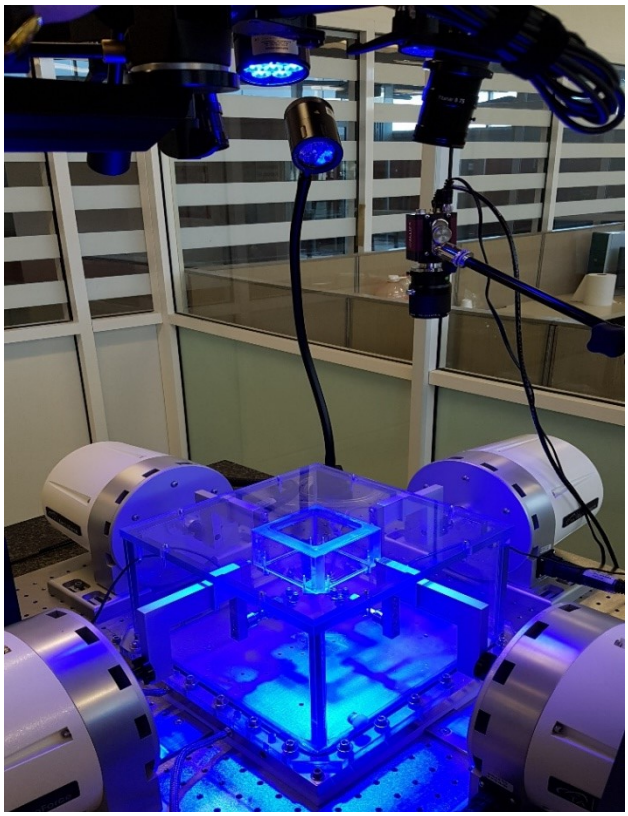

Fig. 96 Electroforce™ Biaxial TestBench with GOM Aramis system

As previously mentioned, GOM Aramis™ was used for acquisition of the experimental test with high-definition cameras and images post processing for deformation analysis. This device has two stereoscopic cameras with a 20 hz rate (shown in Fig. 97), and a glasses array for a measurement surface of 120 x 100 mm.

Fig. 97 GOM Aramis™ equipment set up for superficial deformation measurements based on image processing

Using the GOM Aramis™ Software, it is possible to record the experimental phase and then perform analysis and processing of the images captured.

In this case, the sample has to be prepared with a random pattern of painting marks that allow the system to recognize the surface. With this information, the software creates a 3D surface scanned in space with a triangular mesh that is used to calculate the deformation over time in the recording, as shown in Fig. 98.

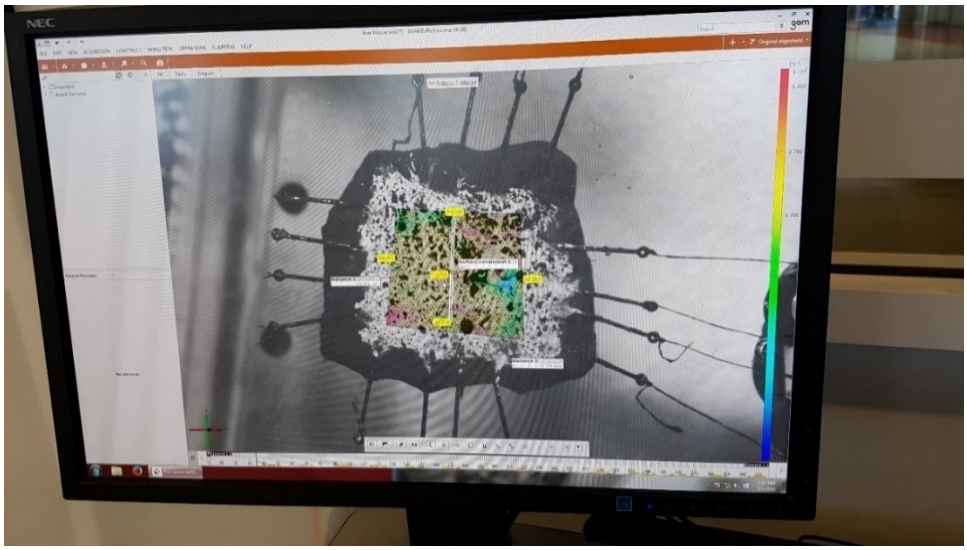

Fig. 98 GOM Aramis software used for calculation of superficial deformation

The fixation method used by this equipment is based on an array of fishing hooks as shown in Fig. 99. This fixation method is an important part of the process for the sample's preparation.

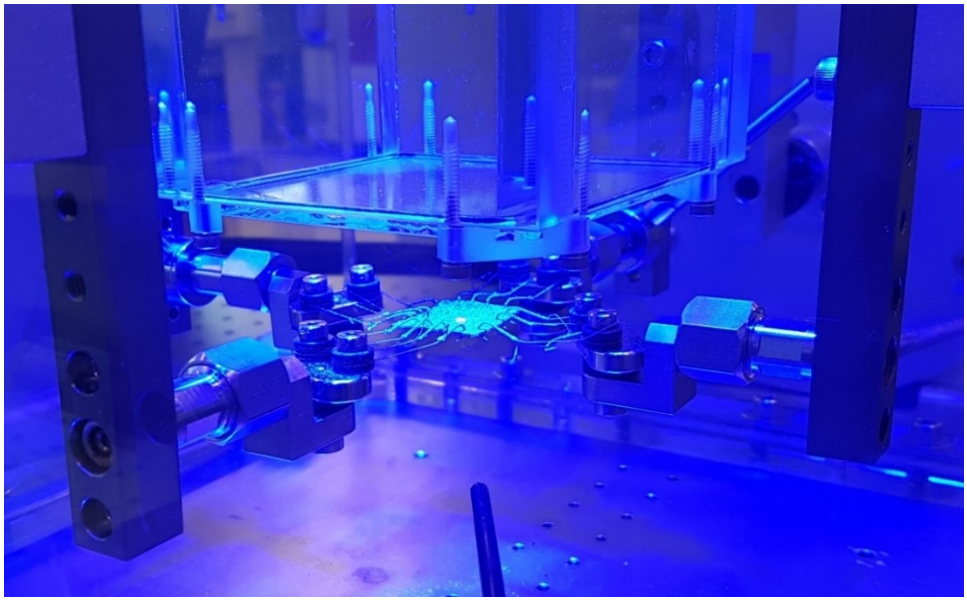

Fig. 99 Fixation method for the tissue sample on the experimental set-up

Each side of a square 20 x 20 mm sample has 4 hooks fixed using tooling that is provided to facilitate the insertion of these attachments having the same spacing across the lateral length of the sample, as shown in Fig. 100. This process is really complex and adds a lot of difficulty and time consumption to the experimental phase. As a proposal in future works, it could be used a different attachment method for testing.

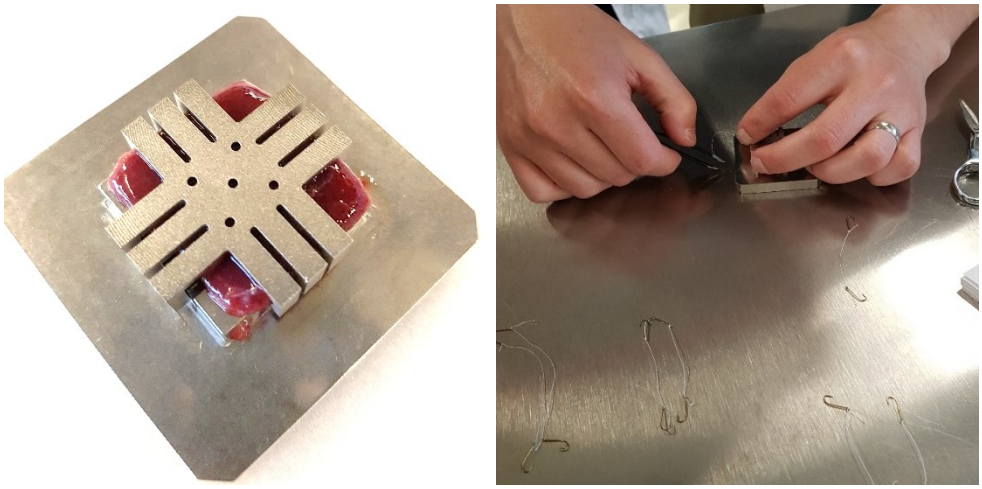

Fig. 100 Tooling provided to attach the fishhooks to the sample during preparation

6.3.1 Samples preparation

In order to perform the biaxial testing, it was used the next procedure for the sample preparation (as is shown in Fig. 101):

a) Cut the sample to the defined squared shape (20 x 20 mm).

b) Position the sample in the fixation tooling with help of a set of tweezers.

c) Insert the fishing hooks in the sample with help of the tooling 4 per side, 16 in total. Take care there is similar spacing between them.

d) Apply a white layer of paint in order to use as a contras background for detection of the sample surface and measurement of the strain with GOM Aramis™.

e) Apply a random set of black dots in the white layer for detection of the sample surface and measurement of the strain with GOM Aramis™.

f) Position the sample in the Biaxial TestBench™, using each side pivot handler to distribute the position without applying an initial deformation.

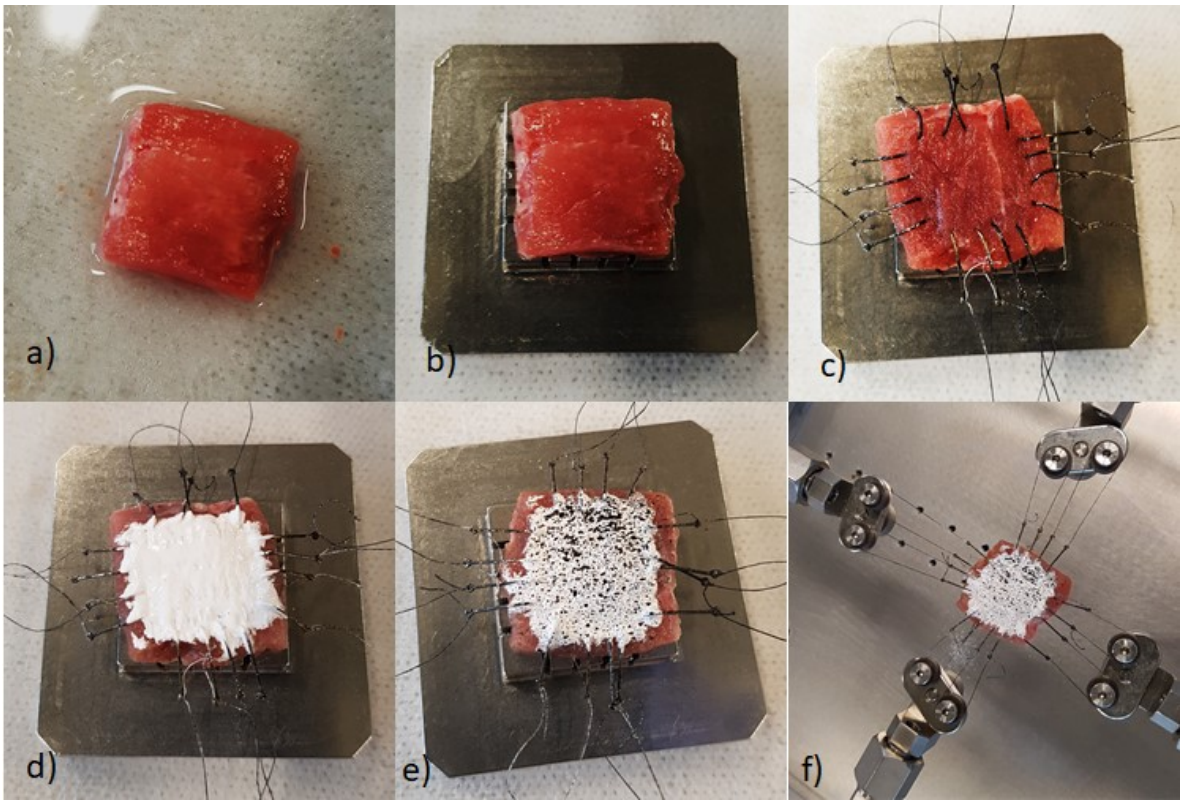

Fig. 101 Preparation process for biaxial mechanical test of porcine abdominal wall tissue with strain analysis

After the tissue sample was prepared and mounted in the Biaxial Testbench™, it is required to do the set-up to define the kind of test that will be performed. Part of this set-up is manual by adjusting and centering the tissue without applying initial deformation but avoiding the sample is bending due to gravity, as shown in Fig. 102.

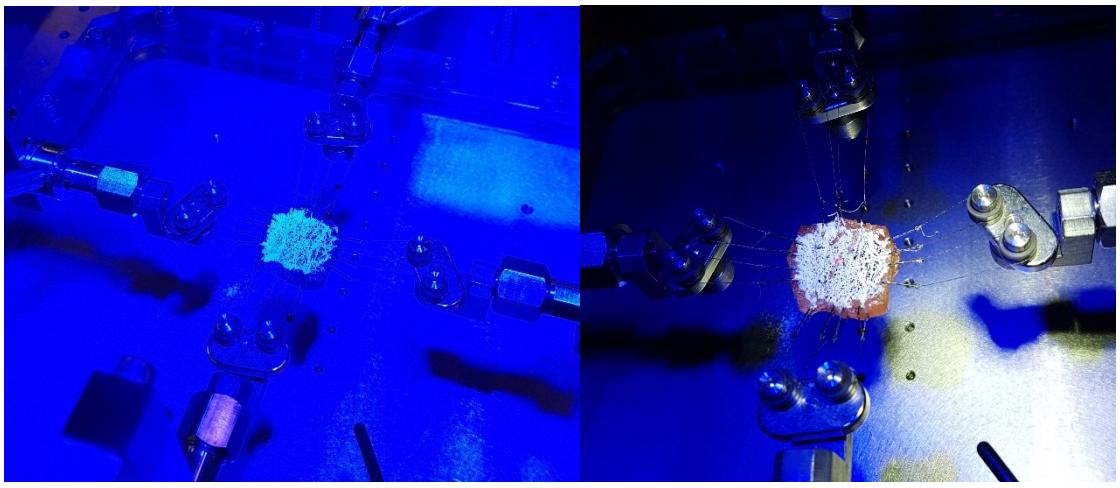

Fig. 102 Biaxial mechanical test set-up of porcine tissue samples

6.3.2 Experimental phase

The experimental phase used the setup as previously specified (shown in Fig. 103), including a Biaxial Testbench™ 200 Nm actuators and 20N loadcells, GOM Aramis™ stereoscopic imaging correlation device for deformation measurements.

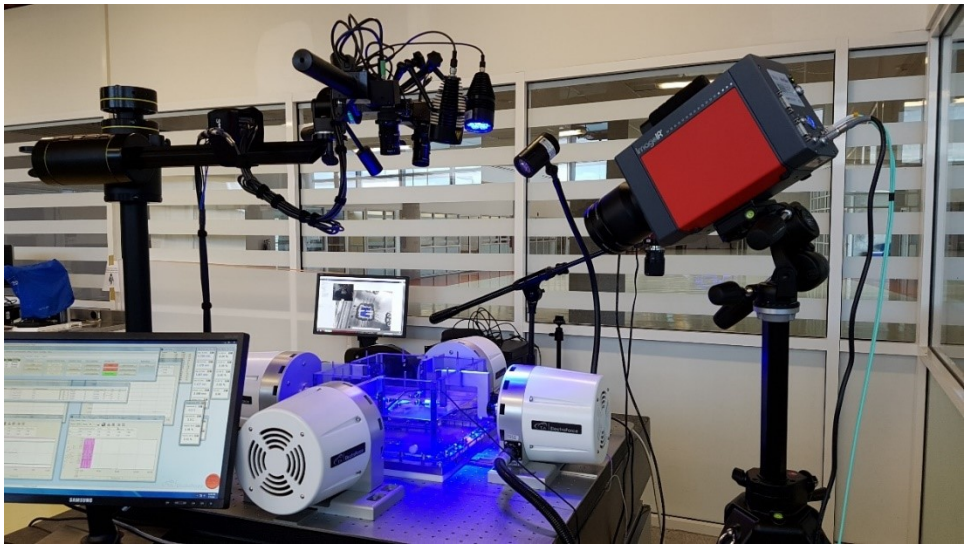

Fig. 103 Instrumentation and experimental set up for biaxial mechanical test of porcine liver tissue with strain analysis

The experimentation tests were performed on 5 porcine liver and abdominal wall tissue samples on a biaxial tensile cyclical test. Initial destructive tests were conducted in order to define the cycle parameters, as shown in Fig. 104. It was concluded to perform 5 cycles for liver to a maximum stretch ratio of $\lambda = 1.22$, and 6 cycles for abdominal wall tissue to a maximum stretch ratio of $\lambda = 1.53$.

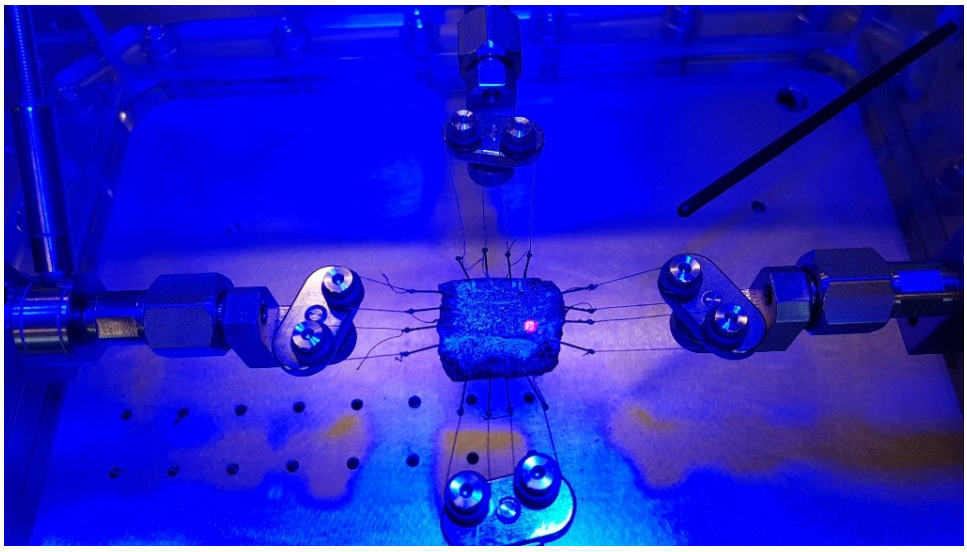

Fig. 104 Liver sample attached on to the biaxial mechanical test

A thermographic camera was used to verify the distribution of the heat in the bath chamber of saline water with temperature control set at 37°C. Higher heat concentrations were found in the central area surrounding the tissue, keeping its temperature to 33 – 35 °C.

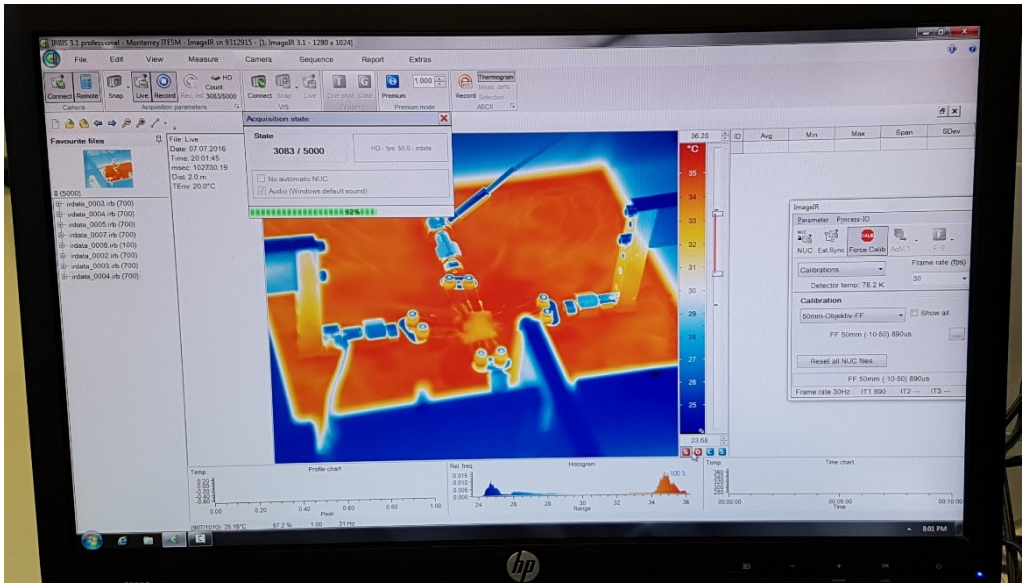

Fig. 105 Thermographic camera visualization of the experimental set-up.

Results were evaluated in the GOM Aramis™ software, in order to calculate the superficial deformations, having the capacity to create a 3D mesh of the sample surface at any time of the biaxial cyclical test. Using this software, it was possible to review the sample's initial state (as shown in Fig. 106) maximal deformation during the cyclical test (as shown in Fig. 107), and all middle deformation levels.

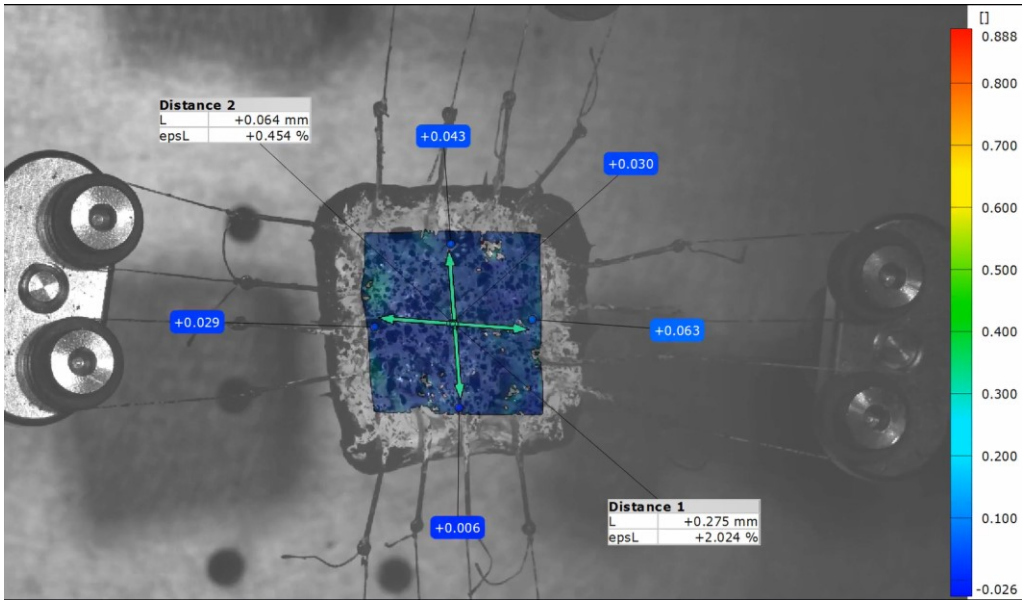

Fig. 106 Initial state of deformation analyzed using GOM Aramis™ with the biaxial mechanical test of porcine liver tissue

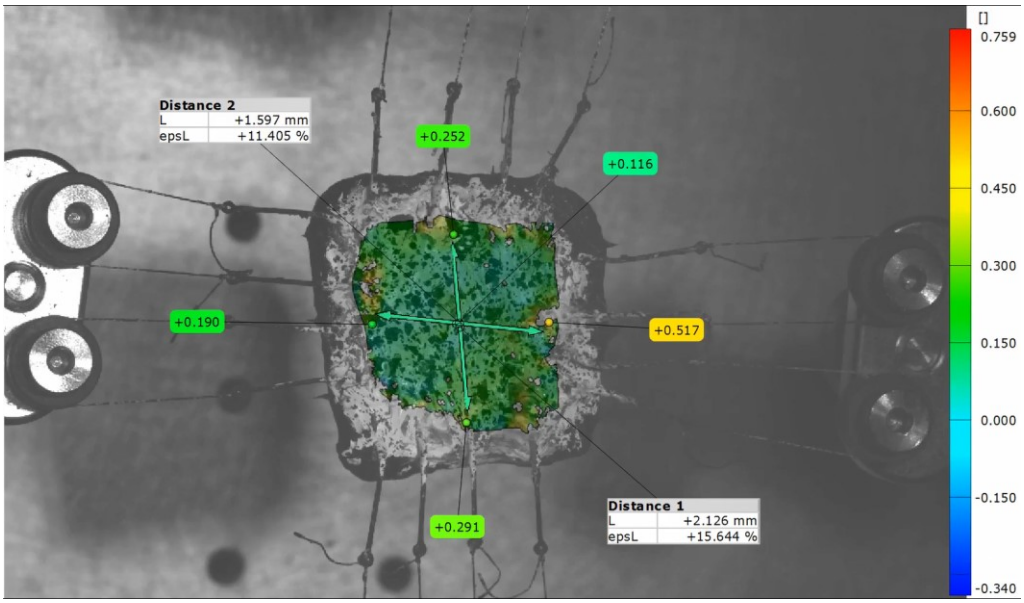

Fig. 107 Maximal deformation during cyclical biaxial testing with the biaxial mechanical test of porcine liver tissue

At the end of this analysis, it was possible to create a report for the samples and to export the deformation over time (as shown in Fig. 108). The information from the deformation analysis with GOM Aramis™ software was used to correlate with the data obtained from the biaxial testbench, that provides load and displacement over time for each axis (X and Y).

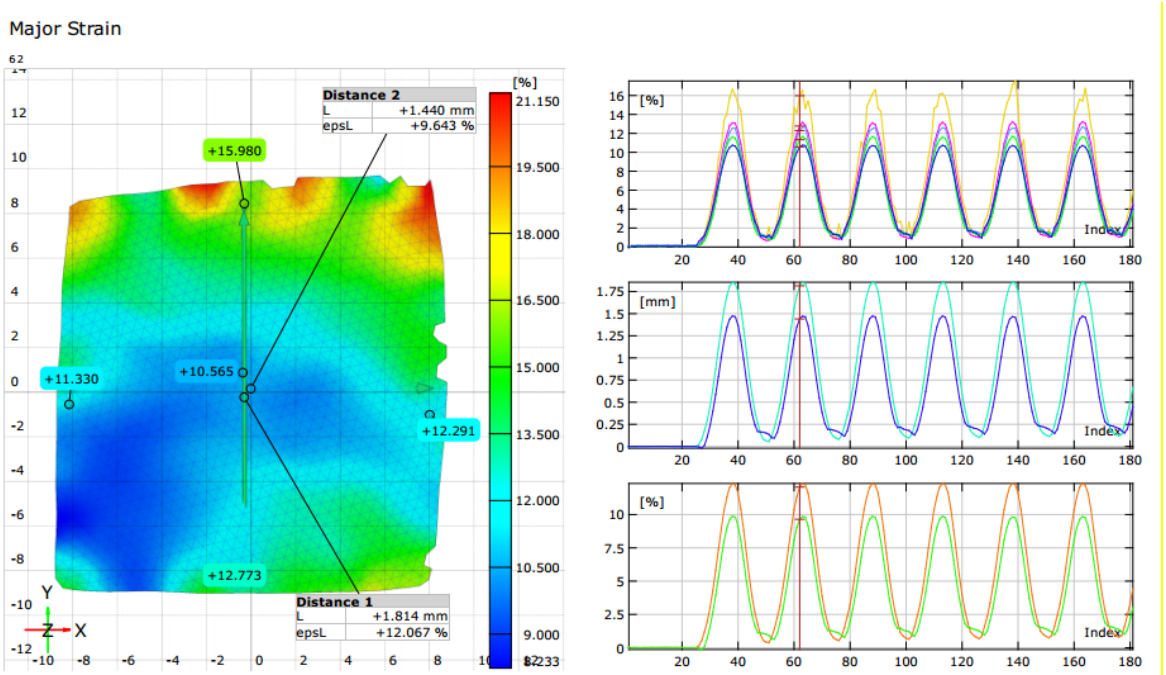

Fig. 108 Example of GOM Aramis™ report of an abdominal wall sample test.

Using this methodology, the experimental data of the mechanical behavior at biaxial tensile test was obtained for porcine liver tissue in X and Y axis. During these tests it was possible to notice that the anisotropy level presented in this tissue was not considered high, having a similar response in both axes, as shown in Fig. 109.

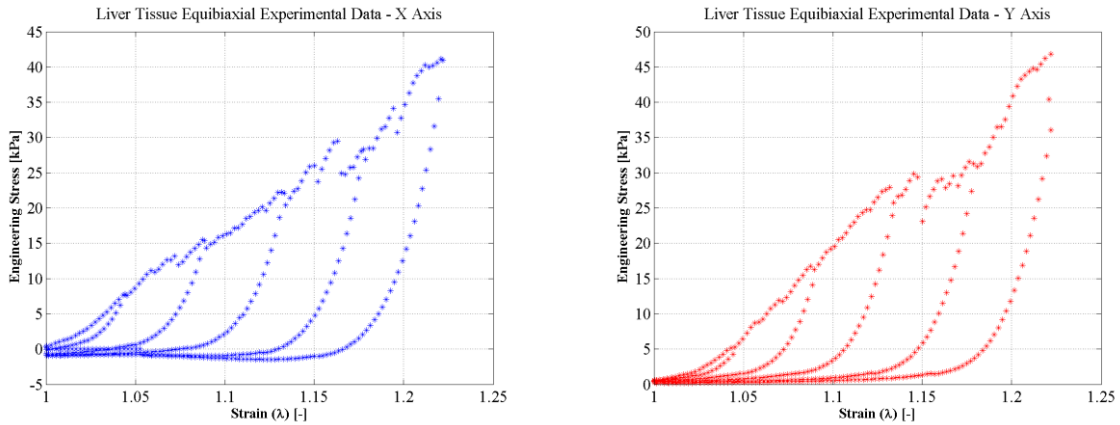

(a) (b)

Fig. 109 Porcine liver tissue biaxial experimental data: (a) X axis Stress-Strain curve; (b) Y axis Stress-Strain curve

Considering that the liver tissue is a random array of parenchyma cells with fibers is expected to have a low anisotropy level and the experimental data used to characterize its behavior confirm it. It shows that there is not a high difference between the X and Y axis response, so a different orientation of the EESM element will not represent a considerable impact on the predictions of the mechanical properties.

If a material with different composition and mechanical behavior was evaluated, like one with higher anisotropy and non-linearity, the impact of the orientation of the EESM element would be more evident.

This would be particularly true for materials with the anisotropic volumetric fraction oriented in a dominant direction. It can be reviewed by comparing the histological compositions of tissue samples, as shown in Fig. 110.

Based on this idea and using the same methodology, it was proposed to evaluate the mechanical behavior of porcine abdominal wall tissue considering that due to its histological construction it has a main orientation in the cell arrays.

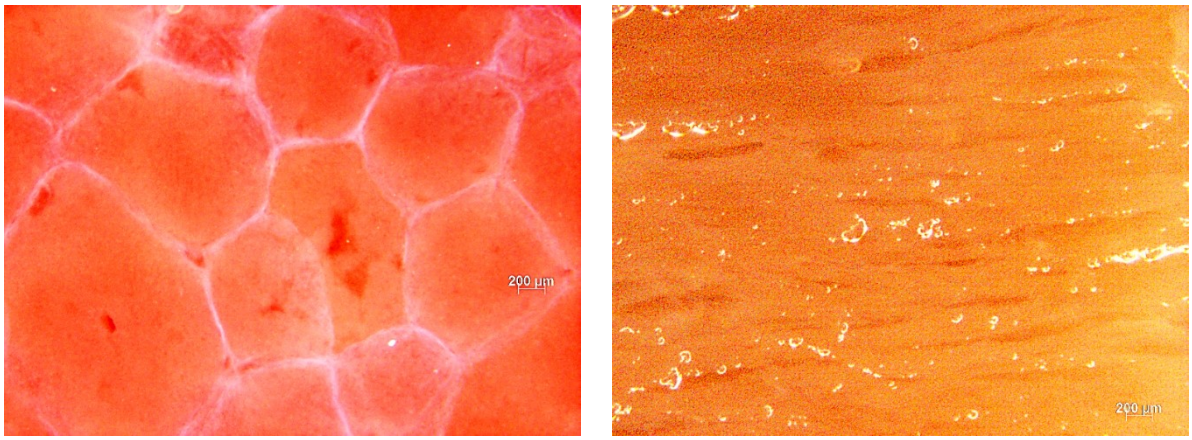

(a) (b)

Fig. 110 Microscopy pictures of tissue samples comparing histological compositions, showing different tissues can have: (a) A randomly distributed structure like porcine liver tissue or (b) A principal orientation in the structure like porcine abdominal wall tissue.

Using the same procedure as in in the previous case, the biaxial tensile cyclical test was performed on porcine abdominal wall tissue, the data was analyzed, and it was obtained the mechanical behavior in the X and Y-axis (as shown in Fig. 111). This experimental data was used for material characterization using the proposed SEDF.

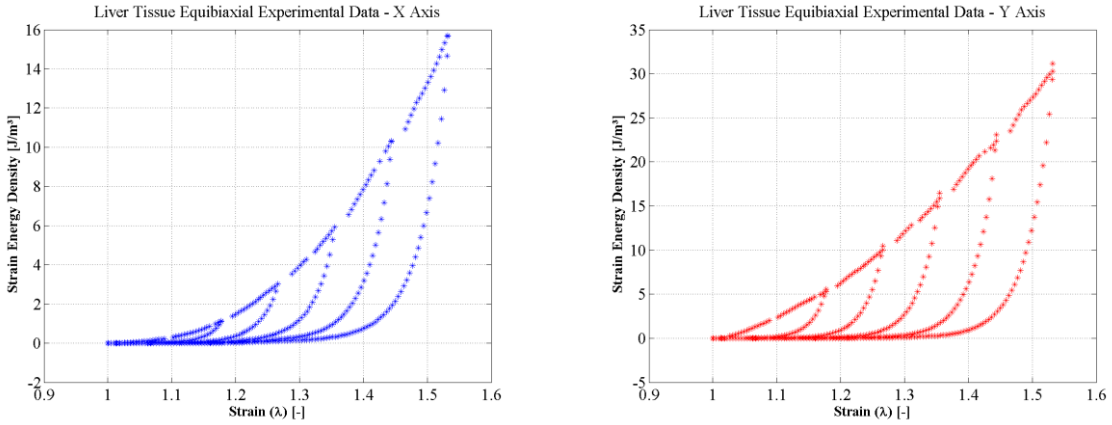

(a) (b)

Fig. 111 Porcine abdominal wall tissue biaxial experimental data: (a) X axis Stress-Strain curve; (b) Y axis Stress-Strain curve

EESM elements that align with the dominant direction would have a higher contribution to the stiffness function and the mechanical behavior than those with a different orientation.

Chapter 7

Material Modeling Final Results

In this chapter, the outcomes and results achieved from the implementation and development of this research process are presented, with a particular focus on material modeling, characterization, and simulation. All these results are a direct consequence of the methodology and tools that were described in detail in the past chapters.

Using the proposed hybrid model (EESM) described in chapter 5 and using the experimental data presented in chapter 6, for characterization of the mechanical properties of soft tissue, the results achieved for the implementation of this research are exposed in the next points. It was considered in three major areas:

(1) Material Characterization and Model Predictions:
In this section, the experimental data is used to find the parameters of the SEDF that characterize the mechanical behavior of the tissue samples at uniaxial and biaxial tension tests.

(2) Simulation Results:
Tests done in the simulation environment are provided as application proof of the proposed method and the EESM formulation in the framework. These were implemented to calculate the deformation presented in a liver mesh composed of EESM elements. The characterization parameters are used to solve the stiffness function of the EESM in an initialization phase, stored, and then used in the real-time simulation.

(3) Simulation Performance:
Measurements of the coefficient of determination and error are provided in order to demonstrate the accuracy of the EESM predictions compared with experimental data

and a simple SMM. Also, the time required by the implemented model was measured to provide evidence that the computational method can deliver a real-time response.

7.1 Material Characterization and Model Predictions

Using the SEDF proposed for the EESM formulation, parameters were found in order to characterize the mechanical behavior considering the total strain energy. The parameters that characterize the mechanical behavior of porcine liver tissue at the uniaxial tensile test are shown in Table *14*. The predictions of the mechanical behavior using these parameters with the SEDF are shown in Fig. 112.

Table 14 Parameters that characterize the porcine liver tissue behavior using SEDF.

Parameter	Porcine Liver Tissue
μ (kPa)	0.1000
f (%)	27.55
A1 (kPa)	9.6754
A2 (kPa)	7543.6
N	1.1974
C (kPa)	9.5273
b	3.3389
v_{ij} (m²)	3.569×10^{-5}

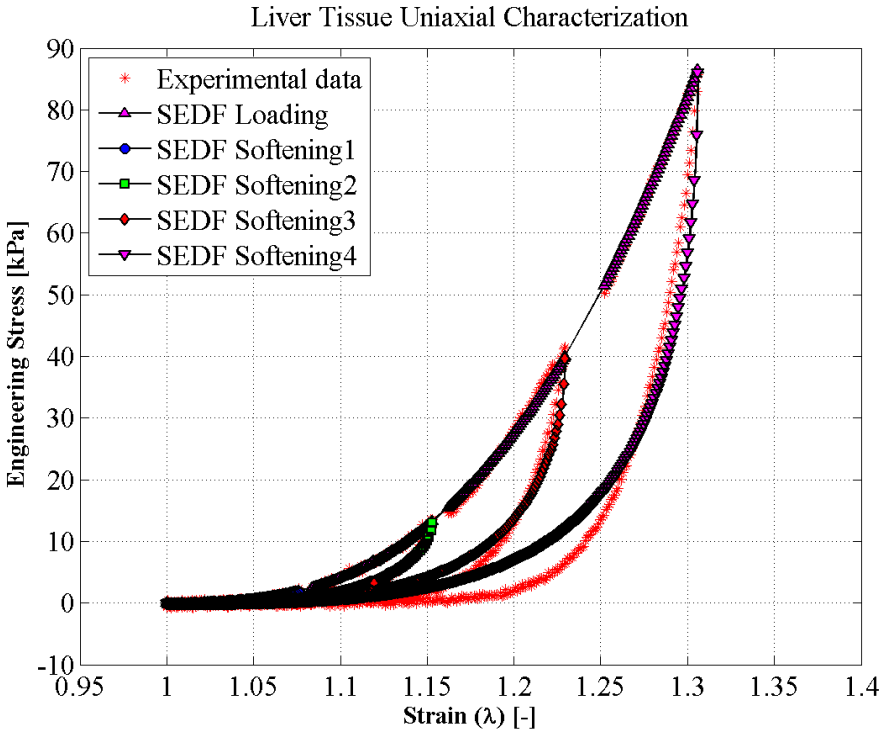

Fig. 112 Predictions of the mechanical behavior of porcine liver tissue using the SEDF and the characterization parameters in Table *14*.

Using this approach, now the EESM will be calculated based on the equivalent energy formulation proposed. Now, it is possible to define the stiffness function of an EESM element that will predict the behavior of the springs as shown in Fig. 113.

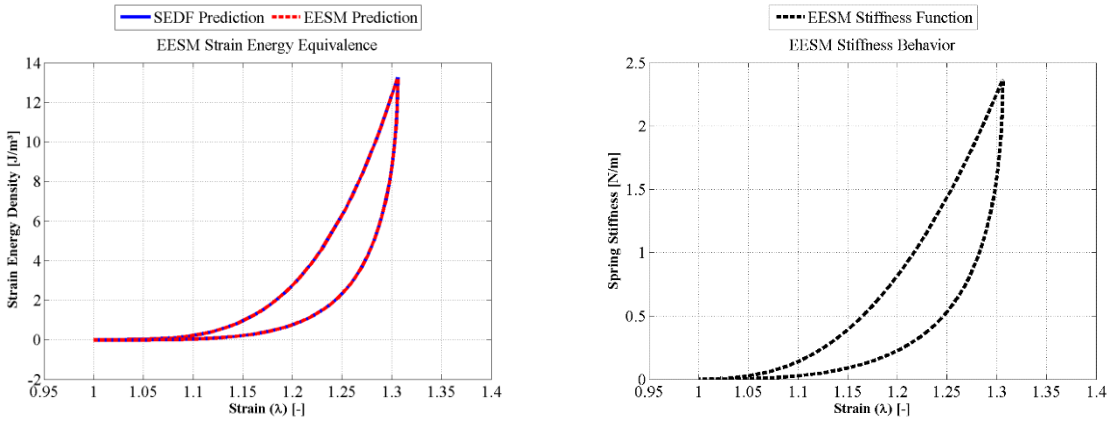

(a) (b)

Fig. 113 EESM results using parameters in Table *14*: (a) Strain Energy Equivalence between SEDF and EESM; (b) Stiffness function of an EESM element that predicts the behavior of the porcine liver tissue.

By applying the stiffness function to a one-dimensional element, it is possible to predict a similar behavior as the one presented in the soft tissue uniaxial tensile test.

In order to have a comparison, Fig. 114 shows the experimental data compared between a simple SMM and EESM elements predictions, showing that the proposed model is able to represent properties like the non-linear behavior of soft tissue and Mullin's Effect. It is considered that the inclusion of the Mullin's effect characterization in the EESM formulation by itself, it's a great contribution to the state of the art of the hybrid improvements proposed in the literature for the SMM.

The capacity of the EESM formulation to predict the material softening described by Mullin's effect is of high relevance for the graphical and force feedback that is going to be represented by this model. Since there was not found any current work on SMM that represent this mechanical property of the soft tissues for real-time simulation, it is considered a novel formulation.

By defining a different set of one-dimensional elements, it is possible to create different test cases for different springs that predict the behavior of porcine liver tissue. In this case, the test used three springs with different initial and final lengths (called Spring1, Spring2, and Spring3).

Spring1 is a liver EESM element submitted to deformation of λ =1.3, Spring2 was submitted to λ = 1.23, and Spring3 to λ = 1.15. These three EESM elements predicted similar behavior to the experimental data as shown in Fig. 115.

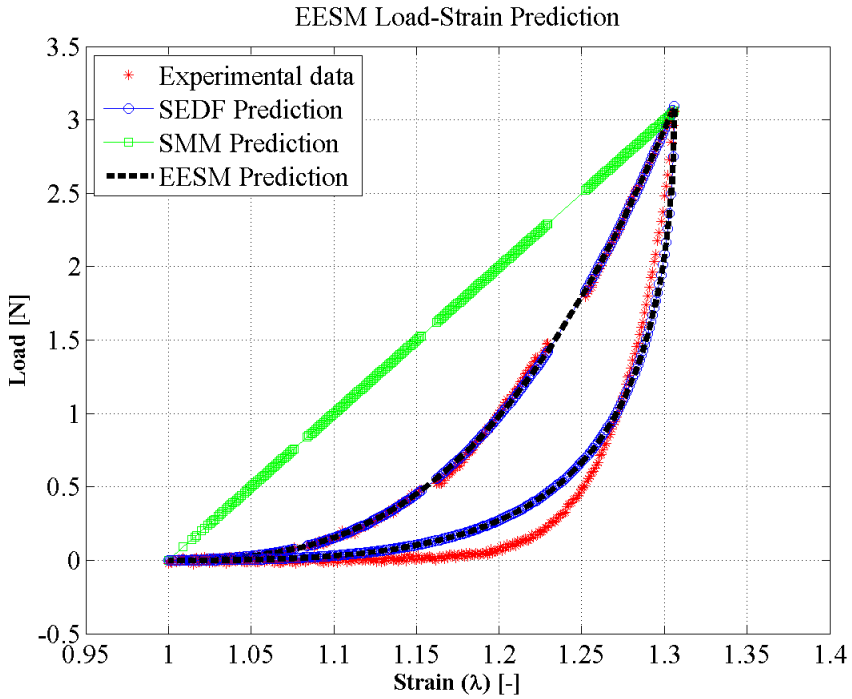

Fig. 114 Comparison between the experimental data of porcine liver tissue in uniaxial tensile test, a simple SMM prediction and the proposed EESM prediction.

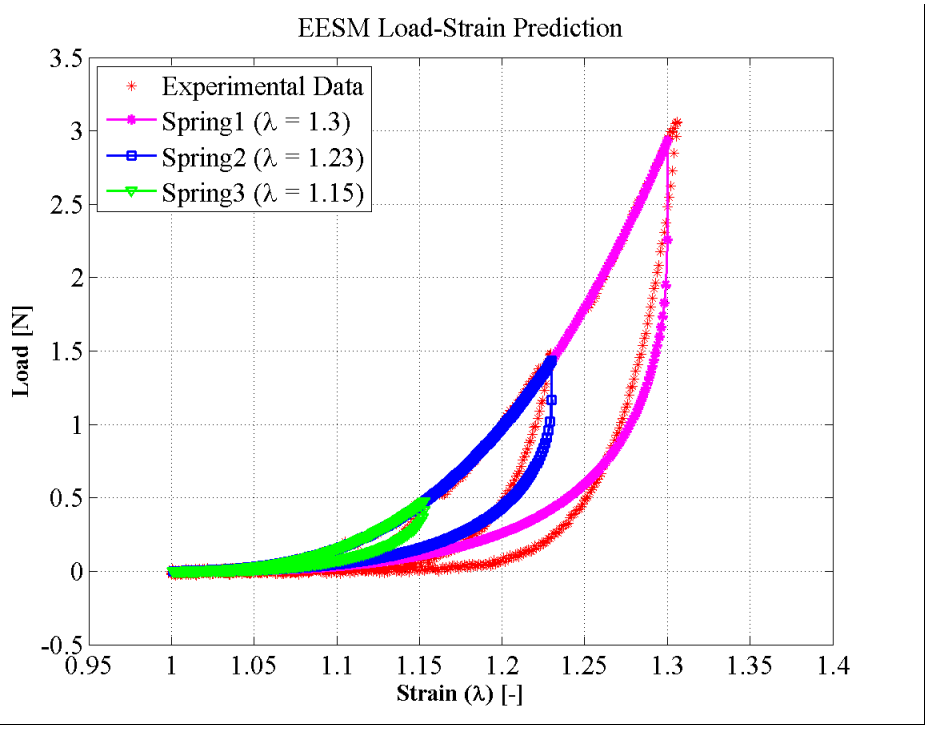

Fig. 115 Predictions of the mechanical behavior of three different EESM elements representing springs with variable stiffness that characterize the behavior of porcine liver tissue.

Using the biaxial formulation of the EESM, it is possible to characterize the behavior that the liver tissue sample shows in the experimental data by finding the parameters as shown in Table *15*. The predictions of the mechanical behavior using these parameters with the SEDF are shown in Fig. 116.

Table 15 Parameters that characterize the porcine liver tissue behavior using SEDF at biaxial tension test for the X and Y-axis.

Parameter	Porcine Liver Tissue X axis	Porcine Liver Tissue Y axis
μ (kPa)	6.7510	9.0871
f (%)	33.11	28.26
A1 (kPa)	-17.5013	-51.5393
A2 (kPa)	-375.1709	-741.5488
N	1.2926	1.2903
C (kPa)	0.0539	1.8483
b	4.2734	4.7536
v_{ij} (m²)	$6.25x10^{-5}$	$6.25x10^{-5}$

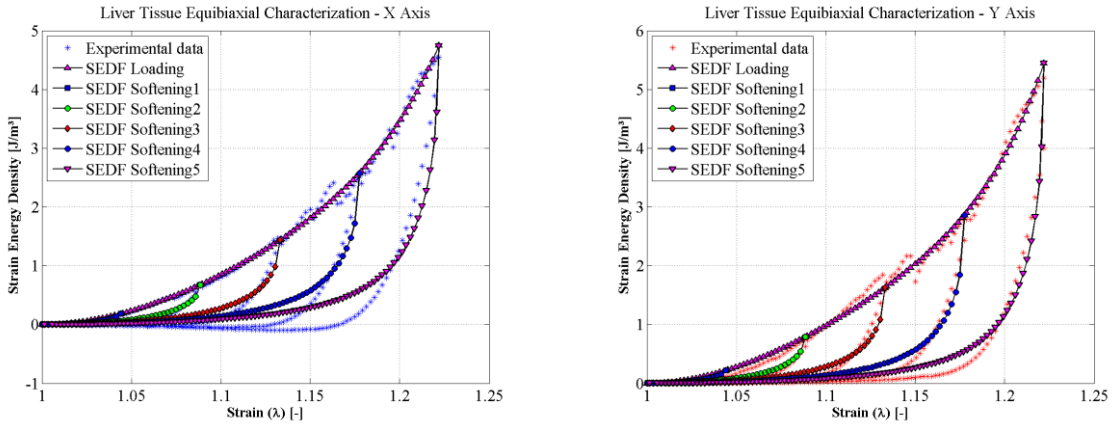

(a) (b)

Fig. 116 Predictions of the mechanical behavior of porcine liver tissue using the SEDF and the characterization parameters in Table *15*.

Following the same methodology applied in the uniaxial tension case, it is performed the equivalence of the EESM with the SEDF proposed in order to define the strain energy density, but now considering the mechanical behavior of the X and Y-axis as shown in Fig. 117.

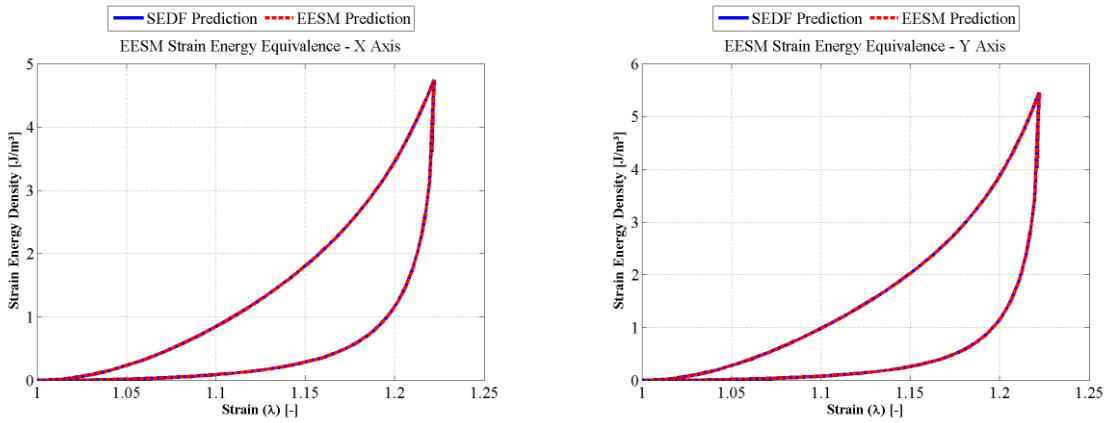

(a) (b)

Fig. 117 Strain Energy Equivalence with EESM using the parameters in Table 15: (a) X-axis strain energy density equivalence curve; (b) Y-axis strain energy density equivalence curve.

Then the stiffness function for the EESM element is defined for each axis, having $\kappa_{Sx}(\lambda_1)$ and $\kappa_{Sy}(\lambda_2)$ with behavior as described in Fig. 118. These functions will be used to calculate the stiffness parameters at each deformation stage, then they will be used in the real-time simulation to describe the variable stiffness properties of the EESM element to achieve the same strain energy level that the one described by the SEDF.

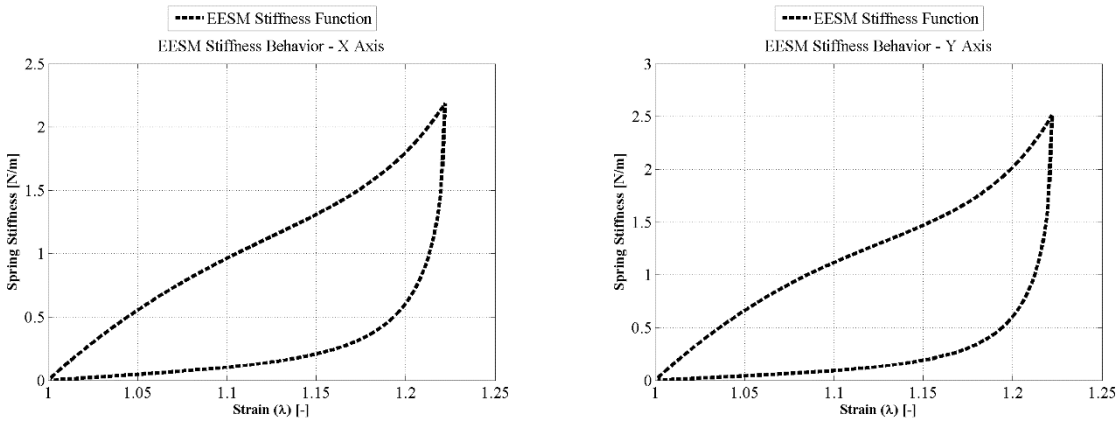

(a) (b)

Fig. 118 Stiffness function of an EESM element that predicts the behavior of the porcine liver tissue, based on the experimental data for (a) X-axis and (b) Y-axis.

Using the proposed biaxial formulation, it is possible to calculate the response of the EESM elements that predicts the mechanical behavior of the porcine liver tissue for the X and Y-axis.

These results are shown in Fig. 119 and were compared with the experimental data and a simple linear SMM element, using a constant stiffness that was calculated with the experimental data to try to predict the mechanical behavior.

Once again, the inclusion of the prediction of the softening described by Mullin's effect using the EESM biaxial formulation is also considered to be a great contribution to the state of the art of real-time simulation models applicable for soft tissues and composite materials.

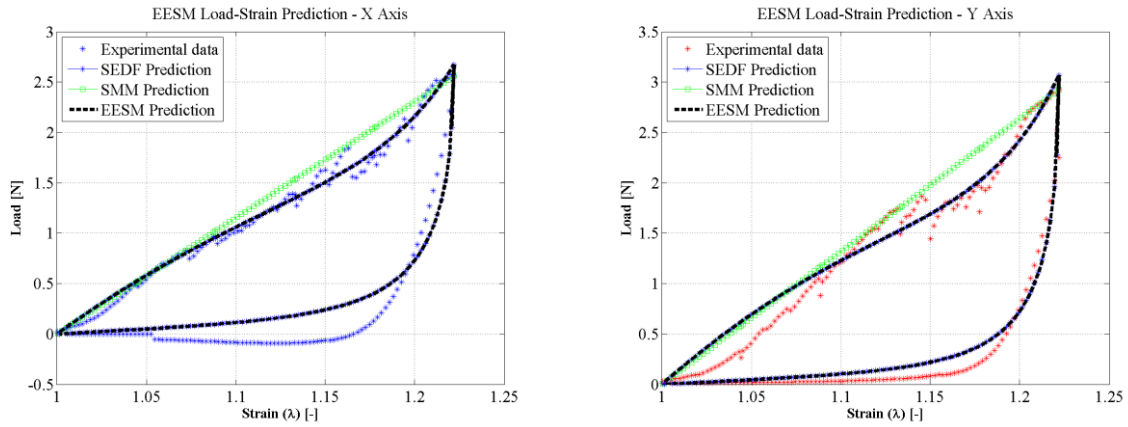

(a) (b)

Fig. 119 Comparison between the experimental data of porcine liver tissue in the biaxial tensile test, a simple SMM calculated with constant stiffness, and the EESM prediction: (a) X-axis Load-Strain curve; (b) Y-axis Load-Strain curve.

As shown in Fig. 119, even when the results of SMM are close to the extension behavior presented in the experimental data (in both axis), the softening at unloading is not possible to be calculated.

ESMM shows better results for extension and softening presented in the experimental data. It is important to mention that the maximum deformation for this biaxial test was $\boldsymbol{\lambda}$ = 1.2. This is relevant for the SMM good performance, considering that for larger deformations it would not be the same case.

Now it is possible to define a set of springs considering the biaxial formulation in order to predict the behavior of porcine liver tissue. Once again, three springs with different initial and final lengths were defined. Spring1 extended to $\boldsymbol{\lambda}$ =1.22, Spring2 to $\boldsymbol{\lambda}$ = 1.18 and Spring3 to $\boldsymbol{\lambda}$ = 1.12. These tests provided predictions with similar behavior to the one presented in the experimental data for each axis, as shown in Fig. 120Fig. 149.

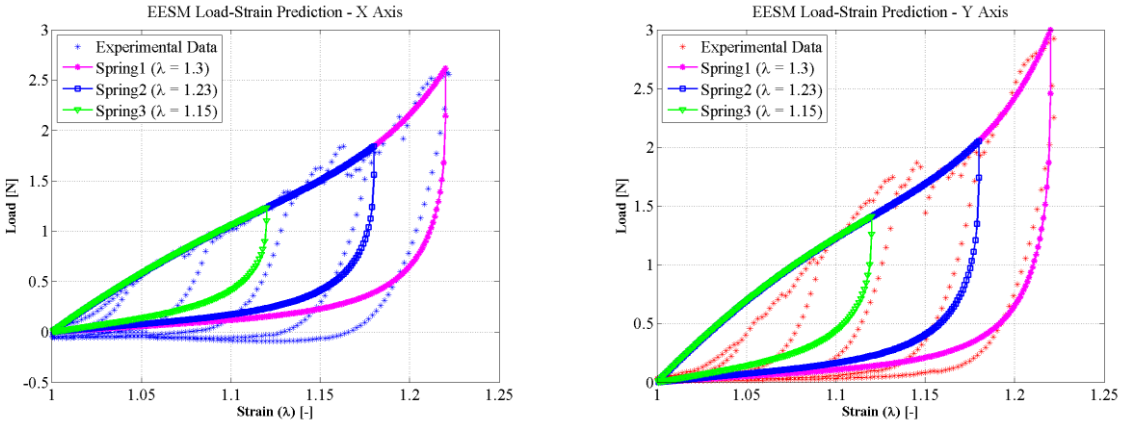

(a) (b)

Fig. 120 Mechanical behavior of three different EESM elements representing springs with variable stiffness that characterize porcine liver tissue: (a) X-axis predictions; (b) Y-axis predictions.

Since this information characterizes the mechanical behavior of the porcine liver tissue on both axis (X and Y), it is possible to use the formulation for the creation of EESM elements with different orientations, based on the directional cosines. As shown in Fig. 121, the formulation has good results to predict the behavior of the proposed orientations.

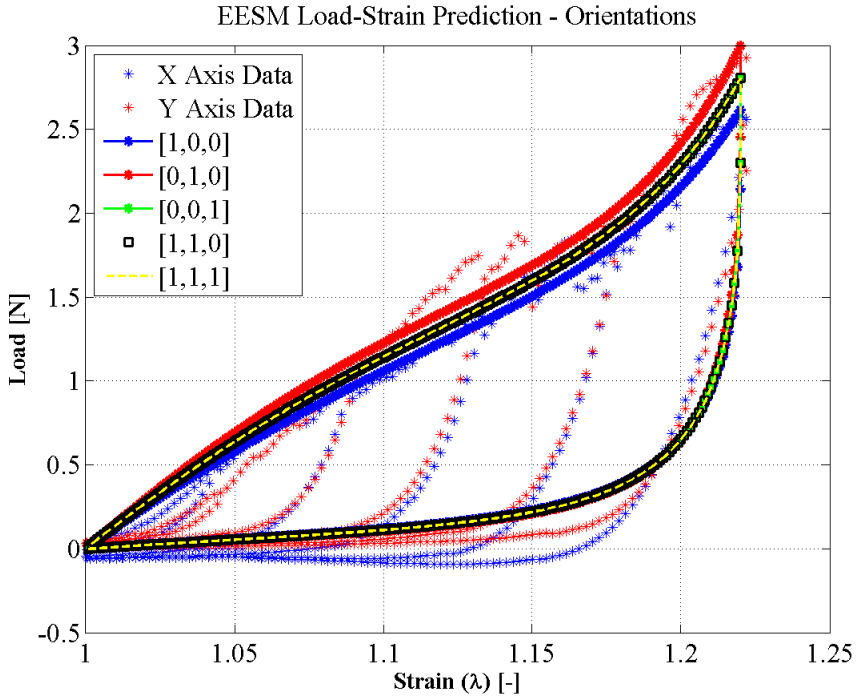

Fig. 121 Using **λ** = 1.22 it was possible to define a set of multiples orientations for EESM elements, and what would be their predictions compared with the mechanical behavior of porcine liver tissue.

As mentioned before, it was expected that due to its histological structure the porcine liver tissue has a low level of anisotropy, considering that the anisotropic fraction of fibers is randomly distributed, as shown in Fig. 110.

Now, the characterization and evaluation of the porcine abdominal wall using the formulation of the biaxial EESM. It is expected that due to its histological structure (shown in Fig. 110), it will present a dominant orientation of the fibers, increasing the level of anisotropy compared with the previous case. Then, the orientation of the EESM elements will have a higher impact on the stiffness function defined for the predictions of the mechanical behavior.

In order to prove this, the characterization and predictions of porcine abdominal wall tissue were performed, obtaining the data included in Table *16* and presenting a considerable difference in behavior between the X and Y-axis, as shown in Fig. 122.

Table 16 Parameters that characterize the porcine abdominal wall tissue behavior using SEDF at biaxial tension test for the X and Y-axis.

Parameter	Porcine Abdominal Wall Tissue X axis	Porcine Abdominal Wall Tissue Y axis
μ (kPa)	0.1080	143.32
f (%)	13.18	10.0
A1 (kPa)	74.2814	-7748.2
A2 (kPa)	175.7885	-1466.3
N	7.9494	5.4077
C (kPa)	0.4750	6.8297
b	2.3485	2.7964
v_{ij} (m²)	6.25×10^{-5}	6.25×10^{-5}

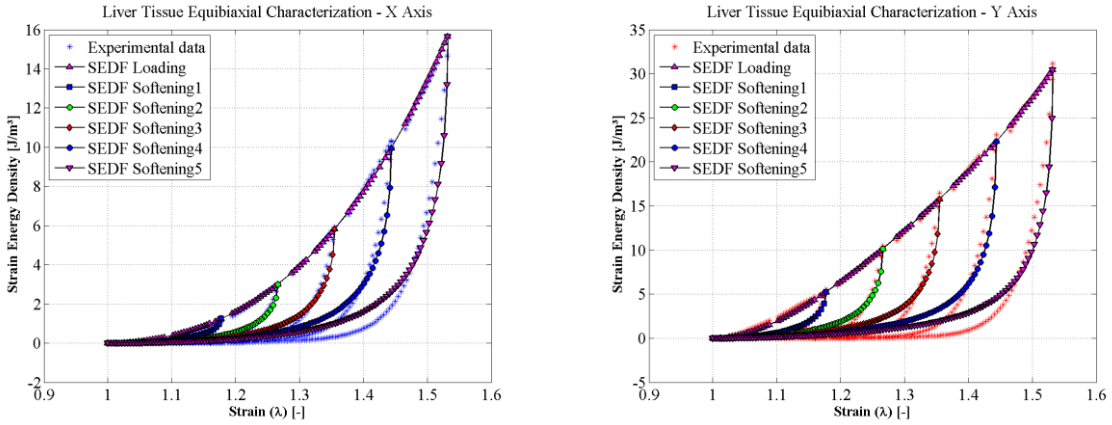

(a) (b)

Fig. 122 Predictions of the mechanical behavior of porcine abdominal tissue using the SEDF and the characterization parameters in Table *16*.

Following the same methodology applied for the biaxial tensile test on the porcine liver tissue samples, it is performed the equivalence of the EESM with the SEDF, considering the mechanical behavior of the X and Y-axis as shown in Fig. 123.

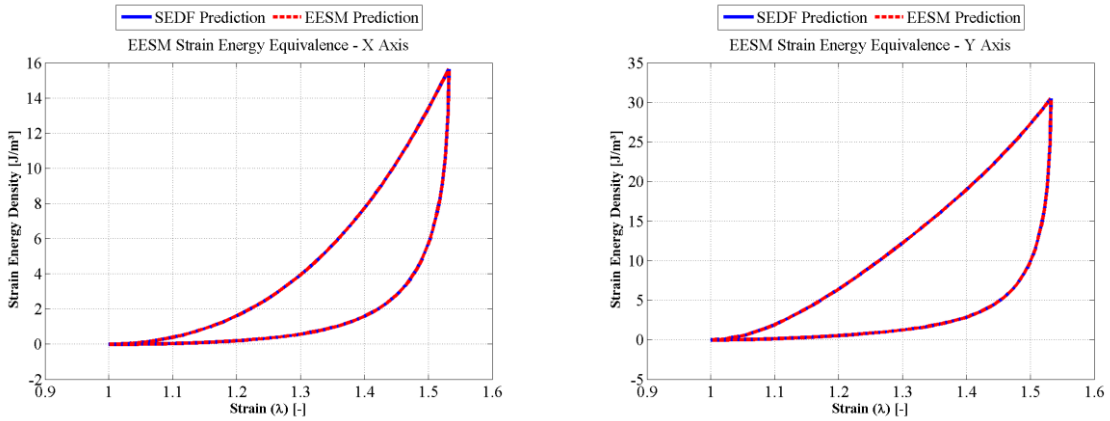

(a) (b)

Fig. 123 Strain Energy Equivalence curve with EESM using the parameters in Table 16: (a) X-axis strain energy density; (b) Y-axis strain energy density.

As performed in the previous cases, the stiffness function has to be obtained from the Strain Energy Density equivalence defined for the EESM element.

This is done for each axis to create $\kappa_{Sx}(\lambda_1)$ and $\kappa_{Sy}(\lambda_2)$ that will be used to describe the mechanical response of the EESM element as shown in Fig. 124.

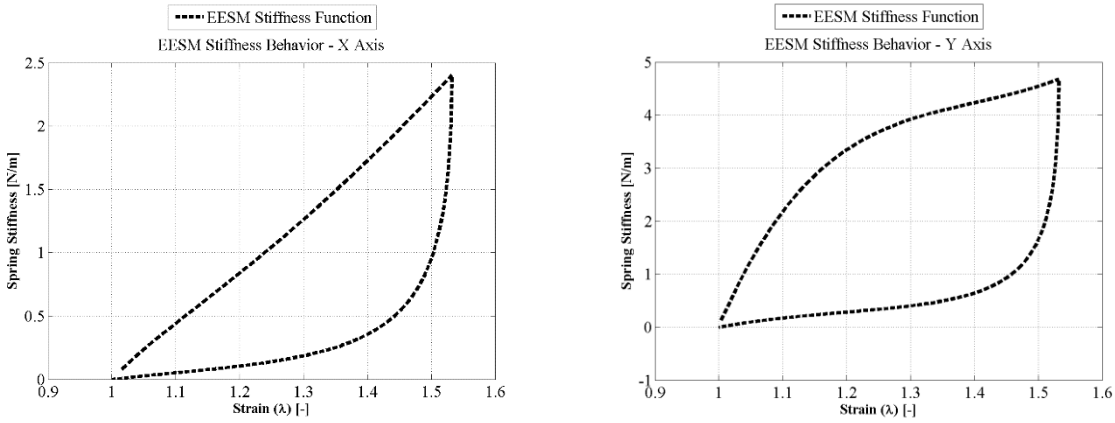

(a) (b)

Fig. 124 Stiffness function of an EESM element that predicts the mechanical behavior of the porcine abdominal wall tissue for (a) X-Axis and; (b) Y-axis.

Using the EESM biaxial formulation, the predictions for the mechanical behavior of the porcine abdominal wall tissue for the X and Y axis were calculated and compared with

the experimental data and a simple linear SMM element. The results are shown in Fig. 125.

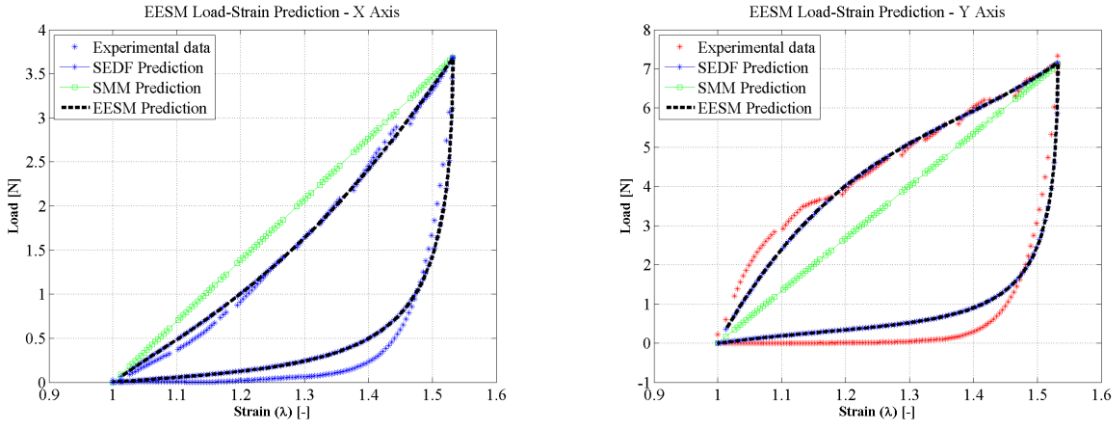

(a) (b)

Fig. 125 Comparison between the experimental data of porcine abdominal wall tissue in biaxial tensile test, a simple SMM prediction and the proposed EESM prediction: (a) X-axis Load-Strain curve; (b) Y-axis Load-Strain curve.

A set of testing EESM elements were defined for different values of **λ**, in order to compare the proposed model predictions versus the experimental data. As shown in Fig. 126, three springs with **λ** = 1.53, **λ** = 1.35, and **λ** = 1.17 were created presenting good results.

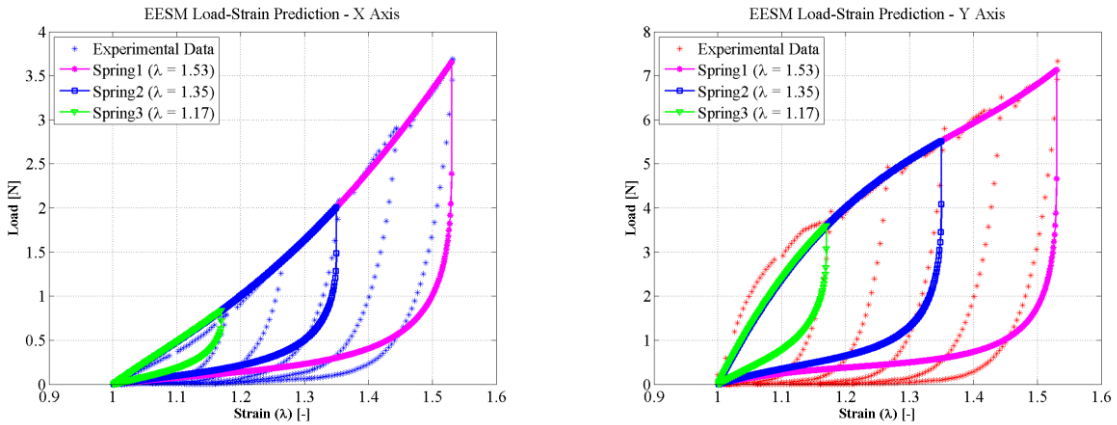

(**a**) (**b**)

Fig. 126 Predictions of three different EESM elements that characterize the mechanical behavior of porcine abdominal wall tissue: (a) X-axis; (b) Y-axis.

As stated previously, the porcine abdominal wall tissue presented a higher level of anisotropy compared with porcine liver tissue, having a big difference between the X and Y-axis mechanical behavior. Using the proposed formulation, it was defined a set of

EESM elements with different orientations were submitted to a large deformation of λ = 1.53, the predictions of their behavior were calculated and is being presented in Fig. 127.

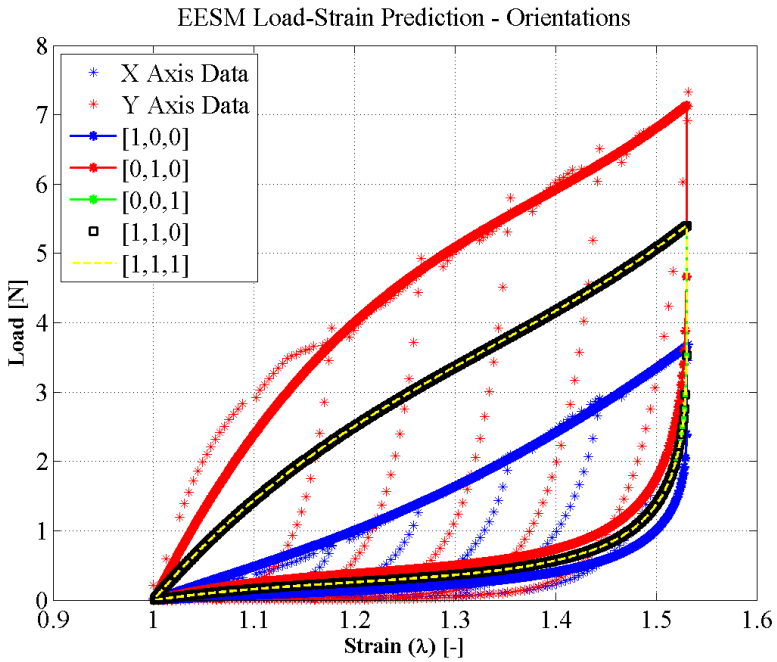

Fig. 127 Using **λ** = 1.53 it was possible to define a set of multiples orientations for EESM elements, and what would be their predictions compared with mechanical behavior of porcine abdominal wall tissue.

The results in Fig. 127 shows the impact of the EESM element initial orientation in defining their stiffness function. In this way, their contribution in the mechanical response to tension is much more evident than in the previous case.

These results demonstrate the capability of the proposed EESM formulation for prediction of mechanical behavior of multiple materials, considering heterogeneous composition, anisotropy, non-linearity, and Mulling's effect at softening.

7.2 Simulation Results

The proposed formulation was implemented on a framework for virtual reality developed on previous works. First, the stiffness parameter of the EESM model is calculated using Eq. 16, in chapter 5.4. Doing this will create a function for the change in the stiffness properties of the spring based on the SEDF and the experimental data. The stiffness behavior would no longer be linear as shown in Fig. 121.

Then, it is possible to calculate the response of any one-dimensional element in order to represent the behavior of soft tissue by determining the force considering the current state of deformation of each element (using a different stiffness parameter in function of the current strain of the element).

Since the main objective is to run on a real-time virtual simulation system, the implementation performance of this model was measured. Running the calculation process on an Intel® Core™ i7-4510U @ 2.00GHz with 8GB RAM for a test mesh of 5322 elements.

The initialization phase to get the parameters from λ = 1 to λmax needed 1430 ms to read, solve and store data of EESM. Then this information was used on the real-time simulation cycle for deformation calculation, presenting 31 fps refresh rate (taking 31.49 ms to calculate each iteration).

Compared with the performance of the initial framework, this implementation represents an improvement. In the original simulation cycle, the framerate achieved was 19.71 fps. This improvement is represented by the fact of doing the pre-calculation of the stiffness function and storing this information, allowing a quicker response by not having to calculate certain forces at each deformation stage.

Considering the improvement in the time response, it was also applied a visual rendering of superficial textures in original meshes, in order to show a better graphical environment as presented in Fig. 128. It is important to mention that the decision of using the same mesh in the simulation framework is to allow a direct comparison of the impact on the performance of the implementation of this research. Using the *VISUALIX* module, new geometries can be created and used for simulation or any other application.

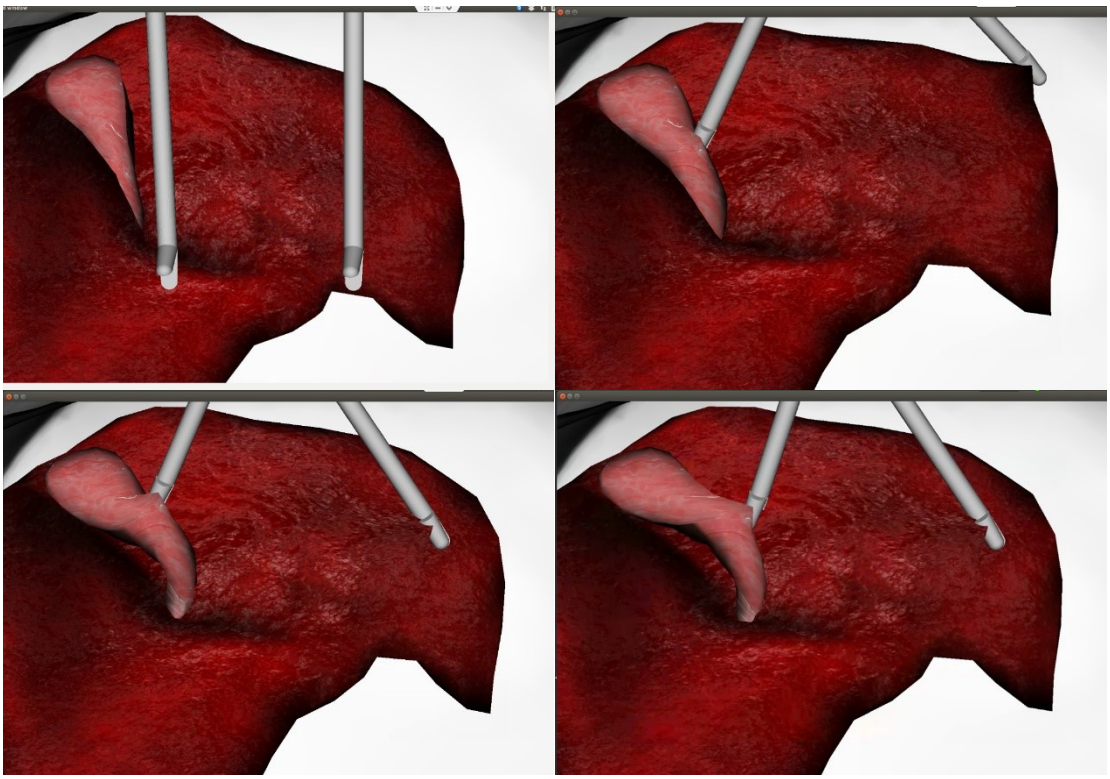

Fig. 128 Virtual application for real-time simulation of liver and gallbladder meshes using the proposed model

7.3 Simulation performance

For validation purposes, a simulation test environment was created as described in section 2.4 to allow interaction with the meshes and simulate the behavior of the material using the proposed model and defined parameters during characterization.

As a measurement of the error for the proposed model versus the experimental data, it was calculated the coefficient of determination R^2 for the formulation at extension and unloading for the different materials that were characterized and compared with an SMM. The result for each case is presented in Table *17*.

Table 17 Coefficient of determination R^2 of the EESM formulation compared with the experimental data at extension and softening.

Material Experimental Data	**R^2 EESM Extension (%)**	**R^2 SMM (%)**	**R^2 EESM Softening (%)**
Porcine Liver Tissue Uniaxial Tension	99.94	15.11	93.23
Porcine Liver Tissue X Axis – Biaxial Tension	98.84	95.73	76.04
Porcine Liver Tissue Y Axis – Biaxial Tension	95.30	92.75	92.76
Porcine Abdominal Wall Tissue X Axis – Biaxial Tension	99.59	90.26	91.05
Porcine Abdominal Wall Tissue Y Axis – Biaxial Tension	97.03	72.57	82.19

As Table *17* shows, the extension prediction of the EESM model has a great fit with the experimental data, representing from 0.06% to 4.7% of error. Compared with SMM, it can be found more consistent performance considering the variation of the error, which goes from 4.3% up to 85%. It should be considered that the cases where SMM showed a low error were the ones with a maximum deformation of $\boldsymbol{\lambda} = 1.2$, as stated before this is important for its performance since for larger deformations the soft tissue is expected to preset non-linear behavior and the error will increase.

As mentioned before, it is considered that the inclusion of the softening characterization in the EESM formulation is a novel proposal and has no comparison point with other hybrid models based on SMM, since there have been no developments that allow predicting this property. In this case, EESM shows from 6.8% to 24% of error, which is considered a good result thinking that softening properties depend on the maximum deformation at each cycle and the model should characterize all of them.

Therefore, it is important to consider that EESM characterization parameters are calculated to predict softening at all possible deformations using each cycle of experimental data. If only the behavior at the last cycle with $\boldsymbol{\lambda}$max was considered, it

would provide the best results for this error test but would not represent as good for **λ** at other cycles.

The calculation of the EESM formulation is performed in an initialization phase, which is not executed in real-time, and it does not affect the graphical rendering refresh cycle. After the calculations for the stiffness functions are stored for all EESM elements in the simulation mesh, the performance in real-time no longer depends on the constitutive model based on the SEDF, but only on the complexity of the simulated mesh, particularly in the number of EESM elements.

In validation tests, the implementation of the proposed model gets a refresh rate of 25 to 32 Hz. An initial test was done with a Liver geometry, conformed by 5322 EESM elements required 1522ms for the initialization process. Each simulation cycle for calculation of deformation and graphical update required 31.49ms, representing a 31fps update rate. The computer used for this test had an Intel® Core ™ i7-4510U @ 2.00GHz / 8GB RAM.

As previously described, the requirement for a system like this to be considered real-time is to allow 25-30 frames per second (FPS) on graphic feedback (Goldenberg et al., 2017, Goulette & Chen, 2015, Nguyen et al., 2020). Under these criteria, the current test provides information that the system allows the virtual simulation to have a real-time response.

Chapter 8

Conclusions & Future Works

In this chapter, it is included the discussion on the results presented in chapter 7, as well as the conclusions of the research project performed for this dissertation. It also includes a section on future works and potential opportunities identified during the development of this work. All code and scripts developed during this research work were uploaded to online repositories, included in the Repository List (Appendix A.2).

8.1 Conclusions

At the end of this research project, it can be defined that a hybrid model based on an energetic equivalence was created. This model allows to represent the mechanical behavior of soft tissue in real-time simulation.

Tension tests were performed, and the experimental data was used to characterize porcine liver mechanical properties. Using this information, the model predictions were validated.

Even when this model was applied to a simulation mesh based on skeleton structure, it can be applied to other meshes with one-dimensional elements.

A method was established for characterization and real-time simulation using the proposed model. This method can be used for other kinds of biomaterials and simulations.

The EESM formulation was implemented, and it was possible to represent the mechanical properties of soft tissue in a real-time simulation. The hybrid construction between the SMM and the SEDF shows good results to create the proposed model, being able to have

the accuracy of a complex constitutive model with the computational performance of a simple model.

As shown in the results, the EESM formulation was possible to represent the non-linear behavior at extension and softening of the soft tissues and composite materials, compared with experimental data. The proposed model presented an error between 0.06 and 4.7% for extension and 6.8% to 24% for softening.

These error values are considered to be good compared with the range of error that the SMM presented at the best possible fit for extension, which was between 4.3% and up to 85%, and without comparison for softening since it is not possible for the model to represent this property.

These results demonstrate that it is possible to use the proposed model EESM to predict the mechanical behavior of soft tissue and other composite materials, applied in a real-time simulation. The proposed model predicts the mechanical properties of soft tissues for large deformation, considering the characterization of non-linearity, anisotropy, and softening.

As it was mentioned before, EESM formulation is a contribution to the state of the art of hybrid models created in order to improve the capacity of the SMM to predict the mechanical behavior of soft tissue.

There have been other formulations, based on SMM with different approaches, that have achieved to represent the non-linearity at large deformation presented by the soft tissues (Nguyen et al., 2020, Omar et al., 2022, Zhang et al., 2017), but it was not found any previous works that provide any prediction of the softening characterized by Mullin's effect, being considered a novel formulation.

Also, another relevant contribution is to consider the orientation of the elements with respect to the dominant direction of the material anisotropic volumetric fraction to calculate their contributions to the stiffness function, using biaxial experimental data to characterize the anisotropic behavior.

This model made it possible to have the benefits of the two main components of the hybrid formulation, having the fast computational time response of the SMM and the accuracy to predict the mechanical behavior of the SEDF that considers the rule of mixture of isotropic and anisotropic energy contributions.

It is important to remember that models based on linear elasticity theory (like SMM) can only be used to predict the behavior of soft tissue in small deformations (< 10%), since it is this strain region that the material can be considered to have a linear response as shown in Fig. 129.

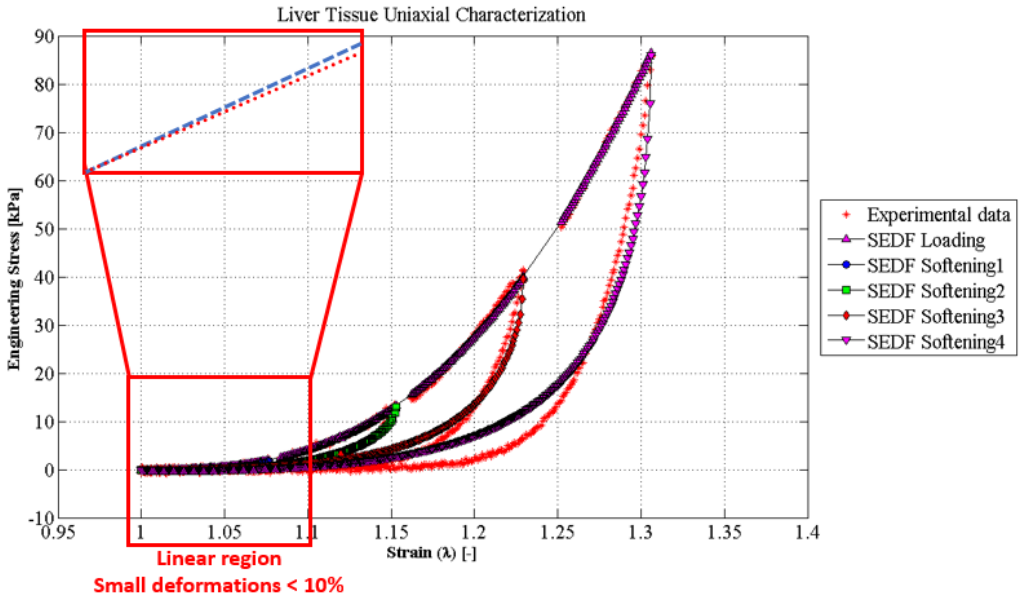

Fig. 129 Graphical description of why linear elastic models like SMM have issues predicting the mechanical properties of soft tissues and biological materials.

The benefits on the accuracy of the EESM model to predict the mechanical behavior over SMM and other linear elastic models are clear when it is used on large deformations (> 10%). Biological tissues and other composite materials have non-linear behavior at large deformations, which require a model that can represent these properties as shown in Fig. 130.

The results shown in Fig. 130 demonstrate that EESM formulation can represent the behavior of soft tissue and biological materials with higher accuracy than SMM. This includes characterization of the nonlinear behavior in large deformation and Mullin's effect.

As mentioned before, it is considered that the inclusion of the softening prediction in the EESM formulation is a novel proposal. It has no comparison point with other hybrid models based on SMM, since there were not found any developments that allow to predict this property.

In this case, the EESM formulation presents a range of error from 6.8% to 24%, which is considered to be good enough since the model should characterize softening at all possible deformation levels, but this property depends on the maximum deformation at each cycle.

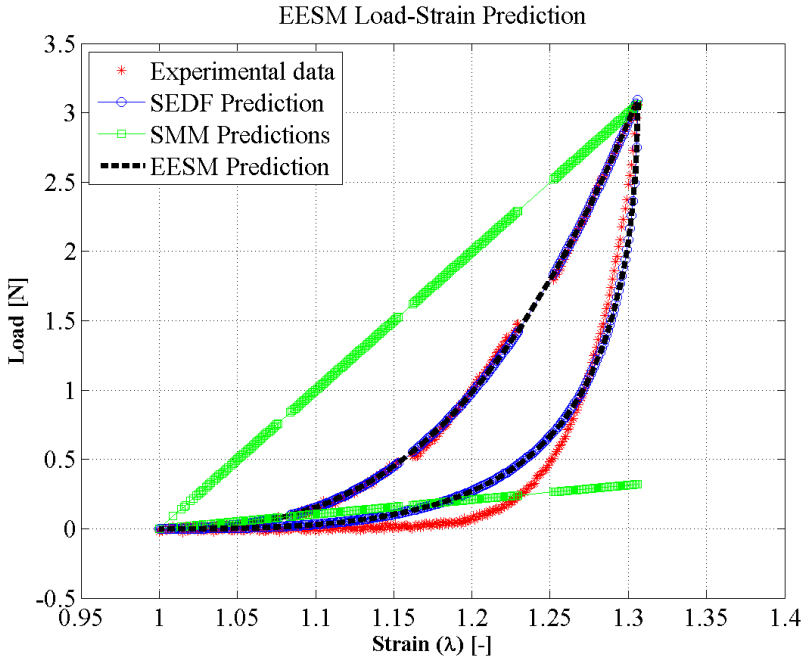

Fig. 130 Comparison of the Load-Strain Predictions obtained using the SMM versus the EESM, showing the benefits of the proposed model.

Another reason that justifies the variation in the error levels is that experimental data from each cycle of the material samples tension tests were used to calculate the EESM characterization parameters presented in this work. This was done in order to predict the softening behavior at different deformation levels with these EESM parameters. The error values presented in this work would be reduced if only the behavior at the $\boldsymbol{\lambda}$max cycle was considered, but then the results for lower $\boldsymbol{\lambda}$ cycles would not match the experimental data.

The calculation of the EESM formulation is performed in an initialization phase, which is not executed in real-time, and it does not affect the graphical rendering refresh cycle. After the calculations for the stiffness functions are stored for all EESM elements in the simulation mesh, the performance in real-time no longer depends on the constitutive model based on the SEDF, but only on the complexity of the simulated mesh, particularly in the number of EESM elements.

This implementation improved the simulation time and allowed the implementation of new tools for the visualization of the simulation environment, as shown in Fig. 128. As was mentioned before, the decision of using the same mesh in the simulation framework is to allow a direct comparison on the performance. It is possible to create new simulation meshes and apply this material model to new geometries by using the *VISUALIX* module.

8.2 Main contributions

A summary of the contributions of this research project is presented, focused on the two areas proposed in the methodology of this research project.

The main contributions identified in this work for material modeling are:

(1) EESM formulation is proposed: A new hybrid model for characterization of soft tissues and composite materials on real-time simulation, with improvements not found in the literature (Nguyen et al., 2020, Omar et al., 2022, Zhang et al., 2017).
- The proposed model can be used in real-time for predictions of other composite materials after its characterization. This shows potential applications not only for training and in medical areas, but also for industrial and technological applications.
- This formulation is able to predict softening described by Mullin's effect. No other work in the literature was found to be able to model this material property using SMM for real-time simulation.
- This formulation also predicts the non-linear behavior of materials at large deformations. This was done applying a hybrid construction never used before in the literature.
- The implemented methodology allows representation of the anisotropic behavior of materials by calculating its stiffness function considering the initial orientation of the element. No other work in the literature was found to apply this geometrical approach to predict anisotropy.

(2) Characterization of soft tissue with EESM formulation using experimental data.
- Biaxial cyclical tension tests were performed in order to characterize the mechanical behavior of porcine liver and abdominal wall tissue using EESM formulation.
- Uniaxial cyclical tension tests were performed in order to characterize the soft tissue behavior of porcine liver tissue using EESM formulation.
- No other works in the literature were found to perform experimental tests to characterize the soft tissue mechanical behavior for real-time simulation (Nguyen et al., 2020, Omar et al., 2022, Zhang et al., 2017).

The main contributions identified in this work for geometrical modeling are:

(1) *VISUALIX* module: An open-source tool was developed implementing a compendium of the state-of-the-art visualization techniques with a different approach (Abdallah et al., 2015, Fajar et al., 2020, Williams & Drew, 2019).
- Module for interactive processing and visualization of medical images.
- Focused on a training approach with virtual reality, not found in the literature.
- This was developed for the specific application of interactive processing and semi-automated segmentation of anatomical structures.

(2) Region growing algorithm with bounding volumes: A new technique for interactive segmentation of medical images not found in the literature (Alakwaa et al., 2017, Hesamian et al., 2019, Kawahara et al., 2016, Shrivastava et al., 2020).
- This methodology is based on a 3D region growing algorithm with an interactive seeding tool. It provides customizable spherical and rectangular boundary volumes, different from the segmentation approaches of current works.
- The result of the semi-automated segmentation process is an STL mesh of triangles representing the surface of the anatomical structure.
- It was based on similar techniques for 2D image segmentation of cars in movement (Mousavian et al., 2017), 2D panoramic pictures (Wu et al., 2017, Yu et al., 2018), and 2D mammographic images (Saeed & Saleh, 2020). It was not found its application for the creation of 3D models based on medical images.

(3) *FractalCells* module: A new open-source tool was developed proposing a methodology for fractal analysis using microtomography images.
- This methodology was not found in the literature (Alomari et al., 2017, Chappard et al., 2015, He & Ain, 2020, Korolj et al., 2019, Gómez-García et al., 2020).
- A similar approach was found on soil samples (Tseng et al., 2018), sand compression (Zhao et al., 2019), foam elements (Borovinsek et al., 2021), and the first one related to fibers were just published last year (Shkarin et al., 2020).
- Preliminary results for the calculation of principal direction vectors on the fractal structure of a rat kidney and a trabecular bone sample were performed.
- This method creates a fractal map of the analyzed structure, that can be used to characterize the distribution of material properties.
- It is left as a proposal for future works to use this methodology to correlate mechanical properties in a solid mesh for the volumetric formulation of the EESM.
- This module creates an open-source framework for the development of new tools based on the fractal analysis for microtomography images with the proposed methodology using GPU volumetric rendering and ray-casting.

8.3 Future works

This dissertation involved several topics, and although the objectives and goals for the scope of this research were achieved, there were detected a lot of opportunity areas for future works in different development paths.

The consideration of the volumetric formulation with tensors for the EESM and the implementation with volumetric elements is proposed to continue in future works, including the process for obtaining the stiffness matrix of equivalence parameters. (An initial development of the volumetric formulation for EESM is included in Appendix B).

In addition, it could be improved the time required for the calculation of each simulation cycle, since this is currently a roadblock to implement higher graphical textures and effects.

As well, it is expected to continue with the integration of commercial haptics devices and a review of comparisons with the results of commercial software, to continue with the optimization of the algorithms for the development of new applications and software.

Furthermore, tests with commercial software based on the Finite Element Method (FEM) could be developed, in order to validate the results of the volumetric formulation. Likewise, the objective is to continue working on the integration with *InVesalius* software.

In the next points, a brief description of the next steps for each part of the multiple contributions and components of this investigation are exposed. It is important to realize that each one of these future works proposed could be developed as a whole new research project.

8.3.1 *VISUALIX* module next steps

One of the biggest challenges was to integrate all the tools without losing performance. Since the main idea of the project is to allow the interactive visualization, real-time response is required in order to provide the user with a feeling of interaction without a delay.

In order to solve this problem, some tools were blocked for not being used at the same time (like the edition of transfer function and segmentation). Also, the segmentation process was defined for parallel computing in order to continue providing a response to interactions of the user even when a segmentation was being done.

Improvement on the customized transfer functions can be done by creating a tool for adding several functions for the same color channel. That could allow, for example, to have multiple triangular functions with several maxims of color on the main peaks of the histogram at different regions. This improvement is proposed for future works.

The segmentation process was improved by adding the boundary tools, but other segmentation methods can be implemented, as well as new tools to improve the results of the segmented mesh.

Even when the interface is functional, it is considered to be difficult to interact with the application. The creation of an intuitive interface that provides access to all the tools developed on this project also is proposed for future works.

8.3.2 *FractalCells* module next steps

Using *VISUALIX* module implementation, a particular case for interactive image visualization and processing was studied, which is microtomography images. This case, as with other imaging techniques, is based on the creation of slides of the material doing the analysis, in this case using X-rays but adding a special array of lenses to allow the acquisition of microscopic details in the sample.

Then, it was possible to visualize the fractal structure of some materials and a proposal for its integration as a part of the material modeling process was created. Using the volumetric formulation of the EESM and adding microtomography analysis for characterization of the fractal structure is an idea that was found during this research. The proposal is to use microtomography images to perform a fractal analysis that will be used to represent the stiffness distribution and its contribution to the anisotropic behavior in a composite material.

An initial approach for fractal analysis was performed by creating *FractalCells* module. This application was developed by implementing the proposed methodology for calculation of the principal direction vectors on the fractal structure using a couple of samples of microtomography studies (the volumetric formulation and this proposal are included in Appendix B and *FractalCells* module scripts are included in the repository link at Appendix A.2).

It is intended to create an open-source framework for fractal analysis using microtomography images. This is in order to characterize the structural and mechanical properties of the sample and consider its fractal nature predict its replicability.

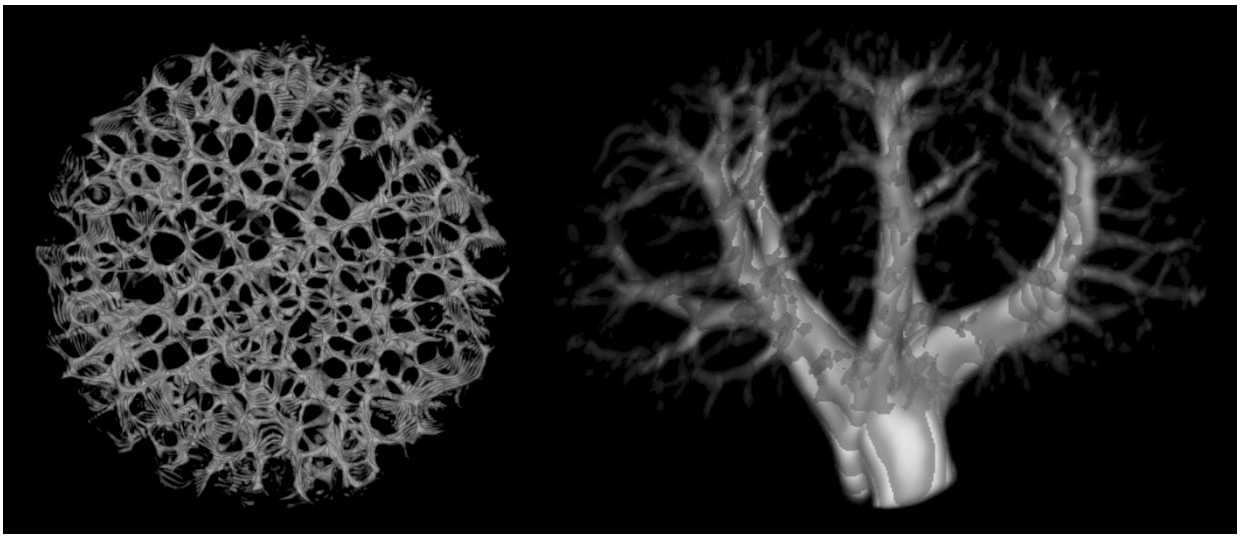

Fig. 131 Interactive processing of microtomography images for visualization of sample fractal structure using *FractalCells* module, developed in this dissertation

It is left to future works to continue analyzing this proposal for tissue characterization and other materials. There is a particular interest in the characterization of the fractal structure in trabecular bone and its contribution to the general mechanical properties of a volumetric mesh created to simulate this material.

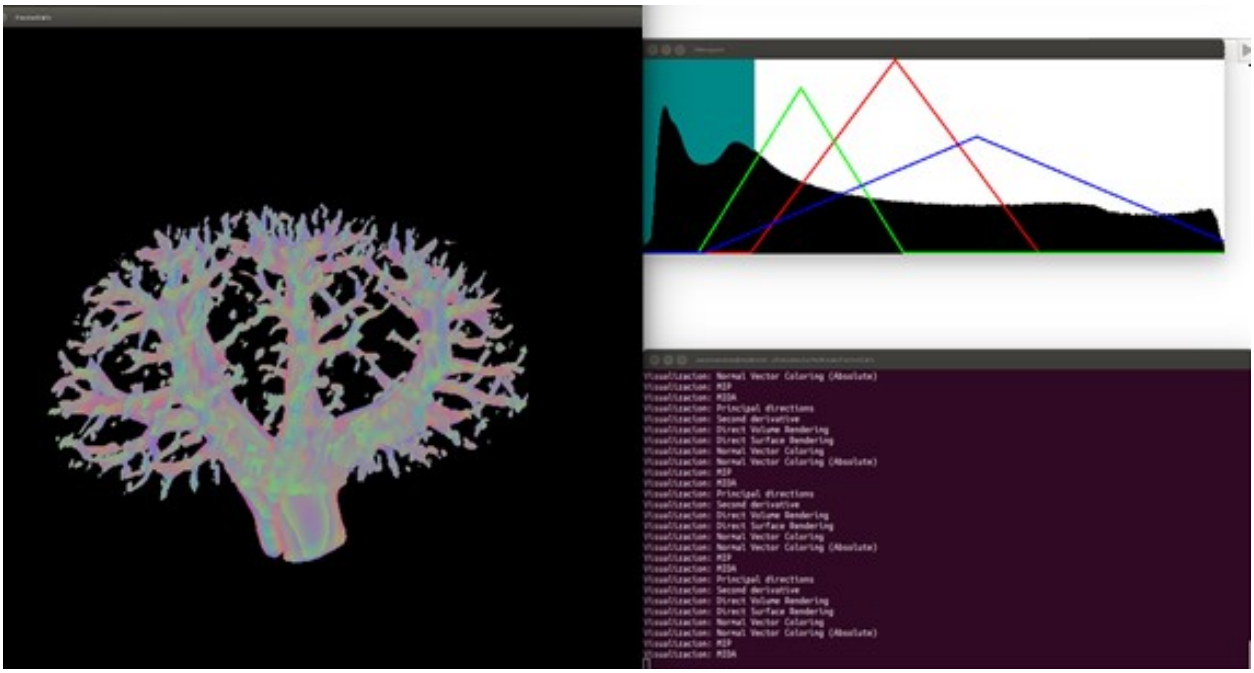

Fig. 132 Interface of *FractalCells* for interactive processing of microtomography images

With this proposal, it would be possible to represent the contribution of the internal fractal structure of biological materials in the general mechanical properties, in order to use this information as the proposed fractal map. This map will help with the assembly process of the global matrixes in the volumetric formulation of the EESM for the distribution of the stiffness properties in each principal direction, as shown conceptually in Fig. 133.

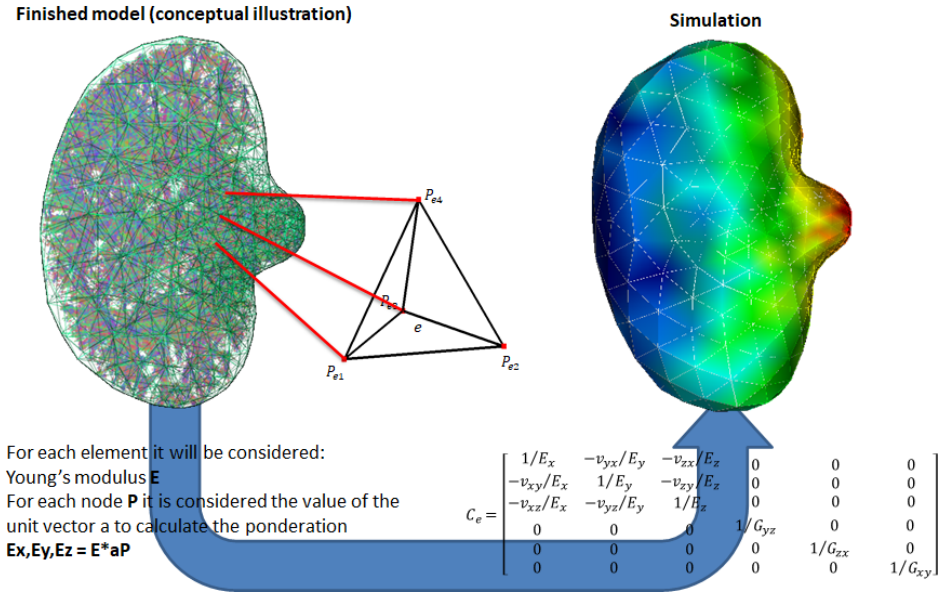

Fig. 133 Conceptual process for the application of the anisotropy map to create the element matrices of the volumetric formulation

If the internal fractal structure was ignored and assumed a solid mesh, it would apply the mechanical properties obtained in experimental tests without considering that the collected data is the resultant of the contribution of different fractions. This proposal would allow the distribution of the stiffness in a homogeneous volumetric mesh, resulting in a solid mesh with variable properties based on its internal fractal structure.

The applicability to define accurately the structure of non-homogenous composite materials, can improve the way that current simulation is being performed. Also, it can help to define the contribution of the fractions when performing a Microtomography scan before a physical test. This can give insights into the relationship between the anisotropic fraction (f) and general fiber orientation vectors.

The full implementation and validation of this proposal are left for future works. This can be included as part of an investigation of biological materials or composite materials. Considering that to represent the contribution of the internal fractal structure in the mechanical properties on a simulation mesh, would require a high level of resolution and number of elements in order to represent said internal geometry.

8.3.3 Surgical procedures with EESM

The research work presented in this dissertation was focused on the improvement of the simulation framework and creation of tools for visualization and processing of medical images, segmentation of anatomical structures, and characterization of soft tissue mechanical behavior with a new hybrid model. These tools are open-source and included in repositories with GNU v3.0 License (more information in Appendix A.2 Repository List).

The development of surgical procedures and applications with these tools is left for future works, as an opportunity to continue creating research projects applying the methodology and tools established in this work.

It is not easy to understand the requirements of medical students and young surgeons, so it is important to interact with the area to understand their needs. The relationship between the medical area and engineering professionals is essential to develop new procedures. It is highly recommended to continue nurturing this interaction in order to get the best results.

It is recommended to have this interaction to define a plan for particular procedures that can be developed to increase the applicability of this work.

8.3.4 Industrial applications of EESM

As was stated before, due to the EESM hybrid construction, this formulation not only can characterize and predict the mechanical behavior of soft tissues but of other composite materials. Then, it is left for future works to implement the proposed model for applications in the industry.

EESM formulation can be used for VR developments focused on learning and training of factory employees or for maintenance procedures, similar to the approaches exposed in the state-of-the-art for VR (Radhakrishnan et al., 2021).

Also, it could be proposed the use of EESM for a real-time prediction of the mechanical properties in parts created by additive manufacturing, similar to an approach proposed for metal parts (Xie et al., 2021).

In addition, considering the current interaction with the truck industry, the author believes there is potential for the application of the proposed model for the characterization of front, rear and cab suspension components and its interaction with steering system. Also, it can be used on elastomeric components included to reduce vibrations of main components, like engine mounting, and cooling packages, among others. Particularly, an opportunity is found for the prediction of the mechanical behavior virtual validations of multiple configurations, as some approaches have been proposed (Rocha-Hoyos et al., 2018, Schmidt et al., 2014).

This could not only reduce the time for validation procedures but also have a huge economic impact by reducing costs on validation before a product is launched. This can be done by reducing the number of vehicles required for physical validation or the amount of full CAE / Multi-body simulations performed for virtual validations.

The number of possible combinations between axles, suspensions, drivetrain, and steering systems configurations is high. It could be performed as a real-time simulation for a quick analysis to find worst-case scenarios, based on a model with low error to predict mechanical properties as shown in the simulation performance section 7.3. This would optimize the Design Verification Plan (DVP), reducing time and cost of operations.

And last, but not least, it could be used for feedback to artificial intelligence systems, both for the manufacturing process and even for Advanced Driver Assistance Systems (ADAS). This could provide information about the predicted behavior of the suspension and steering systems for self-driving vehicles for safety and risk assessment on decision making, as proposed on other approaches for tire forces (Jiang et al., 2019) or testing of ADAS systems (Parra et al., 2020).

8.3.5 Augmented reality applications of EESM

One of the following paths for the next works is to search for other applications of the developed model for Virtual Reality (VR) and Augmented Reality (AR).

The benefits of EESM have been described in this dissertation, but it can be applied for the development of new technological tools that can improve not only training and for academic purposes. This model can have applications on entertainment like animation and video games. It is considered potential implementation for product development of software with Unity™, Vuforia™, or Spark AR™.

During this project, it was detected a great opportunity to develop applications for medical training using the segmented geometries and simulations, as well as other tools. These tools are not open source, which will imply considerable investment in technology development.

However, it is believed by the author of this dissertation that this opportunity could have big commercial potential and a start-up for development of this kind of application for profit could be created.

For this proposal, it was created an initial AR demo using Unity™. This is a commercial software for the development of animation and videogames. This demo was created as an application for Android devices, and it was set up with a QR code (as shown in Fig. 134) and allows the camera to recognize the pattern and insert a 3D scenario in space.

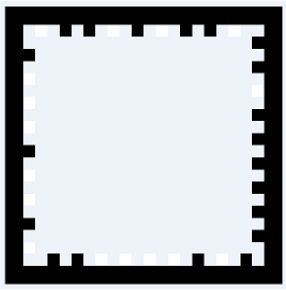

Fig. 134 QR code used for the development of the augmented reality demo

A scenario in Unity™ was created using this QR and the anatomically realistic geometrical models developed in this research. It was achieved a concept in which the mobile device using the application inserted in the camera image the geometry of a liver and a gallbladder as floating in the space, allowing the user to visualize these organs from any angle as shown in Fig. 135.

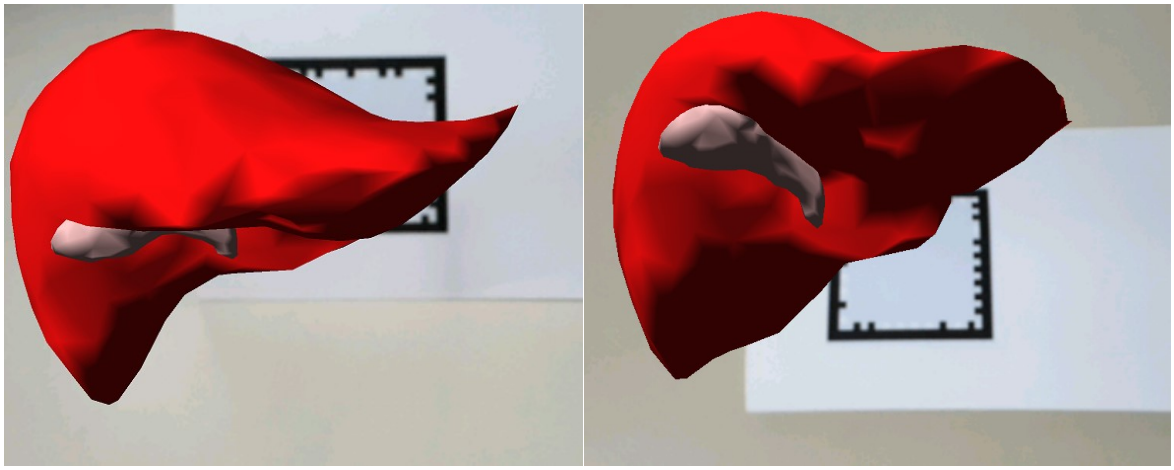

Fig. 135 Screen capture of the demo visualization on a mobile device. The geometry of a human liver and gallbladder is shown in the space and can be displayed at any angle

Based on this, the proposal for future works is to continue researching AR technologies in order to develop applications that can be used for academic, research, and commercial purposes. Such uses could be the training of medical students, to have a tool for remote and interactive learning for virtual classrooms and distance/online classes, surgical planning, and diagnosis, among others using mobile devices as shown in Fig. 136.

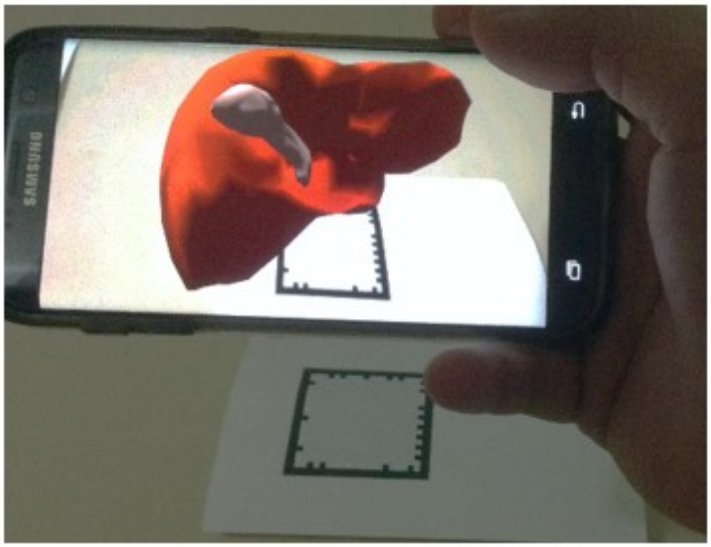

Fig. 136 Mobile device using the demo implemented in this research project for AR visualization of medical geometries, showing potential for future work

These applications are compatible with other current technology like Oculus VR™ for the creation of virtual and augmented reality applications. To explore these commercial technologies as potentially profitable business is left for future works.

Appendix A

Acronyms & Repositories

A.1 Acronym List

Acronyms	**Description**
AAA	Abdominal Aortic Aneurysm
ACL	Anterior Cruciate Ligament
AR	Augmented Reality
BEM	Boundary Element Method
CAE	Computer-Aided Engineering
CFD	Central Finite Differences
CICUAL	Comité Institucional para el Cuidado y Uso de Animales de Laboratorio
CT	Computed Tomography
DICOM	Digital Imaging and Communication in Medicine
DMEM	Dlbecco's Modified Eagle Medium
DVE	Digital Video Extensometer
EESM	Energy Equivalent Spring Model
EM	Euler Method
FDM	Finite Differences Method
FEA	Finite Element Analysis
FEM	Finite Element Method
GPU	Graphics Processing Unit
ITF	Interactive Transfer Function
MIDA	Maximum Intensity Difference Accumulations
MIP	Maximum Intensity Projection
MIS	Minimally Invasive Surgery
MRI	Magnetic Resonance Imaging
RGB	[Red, Green, Blue]
RTD	Resistance Temperature Detector
SDR	Surface Direct Rendering
SEDF	Strain Energy Density Function
SMM	Spring-Mass Model
STL	Stereolithography
TFF	Transfer Function File
TMM	Tensor-Mass Model
UTM	Universal Testing Machine
VDR	Volume Direct Rendering
VR	Virtual Reality
VTK	Visualization Toolkit

A.2 Repository List

Project Scripts	**Repository Link**
A.2.1 FractalCells Module	https://github.com/marioregino/FractalCells
A.2.2 EESM Framework	https://github.com/marioregino/EESM_Framework
A.2.3 EESM Formulation	https://github.com/marioregino/EESM_Formulation
A.2.4 FEMSIM Framework	https://github.com/marioregino/FEMSIM_Framework
A.2.5 SMM Framework	https://github.com/marioregino/SMM_Framework
A.2.6 VISUALIX Module	https://github.com/marioregino/VISUALIX

Appendix B

Volumetric formulation using Finite Element Method (FEM)

B.1 Development of the volumetric formulation

In the case of volumetric elements, a similar formulation can be generated starting from the construction of stiffness matrices of two tetrahedral elements created from the original geometry and calculating the parameters that are modeled in the energy equivalence. This concept is shown in Fig. 137.

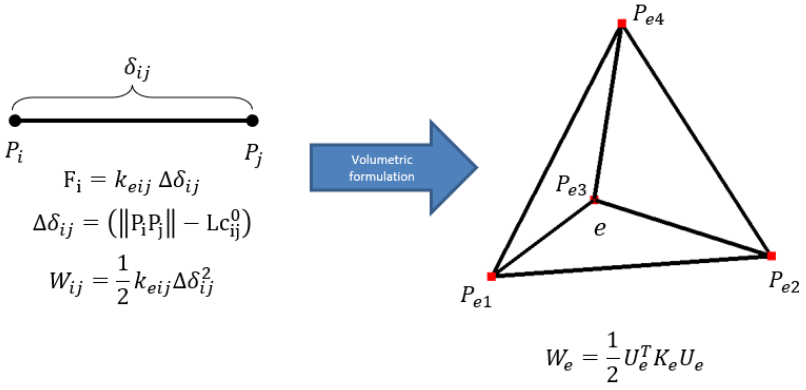

Fig. 137 One-dimensional elements to volumetric elements formulation

To work with volumetric elements, it is necessary to use tensor expressions of Hooke's law:

$$\sigma = \begin{bmatrix}\sigma_{xx}\\ \sigma_{yy}\\ \sigma_{zz}\\ \sigma_{xy}\\ \sigma_{yz}\\ \sigma_{zx}\end{bmatrix} = \begin{bmatrix} C_{11} & C_{12} & C_{13} & C_{14} & C_{15} & C_{16} \\ & C_{22} & C_{23} & C_{24} & C_{25} & C_{26} \\ & & C_{33} & C_{34} & C_{35} & C_{36} \\ & & & C_{44} & C_{45} & C_{46} \\ & & & & C_{55} & C_{56} \\ & & symm & & & C_{66} \end{bmatrix} \begin{bmatrix} e_{xx}\\ e_{yy}\\ e_{zz}\\ 2e_{xy}\\ 2e_{yz}\\ 2e_{zx}\end{bmatrix} = Ce$$

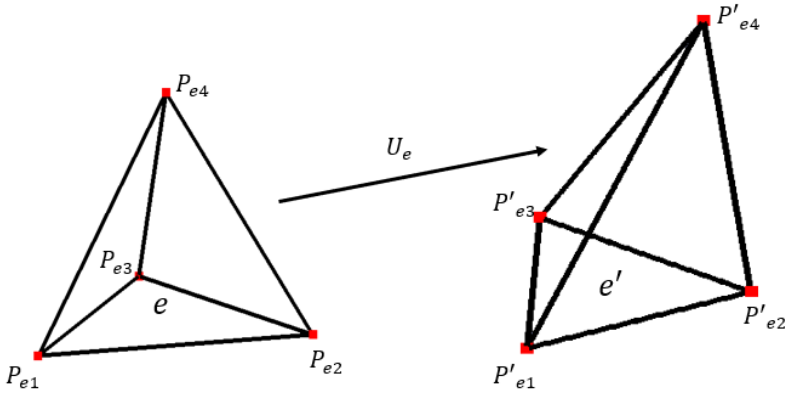

Fig. 138 Deformation of an element based on U_e

$$\begin{bmatrix} x \\ y \\ z \\ 1 \end{bmatrix} = \begin{bmatrix} P_{e1x} & P_{e2x} & P_{e3x} & P_{e4x} \\ P_{e1y} & P_{e2y} & P_{e3y} & P_{e4y} \\ P_{e1z} & P_{e2z} & P_{e3z} & P_{e4z} \\ 1 & 1 & 1 & 1 \end{bmatrix} \begin{bmatrix} N_{e1} \\ N_{e2} \\ N_{e3} \\ N_{e4} \end{bmatrix}$$

$$e = \begin{bmatrix} N_{eix} & 0 & 0 & \dots & N_{eix} & 0 & 0 \\ 0 & N_{eiy} & 0 & \dots & 0 & N_{eiy} & 0 \\ 0 & 0 & N_{eiz} & \dots & 0 & 0 & N_{eiz} \\ N_{eiy} & N_{eix} & 0 & \dots & N_{eiy} & N_{eix} & 0 \\ 0 & N_{eiz} & N_{eiy} & \dots & 0 & N_{eiz} & N_{eiy} \\ N_{eiz} & 0 & N_{xi} & \dots & N_{eiz} & 0 & N_{xi} \end{bmatrix} U_e = \mathrm{BU_e}$$

$$B = \begin{bmatrix} N_{xi} & 0 & 0 \\ 0 & N_{yi} & 0 \\ 0 & 0 & N_{zi} \\ N_{yi} & N_{xi} & 0 \\ 0 & N_{zi} & N_{yi} \\ N_{zi} & 0 & N_{xi} \end{bmatrix}$$

$$K = VB^T CB$$

$$F = Ku$$

To assemble the global matrix of stiffness for the geometrical model, it should be done based on each of the degrees of freedom u_i.

$$K_e = VB^T CB$$

$$M_e = \rho V_e I_3$$

$$C_e = d_1 M_e + d_2 K_e$$

$$K_g = \begin{bmatrix} K_{11} & K_{21} \\ K_{12} & K_{22} \end{bmatrix} \begin{bmatrix} u_{x1} \\ u_{y1} \\ u_{z1} \\ u_{x2} \\ u_{y2} \\ u_{z2} \\ u_{x3} \\ u_{y3} \\ u_{z3} \\ u_{x4} \\ u_{y4} \\ u_{z4} \\ u_{x5} \\ u_{y5} \\ u_{z5} \end{bmatrix}$$

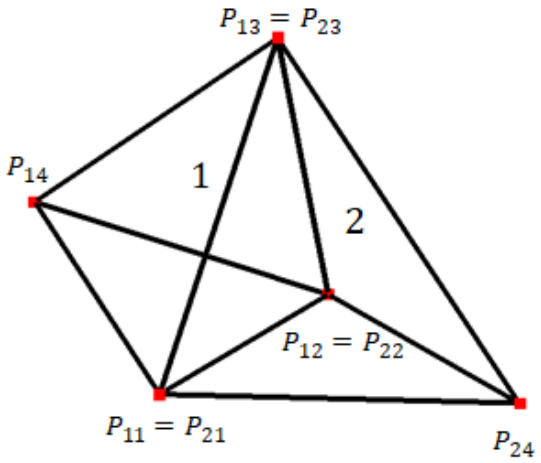

Fig. 139 Assembly of volumetric elements

$$F_{\mathrm{i}} = M_g \ddot{u}_i + C_g \dot{u}_\iota + K_g u_{\mathrm{i}}$$

The parameters used are Young's modulus (*E*), Poisson's Coefficient (*v*), the density, and the damping.

The parameters matrices (Stiffness, Damping, Mass) should be calculated on a pre-computed state for each element and assembled into global matrices based on the degree of freedom. These matrices will be stored in files for reading during the initialization of the real-time simulation.

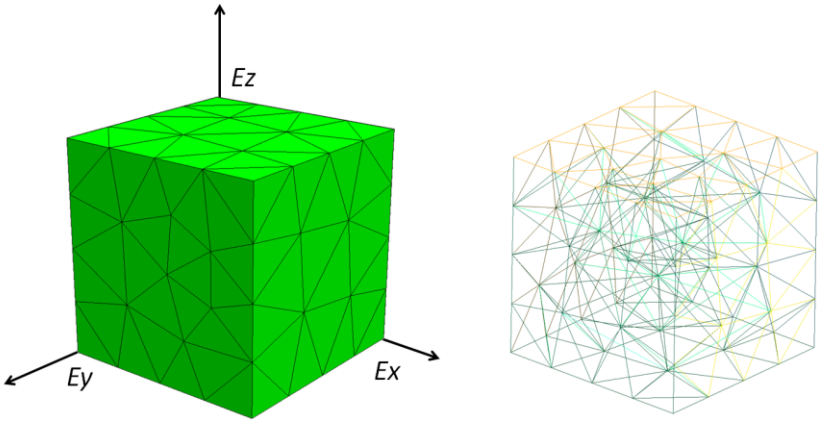

Fig. 140 Example of a mesh constructed with volumetric elements

Considering a material with isotropic behavior, the stiffness matrix can be considered as follows considering that $\boldsymbol{E_x = E_y = E_z}$:

$$C = \frac{E}{(1+v)(1-2v)}\begin{bmatrix} 1-v & v & v & 0 & 0 & 0 \\ v & 1-v & v & 0 & 0 & 0 \\ v & v & 1-v & 0 & 0 & 0 \\ 0 & 0 & 0 & 1/2-v & 0 & 0 \\ 0 & 0 & 0 & 0 & 1/2-v & 0 \\ 0 & 0 & 0 & 0 & 0 & 1/2-v \end{bmatrix}$$

Where E represents Young's modulus and v Poisson's coefficient of the particular material. Using only these parameters, the behavior of an isotropic material can be calculated for the volumetric elements as shown in Fig. 141.

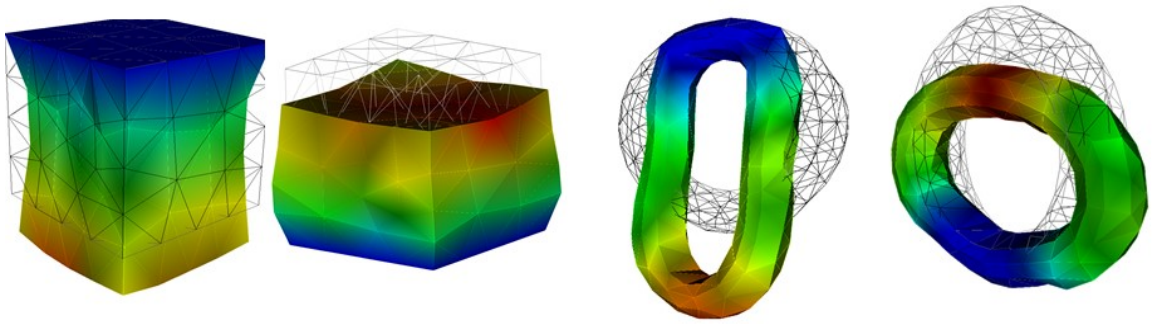

Fig. 141 deformation of an isotropic solid under gravity formed by tetrahedral elements

In this case, to consider the tissue anisotropy, a more complex formulation can be generated where the concept of energy equivalence of the EESM model can be applied in the same way, using $\{\boldsymbol{E_x}, \boldsymbol{E_y}, \boldsymbol{E_z}\}$ and $\{\boldsymbol{v_{xy}}, \boldsymbol{v_{xz}}, \boldsymbol{v_{yx}}, \boldsymbol{v_{yz}}, \boldsymbol{v_{zx}}, \boldsymbol{v_{zy}}\}$ to describe the behavior of the material in the main directions.

$$C = \begin{bmatrix} 1/E_x & -v_{yx}/E_y & -v_{zx}/E_z & 0 & 0 & 0 \\ -v_{xy}/E_x & 1/E_y & -v_{zy}/E_z & 0 & 0 & 0 \\ -v_{xz}/E_x & -v_{yz}/E_y & 1/E_z & 0 & 0 & 0 \\ 0 & 0 & 0 & 1/G_{yz} & 0 & 0 \\ 0 & 0 & 0 & 0 & 1/G_{zx} & 0 \\ 0 & 0 & 0 & 0 & 0 & 1/G_{xy} \end{bmatrix}$$

Using this formulation and the appropriate parameters in the main directions, different behaviors can be obtained (see Fig. 142), which can represent the anisotropic characteristics of the tissues.

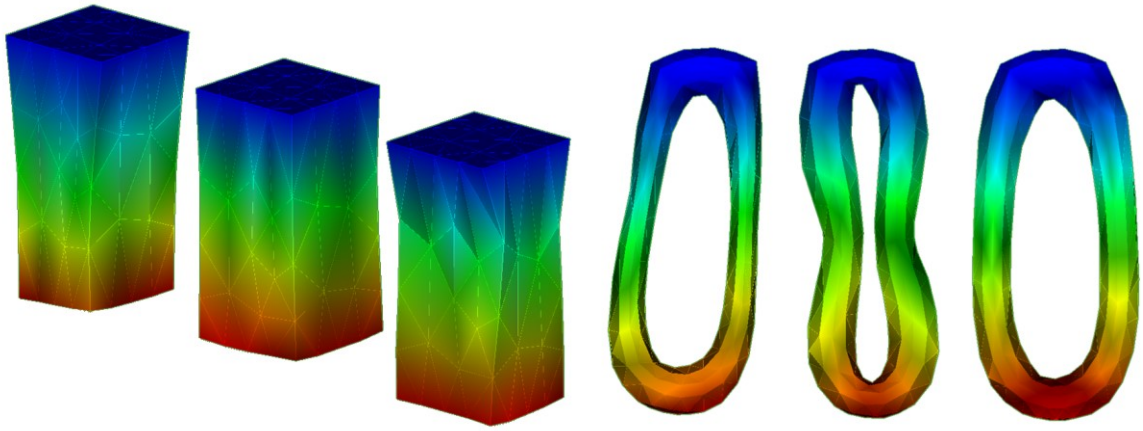

Fig. 142 Deformation of an orthotropic solid under gravity formed by tetrahedral elements

Applying netgen (an open-source tool for mesh processing), the generation of tetrahedral meshes based on STL geometry extracted from medical images can be done. Using the liver geometry obtained from medical images, the mesh of tetrahedral elements was generated to calculate the stiffness matrices as shown in Fig. 143.

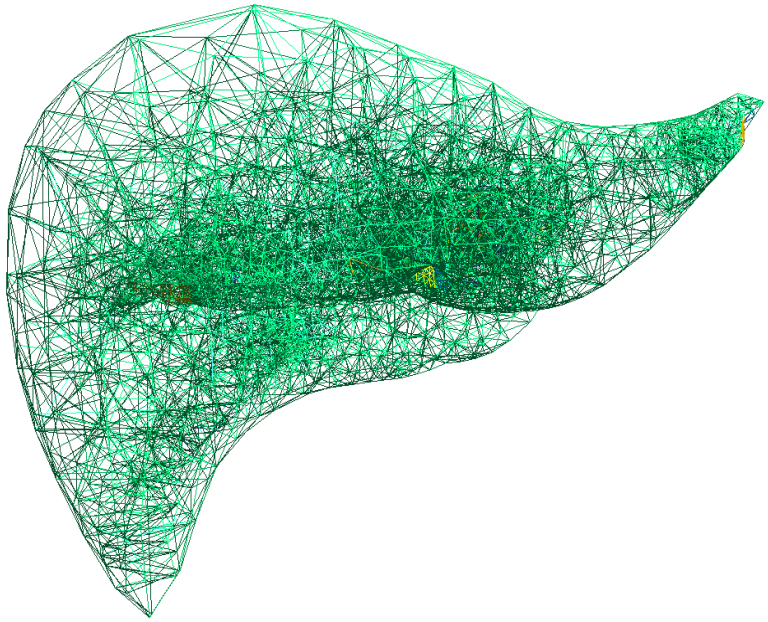

Fig. 143 Example of volumetric element mesh deformation using the proposed model

B.2 Implementation of simulation environment for testing of volumetric formulation

A test module was created for the implementation of the volumetric elements and the calibration of the material model used to characterize the behavior of the soft tissue. This implementation was done using Python and the Visualization Toolkit (VTK).

A simple interface allows to introduce a mesh and run a simulation, as shown on Fig. 144.

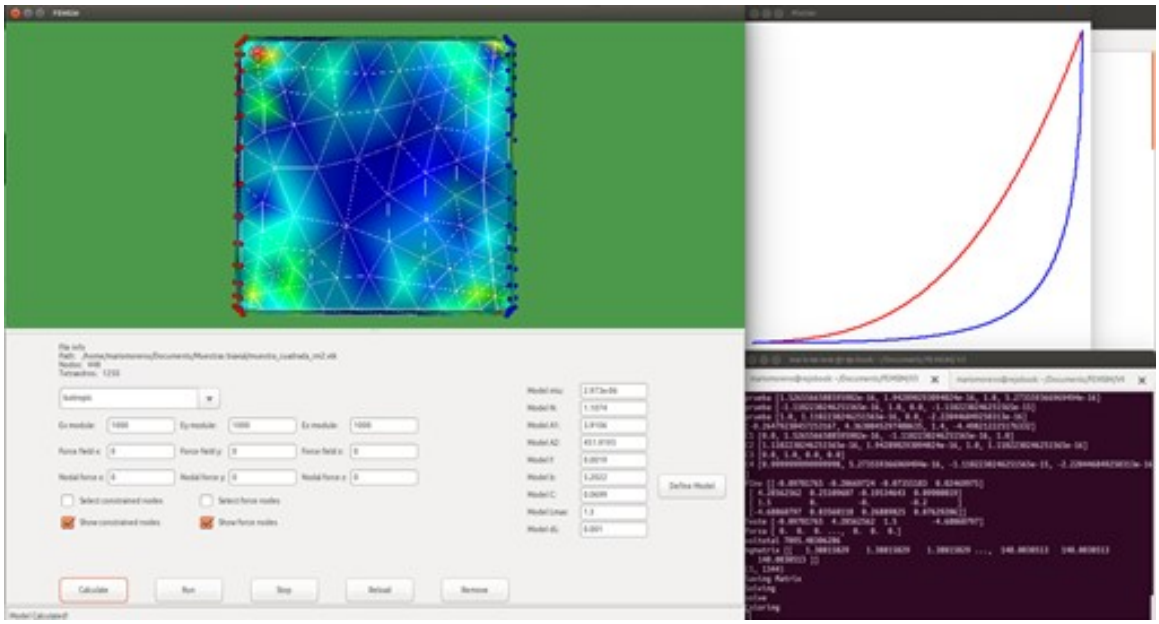

Fig. 144 Main interface of test environment with the proposed model for volumetric elements

With this implementation, it is possible to select nodes and define them as constraints (identified as red spots) or to apply certain load (identified as blue spots). This tool is displayed in Fig. 145.

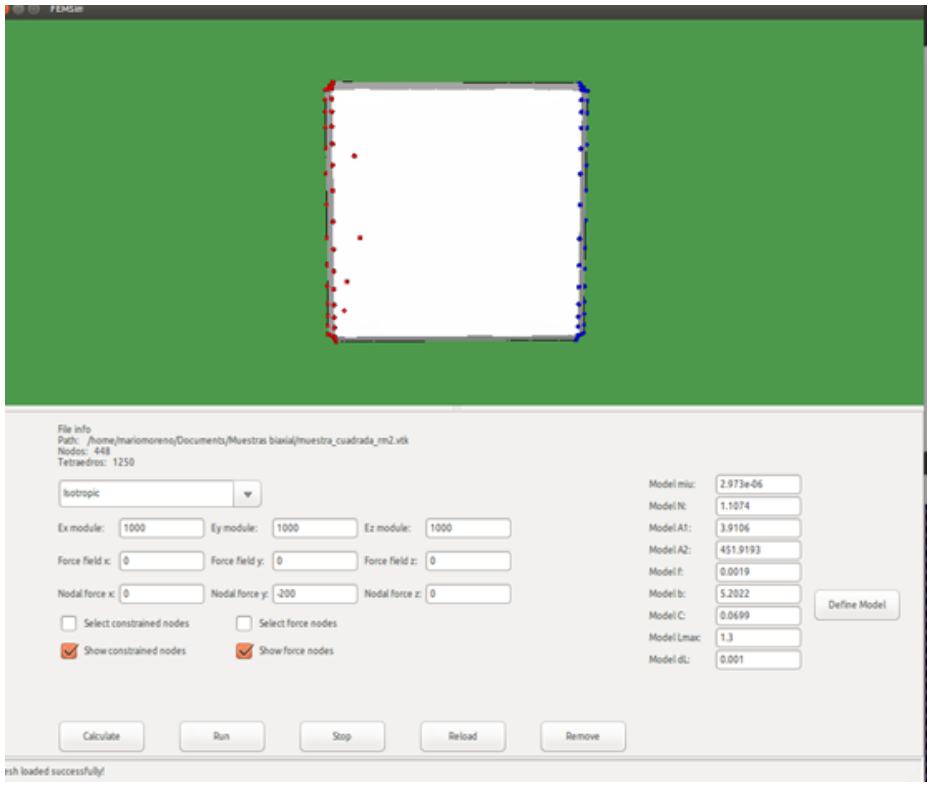

Fig. 145 Test environment for the proposed model using volumetric elements. Constraints on nodes are defined as red spots and forces are applied to blue spot's nodes.

The mesh will be deformed based on the material model calibrated with experimental data and using the matrices that were precalculated for the geometry and storing them for the interactive simulation.

Using this test environment, it is possible to interact with different meshes and try different parameters that characterize certain tissue with the proposed hybrid model.

This module allows to interact and develop the application of the model in an easy way and validate the assumptions of the parameters applied, visualize the deformation on the mesh and compare with the original geometry based on interactions with the mesh nodes, constraints, and loads. Also, this environment allows running effectivity tests in order to verify the time that the pre-calculation takes as well as the interactive simulation, as shown in Fig. 146.

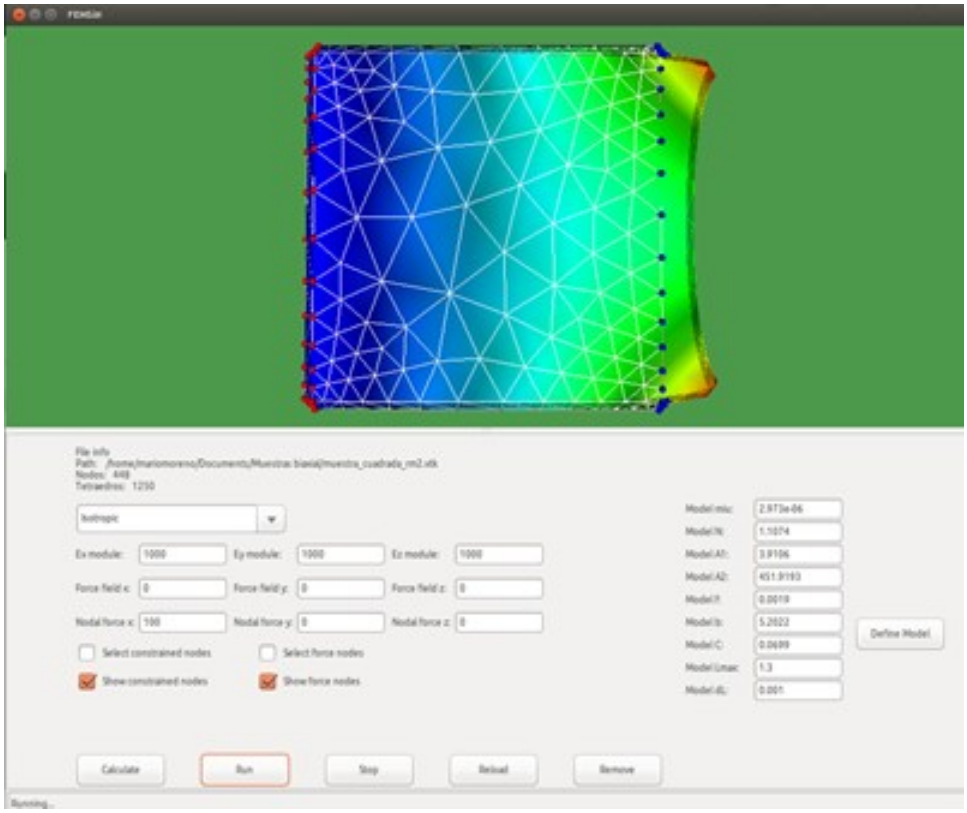

Fig. 146 Test environment for the proposed model using volumetric elements showing deformation of a sample.

B.3 Simulation testing environment results for volumetric formulation

For validation purposes, different cases were run in the test environment that was created to allow interaction with the meshes and simulate the behavior of the material using the proposed model and defined parameters during characterization, as shown in Fig. 147.

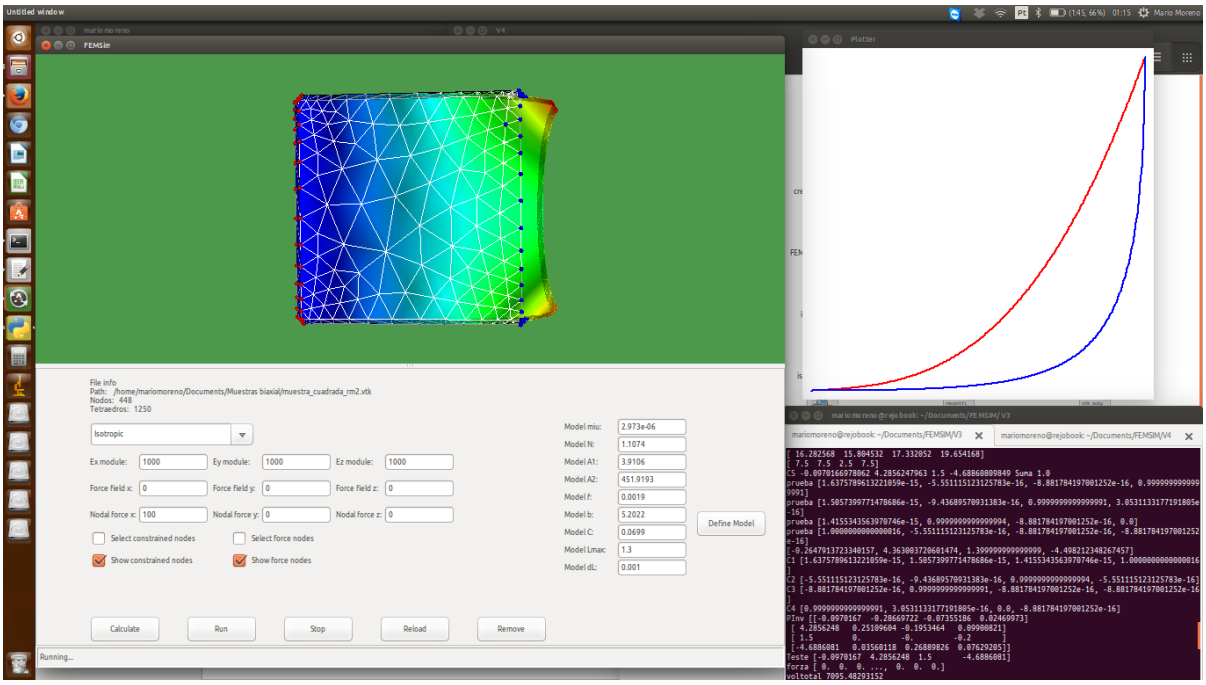

Fig. 147 Test environment for the mathematical model using the constants calibrated with the experimental data.

This test environment can create deformed volumetric meshes based on the constraints, forces, mechanical properties, and characterization parameters for the EESM that are specified by the user, as shown in Fig. 148.

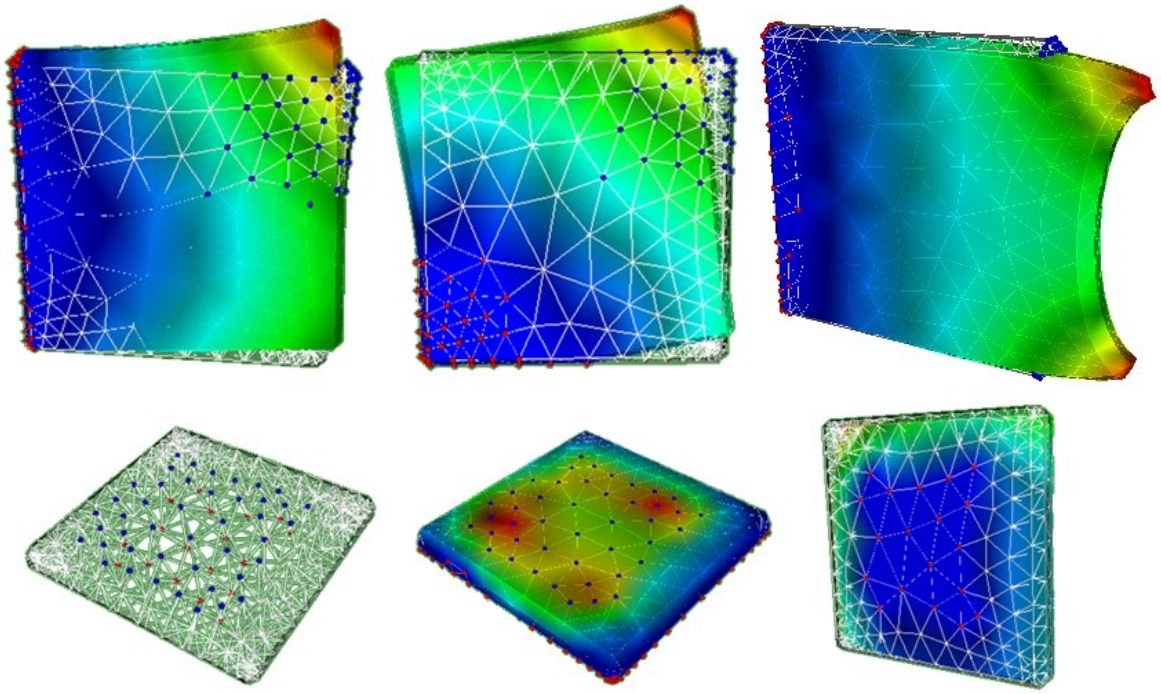

Fig. 148 Interaction with the mesh with the implemented model.

Using the tensor formulation, the calculation of liver deformations under gravity at a given time was calculated as shown in Fig. 149, allowing to prove the applicability of volumetric elements for simulating the behavior of tissues in real-time with an equivalence model.

The calculation of parameters that lead this formulation to represent the actual tissue behavior must be done based on experimental data and is considered one of the next steps.

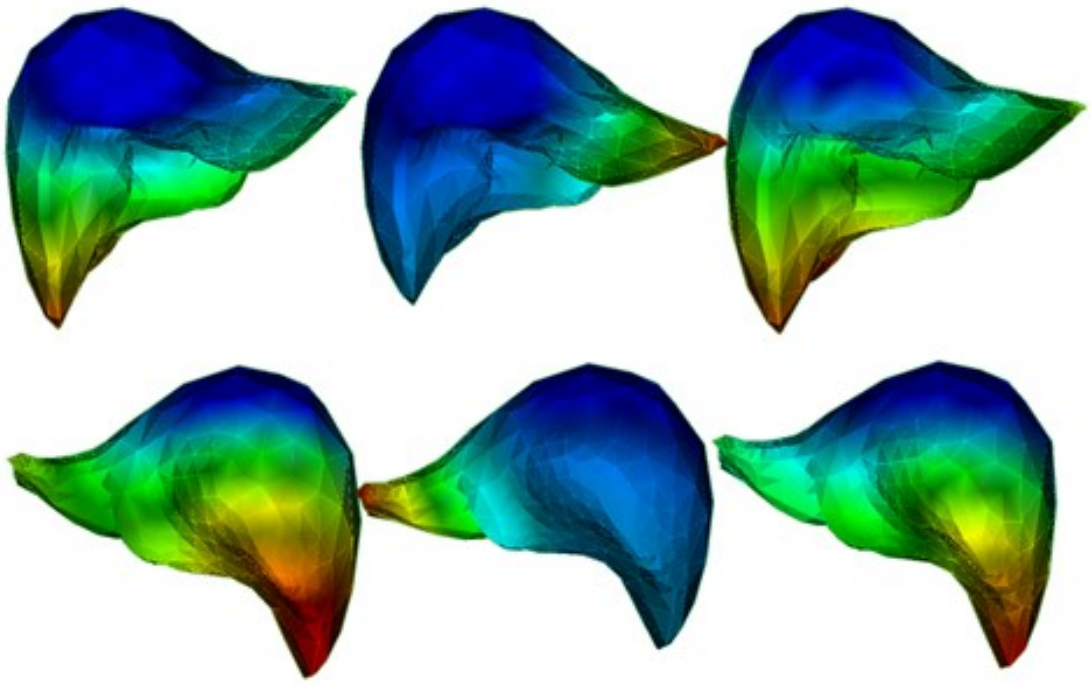

Fig. 149 Liver deformation under gravity using different parameters of $\{E_x, E_y, E_z\}$

Appendix C

Flow diagrams and scripts for initial framework

As an initial framework, it was used the developed simulation work that was performed in previous works.

For the creation of a virtual environment, the appropriate selection of computational tools is essential. These tools will allow the implementation of the algorithms and methods developed for different aspects in the virtual environment, such as the deformation model, the algorithm for creating an internal skeleton structure, the computational method to solve the deformation model equations as well as the collision detection method.

The selection of tools in this research was based on their ability to allow the creation of functions and resources that can be used in different applications, as well as allowing the subsequent integration with platforms already developed or in potential development for a greater objective. Based on this and due to its wide use in the development of computer applications for the area of computer graphics and medical informatics, the Python programming language was selected as the main platform. Python is a high-level, multipurpose programming language with powerful tools for application development.

Within the libraries that were used for the implementation and development of applications in Python, it was necessary to define a tool for the creation, management and visualization of the graphical feedback and rendering interface, as well as for the creation of the virtual environment for the interaction with the user. To cover this aspect, the use of the Visualization Toolkit (VTK) was established, which is a free access tool used for the graphic visualization of data and information in commercial applications, as well as in scientific development and research. At the same time, the Wx library was used to manage and create the interface, as well as to manage times, events and update user actions.

For data management and mathematical calculations, tools from the Numpy and Scipy libraries were used. Both are open access libraries for mathematical, scientific, and engineering applications, which provide tools for managing multidimensional data structures and arrangements, as well as basic operations between them.

On the next points of this Appendix, the flow diagrams that describe the algorithms used for the initial framework and the compendium of scrips will be presented and provided to the reader for a better understanding of this project.

C.1 Flow diagrams for algorithm of initial framework

The implementation of the previous methods occurred in the segmentation of events for the creation of functions in the different cases present in the simulation, as shown in Fig. 150. This simulation process includes the preparation of the models and the creation of the Structures necessary to perform the simulation, generated in the stage referred to as Initialization. After this stage, the interaction cycle of the simulation begins, in which the deformation of the object is considered both by the effect of gravity and by the interaction with the user, as well as the detection of collisions. These functions will be explained in detail in the following points.

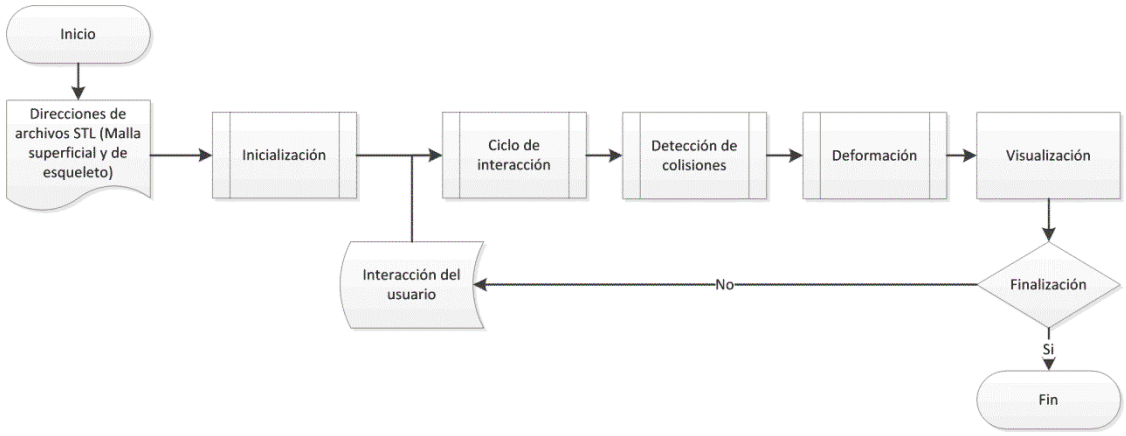

Fig. 150 Flow diagram that shows the algorithm for the main simulation framework

C.1.1 Flow diagrams for algorithm for Initialization Phase Module

To start the application, a function was created to prepare the deformable objects before running the simulation. In this preparation, all the data structures, rendering meshes, matrices and arrangements that will be used in the following functions of the simulation process are created and defined. The diagram shown in Fig. 151 expresses the main flow of this stage of the process.

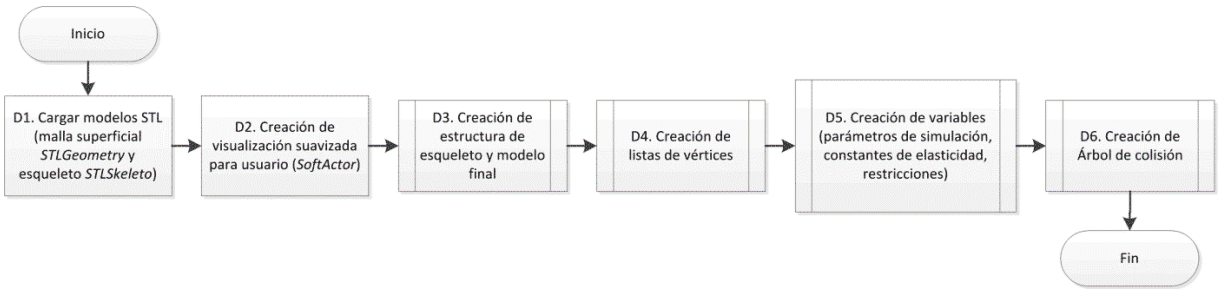

Fig. 151 Flow diagram that shows the algorithm for the Initialization Phase Module

In this application an instance was created which was called SoftBody, which has as inputs in D1 (see Fig. 151) the mesh produced by the procedure presented in chapter 2 (see Fig. 10d) which will be referred to in this section as STLGeometry (formed by Gp points and Gf faces), as well as the simplified mesh of control points for the creation of the skeleton structure, generated as explained in section 3.3, which will be called as STLSkeleto (formed by Sp points and Sf faces).

In the process function in D2, visual filters are applied to create a display mesh with which the user interacts (see Fig. 10e), which will be referred to as SoftActor. The properties for rendering, visualization and color are applied to this mesh.

Later in the D3 process (which is shown descriptively in the diagram in Fig. 152) the algorithm is used to generate the skeleton structure, doing a search for the Gp points of STLGeometry and calculating their proximity to each of the Sp points of STLSkeleto, storing the 4 closest for each vertex in an array (Gpx4) which is called verskel.

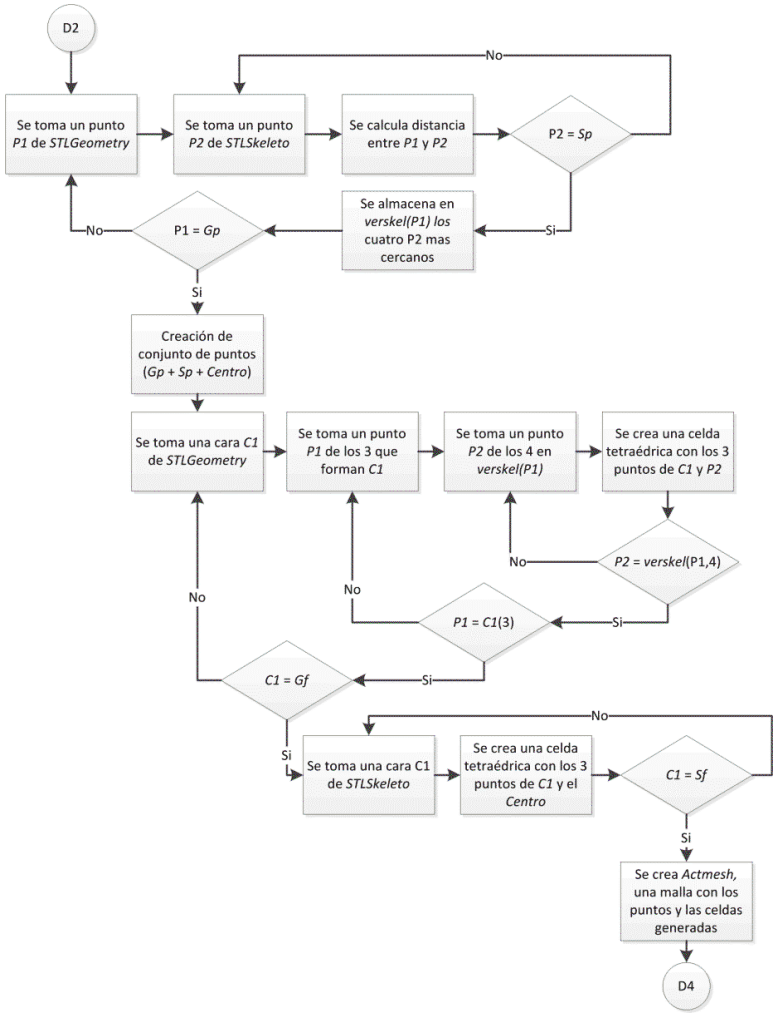

Fig. 152 Flow diagram that shows the algorithm for the creation of a skeleton structure and geometrical model

In this process, a new point structure is created, which will be called Actmesh, which is generated from the vertices of both previous meshes and the center of the geometry (Gp + Sp + 1). One of the Gf triangular faces of STLGeoemtry is taken (which represent the surface of the organ), and the indices of the vertices that make it up are used to define the base of a tetrahedral cell, which is linked at the tip with one of control points Sp.

Using these points, a cell is created in Actmesh for each of the four control points in the verskel arrangement of the three vertices that make up the face (taking care not to repeat control points). Subsequently, the same operation is carried out for the Sf faces of STLSkeleto, linking them with the point in the center of the geometry.

From now on, Actmesh (formed by Ap points and Af faces) is considered as the mesh that will be used to perform the deformation calculations, and in the D4 process (defined in the diagram shown in Fig. 153) they are generated lists to store relevant information about the links that exist between cells and vertices, such as immediate neighboring vertices (veredg) and cells to which it belongs (vercel), for each of the vertices of Actmesh.

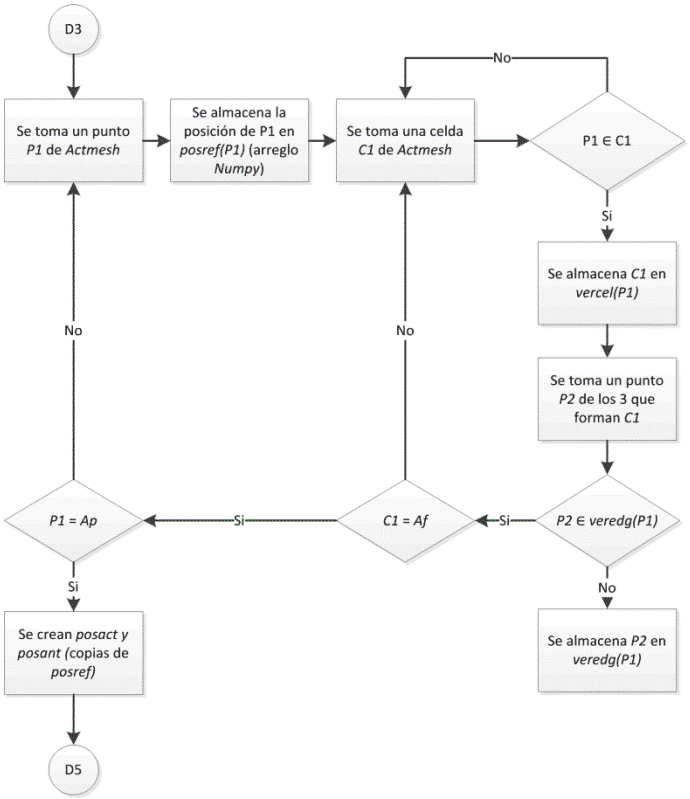

Fig. 153 Flow diagram that shows the algorithm for the creation of the data structure

In the same way NumPy arrays are generated to handle the data of the positions of all its vertices. For this, an arrangement is created for the reference position at rest (posref), the position at the current moment (posact), the position in a previous time differential (posant).

Subsequently, the matrices and the parameter variables are defined in the equations in the D5 process, which is shown in detail in the diagram in Fig. 154. In this step, an arrangement is generated with the indices of the vertices that have movement restriction and by Therefore, it is known that its displacement is null (un = 0, taking it as a boundary condition), which is called a constraint, as well as the matrix of elasticity constants kij (Kspring).

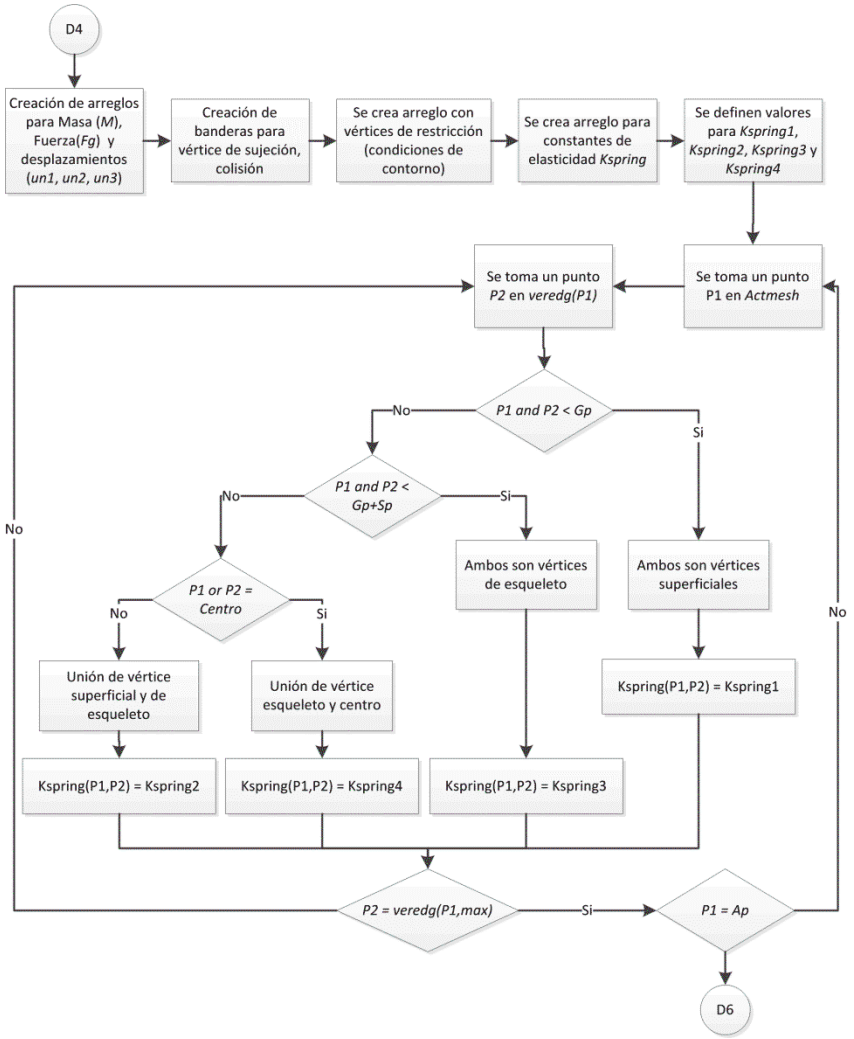

Fig. 154 Flow diagram that shows the algorithm for the variable definition and elasticity constant

Kspring representa la constante de elasticidad del resorte que une el vértice Pi con el vértice Pj, teniendo cuatro niveles de elasticidad los cuales consideran si es un resorte que une 1) un punto superficial con otro superficial, 2) uno superficial con uno de control en el esqueleto, 3) un control con otro control o 4) un control con el centro de la geometría. También se genera la matriz K (Kvertex), que da un parámetro de compensación para cada vértice en función de si es superficial o de control. Se definen el parámetro de masa puntual m, el parámetro de amortiguación d y el determinante de tiempo dt.

Finalmente, se genera una función ColisionTree en el proceso D6 (mostrado en el diagrama de la Fig. 155) para la creación del árbol de esferas de colisión, realizando la segmentación y creación de subdominios en base al procedimiento explicado en el apartado 3.5.

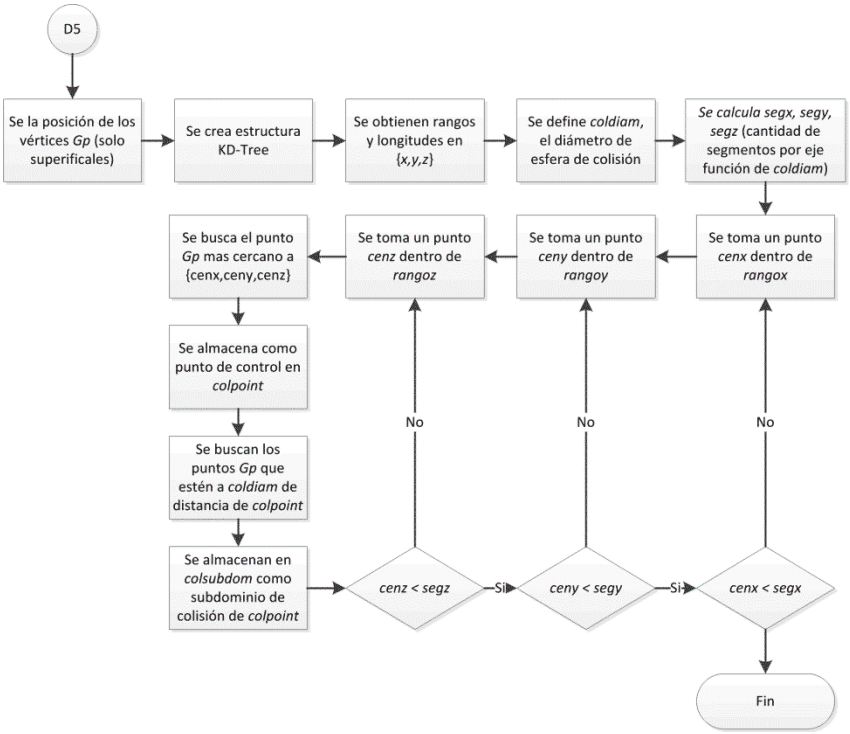

Fig. 155 Flow diagram that shows the algorithm for the creation of the collision tree

The KD-Tree data structure is generated using the Actmesh points, the ranges of distances in the coordinate axes are determined and the space is segmented based on them. A search is made for the vertex in Actmesh closest to the center of each of the segments, which will be used as a collision point with a sphere of diameter $coldiam_1$, and it is stored in an array called colpoint. Subsequently, all the points in the colpoint array are traversed, determining the vertices of Actmesh that are within the diameter (coldiam1) of scope of the sphere defined at the collision point, and they are stored in an array called colsubdom.

In the case of instruments, an instance was created called Instrument. This object takes the mesh modeled with CAD software and exported in STL format to import it into the virtual environment. For this object, only the display actor is generated, an array of points of the collision tree with a diameter (coldiam2), and a function is defined to determine the coordinates of the point in space, based on the position and rotation of geometry.

For further information, the reference codes of the functions of the initialization process are attached, which can be found in Annex II of this research report.

C.1.2 Flow diagrams for algorithm for Interaction Cycle Module

Once the preparation of the models and the creation of the necessary arrangements and structures in the initialization stage have been concluded, the interaction cycle in the simulation process begins.

To carry out this process, a function called Simulation was created, in which the application of the deformation and collision detection methods is managed. The inputs to this function are the outputs of the Initialization process, as well as those of an interface implemented in Wx for the detection of events over time. For this case, the tests with the events were developed with the interaction on the computer keyboard in ASCII code, where it is also shown how it is possible to acquire data from an emulator device of the surgical instrument for interaction with the user.

The purpose of the interaction cycle is to analyze the events thrown by the application in Wx and determine what functions should be carried out, for which it evaluates parameters created in SoftBody and Instrument type objects, such as the instrument status (active or inactive), if it is holding a deformable object or if it is about to do so, and if it is the case, have the vertex which it is holding. This process is best expressed in the diagram in Fig. 156.

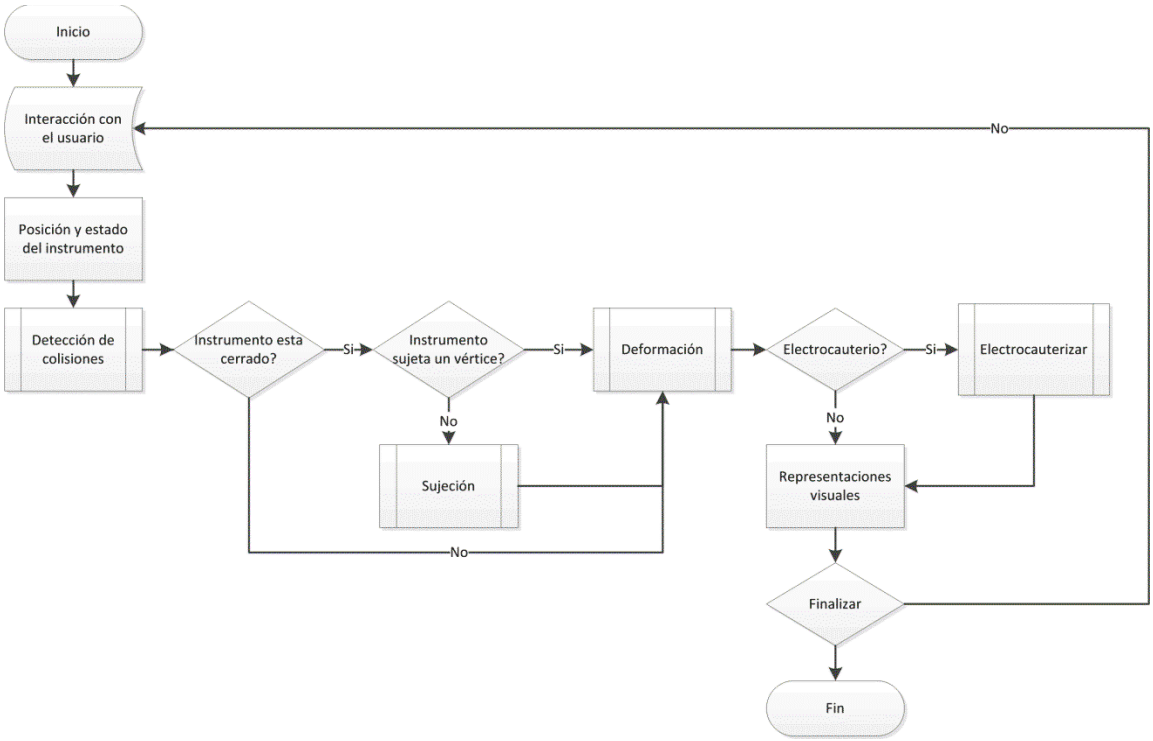

Fig. 156 Flow diagram that shows the algorithm for the Interaction Cycle Module

Based on this information and the collision detection function, an evaluation is performed to determine the present conditions for the deformation calculation. Likewise, it is in this process where additional functions are added for the development of applications, such as the

Electrocautery function in the instrument, which is used in the application developed in section 4.2.2.

The code of the interaction cycle functions can be found in Annex III of this research report.

C.1.3 Flow diagrams for algorithm for Collision Detection Module

Before being able to perform the deformation calculations of the organ being simulated, it is necessary to determine if there is a collision of said object with the interaction instrument, since based on the results of the collision detection, the deformation of the object will be calculated as a response. This is why the collision detection function is performed at the beginning of each repetition of the interaction cycle.

The diagram in Fig. 157 describes in detail the process of the collision detection function, which was implemented applying the method explained, where, based on the collision tree structure generated in the Initialization process, a NumPy array named col_instruments.

Fig. 157 Flow diagram that shows the algorithm for the Collision Detection Module

Said arrangement represents the position of the collision points, being updated each cycle with respect to the position of the instruments and is used to calculate the distance of each of the col_instrument points of the instrument against each of the colpoint points of the organ. If the distance between col_intrumenti and colpointj is less than the sum of the collision radii ((coldiam1)/ 2 + (coldiam2)/ 2), the collision spheres are considered to be penetrating and the distance between col_instrumenti and each one of the points in the colpointj subdomain (colsubdomj).

Once the point in colsubdomj closest to col_instrumenti is known, the vercel array is used to determine the faces of the STLGeometry that contains it. For each of the faces in vercel, it is evaluated whether it has been crossed by one of the preventive points created from col_instrumenti (± tolI3) to detect the collision at a tolerance tol that it occurs and to determine its direction.

To find out if one of the points has crossed a face, a tetrahedral cell is created that joins the face with the preventive point and its volume is evaluated (remembering the consideration that a negative volume means that the point is in the direction of the normal face, and a positive volume means that the point is against the normal). If one of the cells has positive volume, it is considered that there is a collision between the col_instrumenti point and the three points that make up the face of STLGeometry present in the cell.

The points are stored, and based on them and the preventive point that collided with the face of STLGeometry, it is determined in which direction the collision is made. An array of the directions, normal vectors, and collision points is generated and used to calculate the deformation in the next stage of the interaction cycle.

The code implemented for collision detection is included, shown in Appendix B.2.3.

C.1.4 Flow diagrams for algorithm for Deformation Module

Once the collision information is available, we proceed to the deformation calculation stage. As mentioned above, in this stage the conditions present in the system are evaluated to determine different scenarios, having to consider the clamping, the deformation due to the force of gravity and the deformation due to interaction with the user.

The process of this function is shown in the diagram that defines Fig. 158, which will be analyzed considering the start of the simulation. At this moment each Pi of Actmesh are in their rest position, so posref = posact. Subsequently, the distance between Pi and its neighboring points Pj ∈ veredgi is evaluated, both for posact and posref.

The objective of this part of the process is to determine the change in the length of the springs that join Pi with each neighbor Pj from the reference position to the current position (considering that in the first cycle there is still no deformation, the change is null). Taking the change in length, the restoration force is calculated for each Pi using equation (2), considering the vertices with constraint movement restriction, substituting the elasticity constant Kspringij and the spring action vector that directs the restoration force. Subsequently, the summation of the force exerted by all the neighbors for each Pi is stored in an arrangement which will be called Fi.

In the case that the organ has not been held, this function only considers the force of gravity {(0, 9.8 * mi, 0)}, calculating the deformation of the object only under the action of this force.

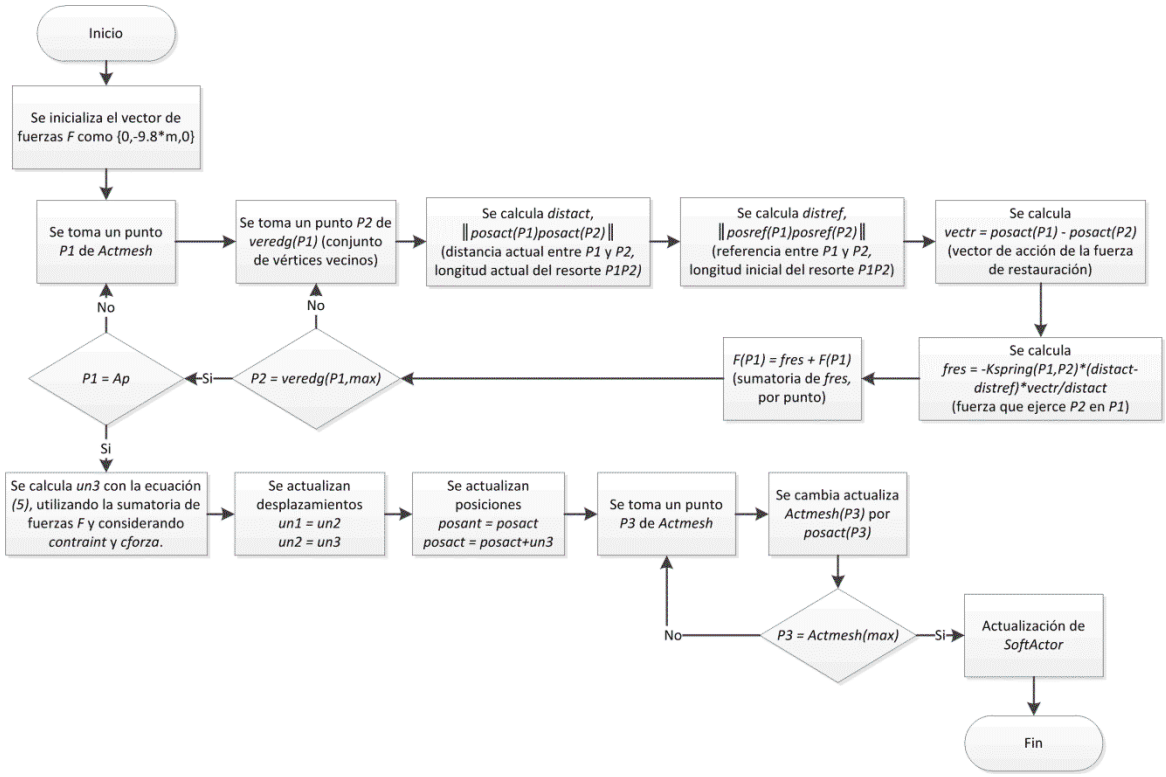

Fig. 158 Flow diagram that shows the algorithm for the Deformation Module

Once we have Fi for all points, we solve equation (5) using Euler's method with central finite difference (as explained in chapter 2). For this, the current and previous displacement (which will be called un2 and un1 respectively) are used, as well as the vector of restoration forces Fi previously calculated and the values of m, d, and Kvertex established in the initialization stage. With this, the displacement for each point in the following dt (un3) can be calculated, considering it to obtain posact and update the position of all points in SoftActor for visualization.

In the following cycle, there is a difference between posact and posref, which represents a deformation in the springs, calculating again Fi for each Pi, and solving equation (5) to calculate un3 in the current dt, considering that now un1 = un2 and un2 = un3. Posact is calculated again, and the points are updated in SoftActor.

When the instrument representing a clamp is operated near the organ, the clamping function begins, in which it is determined whether and what point of the mesh has been clamped by the instrument, as well as its clamping group.

This function is described in the diagram shown in Fig. 159, and is started by calculating the distance from the tip to the surface vertices of Actmesh. If the instrument is "closed" at a distance less than a previously established tolerance (in this case 1 mm) from a point Pi, Pi is

considered to have been clamped and stored together with its neighboring vertices veredgi and veredgveredgi. In this case, it is updated posacti with the position of the tip of the gripper, and the displacements are updated to be used in the deformation function.

Subsequently, the deformation function is executed (see Fig. 159), where now posacti and un2i are considered based on the position and displacement of the tip of the gripper. The change in the position of Pi causes a change in the length of the springs of this vertex and its neighbors, calculating the sum of restoration forces in Fi.

Subsequently the values of Fi are used to calculate un3 using equation (5) for each Pi, considering the constraint boundary restrictions. Taking into account the input of the clamping function, the deformation process is developed in the same way as the case where only gravity is considered, obtaining posact and updating the points in SoftActor, for visualization.

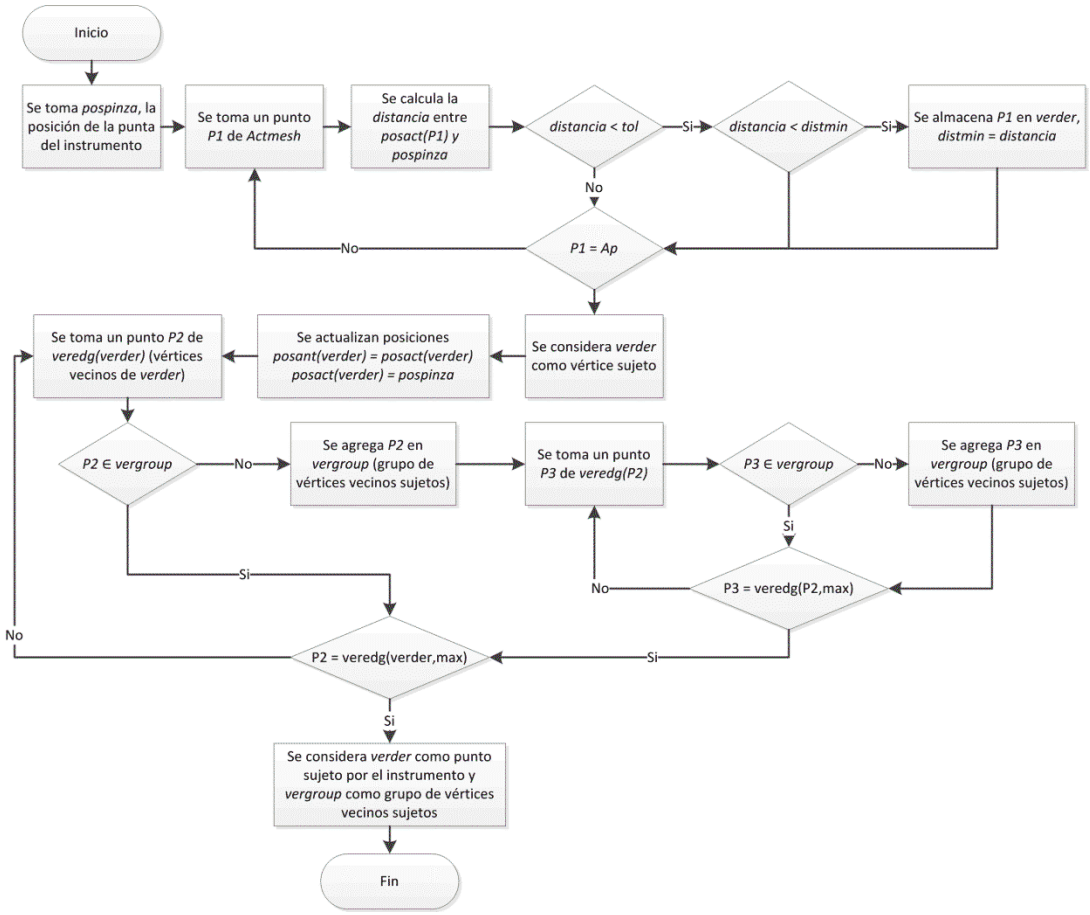

Fig. 159 Flow diagram that shows the algorithm for the grabbing function

The scripts implemented in Python of the functions to calculate the deformations were included in this Appendix next points.

Bibliography

Abdallah, Y.; Abdelhamid, A.; Elarif, T.; M.Salem, A. Intelligent Techniques in Medical Volume Visualization. *Procedia Computer Science* **2015**. *65*. 546-555. 10.1016/j.procs.2015.09.129.

Abdi, E.; Farahmand, F.; Durali, M. A meshless EFG-based algorithm for 3D deformable modeling of soft tissue in real-time. *Studies in health technology and informatics* **2012***. 173.* 1-7. 10.3233/978-1-61499-022-2-1.

Ahn, B.; Kim, J. Measurement and characterization of soft tissue behavior with surface deformation and force response under large deformations. *Medical image analysis* **2009***. 14*. 138-48. 10.1016/j.media.2009.10.006.

Alakwaa, W.; Nassef, M.; Badr, A. Lung Cancer Detection and Classification with 3D Convolutional Neural Network (3D-CNN). *International Journal of Advanced Computer Science and Applications* **2017***. 8.* 10.14569/IJACSA.2017.080853.

Alomari, A.; Wille, M.L.; Langton, C. Bone volume fraction and structural parameters for estimation of mechanical stiffness and failure load of human cancellous bone samples; in-vitro comparison of ultrasound transit time spectroscopy and X-ray μCT. *Bone* **2017***. 107*. 10.1016/j.bone.2017.11.021.

Andrade, H.; Ramos, F.; Kotsarenko, Y. A Multi-Agent System Approach Applied to Light Raycasting. *Journal of applied research and technology* **2012***. 10.* 629-643. 10.22201/icat.16656423.2012.10.4.388.

Arruda, E.; Boyce, M. A Three-Dimensional Constitutive Model of the Large Stretch Behavior of Rubber Elastic Materials. *Journal of the Mechanics and Physics of Solids* **1993***. 41.* 389-412. 10.1016/0022-5096(93)90013-6.

Asmussen, P.; Conrad, O.; Gunther, A.; Kirsch, M.; Riller, U. Semi-automatic segmentation of petrographic thin section images using a "seeded-region growing algorithm" with an

application to characterize wheathered subarkose sandstone. *Computers & Geosciences* **2015***, 83,* 89–99. 10.1016/j.cageo.2015.05.001.

Aspert, N.; Santa-Cruz, D.; Ebrahimi, T. Mesh: Measuring errors between surfaces using the hausdorff distance. *IEEE International Conference in Multimedia and Expo (ICME)* **2002***.* 705-708.

Balsa Rodriguez, M.; Gobbetti, E.; Iglesias Guitián, J.; Makhinya, M.; Marton, F.; Pajarola, R.; Suter, S.K. State-of-the-Art in Compressed GPU-Based Direct Volume Rendering. *Computer Graphics Forum* **2014***. 33.* 10.1111/cgf.12280.

Banihani, S.; De, S. A Comparison of Some Model Order Reduction Methods for Fast Simulation of Soft Tissue Response using the Point Collocation-based Method of Finite Spheres (PCMFS). *Engineering with computers* **2009***. 25.* 37-47. 10.1007/s00366-008-0103-4.

Banihani, S.; Rabczuk, T.; Almomani, T. POD for Real-Time Simulation of Hyperelastic Soft Biological Tissue Using the Point Collocation Method of Finite Spheres. *Mathematical Problems in Engineering* **2013***.* 10.1155/2013/386501.

Basafa, E.; Farahmand, F.; Vossoughi, G.R. A non-linear mass-spring model for more realistic and efficient simulation of soft tissues surgery. *Studies in health technology and informatics* **2008***, 132.* 23-5.

Batagelo, H.; Wu, S.T. What you see is what you snap: snapping to geometry deformed on the GPU. *Proceedings of the 2005 Symposium on Interactive 3D Graphics, SI3D* **2005**. 81-86. 10.1145/1053427.1053440.

Bayazit, U. A Greedy Region Growing Algorithm for Anisotropic Stretch Adaptive Triangulation of Geometry Images. *Graphical Models* **2019***, 106.* 101045. 10.1016/j.gmod.2019.101045.

Baylon-Quinones, K.L.; Moreno-Guerra, M.R.; & Romero, O.M.; Zuniga, A.E.; Rodriguez, C.A.; Villalba, E.F.; Diaz, J.; Silva, J.V.L. Characterization of Porcine Liver Parenchyma Behavior Under Tensile Loading. *XXIV International Materials Research Congress* **2015**.

Beard, D.; Bassingthwaighte, J. The Fractal Nature of Myocardial Blood Flow Emerges from a Whole-Organ Model of Arterial Network. *Journal of vascular research* **2000***, 37,* 282-96. 10.1159/000025742.

Bennai, M.T; Guessoum, Z.; Mazouzi, S.; Cormier, S.; Mezghiche, M. A Stochastic Multi-Agent Approach for Medical-Image Segmentation: Application to Tumor Segmentation in Brain MR Images. *Artificial Intelligence in Medicine* **2020***, 110*. 10.1016/j.artmed.2020.101980.

Beyer, J.; Hadwiger, M.; Pfister, H. State-of-the-Art in GPU-Based Large-Scale Volume Visualization. *Computer Graphics Forum* **2015***, 34.* 10.1111/cgf.12605.

Borovinsek, M.; Koudelka, P.; Sleichrt, J.; Vopalensky, M.; Kumpova, I.; Vesenjak, M.; Kytyr, D. Analysis of Advanced Pore Morphology (APM) Foam Elements Using Compressive Testing and Time-Lapse Computed Microtomography, *Materials* **2021***, 14(19),* 1996-1944. 10.3390/ma14195897.

Bro-Nielsen, M. Finite Element Modeling in Surgery Simulation. *Proceeding of the IEEE* **1998***, 86(3),* 490-503.

Bruckner, S.; Gröller, E. Instant Volume Visualization using Maximum Intensity Difference Accumulation. *Comput. Graph Forum* **2009***, 28,* 775-782. 10.1111/j.1467-8659.2009.01474.x.

Bel-Brunon, A.; Bruyère-Garnier, K.; Coret, M. Mechanical characterization of liver capsule through uniaxial quasi-static tensile tests until failure. *Journal of biomechanics* **2010***, 43,* 2221-7. 10.1016/j.jbiomech.2010.03.038.

Cantournet, S.; Boyce, M.C.; Tsou, A. Micromechanics and macromechanics of carbon nanotube-enhanced elastomers. *Journal of the Mechanics and Physics of Solids* **2007***, 55,* 1321-1339. 10.1016/j.jmps.2006.07.010.

Carter, F.; Frank, T.; Davies, P.; Mclean, D.; Cuschieri, A. Measurements and modelling of the compliance of human and porcine organs. *Medical image analysis* **2002***, 5,* 231-236. 10.1016/S1361-8415(01)00048-2.

Çavuşoğlu, M.C.; Göktekin, T.G.; Tendick, F. GiPSi: A framework for open source/open architecture software development for organ-level surgical simulation. *IEEE Transactions on Information Technology in Biomedicine* **2006***, 10(2),* 312-322.

Chappard, D.; Terranova, L.; Mallet, R.; Mercier, P. 3D Porous Architecture of Stacks of β-TCP Granules Compared with That of Trabecular Bone: A microCT, Vector Analysis, and Compression Study. *Frontiers in Endocrinology* **2015***, 6.* 10.3389/fendo.2015.00161.

Chen, F.; Gu, L.; Huang, P.; Zhang, J.; Xu, J. Soft Tissue Modeling using Nonlinear Mass Spring and Simplified Medial Representation. *Annual International Conference of the IEEE Engineering in Medicine and Biology Society. IEEE Engineering in Medicine and Biology Society* **2007***,* 5083-5086. 10.1109/IEMBS.2007.4353483.

Chu, B.; Gaillard, E.; Mongrain, R.; Reiter, S.; Tardif, J.C. Characterization of fracture toughness exhaustion in pig aorta. *Journal of the mechanical behavior of biomedical materials* **2012***, 17.* 10.1016/j.jmbbm.2012.08.007.

Cignoni, P.; Callieri, M.; Corsini, M.; Dellepiane, M.; Ganovelli, F.; Ranzuglia, G. MeshLab: an Open-Source Mesh Processing Tool. *Computing* **2008***, 1,* 129-136. 10.2312/LocalChapterEvents/ItalChap/ItalianChapConf2008/129-136.

Coles, T.; Meglan, D.; John, N. The Role of Haptics in Medical Training Simulators: A Survey of the State of the Art. *IEEE T. Haptics* **2011***, 4,* 51-66. 10.1109/TOH.2010.19.

Delfino, A.; Stergiopulos, N.; Moore, J.E.; Meister, J.J. Residual strain effects on the stress field in a thick wall finite element model of the human carotid bifurcation. *Journal of biomechanics* **1997***, 30,* 777-786. 10.1016/S0021-9290(97)00025-0.

Delingette, H. (2008). Biquadratic and Quadratic Springs for Modeling St Venant Kirchhoff. *Materials* **2008**, 40-48. 10.1007/978-3-540-70521-5_5.

Delingette, H.; Ayache, N. Soft Tissue Modeling for Surgery Simulation. Computational Models for the Human Body. *Handbook of Numerical Analysis* **2004***, 12*, 453-550. 10.1016/S1570-8659(03)12005-4.

Demiray, H. A note on the elasticity of soft biological tissues. *Journal of Biomechanics* **1972**, *5,* 309-311.

Diani, J.; Fayolle, B.; Gilormini, P. A Review on the Mullins Effect. *European Polymer Journal* **2009***, 45,* 601-612. 10.1016/j.eurpolymj.2008.11.017.

Dirección General de Normas. NOM-062-ZOO-1999, Especificaciones técnicas para la producción, cuidado y uso de los animales de laboratorio, **2001**. Available online: https://www.gob.mx/cms/uploads/attachment/file/203498/NOM-062-ZOO-1999_220801.pdf (accessed on 11 20 2021).

Dorfmann, L.; Ogden, R.W. A constitutive model for the Mullins effect with permanent set in particle-reinforced rubber. *International Journal of Solids and Structures* **2004,** *42,* 1855-1878. 10.1016/j.ijsolstr.2003.11.014.

Duan, Y.; Huang, W.; Chang, H.; Chen, W.; Zhou, J.; Teo, S.K.; Su, Y.; Chui, C.K.; Chang, S. Volume Preserved Mass-Spring Model with Novel Constraints for Soft Tissue Deformation. *IEEE journal of biomedical and health informatics* **2014***, 20.* 10.1109/JBHI.2014.2370059.

Ehrensberger, M.; Hohman, D.; Duncan, K.; Howard, C.; Bisson, L. Biomechanical comparison of femoral fixation devices for anterior cruciate ligament reconstruction using a novel testing method. *Clinical biomechanics* **2013***, 28*. 10.1016/j.clinbiomech.2012.12.007.

Elías-Zúñiga, A.; Baylon, K.; Ferrer, I.; Sereno, L.; Garcia-Romeu, M.L.; Bagudanch, I.; Grabalosa, J.; Pérez-Recio, T.; Martinez-Romero, O.; Ortega, W.; Elizalde, L. On the Rule of Mixtures for Predicting Stress-Softening and Residual Strain Effects in

Biological Tissues and Biocompatible Materials. *Materials* **2014***, 7.* 10.3390/ma7010441.

Elías-Zúñiga, A.; Palacios-Pineda, L.; Perales-Martínez, I.; Martinez-Romero, O.; Olvera Trejo, D.; Jiménez-Cedeño, I. Investigating the Mullins Effect and Energy Dissipation in Magnetorheological Polyurethane Elastomers. *International Journal of Molecular Sciences* **2020***, 21(15).* 10.3390/ijms21155318.

Fajar, A.; & Sarno, R.; Fatichah, C.; Fahmi, A. Reconstructing and resizing 3D images from DICOM files. *Journal of King Saud University - Computer and Information Sciences* **2020**. 10.1016/j.jksuci.2020.12.004.

Fan, M.; Lee, T. Variants of Seeded Region Growing. *IET Image Processing* **2015***, 9*. 10.1049/iet-ipr.2014.0490.

Farshad, M.; Barbezat, M.; Flüeler, P.; Schmidlin, F.; Graber, P.; Niederer, P. Material characterization of the pig kidney in relation with the biomechanical analysis of renal trauma. *Journal of biomechanics* **1999***, 32,* 417-25. 10.1016/S0021-9290(98)00180-8.

Ferraresi, C.; Manuello, A.; Mazza, L.; Maffiodo, D.; Franco, W. One-dimensional experimental mechanical characterisation of porcine aortic root wall. *Medical & biological engineering & computing* **1999***, 37,* 202-207. 10.1007/BF02513288.

Figueroa, D.; Meleán, P.; Calvo, R.; Figueroa, F.; Hube, M.; Labarca, G. (2011). Effect of radiofrequency on partial tears of the anterior cruciate ligament. Ex vivo experimental study in pigs. *Revista Espanola de Cirugia Ortopedica y Traumatologia* **2011***, 55,* 277-281. 10.1016/S1988-8856(11)70319-4.

Flores-Villalba, E.; Díaz-Elizondo, J.; Leyva-Alvizo, A.; Fernandez-Rangel, E.; Villegas-Cabello, O.; Real-Romo, Z. Evaluación de un simulador quirúrgico en función de su desempeño al ser utilizado por residentes con diferentes grados de experiencia. *Cirugía y Cirujanos* **2012***, 80,* 157-161.

Freutel, M.; Schmidt, H.; Durselen, L.; Ignatius, A.; Galbusera, F. Finite element modeling of soft tissues: Material models, tissue interaction and challenges. *Clinical Biomechanics* **2014***, 29(4),* 363-372. 10.1016/j.clinbiomech.2014.01.006.

Fu, Y.; Chui, C.K.; Teo, C.L. Liver tissue characterization from uniaxial stress-strain data using probabilistic and inverse finite element methods. *Journal of the mechanical behavior of biomedical materials* **2013***, 20C,* 105-112. 10.1016/j.jmbbm.2013.01.008.

Fu, Z.; Shi-Kuo, L.; Shi-Da, L.; Qiang, Z. Lame Function and Its Application to Some Nonlinear Evolution Equations. *Communications in Theoretical Physics* **2003***, 40(53).* 10.1088/0253-6102/40/1/53.

Fung, YC. Elasticity of soft tissues in simple elongation. *American Journal of Physiology* **1967***, 213,* 1532-1544. 10.1152/ajplegacy.1967.213.6.1532.

Fung, YC. Biomechanics: Mechanical Properties of Living Tissues. *Springer Verlag Inc*, **1993** New York.

Gao, Z.; Lister, K.; Desai, J. Constitutive Modeling of Liver Tissue: Experiment and Theory. *Annals of biomedical engineering* **2009***, 38,* 505-516. 10.1007/s10439-009-9812-0.

Gent, A.N. A New Constitutive Relation for Rubber. *Rubber Chemistry and Technology* **1996***, 69(1),* 59-61. 10.5254/1.3538357.

Goldenberg, M.; Fok, K.; Ordon, M.; Pace, K.; Lee, J. Simulation-Based Laparoscopic Surgery Crisis Resource Management Training—Predicting Technical and Nontechnical Skills. *Journal of Surgical Education* **2017***, 75*. 10.1016/j.jsurg.2017.11.011.

Gomez-Garcia, F.; Lopez Jornet, P.; Fernández-Martínez, M.; Guerrero Sánchez, Y. The bone density studied through the fractal dimension in patients with periodontal disease. *Fractals* **2020***, 28.* 10.1142/S0218348X20400319.

Goulette, F.; Chen, Z.W. Fast computation of soft tissue deformations in real-time simulation with Hyper-Elastic Mass Links. *Computer Methods in Applied Mechanics and Engineering* **2015***, 295,* 18-38. 10.1016/j.cma.2015.06.015.

Grantcharov, T.P.; Kristiansen, V.B.; Bendix, J.; Bardram, L.; Rosenberg, J.; Funch-Jensen, P. Randomized clinical trial of virtual reality simulation for laparoscopic skills training. *British Journal of Surgery* **2004***, 91(2),* 146-150. 10.1002/bjs.4407.

Guiatni, M.; Riboulet, V.; Duriez, C.; Kheddar, A.; Cotin, S. (2013). A Combined Force and Thermal Feedback Interface for Minimally Invasive Procedures Simulation. *(IEEE/ASME, Ed.) IEEE/ASME Transactions on Mechatronics* **2013***, 18(3),* 1170 - 1181. 10.1109/TMECH.2012.2197862.

He, J.H.; Ain, Q. New promises and future challenges of fractal calculus: From two-scale thermodynamics to fractal variational principle. *Thermal Science* **2020***, 24,* 65-65. 10.2298/TSCI200127065H.

Herman, B.; Hassan Zahraee, A.; Szewczyk, J.; Morel, G.; Bourdin, C.; Vercher, J.; Gayet, B. Ergonomic and Gesture Performance of Robotized Instruments for Laparoscopic Surgery. *IEEE/RSJ International Conference on Intelligent Robots and Systems* **2011***, 11,* 1333-1338. 10.1109/IROS.2011.6048105.

Herman, I. Physics of the Human Body. New York: *Springer-Verlag,* **2007**.

Hernández-Irizarry R.; Zendejas B.; Ali S.M.; Farley D.R. Optimizing training cost-effectiveness of simulation-based laparoscopic inguinal hernia repairs. *American Journal of Surgery* **2016***, 211(2),* 326-335. 10.1016/j.amjsurg.2015.07.027.

Hesamian, M.H.; Jia, W.; He, X.; Kennedy, P. Deep Learning Techniques or Medical Image Segmentation: Achievements and Challenges. *Journal of Digital Imaging* **2019***, 32.* 10.1007/s10278-019-00227-x.

Holzapfel, G.A. Biomecanics of Soft Tissue. *Handbook of Material Behavior: Nonlinear Models and Properties* **2001***, v.3, ch.10,* p. 1057-1071.

Holzapfel, G.A.; Gasser, T.C.; Ogden, R.W. Comparison of a multi-layer structural model for arterial walls with a Fung-type model and issues of material stability. *Journal of Biomechanical Engineering* **2005***, 126(2),* 264-275. 10.1115/1.1695572.

Holzapfel, G.A.; Ogden, R.W. Constitutive modelling of arteries. *Proceedings of The Royal Society A Mathematical Physical and Engineering Sciences* **2008***, 466(2118),* 1551-1597. 10.1098/rspa.2010.0058.

Horgan, C.; Ogden, R.W.; Saccomandi, G. A theory of stress softening of elastomers based on finite chain extensibility. *Proceedings of The Royal Society A Mathematical Physical and Engineering Sciences* **2004***, 460(2046),* 1737-1754. 10.1098/rspa.2003.1248.

Ioffe, S.; Szegedy, C. Batch Normalization: Accelerating Deep Network Training by Reducing Internal Covariate Shift. *Computer Science Machine Learning* **2015**. 10.48550/arXiv.1502.03167.

Ishikawa, M.; Sekine, K.; Okamura, A.; Zheng, Y.W. Ueno, Y.; Koike, N.; Tanaka, J.; Taniguchi, H. Reconstitution of hepatic tissue architectures from fetal liver cells obtained from a three-dimensional culture with a rotating wall vessel bioreactor. *Journal of bioscience and bioengineering* **2011***, 111,* 711-718. 10.1016/j.jbiosc.2011.01.019.

Issenberg, S.M. Features and uses of high-fidelity medical simulations that lead to effective learning: a BEME systematic review. *Medical Teacher* **2005***, 27(1),* 10-28. 10.1080/01421590500046924.

Ito, T. Collaborative implant design using the virtual manufacturing approach. *International Journal of Computer Integrated Manufacturing* **2003***, 16(7-8),* 541-545. 10.1080/0951192031000115741.

Jones, R.S.; Nawana, N.S.; Pearcy, M.J.; Learmonth, D.J.A.; Bickerstaff, D.R. Mechanical properties of the human anterior cruciate ligament. *Clinical Biomechanics* **1995***, 10(7),* 339-344. 10.1016/0268-0033(95)98193-x.

Kauer, M.; Vuskovic, V.; Dual, J.; Szekely, G.; Bajka, M. Inverse Finite Element Characterization of Soft Tissues with Aspiration Experiments. *Medical Image Analysis* **2001***, 6(3),* 275-287. 10.1016/s1361-8415(02)00085-3.

Kawahara, J.; Bentaieb, A.; Hamarneh, G. Deep features to classify skin lesions. *IEEE 13th International Symposium on Biomedical Imaging (ISBI)* **2016***,* 1397-1400. 10.1109/ISBI.2016.7493528.

Kemper, A.R.; Santago, A.C.; Stitzel, J.D.; Sparks, J.L.; Duma, S.M. Biomechanical response of human liver in tensile loading. *Annals of Advances in Automotive Medicine* **2010***, 54,* 15-26.

Kemper, A.R.; Santago, A.C.; Stitzel, J.D.; Sparks, J.L.; Duma, S.M. Biomechanical response of human spleen in tensile loading. *Journal of Biomechanics* **2012***, 45,* 348-355. 10.1016/j.jbiomech.2011.10.022.

Khlebnikov, R.; Voglreiter, P.; Steinberger, M.; Kainz, B.; Schmalstieg, D. Parallel Irradiance Caching for Interactive Monte-Carlo Direct Volume Rendering. *Computer Graphics Forum* **2014***, 33.* 10.1111/cgf.12362.

Kim, Y.; Chang, D.; Kim, J.; Park, S. Gallbladder Removal Simulation for Laparoscopic Surgery Training: A Hybrid Modeling Method. *Journal of Computer Science and Technology* **2013***, 28,* 499-507. 10.1007/s11390-013-1351-3.

Kitware. The VTK User's Guide (11 ed.). *Kitware Inc,* **2010**.

Korndorffer Jr., J.R.; Dunne, J.B.; Sierra, R.; Stefanidis, D.; Touchard, C.L.; Scott, D.J. Simulator training for laparoscopic suturing using performance goals translates to the operating room. *Journal of the American College of Surgeons* **2005***, 201(1),* 23-29. 10.1016/j.jamcollsurg.2005.02.021.

Korolj, A.; Wu, H.T.; Radisic, M. A Healthy Dose of Chaos: Using fractal frameworks for engineering higher-fidelity biomedical systems. *Biomaterials* **2019***, 219,* 119363. 10.1016/j.biomaterials.2019.119363.

Kot, M.; Nagahashi, H.; Szymczak, P. Elastic moduli of simple mass spring models. *The Visual Computer Journal* **2015***, 31,* 1339-1350. 10.1007/s00371-014-1015-5.

Kremer, K.; Platzer, W.; Schreiber, H.; Steichen, F. Minimally Invasive Abdominal Surgery. Stuttgart, Germany: *Georg Thieme Verlag* **2001**.

Lally, C.; Reid, J.; Prendergast, P.J. Elastic behavior of porcine coronary artery tissue under uniaxial and equibiaxial tension. *Annals of Biomedical Engineering* **2004***, 32(10),* 1355-1364. 10.1114/b:abme.0000042224.23927.ce.

Langtangen, H. A Primer on Scientific Programming with Python. Springer-Verlag **2012**.

Liu, F.; Martin, T.; Yeung, S.; Gross, M.H. Efficient direct rendering of deforming surfaces via shared subdivision trees. *Computer-Aided Design* **2015***, 58,* 132-140. 10.1016/j.cad.2014.08.005.

Liu, X.; Xu, S.; Zhang, H.; Hu, L. A New Hybrid Soft Tissue Model for Visio-Haptic Simulation. *IEEE Transactions on Instrumentation and Measurement* **2011***, 60(11),* 3570-3581. 10.1109/TIM.2011.2161142.

Lloyd, B.; Székely, G.; Harders, M. Identification of Spring Parameters for Deformable Object Simulation. *IEEE Transactions on Visualization and Computer Graphics* **2007***, 13(5),* 1081-1094*.* 10.1109/TVCG.2007.1055.

Lloyd, J.; Stavness, I.; Fels, S. (2012). ArtiSynth: A Fast Interactive Biomechanical Modeling Toolkit Combining Multibody and Finite Element Simulation. *Studies in Mechanobiology, Tissue Engineering and Biomaterials* **2012***, 11,* 355–394. 10.1007/8415_2012_126.

Lu, X.; Wu, J.; Ren, X.; Zhang, B.; Li, Y. The Study and application of the improved region growing algorithm for liver segmentation. *Optik - International Journal for Light and Electron Optics* **2014***, 125,* 2142–2147. 10.1016/j.ijleo.2013.10.049.

Ma, A.; Payandeh, T. Analysis and Experimental Study of a 4-DOF Haptic Device. Symposium on Haptic Interfaces for Virtual Environment and Teleoperator Systems **2008**, 351-356. 10.1109/HAPTICS.2008.4479970

Maehara, J.; Masugi, Y.; Abe, T.; Tsujikawa, H.; Kurebayashi, Y.; Ueno, A.; Ojima, H.; Okuda, S.; Jinzaki, M.; Shinoda, M.; Kitagawa, Y.; Oda, Y.; Honda, H.; Sakamoto, M. Quantification of intratumoral collagen and elastin fibers within hepatocellular carcinoma tissues finds correlations with clinico-patho-radiological features. *Hepatology Research* **2019***, 50*. 10.1111/hepr.13484.

Mansoor, S.B.; Mukhtar, Z.; Malik, M.; Amjad, Z.; Qureshi, H. Parameter evaluation for virtual Laparoscopic simulation. *7th International Conference on Emerging Technologies* **2011***.* 10.1109/ICET.2011.6048481.

Martins, P.; Peña, E.; Calvo, B.; Doblaré, M.; Mascarenhas, T.; Natal Jorge, R.; Ferreira, A. Prediction of nonlinear elastic behavior of vaginal tissue: experimental results and model formulation. *Computer Methods in Biomechanical and Biomedical Engineering* **2010***, 13(3),* 327-337. 10.1080/10255840903208197.

Martins, TACP.; Barbara, A.S.; Silva, G.B.C.; Faria, T.V.; Dalava, B.C.; da Silva, J.V.L (2007). InVesalius: three-dimensional medical reconstruction software. Virtual and rapid manufacturing. 135-141.

Mavrikios, D.; Karabatsoua, V.; Fragosa, D.; Chryssolourisa, G. A prototype virtual reality-based demonstrator for immersive and interactive simulation of welding processes. *International Journal of Computer Integrated Manufacturing* **2006***, 19(3),* 294-300. 10.1080/09511920500340916.

Mensmann, J.; Ropinski, T.; Hinrichs, K. An Advanced Volume Raycasting Technique using GPU Stream Processing. *Proceedings of the International Conference on Computer Graphics Theory and Applications GRAPP* **2010***,* 190-198.

Misra, S.; Ramesh, K.T.; Okamura, A.M. Modeling of Tool-Tissue Interactions for Computer-Based Surgical Simulation: A Literature Review. *Presence-Teleoperators and Virtual Environments* **2008***, 17(5),* 463-491, MIT. 10.1162/pres.17.5.463.

Mohr, M.B.; Blumcke, L.; Sachse, F.B.; Seemann, G.; Dossel, O. Hybrid Deformation Model of Myocardium. *Computers in Cardiology* **2003**, 319 - 322. 10.1109/CIC.2003.1291155.

Mooney, M. A theory of large elastic deformation. *Journal of Applied Physics* **1940***, 11(9),* 582-592. 10.1063/1.1712836.

Moore, K.L.; Agur, A.M.R.; Dalley, A.F. Essential Clinical Anatomy. *Lippincott Williams & Wilkins* **2010**.

Moraes, T.; Amorim, P.; Azevedo, F.A. Invesalius - an open-source imaging application. *Computational Vision and Medical Image Processing: VipIMAGE* **2011**, 405-408. Olhão, PT: CRC Press.

Moreno-Guerra, M.R. Simulación del comportamiento de tejidos en aplicaciones de realidad virtual con enfoque en procedimientos de cirugía laparoscópica, Thesis for Master's degree, *Tecnológico de Monterrey* **2012**.

Moreno-Guerra, M.R.; Marban, A.; Rojas, J.; Bosque, G.; Escamilla, D.; Silva, J.V.L.; Diaz, J. Simulator for Laparoscopic Surgery with Open-Source approach. In: Proceedings of the *1st International Conference on Design and Processes for Medical Devices* **2012**. *Proceedings of the 1st International Conference on Design and Processes for Medical* Devices 2012. V. 1. P. 207-210.

Moreno-Guerra, M.R.; Moraes, T.F.; Amorim, P.H.J.; Silva, J.V.L.; Rodriguez, C.A. Virtual Open-Source Environment for Training and Simulation of Laparoscopic Surgery. *XII Workshop De Informática Médica (WIM)* **2012**, Curitiba-PR. *XXXII Congresso Da Sociedade Brasileira De Computação - XII Workshop De Informática Médica, 2012*.

Moreno-Guerra, M.R.; Amorim, P.H.J.; Moraes, T.F.; Silva, J.V.L.; Quinones, K.L.B.; Villalba, E.F.; Elias-Zuniga, A.; Rodriguez, C.A. Soft Tissue Modeling for Virtual Surgery Simulation. *XXIV Congresso Brasileiro de Engenharia Biomédica (CBEB),* **2014**.

Moreno-Guerra, M.R.; Junqueira Amorim, P.H.; Franco De Moraes, T.; Martínez Romero, O.; Elías Zúñiga, A.; Flores Villalba, E.; Díaz Elizondo, J.A.; Lopes Da Silva, J.V.; Rodríguez-González, C.A. A Hybrid Formulation for Soft Tissue Modeling on Real-Time Surgery Simulation. *XXXVI Iberian Latin American Congress on Computational Methods in Engineering* **2015**. 10.20906/cps/cilamce2015-0633

Moreno-Guerra, M.R.; Martínez-Romero, O.; Palacios-Pineda, L.M.; Olvera-Trejo, D.; Diaz-Elizondo, J.A.; Flores-Villalba, E.; da Silva, J.V.L.; Elías-Zúñiga, A.; Rodriguez, C.A. Soft Tissue Hybrid Model for Real-Time Simulations. *Polymers* **2022**, *14, 1407*. https://doi.org/10.3390/polym14071407

Mousavian, A.; Anguelov, D.; Flynn, J.; Košecká, J. (2017). 3D Bounding Box Estimation Using Deep Learning and Geometry. *IEEE Conference on Computer Vision and Pattern Recognition (CVPR)* **2017**, 5632-5640. 10.1109/CVPR.2017.597.

Mroz, L.; Hauser, H.; Gröller, E. Interactive High-Quality Maximum Intensity Projection. *Computer Graphic Forum* **2000***, 19(3),* 341-350. 10.1111/1467-8659.00426.

Murdock, K.; Martin, C.; Sun, W. Characterization of mechanical properties of pericardium tissue using planar biaxial tension and flexural deformation. *Journal of the mechanical behavior of biomedical materials* **2017***, 77,* 148-156. 10.1016/j.jmbbm.2017.08.039.

Natsupakpong, S.; Çavusoglu, M.C. Determination of elasticity parameters in lumped element (mass-spring) models of deformable objects. *Graphical Models* **2010***, 72,* 61-73. 10.1016/j.gmod.2010.10.001.

Nguyen, T.N.; Ho Ba Tho, M.C.; Dao, T.T. A Systematic Review of Real-Time Medical Simulations with Soft-Tissue Deformation: Computational Approaches, Interaction Devices, System Architectures, and Clinical Validations. *Applied Bionics and Biomechanics.* **2020***, 19*, 1-30. 10.1155/2020/5039329.

Nikolaev, S. Non-linear mass-spring system for large soft tissue deformations modeling. *Scientific and Technical Journal of Information Technologies, Mechanics and Optics* **2013***, 5(87),* 88-94. 10.48550/arXiv.1403.2294.

Okuyan, E.; Gudukbay, U.; Bulutay, C.; Heinig, K.H. MaterialVis: Material visualization tool using direct volume and surface rendering techniques. *Journal of molecular graphics & modelling* **2014***, 50C,* 50-60. 10.1016/j.jmgm.2014.03.007.

Oliveira, M.L.; Saraiva, J.A.; Loffredo, L.C.; Scaf, G. Tosoni, G. Fractal dimension of the mandibular trabecular bone measured on digital and digitized images. *Journal of Oral and Maxillofacial Radiology* **2015***, 3*. 10.4103/2321-3841.157519.

Omar, M.N.; Zhong, Y. Flexible Mass Spring Method for Modelling Soft Tissue Deformation. *International Journal of Engineering Technology and Sciences* **2020**, *7,* 24-41. 10.15282/ijets.7.2.2020.1003.

Omar, M.N.; Zhong, Y. A Review of Mass Spring Method Improvements for Modeling Soft Tissue Deformation. *Human-Centered Technology for a Better Tomorrow* **2022***,* 203-215. 10.1007/978-981-16-4115-2_16.

Palacios-Pineda, L.; Perales-Martínez, I.; Moreno-Guerra, M.R.; Elías-Zúñiga, A. An Optimum Specimen Geometry for Equibiaxial Experimental Tests of Reinforced Magnetorheological Elastomers with Iron Micro- and Nanoparticles. Nanomaterials **2017***, 7(9),* 254. 10.3390/Nano7090254

Palter, V.; Grantcharov, T. Simulation in surgical education. *Canadian Medical Association Journal* **2010**, *182(11)*, 1191-1196. 10.1503/cmaj.091743.

Pang, W.M.; Qin, J.; Chui, Y.P.; Heng, P.A. Fast Prototyping of Virtual Reality Based Surgical Simulators with PhysiX-enabled GPU. *Transactions on Edutainment IV LNCS* **2010**, 6250, 176-188. 10.1007/978-3-642-14484-4_15.

Parra, A.; Rodríguez, A.; Zubizarreta, A.; Pérez, J. Validation of a Real-Time Capable Multibody Vehicle Dynamics Formulation for Automotive Testing Frameworks Based on Simulation. *IEEE Access* **2020***, 8,* 213253-213265. 10.1109/ACCESS.2020.3040232.

Patete, P.; Iaconoa, M.; Spadeaa, M.; Trecatec, G.; Vergnaghi, D.; Mainardi, L.; Baroni, G. A multi-tissue mass-spring model for computer assisted breast surgery. *Medical Engineering & Physics* **2013***, 35,* 47-53. 10.1016/j.medengphy.2012.03.008.

Picinbono, G.; Delingette, H.; Ayache, N. Nonlinear and anisotropic elastic soft tissue models for medical simulation. *Proceedings - IEEE International Conference on Robotics and Automation* **2001***, 2,* 1370 - 1375. 10.1109/ROBOT.2001.932801.

Pietroszek, K. Raycasting in Virtual Reality. *Springer Encyclopedia of Computer Graphics and Games* **2018**. 10.1007/978-3-319-08234-9_180-1.

Radhakrishnan, U.; Konstantinos, K.; Chinello, F. A systematic review of immersive virtual reality for industrial skills training. *Behaviour and Information Technology* **2021***, 40*. 10.1080/0144929X.2021.1954693.

Rickaby, S.R.; Scott, N. A cyclic stress softening model for the Mullins effect. *International Journal of Solids and Structures* **2013***, 50,* 111–120. 10.1016/j.ijsolstr.2012.09.006.

Rivlin, R.S. Large elastic deformations of isotropic materials. IV. Further developments of the general theory. *Philosophical Transactions of the Royal Society of London. Series A, Mathematical and Physical Sciences* **1948***, 241(835),* 379-397. 10.1098/rsta.1948.0024.

Rocha-Hoyos, J.; Cedeño, E.A.; & Vega, W.; Molina-Osejos, J. Review of the Modeling and Optimization Characteristics for the Design of the Macpherson Suspension System. *Informacion Tecnológica* **2018***, 29(6).* 221-233.

Rodríguez, C.; Maestro, A.; García, T.E.; Montes, S. Static load biomechanical behaviour of different femoral fixation systems for anterior cruciate ligament reconstruction. *Revista Española de Cirugía Ortopédica y Traumatología* **2011***, 55(6),* 428-436. 10.1016/j.recote.2011.07.001.

Rosskopf, J.; Kloth, C.; Dreyhaupt, J.; Braun, M.; Schmitz, B.; Graeter, T. Thin Slices and Maximum Intensity Projection Reconstructions Increase Sensitivity to Hyperdense Middle Cerebral Artery Sign in Acute Ischemic Stroke. *Cerebrovascular Diseases* **2020**, *49,* 1-5. 10.1159/000509378.

Rubio, E.; Sanz-Lobera, A.; Sebastián, M. Virtual reality applications for the next-generation manufacturing. *International Journal of Computer Integrated Manufacturing* **2005***, 18(7),* 601-609. 10.1080/09511920500069259.

Saeed, E.; Saleh, H. Pectoral Muscles Removal in Mammogram Image by Hybrid Bounding Box and Region Growing Algorithm, *International Conference on Computer Science and Software Engineering (CSASE)* **2020**, 146-151. 10.1109/CSASE48920.2020.9142055.

Sanchez-Molina, D.; Velazquez-Ameijide, J.; Quintana, V.; Arregui-Dalmases, C.; Crandall, J.; Subit, D.; Kerrigan, J. Fractal dimension and mechanical properties of human cortical bone. *Medical engineering & physics* **2012***, 35*. 10.1016/j.medengphy.2012.06.024.

San-Vicente, G.; Aguinaga, I.; Celigueta, J.T. Cubical Mass-Spring Model Design Based on a Tensile Deformation Test and Nonlinear Material Model. *IEEE Transactions on Visualization and Computer Graphics* **2012***, 18(2),* 228-241. 10.1109/TVCG.2011.32.

Scalese, R.; Obeso, V.; Issenberg, S. Simulation Technology for Skills Training and Competency Assessment in Medical Education. *Journal of General Internal Medicine* **2007***, 23(1),* 46-49. 10.1007/s11606-007-0283-4.

Schijven, M.J. Virtual reality surgical laparoscopic simulators. *Surgical Endoscopy and other Interventional Techniques* **2003***, 17,* 1943-1950. 10.1007/s00464-003-9052-6.

Schmidt, S.; Schmidt, E.; Schick, W.; Henning, J. Optimization of Vehicle Handling Performance Using a Full Vehicle Model with Multi-Body System (MBS) Suspensions in Multiple Real Time - Applying the DoE Method. *International Journal of Automotive Engineering* **2015***, 6(2),* 53-57. 10.20485/jsaeijae.6.2_53.

Schwartz, J.M.; Dellinger, M.; Rancourt, D.; Moisan, C.; Laurendeau, D. Modelling liver tissue properties using a non-linear viscoelastic model for surgery simulation. *European Series in Applied and Industrial Mathematics (ESAIM): Proceedings* **2002***, 12,* 146-153. 10.1051/proc:2002024.

Secretaría de Salud. Reglamento de la Ley General de Salud en materia de control sanitario de la disposición de órganos, tejidos y cadáveres de seres humanos **2014**. Available online: http://www.ordenjuridico.gob.mx/Documentos/Federal/pdf/wo88534.pdf (accessed on 11 20 2021).

Secretaría de Salud (B). Reglamento de la Ley General de Salud en Materia de Investigación para la Salud **2014**. Available online: http://www.ordenjuridico.gob.mx/Documentos/Federal/pdf/wo88535.pdf (accessed on 11 20 2021).

SENASICA (Servicio Nacional de Sanidad, Inocuidad y Calidad Agroalimentaria). Ley Federal De Sanidad Animal **2012**. Available online:

https://www.gob.mx/cms/uploads/attachment/file/118761/LFSA.pdf (accessed on 20 11 2021).

SENASICA (Servicio Nacional de Sanidad, Inocuidad y Calidad Agroalimentaria) (B). Reglamento De La Ley Federal De Sanidad Animal **2012**. Available online: https://www.gob.mx/cms/uploads/attachment/file/118762/Reg_LFSA.pdf (accessed on 11 20 2021).

Serna-Ojeda, J.; Borunda-Nava, D.; Domínguez-Cherit, G. La simulación en medicina. La situación en México. *Cirugía y Cirujanos* **2012***, 80(3),* 301-305.

Seymour, N.; Gallaghe, A.; Roman, S.; O'Brien, M.; Bansal, V.; Andersen, D.; Satava, R.M. Virtual Reality Training Improves Operating Room Performance. *Annals of Surgery* **2002***, 236(4)*, 458-464. 10.1097/00000658-200210000-00008.

Shetty, S.; Zevin, B.; Grantcharov, T.; Roberts, K.; Duffy, A. Perceptions, Training Experiences, and Preferences of Surgical Residents Toward Laparoscopic Simulation Training: A Resident Survey. *Journal of surgical education* **2014***, 71(5),* 727-733. 10.1016/j.jsurg.2014.01.006.

Shkarin, R.; Shkarina, S.; Weinhardt, V.; Surmenev, R.; Surmeneva, M.; Shkarin, A.; Baumbach, T.; Mikut, R. GPU-accelerated ray-casting for 3D fiber orientation analysis. *PLoS ONE* **2020***, 15(7),* e0236420. 10.1371/journal.pone.0236420.

Shrivastava, N.; Bharti, J. Automatic Seeded Region Growing Image Segmentation for Medical Image Segmentation: A Brief Review. *International Journal of Image and Graphics* **2020***, 20(3),* 2050018. 10.1142/S0219467820500187.

Simonyan, K.; Zisserman, A. Very Deep Convolutional Networks for Large-Scale Image Recognition. *Computer Vision and Pattern Recognition* **2015**. 10.48550/arXiv.1409.1556.

Singarayan, J.; Therese, B.; Rangasami, R. A novel segmentation of cochlear nerve using region growing algorithm. *Biomedical Signal Processing and Control* **2018***, 39,* 117-129. 10.1016/j.bspc.2017.07.014.

Smutny, P.; Babiuch, M.; Foltynek, P. A Review of the Virtual Reality Applications in Education and Training. *20th International Carpathian Control Conference (ICCC)* **2019**, 1-4. 10.1109/CarpathianCC.2019.8765930.

Soper, N.; Swanstöm, L.; Eubanks, W. Mastery of Endoscopic and Laparoscopic Surgery. Philadelphia: *Lippincott Williams & Wilkins* **2009**.

Spencer, A.J.M. Constitutive Theory for strongly Anisotropic Solids. Springer-Verlag, Wien, in *Continuum theory of the mechanics of fiber-reinforced, International Centre for Mechanical Sciences* **1984***, 282,* 1-32. 10.1007/978-3-7091-4336-0_1.

Stevens, L.; Lynm, C.; Glass, R. Laparoscopia. *The Journal of the American Medical Association* **2002***, 287(3).*

Stingl, J.; Báĉa, V.; Ĉech, P.; Kovanda, J. Morphology and some biomechanical properties of human liver and spleen. *Surgical and Radiologic Anatomy* **2002***, 24(5),* 285-289. 10.1007/s00276-002-0054-1.

Tan, W.; Kang, Y.; Dong, Z.; Chao, C.; Y, X.; Su, Y.; Zhang, Y.; Zhang, L.; Xu, L. An Approach to Extraction Midsagittal Plane of Skull From Brain CT Images for Oral and Maxillofacial Surgery. *IEEE Access* **2019***, 7,* 118203-118217. 10.1109/ACCESS.2019.2920862.

Tomasina, C.; Bodet, T.; Mota, C.; Moroni, L.; Camarero-Espinosa, S. Bioprinting Vasculature: Materials, Cells and Emergent Techniques. *Materials* **2019***, 12,* 2701. 10.3390/ma12172701.

Tortora, G.J.; Derrickson, B.; Principles of Anatomy and Physiology. New Jersey, *John Wiley and Sons Inc* **2009**.

Tseng, C.; Alves, M.; Milori, D.; Crestana, S. Geometric characterization of soil structure through unconventional analytical tools. *Soil and Tillage Research* **2018***, 181*. 10.1016/j.still.2018.03.018.

Ueda, M.; Saito, S.; Murata, T.; Hirano, T.; Bise, R.; Kabashima, K.; Suzuki, S. Combined multiphoton imaging and biaxial tissue extension for quantitative analysis of geometric fiber organization in human reticular dermis. *Scientific Reports* **2019***, 9*. 10.1038/s41598-019-47213-5.

Umale, S.; Deck, C.; Bourdet, N.; Dhumane, P.; Soler, L.; Marescaux, J.; Willinger, R. Experimental mechanical characterization of abdominal organs: liver, kidney & spleen. *Journal of the Mechanical Behavior of Medical Materials* **2013***, 17,* 22-33. 10.1016/j.jmbbm.2012.07.010.

Van-Verth, J.; Bishop, L. Essential Mathematics for Games and Interactive Applications: A Programmer's Guide. Burlington: Elsevier, Morgan Kaufmann Publishers **2008**.

Vázquez, J. Simuladores médicos, una elección racional y ética del manejo de cadáveres. *EN-CLAVES del pensamiento* **2013**, 13.

Wang, X.; Schoen, J. A.; Rentschler, M.E. A quantitative comparison of soft tissue compressive viscoelastic model accuracy. *Journal of the Mechanical Behavior of Biomedical Materials* **2013***, 20,* 126-136. 10.1016/j.jmbbm.2013.01.007.

Waters, J.; Kim, H. Force distribution in a semiflexible loop. *Physical Review E* **2016***, 93*. 10.1103/PhysRevE.93.043315.

Weiss, S.; Westermann, R. Differentiable Direct Volume Rendering. *Graphics* **2021**. 10.48550/arXiv.2107.12672

Wen, Y.; Su, D.; Lin, Q. Region-Growing Algorithm on CT Angiography Images for Detection of Gynecological Malignant Tumor. *Scientific Programming* **2021***,* 1-7. 10.1155/2021/9875886.

Williams, L.; Drew, T. What do we know about volumetric medical image interpretation?: a review of the basic science and medical image perception literatures. *Cognitive Research: Principles and Implications* **2019***, 4(21).* 10.1186/s41235-019-0171-6.

Wu, S.; Nakao, M.; Matsuda, T. SuperCut: Superpixel Based Foreground Extraction With Loose Bounding Boxes in One Cutting. *IEEE Signal Processing Letters* **2017***, 24(12),* 1803-1807. 10.1109/LSP.2017.2761393.

Wu, Y.; Adeeb, S.; Doschak, M. Using Micro-CT Derived Bone Microarchitecture to Analyze Bone Stiffness – A Case Study on Osteoporosis Rat Bone. *Frontiers in endocrinology* **2015***, 6, 80.* 10.3389/fendo.2015.00080.

Xi, T.; Schreurs, R.; Heerink, W.; Berge, S.; Maal, T. A Novel Region-Growing Based Semi-Automatic Segmentation Protocol for Three-Dimensional Condylar Reconstruction Using Cone Beam Computed Tomography (CBCT). *PloS ONE* **2014***, 9(11),* e111126. 10.1371/journal.pone.0111126.

Xiao, J. Contact and Deformation Modeling for Interactive Environments. *IEEE Transactions on Robotics* **2007***, 23(3),* 416-430. 10.1109/TRO.2007.895058.

Xie, X.; Bennett, J.; Saha, S.; Lu, Y.; Cao, J.; Liu, W.; Gan, Z. Mechanistic data-driven prediction of as-built mechanical properties in metal additive manufacturing. *npj Computational Materials* **2021***, 7(86).* 10.1038/s41524-021-00555-z.

Yaacoub, F.; Hamam, Y.; Abche, A. Computer-Based Training System for Simulating Wrist Arthroscopy. *21st IEEE International Symposium on Computer-Based Medical Systems CBMS* **2008***,* 421-423. 10.1109/CBMS.2008.67.

Yeoh, O.H. Some Forms of the Strain Energy Function for Rubber. *Rubber Chemistry and Technology* **1993***, 66(5),* 754-771. 10.5254/1.3538343.

Yin, G.; Li, Y.; Zhang, J.; Ni, J. Soft Tissue Modeling using Tetrahedron Finite Element Method in Surgery Simulation. *First International Conference on Information Science and Engineering* **2009***,* 3705-3708. 10.1109/ICISE.2009.1071.

Yu, Y.; Zhu, J.; Pei, J. Foreground Target Extraction in Bounding Box Based on Sub-block Region Growing and Grab Cut. *14th IEEE International Conference on Signal Processing (ICSP)* **2018***,* 344-349. 10.1109/ICSP.2018.8652318.

Yuan, Y.; Chen, D.; Yan, L. Interactive Three-Dimensional Segmentation Using Region Growing Algorithms. *Journal of Algorithms & Computational Technology* **2015***, 9,* 199-214. 10.1260/1748-3018.9.2.199.

Zhang, J.; Gu, L.; Zhu, B.; Li, X.; Zheng, G.; Xu, J. A Novel laparoscopic surgery simulator: System and Evaluation. *International Conference on Information Technology and Application in Biomedicine* **2008***, 8,* 467-470. 10.1109/ITAB.2008.4570601.

Zhang, J.; Zhong, Y.; Gu, C. Deformable Models for Surgical Simulation: A Survey. *IEEE Reviews in Biomedical Engineering* **2017***, 11,* 143-164. 10.1109/RBME.2017.2773521.

Zhang, J.; Zhong, Y.; Gu, C. Soft tissue deformation modelling through neural dynamics-based reaction-diffusion mechanics. *Medical & Biological Engineering & Computing* **2018***, 56,* 2163-2176. 10.1007/s11517-018-1849-5.

Zhao, B.; Wang, J.; Andò, E.; Viggiani, G.; Coop, M. An Investigation of Particle Breakage under One-Dimensional Compression of Sand Using X-ray Micro-Tomography. *Canadian Geotechnical Journal* **2019***, 57*. 10.1139/cgj-2018-0548.

Zheng, S.; Guo, J.; Cui, X.; Veldhuis, R.; Oudkerk, M.; Van Ooijen, P. Automatic Pulmonary Nodule Detection in CTScans Using Convolutional Neural Networks Based on Maximum Intensity Projection. *IEEE Transactions on Medical Imaging* **2020***, 39(3),* 797-805. 10.1109/TMI.2019.2935553.

Zhu, B.; Gu, L. A hybrid deformable modecl for real-time surgical simulation. *Computerized Medical Imaging and Graphics* **2012***, 36(5),* 356-365. 10.1016/j.compmedimag.2012.03.001.

Published Papers & Conferences

Mario Regino Moreno Guerra

https://www.researchgate.net/profile/Mario-Moreno-Guerra

https://www.scopus.com/authid/detail.uri?authorId=57191110530

https://orcid.org/0000-0002-5145-1819

1. Moreno-Guerra, M.R.; Martínez-Romero, O.; Palacios-Pineda, L.M.; Olvera-Trejo, D.; Diaz-Elizondo, J.A.; Flores-Villalba, E.; da Silva, J.V.L.; Elías-Zúñiga, A.; Rodriguez, C.A. Soft Tissue Hybrid Model for Real-Time Simulations. Polymers 2022, 14, 1407. https://doi.org/10.3390/polym14071407

2. Palacios-Pineda, Luis & Perales-Martínez, I. & Moreno-Guerra, Mario & Elías-Zúñiga, Alex. (2017). An Optimum Specimen Geometry for Equibiaxial Experimental Tests of Reinforced Magnetorheological Elastomers with Iron Micro- and Nanoparticles. Nanomaterials. 7. 254. 10.3390/nano7090254.

3. Dinis, J. C. & Moraes, T. F. & Junqueira Amorim, P. H. & Moreno-Guerra, M. R. & Nunes, A. A. & Lopes Da Silva, J. V. (2016). Pomes: An Open Source Software Tool to Generate Roughness/Porous Surfaces. Procedia CIRP, 2016.

4. Moreno-Guerra, M.R. & Junqueira Amorim, P. & Moraes, T. & Martínez Romero, O., Elías Zúñiga, A. & Flores Villalba, E. & Díaz Elizondo, J.A. & Lopes Da Silva, J. & Rodríguez-González, C. A. (2015). A Hybrid Formulation for Soft Tissue Modeling on Real-Time Surgery Simulation. In: XXXVI Iberian Latin American Congress on Computational Methods in Engineering, 2015, Rio De Janeiro. V. 2015. 2178-4949, doi: http://dx.doi.org/10.20906/cps/cilamce2015-0633

5. Baylon Quinones, K. L. & Moreno Guerra, M. R. & Romero, O. M. ; Zuniga, A. E. & Rodriguez, C. A. & Villalba, E. F. & Diaz, J. & Silva, J. V. L. (2015). Characterization of Porcine Liver Parenchyma Behavior Under Tensile Loading. 2015.

6. Moreno-Guerra, M. R. & Amorim, P. H. J. & Moraes, T. F. & Silva, J. V. L. & Quinones, K. L. B. & Villalba, E. F. & Elias-Zuniga, A. & Rodriguez, C. A. (2014). Soft Tissue Modeling for Virtual Surgery Simulation. In: XXIV Congresso Brasileiro de Engenharia Biomédica (CBEB2014), 2014, Uberlândia, MG. XXIV Brazilian Congress on Biomedical Engineering, CBEB, 2014.

7. Moreno-Guerra, M. R. & Moraes, T. F. & Amorim, P. H. J. & Silva, J. V. L. & Rodriguez, C. A. (2012). Virtual Open-Source Environment for Training and Simulation of Laparoscopic Surgery. In: XII Workshop De Informática Médica (WIM2012), 2012, Curitiba-PR. XXXII Congresso Da Sociedade Brasileira De Computação - XII Workshop De Informática Médica, 2012. V. 1. P. 1-4.

8. Moreno-Guerra, M. R. & Marban, A. & Rojas, J. & Bosque, G. & Escamilla, D. & Silva, J. V. L., Diaz, J. (2012). Simulator For Laparoscopic Surgery with Open-Source approach. In: Proceedings of the 1st International Conference on Design and Processes for Medical Devices, 2012, Brescia. Proceedings of the 1st International Conference on Design and Processes for Medical Devices, 2012. V. 1. P. 207-210.

polymers

MDPI

Article

Soft Tissue Hybrid Model for Real-Time Simulations

Mario R. Moreno-Guerra [1], Oscar Martínez-Romero [1,2], Luis Manuel Palacios-Pineda [3], Daniel Olvera-Trejo [1,2], José A. Diaz-Elizondo [4], Eduardo Flores-Villalba [4], Jorge V. L. da Silva [5], Alex Elías-Zúñiga [1,2,*] and Ciro A. Rodriguez [1,2,*]

[1] Mechanical Engineering and Advanced Materials Department, School of Engineering and Science, Tecnologico de Monterrey, Ave. Eugenio Garza Sada 2501 Sur, Monterrey 64849, NL, Mexico; marioregino@hotmail.com (M.R.M.-G.); oscar.martinez@tec.mx (O.M.-R.); daniel.olvera.trejo@tec.mx (D.O.-T.)
[2] Laboratorio Nacional de Manufactura Aditiva y Digital MADiT, Apodaca 66629, NL, Mexico
[3] Tecnológico Nacional de Mexico, Instituto Tecnológico de Pachuca, Carr. México-Pachuca Km 87.5, Pachuca de Soto 42080, HG, Mexico; luis.pp@pachuca.tecnm.mx
[4] Escuela de Medicina y Ciencias de la Salud, Tecnológico de Monterrey, Avenida Eugenio Garza Sada 2501, Monterrey 64849, NL, Mexico; jadiaze@tec.mx (J.A.D.-E.); eduardofloresvillalba@tec.mx (E.F.-V.)
[5] DT3D/CTI, Rodovia Dom Pedro I (SP-65), Km 143,6-Amarais-Campinas, Campinas 13069-901, SP, Brazil; jorge.silva@cti.gov.br
* Correspondence: aelias@tec.mx (A.E.-Z.); ciro.rodriguez@tec.mx (C.A.R.)

Abstract: In this article, a recent formulation for real-time simulation is developed combining the strain energy density of the Spring Mass Model (SMM) with the equivalent representation of the Strain Energy Density Function (SEDF). The resulting Equivalent Energy Spring Model (EESM) is expected to provide information in real-time about the mechanical response of soft tissue when subjected to uniaxial deformations. The proposed model represents a variation of the SMM and can be used to predict the mechanical behavior of biological tissues not only during loading but also during unloading deformation states. To assess the accuracy achieved by the EESM, experimental data was collected from liver porcine samples via uniaxial loading and unloading tensile tests. Validation of the model through numerical predictions achieved a refresh rate of 31 fps (31.49 ms of computation time for each frame), achieving a coefficient of determination R^2 from 93.23% to 99.94% when compared to experimental data. The proposed hybrid formulation to characterize soft tissue mechanical behavior is fast enough for real-time simulation and captures the soft material nonlinear virgin and stress-softened effects with high accuracy.

Keywords: spring–mass model; stress softening effects (Mullin's effect); non-Gaussian model; biomaterial residual strains; biological tissues; real-time simulations

Citation: Moreno-Guerra, M.R.; Martínez-Romero, O.; Palacios-Pineda, L.M.; Olvera-Trejo, D.; Diaz-Elizondo, J.A.; Flores-Villalba, E.; da Silva, J.V.L.; Elías-Zúñiga, A.; Rodriguez, C.A. Soft Tissue Hybrid Model for Real-Time Simulations. *Polymers* **2022**, *14*, 1407. https://doi.org/10.3390/polym14071407

Academic Editor: Antonio Gloria

Received: 4 February 2022
Accepted: 16 March 2022
Published: 30 March 2022

1. Introduction

Modeling the mechanical behavior of soft biological tissue is a complex task that has derived in the development of a great number of constitutive material models. Some of the material models that have been used in the literature for predicting the nonlinear behavior observed in experimental data are those proposed by Dorftmann and Ogden [1], Holzapfel [2–4], Arruda-Boyce [5], Cantournet et al. [6], Elías-Zúñiga et al. [7], and references listed therein. These models consider a different number of material constants that need to be determined using experimental data [8,9]. It is also known that the majority of these constitutive material models are not appropriate to perform real-time simulations and thus, simplified models such as the Spring–Mass Model (SMM) formulation have been developed [10–14]. These SMM formulations are based on the linear elasticity theory and Hooke's law. Therefore, these are used for small material elongations ($\lambda < 10\%$). The SMM is easy to implement, and computer simulations of the material response are performed in real-time, but its accuracy is lower than that attained by finite element methods. In an attempt to improve the SMM accuracy for larger materials elongations, several approaches

nanomaterials

MDPI

Article

An Optimum Specimen Geometry for Equibiaxial Experimental Tests of Reinforced Magnetorheological Elastomers with Iron Micro- and Nanoparticles

Luis Manuel Palacios-Pineda [1,2], Imperio Anel Perales-Martínez [1], Mario Regino Moreno-Guerra [1] and Alex Elías-Zúñiga [1,*]

[1] Escuela de Ingeniería y Ciencias, Tecnológico de Monterrey, Monterrey 64849, Mexico; palacios@itpachuca.edu.mx (L.M.P.-P.); anel.perales@itesm.mx (I.A.P.-M.); marioregino@hotmail.com (M.R.M.-G.)

[2] División de Estudios de Posgrado e Investigación, Instituto Tecnológico de Pachuca, Pachuca 42082, Mexico

* Correspondence: aelias@itesm.mx; Tel.: +52-818-358-2000

Received: 14 August 2017; Accepted: 31 August 2017; Published: 3 September 2017

Abstract: The aim of this paper focused on obtaining the optimum cruciform geometry of reinforced magnetorheological elastomers (MRE) to perform homogeneous equibiaxial deformation tests, by using optimization algorithms and Finite Element Method (FEM) simulations. To validate the proposed specimen geometry, a digital image correlation (DIC) system was used to compare experimental result measurements with respect to those of FEM simulations. Moreover, and based on the optimum cruciform geometry, specimens produced from MRE reinforced with carbonyl-iron microparticles or iron nanoparticles were subjected to equibiaxial loading and unloading cycles to examine their Mullin's effect and their residual strain deformations.

Keywords: biaxial tests; cruciform specimen; Mullin's effect; nanoparticles

1. Introduction

The addition of materials of different nature, size, and morphology to neat polymers leads to new reinforced polymeric composites with physical and mechanical properties that need to be determined, since during their manufacturing processes or service conditions [1–3] these could be subjected to three-dimensional deformation states that require a good understanding of their mechanical properties to predict their qualitative and quantitative behavior [4,5]. In this sense, the common practice of using tensile testing to predict the material's response is insufficient to account for anisotropic effects that could arise in reinforced polymeric materials. Therefore, the experimental data obtained from these tensile tests do not provide sufficient information to appropriately identify constitutive equations to describe the material behavior under a variety of complex loading conditions.

Most of the research done on characterizing material behavior relies on uniaxial deformation tests. However, when the material is of anisotropic nature, uniaxial deformation tests are not enough to describe their mechanical response when subjected to multiaxial load conditions. Therefore, it is desirable to perform other experimental tests that includes pure shear, biaxial, or equibiaxial deformation states [6], if constitutive material models need to be used to describe the mechanical behavior of polymeric materials. However, there exist major difficulties when performing biaxial tests, starting from the definition of the specimen's design geometry, clamping and loading devices, technology lab equipment, and sample preparation, to say a few [7,8]. Therefore, one of the goals of this study consists of determining the optimum specimen design geometry to perform equibiaxial tests. We shall start the next section by briefly discussing some of the main previous research related to the identification of the specimen geometry needed to collect equibiaxial experimental data.

Available online at www.sciencedirect.com

ScienceDirect

Procedia CIRP 49 (2016) 178 – 182

www.elsevier.com/locate/procedia

The Second CIRP Conference on Biomanufacturing

POMES: An Open-Source Software Tool to Generate Porous/Roughness on Surfaces

Jairson C. Dinis[a], Thiago F. Moraes[a], Paulo H. J. Amorim[a], Mario R. Moreno[a], Amanda A. Nunes[a], Jorge V. L. Silva[a]

[a]DT3D/CTI,Rodovia Dom Pedro I (SP-65), Km 143,6-Amarais-Campinas, SP-CEP 13069-901, Brasil

* Corresponding author. Tel.: +55-19-3746-6035; *E-mail address:* jairson.dinis@gmail.com

Abstract

The long-term success of implants depends on rapid healing and safe integration with body. In the case of orthopaedic and dental implants it was found that geometry and surface topography are crucial for short and long-term success of the implant, due to its effects in osseointegration. Properties of implant surfaces have been studied in the last decade in a concentrated effort to improve osseointegration process and implant success. Several researchers have proved that roughness of implant surface is related to healing time and integration between the implants and the bone, but the parameters on the surface creation are not fully controllable with current processes. In this work, computational algorithms are proposed for implant surface design in order to control the parameters required for this application. As a result it is presented an open-source software tool, called POMES - Porous and Modifications for Engineering Surfaces - , to design porous/roughness on top of surfaces in any geometry. Additionally, an example model was fabricated using POMES and additive manufacturing.

Peer-review under responsibility of the scientific committee of The Second CIRP Conference on Biomanufacturing

Keywords: Software Tool, Roughness, Modeling, Porous Surface, Biodesign, Biomimetic, Biofabrication;

1. Introduction

Osseointegration, defined as a direct structural and functional connection between ordered, living bone and the surface of a load-carrying implant, is critical for its stability, and is considered a prerequisite for its loading and long-term clinical success. A porous implant surface provides considerably more volume to promote cell attachment and bone tissue ingrowth, thereby facilitating a higher level of bone-implant interaction for cell migration and osteoblast adhesion into the implant surfaces [1]. This structural and functional union of the implant with living bone is strongly influenced by the surface properties of the implant. The performance of porous surface relies on a number of topographical features, including porosity, pore/particle size, pore orientation, etc [1]. Scientific researches assessing the influence of implant surface properties on bone healing have identified several factors which are important for osseointegration [2]. The surface characteristics of implant which influence the speed and strength of osseointegration include surface chemistry, topography, roughness, load, surface energy, crystal structure and crystallinity, chemical potential, among others.

According to Wennerberg et al.[3] and Shalabi et al.[4], the roughness surface of implants is divided into macro, micro, and nano-roughness. The macro roughness comprises features in the range of millimetres to tens of microns. This scale directly relates to implant geometry, with threaded screw and macro porous surface treatments. The primarily implant fixation and long-term mechanical stability can be improved by an appropriate macro roughness. This will enhance the mechanical interlocking between the macro roughness features of the implant surface and the surrounding bone [3]. Micro roughness is defined as being in the range of 1 μm to 10 μm. This range of roughness maximizes the interlocking between mineralized bone and implant surface. Studies supported by some clinical evidences suggest that the micron-level surface topography results in greater accrual of bone at the implant surface [4,5]. Nanometre roughness plays an important role in the adsorption of proteins, adhesion of osteoblastic cells and thus the rate of osseointegration [6].

Some studies have demonstrated that there is a predominant relationship between the roughness surface of the implants in the osseointegration process. Wennerberg and Albrektsson[7] had shown that titanium implants with adequate roughness may influence its primary stability, enhance bone-to-implant contact, and may increase removal torque forces. According to Boyan et al.[8], the surface roughness of the implants can significantly change the process of osseointegration because the cells react differently to smooth and rough surfaces. Fibro-

Peer-review under responsibility of the scientific committee of The Second CIRP Conference on Biomanufacturing
doi:10.1016/j.procir.2015.07.085

A HYBRID FORMULATION FOR SOFT TISSUE MODELING ON REAL-TIME SURGERY SIMULATION

Mario Regino Moreno Guerra
Paulo Henrique Junqueira Amorim
Thiago Franco de Moraes
Jorge Vicente Lopes da Silva
mario.guerra@cti.gov.br
paulo.amorim@cti.gov.br
tfmoraes@cti.gov.br
jorge.silva@cti.gov.br
Three Dimensional Technologies Division, Renato Archer Information Technology Center
SP 65 km 143,6, Campinas, SP 13069-901, Brazil
Ciro Ángel Rodríguez González
Alex Elías Zúñiga
Oscar Martínez Romero
ciro.rodriguez@itesm.mx
aelias@itesm.mx
oscar.martinez@itesm.mx
School of Engineering and Sciences, Tecnológico de Monterrey, ITESM
Eugenio Garza Sada 2501 Sur, Monterrey 64849, Nuevo León, México
José Antonio Díaz Elizondo
Eduardo Flores Villalba
jadiaze@itesm.mx
eduardofloresvillalba@itesm.mx
Medical School and Health Sciences, Tecnológico de Monterrey, ITESM
Eugenio Garza Sada 2501 Sur, Monterrey 64849, Nuevo León, México

CILAMCE 2015
Proceedings of the XXXVI Iberian Latin-American Congress on Computational Methods in Engineering
Ney Augusto Dumont (Editor), ABMEC, Rio de Janeiro, RJ, Brazil, November 22-25, 2015

XXIV INTERNATIONAL MATERIALS RESEARCH CONGRESS

MRS MATERIALS RESEARCH SOCIETY Advancing materials. Improving the quality of life.

Sociedad Mexicana de Materiales, A.C.

CHARACTERIZATION OF PORCINE LIVER PARENCHYMA BEHAVIOR UNDER TENSILE LOADING

K. Baylon[1], M.R. Moreno-Guerra[1], O. Matrínez-Romero[2], A. Elías-Zuñiga[2], E. Flores[3], J.A. Díaz-Elizondo[3], J.V.L. da Silva[4], C.A. Rodríguez[2]

[1]*Department of Mechanical Engineering, Tecnológico de Monterrey, ITESM, Eugenio Garza Sada 2501 Sur, Monterrey 64849, México*

[2]*School of Engineering and Sciences, Tecnológico de Monterrey, ITESM, Eugenio Garza Sada 2501 Sur, Monterrey 64849, México*

[3]*Medical School and Health Sciences, Tecnológico de Monterrey, ITESM, Eugenio Garza Sada 2501 Sur, Monterrey 64849, México*

[4]*Three Dimensional Technologies Division Renato Archer Information Technology Center. Address: SP 65, km 143,6 – Campinas, SP, CEP 13069-901, Brazil*

Design and development medical devices as safety car components require the understanding of tissue behavior, where an appropriated characterization is needed. Liver´s mechanical properties are required to analyze tissue trauma on car accident and predict the real behavior of tissue by the interaction with implants as well as surgery´s virtual planning and simulation. Therefore, the aim of this paper focus on describing the mechanical properties of liver tissue in order to achieve an appropriated characterization of this particular material. On this approach, an equivalent strain energy density function was used to model the material response, based on the interpolation of the volumetric fraction with isotropic behavior and the contribution of the anisotropic volumetric fraction. Uniaxial tensile tests were cyclically performed on 15 tissue samples of porcine liver parenchyma, and the experimental data for longitudinal and transversal directions were used to model the mechanical behavior, considering the Mullins and permanent set effects. Results for model´s theoretical prediction compared with experimental data are presented in this study, showing good approximation by the proposed model.

Keywords: Porcine liver parenchyma, Liver characterization and modeling, Tissue mechanical tests

Presenting authors email: aelias@itesm.mx

XXIV Brazilian Congress on Biomedical Engineering – CBEB 2014

SOFT TISSUE MODELING FOR VIRTUAL SURGERY SIMULATION

M. R. Moreno*, P. H. J. Amorim*, T. F. Moraes*, J. V. L. Silva*,
K. L. Baylon**, E. Flores***, A. Elías**, C. A. Rodriguez**

*Centro de Tecnologia da Informação Renato Archer (CTI), Campinas, Brazil
**Centro de Innovación en Diseño y Tecnología - Tecnológico de Monterrey, Monterrey, Mexico
*** Escuela de Medicina y Ciencias de la Salud - Tecnológico de Monterrey, Monterrey, Mexico

e-mail: ciro.rodriguez@itesm.mx

Abstract: Nowadays on medical and healthcare areas, training and learning methods for surgeons are based on skills development. In order to improve this learning process, virtual reality simulators have been proposed due its capacity to reproduce surgical procedures without any risk or harm on patient. These devices represent a wide research area that involves multiple fields of knowledge, such as mechatronics, computational mechanics and information technology.

In this work are exposed the improvements for soft tissue modeling on the virtual environment of an open-source laparoscopic surgery simulator.

In this paper, the *Exoskeleton Structure* (ES) method was developed and applied on a 3D mesh in order to create interactive simulations for concave geometries on the simulation core. Moreover, the *Equivalent Strain Energy Density* (ESED) model was implemented, showing good performance in prediction of soft tissue behavior on preliminary results for a one-dimensional element on uniaxial testing.

These results validate the application of both proposals for soft tissue modeling on the development of real-time surgery simulations.

Keywords: Virtual reality, InVesalius, Surgery simulation, Tissue modeling.

Introduction

Currently, medical training on surgical procedures is focused on skills development and practical learning. For this application, several technologies have been proposed to create tools for training, trying to improve the process in which physicians acquire experience and practical knowledge, avoiding any risk on patients.

For instance, virtual reality has been applied to create learning tools and devices for surgical training, due its capacity to generate controlled environments without any risk or harm on patients. Simulation systems created with this technology allow the physician to interact with the device in order to complete several tasks (with failure detection and improvement measurement) over and over until the user achieve the quality level required for the procedure [1].

One of the most important parts on the development of a virtual surgery simulator is the functional integration of multiple concepts in order to create a training system as close as possible to reality. Therefore, virtual simulators intended to support skills development on surgical procedures should involve an appropriated combination of graphical tools, physics and mechatronics, and considering computational performance and visual response.

In this work, the new developments of an open-source laparoscopic surgery simulator are exposed, focusing on improvement for soft tissue modeling on the virtual environment.

Background

This work is based on the integration of three major parts: 1) InVesalius software for 3D reconstruction of medical images, 2) a simulation core of mechanical properties for soft tissue characterization and 3) a mechatronic design for user interaction. The main concept of this framework is presented on Figure 1, showing the interaction between fields.

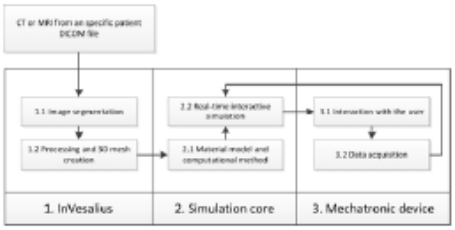

Figure 1: Main concept of this framework

InVesalius is an open-source software used to create 3D reconstructions from medical images, such as CT (*Computed Tomography*) and MRI (*Magnetic Resonance Imaging*) on DICOM (*Digital Imaging and Communication in Medicine*) format [2,3]. It was developed with Python programming language and VTK (Visualization Toolkit) and includes segmentation and measurement tools for geometrical features [4].

Given that InVesalius is open-source software with GNU General Public License, it represents a platform that allows the development of new tools for research purposes on a wide range of medical applications [5-8].

Virtual Open Source environment for training and Simulation of Laparoscopic Surgery

Mario R. Moreno[1], Thiago Franco Moraes[2], Paulo H. J. Amorim[2]
Jorge V. Lopes da Silva[2], Ciro A. Rodriguez[1]

[1]Centro de Innovación en Diseño y Tecnología, Tecnológico de Monterrey – MÉXICO

[2]Centro de Tecnologia da Informação Renato Archer – BRASIL

jorge.silva@cti.gov.br, ciro.rodriguez@itesm.mx

Abstract. *In the Medical area the use of technological tools for the training process of surgical procedures is an attractive solution, free of risks and implications. In this work the preliminary results of the development of an interactive virtual environment for medical training are exposed. This is developed in the context of an open source simulator of laparoscopic surgery. The geometrical and physical modeling of the anatomical structures or organs involved in surgical procedures are the main focus of this work. Medical images were used to obtain the real anatomical geometries and the Spring-Mass model was applied with a skeleton structure for modeling the mechanical behavior of the soft-tissues. The experimental results for a pancreas are exposed.*

1. Introduction

The Laparoscopic surgery is a technique of Minimally Invasive Surgery, based in performing the surgical procedure by using specialized instruments and a laparoscope video camera inserted through small incisions in the abdominal wall. In this case, the surgeon must guide his actions by relying in the monitor video image, having difficulties by the limited visualization, the loose of depth perception in a 2D video image, a reduced motion range and a limited force feedback.

There are a few training methods for laparoscopic surgery, such as training on cadavers, animals, trainer box, virtual simulators and even on patients, having different ethical and legal implications. The virtual simulator represents a method free of implications, and its effectiveness as a teaching tool has been previously validated by several studies [Schijven and Jakimowicz 2003], [Issenberg et al. 2005], [Palter and Grantcharov 2010]. The idea of this project is to provide a laparoscopic surgery virtual simulator in an open source approach, by releasing the software, manufacturing drawings and electronic circuit designs of the project in a freely and cooperative way. In a first stage, a prototype of the device was developed and exposed in a previous work [Moreno et al. 2012]. In this work, the development progress of the virtual environment is the main focus, including the geometry acquisition from medical images, the graphic structure and the mechanical modeling to simulate the behavior of the soft-tissue involved in the surgical procedures.

2. Anatomically Realistic Geometry

The anatomical geometries are complex surfaces and their acquisition is really important for the simulation process of the surgical procedures that will be included in the virtual

PROCEEDINGS OF THE 1st INTERNATIONAL CONFERENCE ON DESIGN AND PROCESSES
FOR MEDICAL DEVICES – Ceretti et alii. PROMED, ISBN: 978 88 6608 058 9

SIMULATOR FOR LAPAROSCOPIC SURGERY WITH OPEN SOURCE APPROACH

Mario R. Moreno[1], Arturo Marban[1], Juan C. Rojas[1], Gabriela del Bosque[1], Diego Escamilla[1], Jose Antonio Diaz[2], Ciro Rodriguez[1*], Jorge V. Lopes da Silva[3]

[1]Tecnologico de Monterrey – Centro de Innovación en Diseño y Tencología (Mexico)
[2]Tecnologico de Monterrey – Departamento de Ciencias Clínicas (Mexico)
[3]Centro de Tecnologia da Informação Renato Archer (Brazil)

ABSTRACT: The development of skills for laparoscopic surgery imposes a significant challenge in medical schools. Currently, the use of simulators for laparoscopic surgery is one of the most effective techniques for this type of medical skills development. This study shows the design and prototyping of a new kind of low cost simulator for laparoscopic surgery. The simulator developed by an international and multidisciplinary team is based on the open source approach. The simulator includes the following elements: a) surgeon's practice knowledge management, b) emulators for laparoscopic surgery instruments, and c) virtual interactive environment. The simulators concept presented here is intended for free and open distribution, allowing the development of basic laparoscopic surgery skills at low cost. The surgery instrument emulators are designed for construction with simple materials and tools by the end user. The virtual interactive environment is based on video game technology (i.e., open source software Blender). Realistic models of human organs are prepared with open access software InVesalius. Surgery specialization students and teachers currently test the simulator prototype shown in this study. Preliminary results of the simulator testing are presented.

KEYWORDS: Laparoscopic Surgery Simulator, Video Game Technology, Medical Imaging.

1 INTRODUCTION

One of the most important advances in the field of surgical procedures is the Minimally Invasive Surgery (MIS). The MIS represent an alternative to the conventional open surgery, with the main advantages of reducing the surgery risk, trauma and pain and decreasing the recovery time thereby reducing the hospital stay and cost [1].

The Laparoscopic surgery is one kind of MIS technique, and the main idea is to accomplish surgical procedures insufflating the abdominal cavity with CO_2 to create an open workspace inside, and then insert a video camera and specialized instruments trough small incisions in the abdominal walls. The surgical procedure is performed by the surgeons using the instruments and guiding their actions by the video image, in a high-resolution monitor, of the camera inside the body.

The main challenges of the laparoscopic surgery are the following:

- *Visualization:* The surgeon cannot directly see the operating site, but must rely on a 2D video image in a monitor, causing problems of spatial orientation due to the lack of depth perception, increasing stress and affecting the learning curve of procedures.
- *Motion Range:* Since the instruments and the camera are introduced trough small holes into a narrow space, their movements are restricted.
- *Limited Feedback:* Surgeons have reduced visual and haptic feedback during these interventions, and cannot rely on traditional hand-eye coordination.
- *Learning Curve:* Training a procedure in this technique takes more practice than learning traditional surgical procedures [1-3].

1.1 TRAINING METHODS IN LAPAROSCOPIC SURGERY

There are several training methods for laparoscopic surgery: (1) *Training on patients:* This is only allowed for experienced physicians due to the patient risk. (2) *Training on cadavers:* Not all the medical institutions have access to this method, and involve several ethical and legal implications. (3) *Training on animals:* This method also involves several ethical and legal implications, and with limited access to anatomical properties of a real human surgery. (4) *Box Trainer:* This method is basic and accessible, but it does not intend to reproduce the real surgery. It is based on represent the abdominal cavity with a box, inserting real instruments

* Corresponding author: Av Eugenio Garza Sada #2501 Monterrey 64849 Mexico, +52 81 83582000 ext 5105, ciro.rodriguez@itesm.mx

Curriculum Vitae: Mario Regino Moreno Guerra

Education

01/2014 – Current Doctor of Science in Engineering (CANDIDATE)
Instituto Tecnológico y de Estudios Superiores de Monterrey (ITESM)

01/2011 – 12/2012 Master of Science in Manufacturing systems with honors
Instituto Tecnológico y de Estudios Superiores de Monterrey (ITESM)

08/2004 – 07/2009 Bachelor's degree in Mechatronic engineering
Facultad de Ingeniería Mecánica y Eléctrica (FIME) of the
Universidad Autónoma de Nuevo León (UANL)

Work Experience

11/2018 – Current Chassis Engineering Manager – Steering and Suspension PE Coord
Navistar Mexico S. de R.L de C.V, Escobedo, N.L, Mexico

- Functional manager of two engineering teams for new product development (more than 20 direct reports)
- Approver of design changes on engineering releases for new products, optimization of current products or solution of complex issues.
- Performance reviews and development of direct reports.
- Forecast of programs and workload capacity between US/MX/IN resources.
- Budget and cost management of two departments for cost accounts and labor.

12/2016 – 11/2018 Product Engineer – Steering Systems
Navistar Mexico S. de R.L de C.V, Escobedo, N.L, Mexico

- Design of steering components for trucks, tractors and heavy-duty vehicles.
- Project lead on major programs for design and analysis of steering, front suspension and axle integration components.
- Kinematic analysis of front axles articulations for design and functionality review of components like tires, wheels, brakes chambers, axles, suspension springs and steering linkage.

08/2014 – 07/2016 PhD research internship for project development
CTI Renato Archer, Campinas, Sao Paulo, Brazil

- Project lead of a medical training real-time simulation as an open-source software and hardware platform.
- Modeling and simulation of the mechanical properties of soft tissue on anatomically realistic geometries obtained by processing medical images.

02/2013 – 02/2014 Product engineer – Global engineering
Navistar Mexico S. de R.L de C.V, Escobedo, N.L, Mexico

- New product development engineer working on design of multiple subsystems for trucks, tractors and heavy-duty vehicles. Problem solving of current production issues and field claims on global market.
- Support to manufacturing plant for implementation of engineering changes.

10/2009 – 01/2011 Design engineer of automotive components
Yazaki Service S. de R.L de C.V, San Nicolás de los Garza, N.L, Mexico

- Design of automotive components for wire harnesses like connectors, terminals, gromets, gutters and covers, etc. (3D modeling and 2D views.

This document was typed in using Microsoft Word by Mario Regino Moreno Guerra.